M. E.

JOURNAL OF THE

AERO/SPACE SCIENCES

VOLUME 27 FEBRUARY, 1960 NUMBER 2

MECHANICAL ENGINEERING
LIBRARY

CONTENTS

Boundary-Layer Transition on Blunt Bodies With Highly Cooled Boundary Layers.. KENNETH F. STETSON 81

Transition in a Separated Laminar Boundary Layer..... B. H. LOCHTENBERG 92

Large Deflections of Structures Subjected to Heating and External Loads..... M. J. TURNER, E. H. DILL, H. C. MARTIN, AND R. J. MELOSH 97

Application of Power Spectral Methods in Airplane and Missile Design..... KENNETH R. THORSON AND QUENTIN R. BOHNE 107

Propagation of Weak Disturbances in a Gas Subject to Relaxation Effects..... FRANKLIN K. MOORE AND WALTER E. GIBSON 117

A Statistically Averaged Error Criterion for Feedback-System Synthesis..... JOHN ZABORSZKY AND JOHN W. DIESEL 128

Readers' Forum..... 135

PURDUE UNIVERSITY
LIBRARY

Published by
INSTITUTE OF THE AERONAUTICAL SCIENCES, INC.

JOURNAL OF THE AERO/SPACE SCIENCES

Editor: W. R. SEARS
Director, Graduate School of Aeronautical Engineering, Cornell University

Associate Editor: ROBERT R. DEXTER *Managing Editor:* RITA J. TURINO
Editorial Assistant: CAROLINE TAYLOR

Editorial Committee

Aerodynamics and Fluid Mechanics
H. Julian Allen
Holt Ashley
Dean R. Chapman
Francis H. Clauser
Hugh L. Dryden
John C. Evvard
Antonio Ferri
Alexander Flax
Wallace D. Hayes
R. T. Jones
Carl Kaplan
H. W. Liepmann
C. C. Lin
H. F. Ludloff
Harold Luskin
Clark B. Millikan
Henry T. Nagamatsu
H. J. E. Reid
George S. Schairer
G. B. Schubauer
John Stack
Theodore Theodorsen
Arthur N. Tifford
Th. von Kármán

Flight Testing
R. R. Gilruth
Melvin N. Gough
W. L. Howland
W. F. Milliken, Jr.

Rotating Wing Aircraft
F. B. Gustafson
K. H. Hohenemser
Bartram Kelley
R. B. Maloy
Ralph McClarren
R. H. Miller
R. H. Prewitt
Igor I. Sikorsky

Structures
John E. Duberg
R. R. Heldenfels
N. J. Hoff
Samuel Levy
J. F. McBrearty
W. Ramberg
E. E. Sechler
F. R. Shanley
C. R. Strang
S. Timoshenko

Meteorology
C. F. Brooks
D. M. Little
F. W. Reichelderfer
K. C. Spengler

Vibration and Flutter
Lee Arnold
M. A. Biot
R. L. Bisplinghoff
Harold A. Cheilek
I. E. Garrick
Martin Goland

Aircraft Design
W. E. Beall
E. H. Heinemann
Hall L. Hibbard
Richard Hutton
C. L. Johnson
A. A. Kartveli
F. K. Teichmann

Electronics
K. C. Black
M. V. Kiebert, Jr.
David S. Little
Paul Rosenberg
Giles J. Strickroth

Physiologic Problems
H. G. Armstrong
Louis H. Bauer
Robert J. Benford
W. Randolph Lovelace, II
Ross A. MacFarland

Flight Propulsion
William Bollay
George W. Brady
R. P. Kroon
Frank E. Marble
Abe Silverstein
E. S. Taylor

Instruments
Alan G. Binnie
Charles H. Colvin
Frank R. Cook
C. S. Draper
S. G. Eskin
C. F. Savage
R. C. Sylvander

SUBSCRIPTION RATES

JOURNAL OF THE AERO/SPACE SCIENCES (formerly Journal of the Aeronautical Sciences), Published Monthly. United States and Possessions: 1 Year, $15.00; Single Copies, $1.50. Foreign Countries Including Canada (American Currency Rates): 1 Year, $16.00; Single Copies, $1.50.

AERO/SPACE ENGINEERING, Published Monthly. United States and Possessions: 1 Year, $5.00; Single Copies, $0.50. Foreign Countries Including Canada (American Currency Rates): 1 Year, $6.00; Single Copies, $0.50.

Notices of change of address should be sent to the Institute at least 30 days prior to actual change of address.

Manuscripts for publication, proofs, and all correspondence should be addressed to the Editorial Office of the JOURNAL.

Publication Office, 20th and Northampton Sts., Easton, Pa. Correspondence regarding subscriptions may be addressed to the Editorial Office of the JOURNAL OF THE AERO/SPACE SCIENCES, 2 East 64th Street, New York 21, N.Y.

© *Copyright, 1960, by the Institute of the Aeronautical Sciences, Inc.*

Second-Class Mail Privileges Authorized at Easton, Pa. Acceptance for mailing at a special rate of postage provided for in Section 1103, Act of October 3, 1917, authorized April 29, 1937.

JOURNAL OF THE AERO/SPACE SCIENCES

VOLUME 27 FEBRUARY, 1960 NUMBER 2

Boundary-Layer Transition on Blunt Bodies With Highly Cooled Boundary Layers†

KENNETH F. STETSON*

Avco-Everett Research Laboratory

Summary

The shock tube is shown to be a feasible research tool for conducting boundary-layer transition experiments. The use of the shock tube permits the study of transition with highly cooled boundary layers, as may be encountered on hypersonic vehicles.

Boundary-layer transition investigations have been made on optically polished pyrex hemisphere-cylinder and ellipse-cylinder models with stagnation-to-wall enthalpy ratios between 4.5 and 30. The models were 1/2 and 1 in. in diameter with a surface roughness estimated to be less than 1 microinch (*rms*). Transition was detected by measurements of the heat-transfer rates on the model surface.

The shock tube experiments indicated that a characteristic feature of transition of a highly cooled boundary layer on a hemisphere was the simultaneous occurrence of transition over the entire supersonic portion of the hemisphere. This implies that transition first occurred in the sonic region. The transition Reynolds Number (based on local fluid properties at the outer edge of the boundary layer and the momentum thickness) in the sonic region increased from about 225 to 325 as the stagnation-to-wall enthalpy ratio increased from about 9.5 to 29.5. Transition occurred along the cylindrical portion of the hemisphere-cylinder model at a nearly constant momentum thickness Reynolds Number, increasing from about 400 to 625 as the stagnation-to-wall enthalpy ratio increased from about 9.5 to 29.5.

The highly cooled boundary layers obtained on the cylindrical portion of the shock tube hemisphere-cylinder model provided an extension of NASA transition results obtained on a cooled hemisphere-cone-cylinder model in a wind tunnel. The transition Reynolds Numbers obtained from these shock tube data were of the same order of magnitude as the minimum transition Reynolds Numbers obtained in the wind-tunnel experiments. The results indicate that, for practical purposes, boundary-layer cooling is not a critical transition parameter for blunt bodies with a highly cooled boundary layer resulting from a stagnation-to-wall enthalpy ratio of about 3 to 30. That is, the transition Reynolds Number did not vary significantly with boundary-layer cooling in this cooling range, but transition always occurred at a low Reynolds Number (between about 350,000 and 750,000 based on local external properties and a distance along the body surface from the stagnation point).

The boundary-layer history (body shape history) appeared to be an important parameter affecting the magnitude of the Reynolds Number for transition and the amount of increase in the transition Reynolds Number with increased boundary-layer cooling. That is, transition occurred at a lower Reynolds Number on the ellipse-cylinder configuration than on the hemisphere-cylinder. Also, the increase in transition Reynolds Number with an increase in boundary-layer cooling was even less significant for the ellipse-cylinder than the hemisphere-cylinder.

Presented at the Aerodynamics-II Session, IAS 27th Annual Meeting, N.Y., Jan. 26–29, 1959. Revised and received July 3, 1959.

† This work was sponsored by the Ballistic Missile Division, ARDC, USAF, under Contract AF 04(645)-18.

* Senior Engineer.

The author wishes to acknowledge that this program was suggested by Dr. Mac C. Adams, Deputy Director of the Avco-Everett Research Laboratory, and was carried out under his able guidance. Thanks are also due many members of the Laboratory, especially to Dr. R. Probstein (Consultant) and H. Hidalgo for their helpful discussions and suggestions and to R. McMillan who very meticulously conducted the shock-tube experiments.

Symbols

h = static enthalpy
H = stagnation enthalpy
M = Mach Number
M_s = shock Mach Number (referred to speed of sound in quiescent gas in front of shock)
Nu = Nusselt Number
Nu^* = modified Nusselt Number (Nu/σ)
p = pressure
p_1 = initial pressure in shock tube
q = heat-transfer rate
R = body radius
r = body radius perpendicular to the longitudinal axis of body
Re_θ = Reynolds Number based on momentum thickness
Re_x = Reynolds Number based on body dimension
rms = root mean square
S = distance from stagnation point along the body surface
T = absolute temperature
u = velocity
α = body angle on hemisphere away from the stagnation point
β = pressure gradient parameter = $2d \ln u_e/d \ln \xi$
$\bar{\gamma}$ = approximate ratio of specific heats
θ = laminar boundary-layer momentum thickness
μ = viscosity

$\xi(s) = \int_0^S \rho_w \mu_w u_e r^{2*} ds$

ρ = density

σ = Prandtl Number

Subscripts

e = external flow conditions

st = stagnation point conditions

w = wall conditions

∞ = free-stream conditions

Introduction

THE PROBLEM of the transition to turbulence of the laminar boundary layer is one which has been with us for many years, yet, in most cases, there still does not exist sufficient knowledge regarding the general nature of transition to make reliable predictions of boundary-layer transition on new configurations, or under a different set of conditions. Therefore, it is usually necessary to conduct additional experimentation to answer specific questions regarding transition. For the case of hypersonic configurations, laboratory simulation is not a simple problem, since "conventional" wind-tunnel facilities do not provide the high gas enthalpies encountered locally about bodies traveling at very high velocities.

Lewis Research Center of NASA has obtained considerable boundary-layer transition data under moderate boundary-layer cooling by pre-cooling the models with liquid nitrogen to a stagnation-to-wall enthalpy ratio of 4.4, and have reported finding a transition reversal.[1–4] That is, contrary to small disturbance stability theory (see, for example, reference 5), an increase in boundary-layer cooling may result in a reduction of the transition Reynolds Number. By using a heater capable of producing temperatures of about 3,000°R., the Polytechnic Institute of Brooklyn has extended the boundary-layer cooling range for an uncooled model in a wind tunnel.[6, 7]

Blunt bodies with strong favorable pressure gradients and high boundary-layer cooling were expected by many people to have a relatively high transition Reynolds Number, yet experiments (such as those conducted in the above mentioned facilities) showed that this was not the case and transition consistently occurred at lower Reynolds Numbers than expected from slender body results and small disturbance stability theory. Unfortunately, current data do not cover the flight range where the most severe conditions are expected by future hypersonic vehicles.

The shock tube showed promise as a research tool to investigate hypersonic boundary-layer problems, particularly under conditions of high surface cooling, since it had the capability of producing a wide range of stagnation pressure and enthalpy conditions (see Table 1). However, it was necessary to tolerate limitations in regard to flow Mach Number, testing time, and model instrumentation. The maximum flow Mach Number obtainable in a constant area shock tube is given by the equation

$$M_{max} = \sqrt{2/\gamma(\gamma - 1)}$$

TABLE 1

Theoretical Flow Properties for Several Shock Tube Test Conditions (Values Obtained Reference 20).

p_1, cm. Hg.	T_∞, °R.	ρ_∞, slugs/ft.³	p_∞, lb./ft.²	U_∞, ft./sec.	M_∞	Equivalent* Flight Velocity, ft./sec.	T_{st}, °R.	ρ_{st}, slugs/ft.³	p_{st}, lb./ft.²	h_{st}/h_w**	T_{st}/T_w**
					$M_s = 5$						
5	2,900	0.000923	4,450	4,480	1.80	7,400	4,430	0.00272	18,050	9.3	8.2
10	2,900	0.00184	8,900	4,480	1.80	7,400	4,430	0.00543	36,100	9.3	8.2
20	2,900	0.00369	17,800	4,480	1.80	7,400	4,430	0.01085	72,200	9.3	8.2
30	2,900	0.00555	26,700	4,480	1.80	7,400	4,430	0.01635	108,500	9.3	8.2
40	2,900	0.00736	35,500	4,480	1.80	7,400	4,430	0.02170	144,000	9.3	8.2
50	2,900	0.00920	44,500	4,480	1.80	7,400	4,430	0.02710	180,500	9.3	8.2
60	2,900	0.01105	53,500	4,480	1.80	7,400	4,430	0.03260	217,000	9.3	8.2
76	2,900	0.01400	67,700	4,480	1.80	7,400	4,430	0.04120	275,000	9.3	8.2
					$M_s = 7$						
5	4,750	0.001115	8,350	6,880	2.18	10,400	6,700	0.00450	47,250	17.3	12.4
10	4,750	0.00224	16,700	6,880	2.18	10,400	6,800	0.00872	94,500	17.3	12.6
20	4,750	0.00448	33,300	6,880	2.18	10,400	6,850	0.01745	189,000	17.3	12.7
30	4,750	0.00673	50,100	6,880	2.18	10,400	6,900	0.02580	283,500	17.3	12.8
40	4,750	0.00888	66,700	6,880	2.18	10,400	6,950	0.03390	378,000	17.3	12.9
50	4,750	0.01110	83,500	6,880	2.18	10,400	7,020	0.04230	472,500	17.3	13.0
60	4,750	0.01330	100,000	6,880	2.18	10,400	7,070	0.05080	567,000	17.3	13.1
76	4,750	0.01685	127,000	6,880	2.18	10,400	7,070	0.06440	718,000	17.3	13.1
					$M_s = 9$						
5	6,250	0.00137	14,200	8,960	2.49	13,600	9,070	0.00635	103,000	29.5	16.8
10	6,430	0.00268	28,400	9,000	2.49	13,600	9,400	0.01235	203,000	29.5	17.4
20	6,530	0.00530	56,600	9,050	2.48	13,600	9,600	0.02400	402,000	29.5	17.8
30	6,580	0.00792	85,100	9,070	2.47	13,600	9,770	0.03560	601,000	29.5	18.1
40	6,630	0.01045	113,100	9,090	2.46	13,600	9,880	0.04670	788,000	29.5	18.3
50	6,670	0.01300	142,000	9,100	2.46	13,600	10,000	0.05750	974,000	29.5	18.5
60	6,700	0.01560	170,000	9,110	2.45	13,600	10,050	0.06850	1,152,000	29.5	18.6
76	6,750	0.01960	216,000	9,120	2.45	13,600	10,050	0.08550	1,440,000	29.5	18.6

* Flight velocities where same stagnation enthalpy is encountered.

** Wall temperature equals 540°R. (the temperature and enthalpy ratios do not change significantly during the shock tube tests).

For an ideal diatomic gas this limiting value is 1.89. When real gas properties are considered, the flow Mach Number is limited to about 3.2. This Mach Number restriction is not a severe limitation for many investigations concerning boundary layers on blunt shapes since the "Mach Number independence principle" can be applied (see, for example, reference 8). That is, for a blunt body, hypersonic free flight stagnation point conditions and pressure distribution along the body can be simulated without matching free-stream Mach Numbers. Shock tube heat-transfer instrumentation had been developed (for example, see references 9, 10, and 11), thus providing a method for detecting boundary-layer transition. Preliminary boundary-layer transition experiments were performed on a hemisphere-cylinder configuration to determine the feasibility of the shock tube for transition investigations. These data were found to be consistent and repeatable, and transition was clearly evident.

The experiments reported here are the results of an investigation of the effect of boundary-layer cooling on two shapes—the hemisphere-cylinder and the ellipse-cylinder.

Experimental Equipment

Two constant area shock tubes were utilized for this boundary-layer transition investigation—one with a 4-in. inside diameter and 50 ft. in length, and the other a $1^1/_2$-in. inside diameter and 16 ft. in length. The useful testing times were normally between 300 and 500 microsec. for the large shock tube and between 80 and 150 microsec. for the small shock tube (testing time was a function of initial pressure in the tube and shock Mach Number). Two model configurations were used for the experiments—a hemisphere-cylinder and an ellipse-cylinder. Transition was detected by observing the changes in heat-transfer rates on the model surface. The heat-transfer rates were determined by thin platinum resistance thermometer type gages (approximately 0.3 micron thick). These gages were mounted directly on the model surface in the manner of a printed circuit,[9-11] hence the model material in the neighborhood of the gage had to be an insulator. This was accomplished by constructing the entire model from pyrex. The models were 1/2 and 1 in. in diameter and contained from two to four heat-transfer gages. 1/2-in. diameter models were tested in the $1^1/_2$-in. shock tube and both 1/2 and 1-in. diameter models were tested in the 4-in. shock tube. Typical models and arrangement for mounting gages can be seen in Fig. 1. Electrical leads were internally housed and all junctions were insulated to eliminate electrical interference from ionization. The gages were mounted, calibrated, and utilized in the manner outlined in reference 11.

Both shock tubes were equipped with schlieren systems and occasional schlieren photographs were taken for general observation of the flow and to obtain pressure distributions.

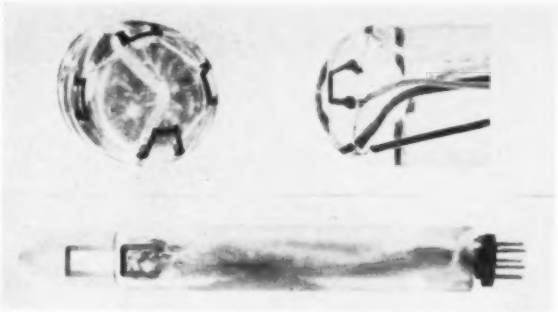

FIG. 1. Transition models. (*Top*) 1-in. diameter hemisphere-cylinder model with four heat-transfer gages. (*Bottom*) 1/2-in. diameter ellipse-cylinder model with two heat-transfer gages.

The shock tube test conditions were varied over a wide range, yet the full range of the shock tube could not be utilized, since only those test conditions which provided Reynolds Numbers in the neighborhood of transition were desired. Most of the data were obtained at three states of boundary-layer cooling, corresponding to stagnation-to-wall enthalpy ratios (h_{s1}/h_w) of about 9.5, 17.5, and 29.5.

Specific values of the flow properties for several shock tube test conditions may be found in Table 1. Reynolds Numbers (based on conditions at the outer edge of the boundary layer) obtainable on the 1/2-in. diameter models can be seen in Figs. 6, 7, 9, and 10. Reynolds Numbers based on momentum thickness (Re_θ) for the 1-in. diameter hemisphere may be obtained by multiplying the values for the 1/2-in. diameter model by $\sqrt{2}$. (If identical test conditions and body angle locations on a hemisphere are compared, Re_θ varies as the square root of the radius.)

The surface condition of individual models used for these experiments was not known precisely. However, an estimate of the surface finish could be obtained from information resulting from the examination of sample models under an electron microscope. The sample models were prepared in the same manner as those utilized in the experiments, and it seems reasonable to expect that the experimental models had a surface finish of the same type as the sample models. The surface roughness which was predominantly in the form of pits, was estimated to be less than 1 microinch (*rms*). The maximum pit depth measured on the sample models was 12 microinches. The Appendix contains the results of the surface finish experiments.

Results

It has been shown that such factors as pressure gradient and surface cooling significantly affect the Reynolds Number at which transition occurs (for example, see reference 12). Such effects are not accounted for in a Reynolds Number based on free-stream properties and a body dimension. In order to incorporate boundary-layer history into the Reynolds Number, recent transition data on blunt shapes have often been correlated with a Reynolds Number (Re_θ) based on local

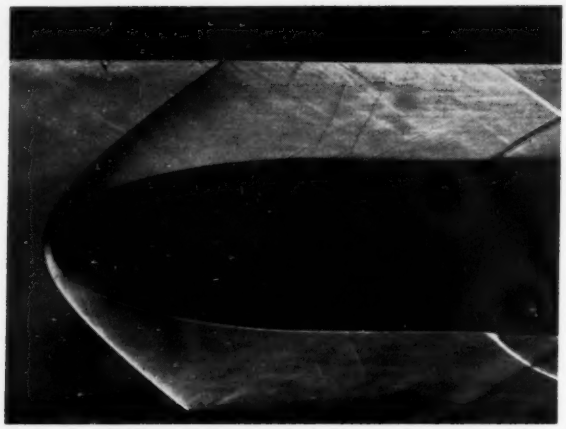

FIG. 2. Schlieren photograph of ellipse-cylinder model with scratches to produce Mach lines (test conditions: $p_1 = 5$ cm. Hg, $M_s = 7.7$).

fluid properties at the outer edge of the boundary layer and the laminar boundary-layer momentum thickness (θ). For the most part, the data from these current experiments have been correlated with Re_θ. It should not be interpreted, however, that Re_θ necessarily provides the best correlation. For comparison purposes some of the transition data was correlated with a Reynolds Number (Re_x) based on local fluid properties at the outer edge of the boundary layer and a length along the body surface from the stagnation point.

Calculations of Re_θ were made with the assumption of isentropic flow from the stagnation point along the surface streamline and utilized an approximate ratio of specific heats ($\bar{\gamma}$) which included a correction for real gas effects. The calculations of momentum thickness were based on the assumption of local similarity as discussed by Kemp, Rose and Detra[13] (they obtained their solutions numerically by an extension of the method which Fay and Riddell[14] used at the stagnation point). From these numerical solutions θ can be empirically correlated by the following equation:

$$\theta = (\sqrt{2\xi}/\rho_e u_e r^\epsilon)[0.491(1 - 0.090\beta^{0.4})(\rho_e\mu_e/\rho_w\mu_w)^{0.386}]$$

where ξ is

$$\xi(S) = \int_0^S \rho_w\mu_w\mu_e r^{2\epsilon} dS$$

$\epsilon = 0$ for two-dimensional bodies, $\epsilon = 1$ for axially symmetric bodies, β is a pressure gradient parameter expressed as

$$\beta = 2d \ln u_e / d \ln \xi$$

and r is the body radius perpendicular to the longitudinal axis of the body. Subscripts e and w denote values obtained at the outer edge of the boundary layer and at the wall.

It is not possible to obtain a pressure distribution on a model in a shock tube as customarily obtained in a wind tunnel, due to inadequate pressure instrumentation. However, a pressure distribution may be obtained in the shock tube in regions of supersonic flow by making small scratches on the model (about 0.001 in. deep) and measuring the Mach lines on a schlieren photograph. The local Mach Number is obtained from the Mach angle, and, with the assumption of isentropic flow, the local pressure ratio (p/p_{st}) may be related to the local Mach Number. A number of such pressure distributions have been obtained on a hemisphere-cylinder configuration[13] and the pressure distribution was found to be very close to that predicted by a modified Newtonian pressure distribution without the centrifugal correction {given by the following equation: $p/p_{st} = 1 - [(p_{st} - p_\infty)/p_{st}] \sin^2 (S/R)$}. Fig. 3(A) is a typical pressure distribution on a hemisphere-cylinder model (from reference 13). This same technique was used to obtain the pressure distribution on an ellipse-cylinder model in a shock tube. Fig. 2 is a schlieren photograph of the ellipse-cylinder model showing the Mach lines obtained from 0.001 in. scratches on the model. Fig. 3(B) is the pressure distribution obtained from this photograph. It can be seen that the pressure distribution on the ellipse-cylinder in a shock tube also follows very closely the pressure distribution given by the above equation. The assumption of isentropic flow and a pressure distribution given by the above equation was then made in the calculations of Re_θ and other information needed in analyzing these data.

Before presenting the experimental transition results, the reader is reminded of the following significant features which pertain to these data:

(a) Testing times were a fraction of a millisecond.

(b) The transition models were 1/2 and 1 in. in diameter.

(c) Only general surface finish information of the test models was known.

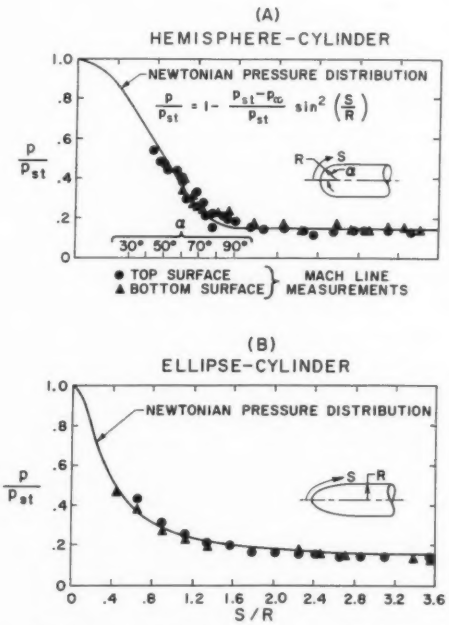

FIG. 3. Typical pressure distributions obtained in a shock tube.

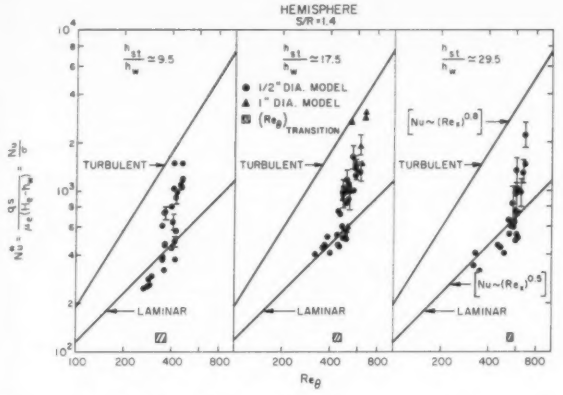

FIG. 4. Typical shock tube boundary-layer transition data.

(d) The heat-transfer gages (about 0.3 micron thick) were mounted on the model surface. The effect of gage height on transition is not known; however, the thickness of the gage was no greater than the maximum pit depth measured.

(e) The gages were nearly 1 millimeter wide, which meant that for the 1/2-in. diameter hemisphere the gage covered about a 9° arc and for the 1-in. diameter model the gage covered about $4^1/_2°$. That is, for the 1/2-in. hemisphere, a gage referred to as an 80° gage had the leading edge of the gage at about $75^1/_2°$ and the trailing edge at about $84^1/_2°$. The heat-transfer rate measured was then the average rate for the 9° arc.

(f) Some scatter of the data was introduced by deviation in gage location from the desired station.

(g) Previous shock tube heat-transfer data have had scatter of about ±10 to 20 per cent.

(h) Flow Mach Number changed with a change in boundary-layer cooling (see Table 1).

Only a sample of the shock tube transition data has been shown. Fig. 4 is typical of the type of data obtained from shock tube experiments at all stations. The laminar heat-transfer rates were steady, whereas the transition heat-transfer rates were often unsteady. When the rates varied with time the range of variation was indicated by a vertical line through the test point. The variation of heat-transfer rates in the transition region and the randomness associated with the transition location are not surprising in view of the fluctuations normally observed in transition data. Transition was assumed to occur in the region where the heat-transfer rate departed from the laminar value, as indicated on Fig. 4 by the shaded rectangular areas. This probably results in transition Reynolds Numbers which are lower than would be encountered under comparable conditions in free flight. This is to be expected as the consequence of such factors as a higher turbulence level in the shock tube test gas, the close proximity of the walls, and disturbances caused by the external heat-transfer gages. Most of the transition experiments were performed with the 1/2-in. diameter model. A limited amount of data obtained with the 1-in. diameter hemisphere-cylinder model agreed, within experimental accuracy, with that obtained with the 1/2-in. diameter model.

Fig. 5 contains heat-transfer data from four typical experiments with the 1/2-in. diameter hemisphere-cylinder model. Each model contained three heat-transfer gages (30°, 45°, and 70°) to provide simultaneous comparison of the boundary-layer condition. It can be seen that the 45° and 70° stations followed a consistent trend. They departed from the laminar curve at the same time and maintained a consistent departure as the Reynolds Number was increased. This would imply that transition first occurred at, or before, the 45° gage, but after the 30° gage.

Fig. 6 shows the transition Reynolds Number distribution for the hemisphere-cylinder model under three boundary-layer cooling conditions ($h_{st}/h_w \cong 9.5$, 17.5, and 29.5). The dashed lines represent the Reynolds Number distribution on the 1/2-in. diameter model for the indicated shock tube test conditions and with the assumption of a modified Newtonian pressure distribution without centrifugal corrections, as previously mentioned. All three figures are similar in shape, with the magnitude of Re_θ for transition being related to the amount of boundary-layer cooling in such a manner that an increase in cooling gave an increase in the transition Reynolds Number At a given location the Reynolds Number per unit length increased with an increase in boundary-layer cooling. However, any variations in transition Reynolds Number due to unit Reynolds Number changes are not large enough to be clearly distinguished above the scatter of the data. For a given amount of boundary-layer cooling, transition occurred on the cylindrical portion of the model at

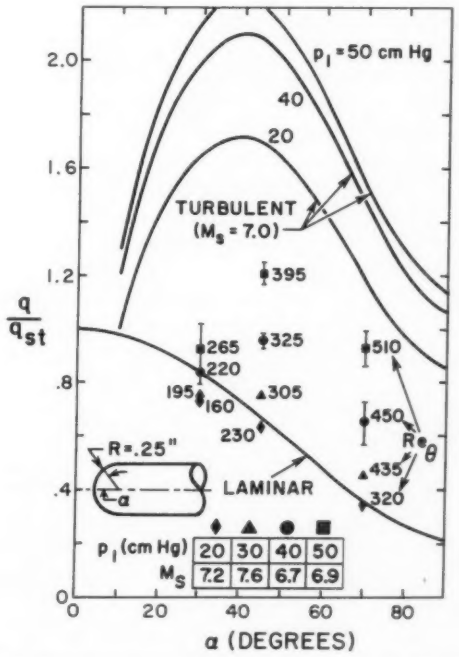

FIG. 5. Typical heat-transfer rates obtained on a hemisphere-cylinder model with three heat-transfer gages.

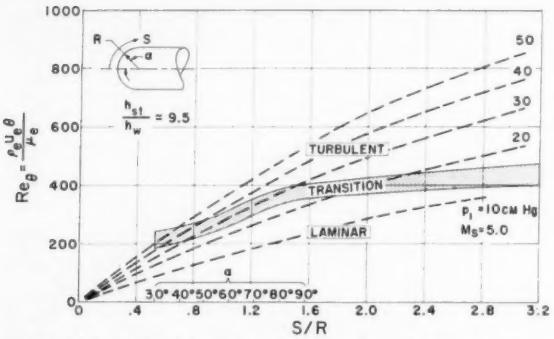

FIG. 6(a). Transition Reynolds Number distribution on a hemisphere-cylinder configuration ($h_{st}/h_w \simeq 9.5$). *Note:* Dashed lines represent the Re_θ distribution for the hemisphere-cylinder model under the shock tube test conditions indicated (1/2-in. diameter model and $M_s = 5.0$).

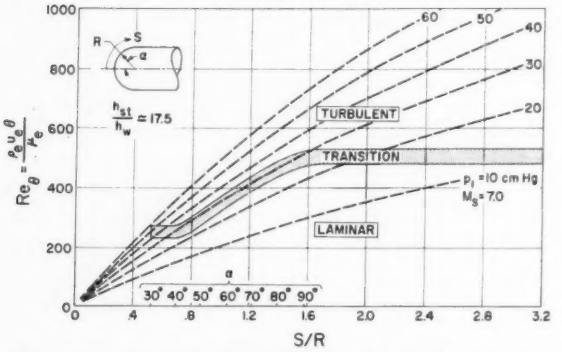

FIG. 6(b). Transition Reynolds Number distribution on a hemisphere-cylinder configuration ($h_{st}/h_w \simeq 17.5$). *Note:* Dashed lines represent the Re_θ distribution for the hemisphere-cylinder model under the shock tube test conditions indicated (1/2-in. diameter model and $M_s = 7.0$).

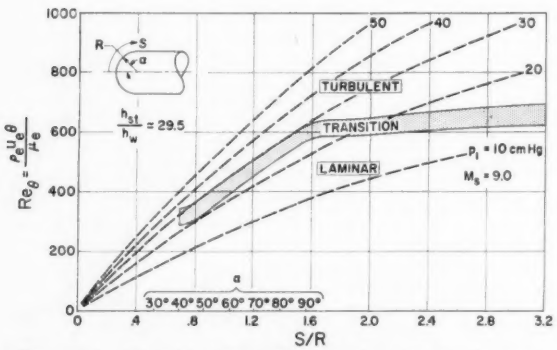

FIG. 6(c). Transition Reynolds Number distribution on a hemisphere-cylinder configuration ($h_{st}/h_w \simeq 29.5$). *Note:* Dashed lines represent the Re_θ distribution for the hemisphere-cylinder model under the shock tube test conditions indicated (1/2-in. diameter model and $M_s = 9.0$).

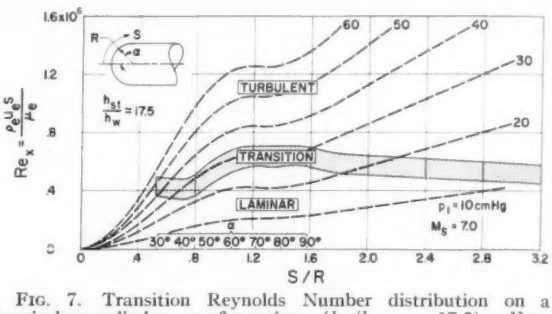

FIG. 7. Transition Reynolds Number distribution on a hemisphere-cylinder configuration ($h_{st}/h_w \simeq 17.5$). *Note:* Dashed lines represent the Re_x distribution for the hemisphere-cylinder model under the shock tube test conditions indicated (1/2-in. diameter model and $M_s = 7.0$).

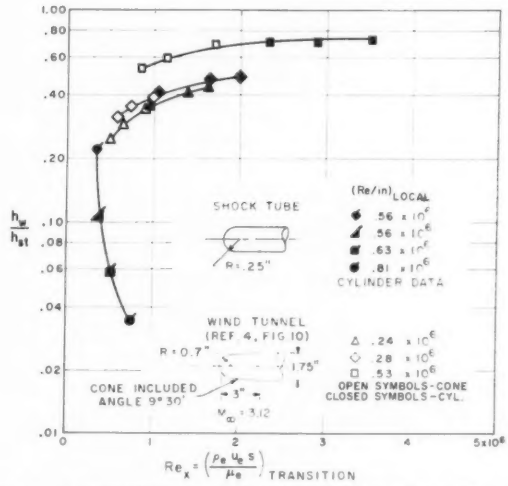

FIG. 8. A comparison of shock tube transition data with wind-tunnel transition reversal data.

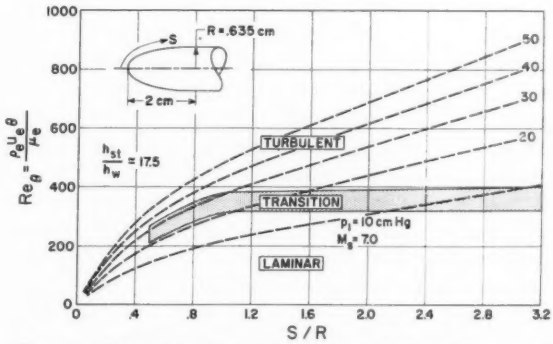

FIG. 9. Transition Reynolds Number distribution on an ellipse-cylinder configuration ($h_{st}/h_w \simeq 17.5$). *Note:* Dashed lines represent the Re_θ distribution for the ellipse model under the shock tube test conditions indicated (1/2-in. diameter model and $M_s = 7.0$).

a nearly constant momentum thickness Reynolds Number; that is, the transition Reynolds Number was essentially independent of location on the cylinder. The subsonic portion of the hemisphere also had a nearly constant Re_θ for transition A significant characteristic of these figures can be seen in the supersonic portion of the hemisphere ($\approx 45° < \alpha < 90°$), where transition occurred simultaneously over the entire region This is indicated on the figure by the fact that the transition Reynolds Number distribution curve in the supersonic region coincides with the calculated distribution curve for a specific test condition. (This could also be observed in individual experiments, such as shown in Fig. 5.) It appears likely that the simultaneous appearance of transition on the hemisphere was a consequence of transition first occurring in the sonic region (in the neighborhood of $\alpha = 45°$). In any case, this result would indicate that the minimum transition Reynolds Number associated with the first appearance of transition on the highly cooled hemisphere was the Reynolds Number calculated for the sonic region.

Fig. 7 contains the same experimental data as Fig. 6(b), with the difference being that Reynolds Number is now based on a distance along the body surface from the stagnation point, instead of momentum thickness. It was believed to be of interest to see the same data correlated with two different Reynolds Numbers.

The highly cooled boundary layers obtained on the shock tube models allowed an extension to the boundary-layer cooling results obtained in wind tunnels. Diaconis, Wisniewski and Jack[4] obtained wind-tunnel transition data on a hemisphere-cone-cylinder under the influence of boundary-layer cooling by precooling the models with liquid nitrogen to a stagnation-to-wall enthalpy ratio of 4.4. This configuration was not far different from the hemisphere-cylinder used in the shock tube experiments and was considered suitable for the desired comparison.

Fig. 8 shows the comparison of the wind tunnel and shock tube data for the above mentioned configurations. The three smallest enthalpy ratios for the shock tube data correspond to cylinder data as presented in Fig. 6. In order to obtain an experimental point closer to the wind-tunnel data, shock tube experiments were conducted just above the choking limit of the shock tube. That is, for a 1/2-in. diameter model in the 4-in. diameter 50-ft. long shock tube, choking occurred at the model at shock Mach Numbers below about 3.0. Therefore, the data in question were obtained in the shock Mach Number range of 3.2 to 3.5, with a corresponding flow Mach Number of about 1.5.

According to reference 4. the wind-tunnel models were precooled to a temperature of −340°F., so that at the start of the test there existed a wall-to-stagnation enthalpy ratio of 0.23. The experiments were conducted with thin-walled models instrumented to obtain temperature time histories. As the surface of the models heated during the test, the transition location moved downstream, as indicated in Fig. 8 by the increase in transition Reynolds Number with an increase in enthalpy ratio. This trend is consistent with the transition reversal data presented in references 1, 2, 3, and 4. As can be seen in Fig. 8, low transition Reynolds Numbers (less than one million) were obtained initially when there existed a large degree of boundary-layer cooling. This result suggested that low transition Reynolds Numbers may be a characteristic feature of very highly cooled boundary layers. In a boundary-layer cooling range which extended that of the wind-tunnel experiments, these shock tube data were consistent with this trend, and the transition Reynolds Numbers obtained in the shock tube were of the same order of magnitude as the minimum transition Reynolds Numbers obtained in the wind-tunnel experiments. (With the shock tube equipment available, it was not possible to duplicate in the shock tube the same cooling range obtained in the wind-tunnel experiments.)

These shock tube data have significant implications for a vehicle with a highly cooled boundary layer (as, for example, a vehicle re-entering the atmosphere). Although these data show a slight increase in the transition Reynolds Number with an increase in boundary-layer cooling, there appears to be no connection between the very low transition Reynolds Numbers found and those which would be predicted by small disturbance stability theory. Two very important conclusions may be obtained from this figure and stated as follows: (1) Low transition Reynolds Numbers occur on a highly cooled blunt body. (2) It would appear that for blunt bodies boundary-layer cooling is not a critical transition parameter for a wall-to-stagnation enthalpy ratio in the range of about 0.03 to 0.3.

Shock tube transition experiments on a hemisphere configuration implied that transition first occurred in the sonic region. This result suggested that higher transition Reynolds Numbers might be obtained on a more slender shape, such as an ellipse, which had the sonic region located closer to the stagnation point and therefore would always maintain a relatively low Reynolds Number (and presumably a stable boundary layer) in this region. A number of shock tube experiments were performed on an ellipse-cylinder configuration (semimajor axis/semiminor axis = 2.0 cm./0.635 cm. = 3.15), with most of the data being obtained at a stagnation-to-wall enthalpy ratio of about 17.5. The results of these experiments are presented in Fig. 9. Contrary to the above reasoning, transition occurred at a lower Reynolds Number than on the hemisphere-cylinder tested under similar conditions. For the region of the ellipse with a weak pressure gradient ($S/R > 1.0$, see Fig. 3) transition occurred at essentially a constant Re_θ. Nearer the stagnation point, where the pressure gradient was stronger ($0.5 < S/R < 1.0$), transition occurred simultaneously over the entire region, as was experienced on the supersonic portion of the hemisphere. Data could not be obtained at S/R values below 0.5 due to the relative size of the heat-transfer gage and model nose radius; therefore, no information is available concerning the subsonic region of the el-

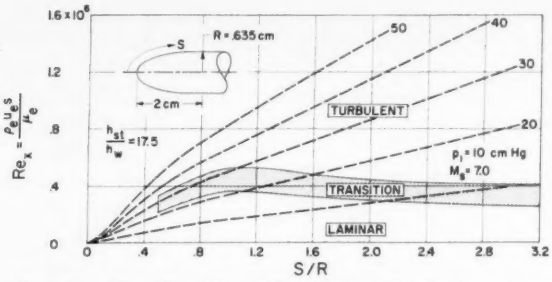

FIG. 10. Transition Reynolds Number distribution on an ellipse-cylinder configuration ($h_{st}/h_w \simeq 17.5$). *Note:* Dashed lines represent the Re_x distribution for the ellipse model under the shock tube test conditions indicated (1/2-in. diameter model and $M_s = 7.0$).

lipse. In comparing the transition Reynolds Number distribution on the ellipse-cylinder with the hemisphere-cylinder, it appears that the subsonic region of the ellipse has a strong influence on the transition Reynolds Number in a similar manner as on the hemisphere. The reason for the ellipse-cylinder having lower transition Reynolds Numbers than the hemisphere-cylinder is not clear at this time. The indications are, however, that the effect of body curvature in the nose region of a highly cooled body is important. Discussion of this point has been given by Ferri and Vaglio-Laurin,[15] Lees,[16] Kuethe,[17, 18] and Jack.[19]

Another comparison of the two configurations may be made by considering the cylindrical portion of both models at a location well downstream from the stagnation point [Figs. 6(b) and 9]. One might speculate that here we have two regions of zero pressure gradient, some distance downstream of a blunt nose where boundary-layer history is no longer important, and therefore we could expect similar Reynolds Numbers for transition. This was not found to be the case, however, and the experiments showed that the cylinder preceded by a hemisphere had an Re_θ for transition of about 500 and the cylinder preceded by an ellipse had an Re_θ for transition of about 375 (both for $h_{st}/h_w \simeq 17.5$). An interesting point is that the two curves show no definite indication of converging, as they should do as the effect of history loses its significance. Apparently the influence of boundary-layer history does not wear off for a considerable distance downstream on the cylinder.

Fig. 10 is the same data as shown in Fig. 9, with the Reynolds Numbers being based on a distance along the body surface from the stagnation point, instead of boundary-layer momentum thickness.

Fig. 11 is a cross plot of the transition data to show the effect of a highly cooled boundary layer on transition. The increase in the transition Reynolds Number with increased boundary-layer cooling on the hemisphere has been apparent from previous figures. An important point of this figure is obtained from a comparison of the ellipse data with the hemisphere and cylinder data. At the location on the ellipse where these data were obtained the pressure gradient was very weak and essentially zero, as on the cylinder. The fact that the ellipse showed little increase in the transition Reynolds Number with increased boundary-layer cooling, in comparison with the cylinder (hemisphere nose) which had similar local flow characteristics, suggests that the amount of increase in transition Reynolds Number with boundary-layer cooling depends upon boundary-layer history (body shape history).

For comparison purposes the momentum thickness occurring at transition at various stations on the 1/2-in. diameter hemisphere-cylinder and ellipse-cylinder models are shown in Fig. 12. Also, the momentum thickness distribution on the models for several shock tube test conditions are given. The reader is reminded that the momentum thickness on a hemisphere increases as the square root of the model radius. This means that, for similar locations and shock tube test conditions, Re_θ for the 1-in. diameter hemisphere is $\sqrt{2}$ times the Re_θ for the 1/2-in. diameter hemisphere. Reynolds Number per unit length (Re/in.) at a given station and given shock tube conditions may be obtained by dividing Re_θ (Fig. 6) by θ (Fig. 12).

Conclusions

Boundary-layer transition has been investigated in shock tube experiments on hemisphere-cylinder and ellipse-cylinder configurations under conditions of extreme boundary-layer cooling. Transition Reynolds Number distribution curves have been obtained at stagnation-to-wall enthalpy ratios of about 9.5, 17.5, and 29.5 (corresponding stagnation-to-wall tempera-

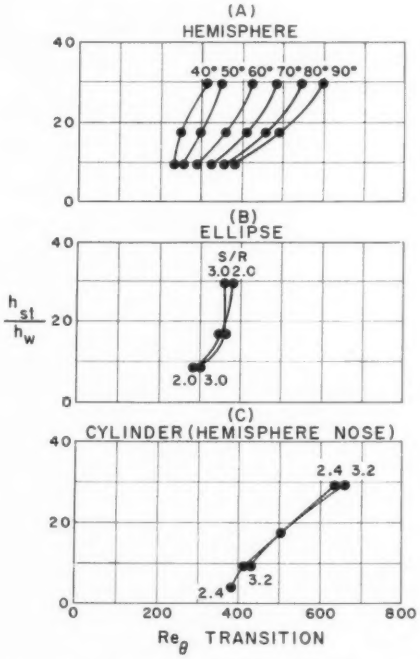

FIG. 11. Variation of transition Reynolds Number with enthalpy ratio.

ture ratios of about 8.5, 13, and 18). The following conclusions were derived from the experiments:

(1) A characteristic feature of transition of a highly cooled boundary layer on a hemisphere was the simultaneous occurrence of transition over the entire supersonic portion of the hemisphere. This implied that transition first occurred in the sonic region. The minimum transition Reynolds Number associated with the first appearance of transition was then the Reynolds Number calculated for the sonic region. The transition Reynolds Number (based on local fluid properties at the outer edge of the boundary layer and the momentum thickness) in the sonic region increased from about 225 to 325 as the stagnation-to-wall enthalpy ratio increased from about 9.5 to 29.5.

(2) Transition occurred along the cylindrical portion of the hemisphere-cylinder model at a nearly constant momentum thickness Reynolds Number, increasing from about 400 to 625 as the stagnation-to-wall enthalpy ratio increased from about 9.5 to 29.5.

(3) The highly cooled boundary layers obtained on the cylindrical portion of the shock tube hemisphere-cylinder model provided an extension of NASA transition results obtained on a cooled hemisphere-cone-cylinder model in a wind tunnel. The results indicate that, for practical purposes, boundary-layer cooling is not a critical transition parameter for blunt bodies with a highly cooled boundary layer resulting from a stagnation-to-wall enthalpy ratio in the range of about 3 to 30. That is, the transition Reynolds Number did not vary significantly with boundary-layer cooling in this cooling range, but transition always occurred at a low Reynolds Number (between about 350,000 and 750,000, based on local external properties and a distance along the body surface from the stagnation point).

(4) Transition occurred at a lower Reynolds Number on the ellipse-cylinder configuration than on the hemisphere-cylinder under similar conditions, indicating that the effect of body curvature in the nose region of a highly cooled body is important.

(5) In comparing data obtained on the cylindrical portion of the ellipse-cylinder and hemisphere-cylinder configurations, it appears that the influence of boundary-layer history on transition is significant for a considerable distance downstream on the cylinder.

(6) The amount of increase in the transition Reynolds Number with increased boundary-layer cooling depends upon boundary-layer history (body shape history). That is, an increase in boundary-layer cooling did not increase the transition Reynolds Number for the ellipse-cylinder as much as for the hemisphere-cylinder.

Appendix

The surfaces of three highly polished, hemisphere-cylinder pyrex models were examined with an electron microscope. The areas examined (the stagnation and 45° regions) were first cleaned by applying a collodion in amyl acetate and stripping when dry. Collodion

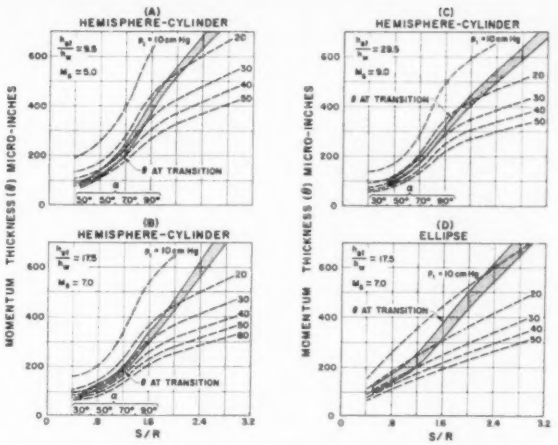

FIG. 12. Momentum thickness on transition models. *Note:* Dashed lines represent the momentum thickness distribution for the hemisphere-cylinder model [see (A), (B), and (C)] and the ellipse model [see (D)] under the shock tube test conditions indicated (1/2-in. diameter models).

replicas were made of these areas and then made into shadowed carbon replicas. Shadow length was calibrated by putting a collodion film (stripped from a glass microscope slide) with calibrating spheres, alongside the replicas of the models during shadowing. Figs. 13–16 are typical photographs obtained by this method. Following is a summary of surface information obtained from the three sample models:*

	Stagnation Region	45° Region
Model A	Several small pits, the largest 10 μ in. deep; one scratch less than 1 μ in. deep.	Several small pits, the largest 12 μ in. deep; several scratches of 1 μ in. and less.
Model B	A short gouge, 3 μ in. deep; no pits or scratches of appreciable size.	One small pit, 5 μ in. deep; two scratches 1 and 2 μ in.
Model C	Two scratches, 1 μ in. and less than 1 μ in.	A gouge 5 μ in. deep; one scratch $1\frac{1}{2}$ μ in.

References

[1] Evvard, John C., *The Effects of Extreme Cooling on Boundary Layer Transition at Supersonic Speeds*, paper presented at the American Physical Society Meeting, New York, January 31, 1957.

[2] Diaconis, N. S., Jack, J. R., and Wisniewski, R. J., *Boundary Layer Transition at Mach 3.12 as Affected by Cooling and Nose Blunting*, NACA TN 3928, January 1957.

[3] Jack, J. R., Wisniewski, R. J., and Diaconis, N. S., *Effects of Extreme Surface Cooling on Boundary Layer Transition*, NACA TN 4094, October, 1957.

[4] Diaconis, N. S., Wisniewski, R. J., and Jack, J. R., *Heat Transfer and Boundary Layer Transition on Two Blunt Bodies at Mach Number 3.12*, NACA TN 4099, October 1957.

* This investigation of surface finish was done under subcontract to Ladd Research Industries, Inc., Roslyn Heights, New York.

FIG. 13. Model A, stagnation region showing several pits, the largest 10 microinches deep.

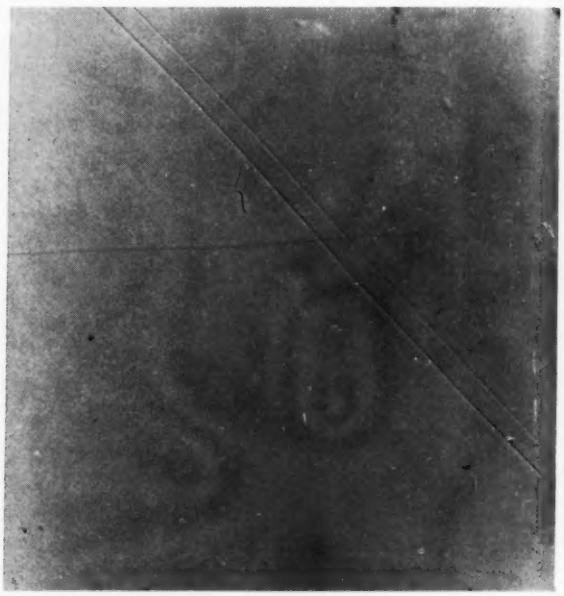

FIG. 15. Model B, 45° region showing two scratches 1 and 2 microinches deep.

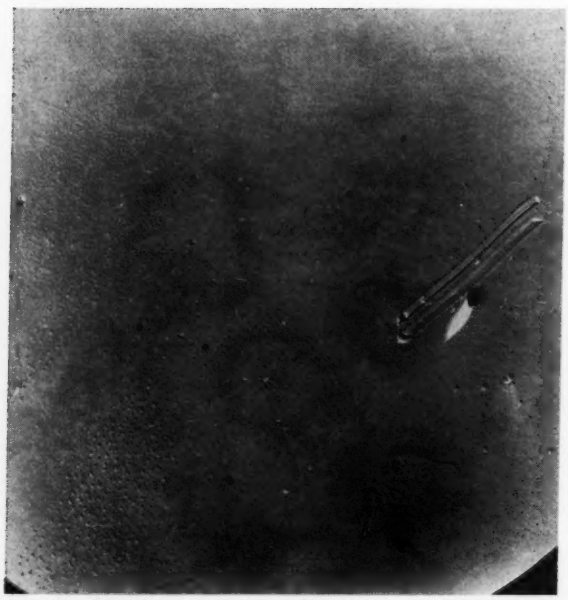

FIG. 14. Model B, stagnation region showing a gouge 3 microinches deep.

FIG. 16. Model 45° region showing a smooth surface.

[5] Lin, C. C., *The Theory of Hydrodynamic Stability*, Cambridge University Press, 1955.

[6] Ferri, A., and Libby, P. A., *The Hypersonic Facility of the Polytechnic Institute of Brooklyn and Its Application to Problems of Hypersonic Flight*, WADC TR 57-369, August, 1957.

[7] Cresci, R. J., *Preliminary Experimental Results Indicating the Effect of Centrifugal Forces on Hypersonic Boundary Layer Transition*, WADC TN 57-98, March, 1957.

[8] Hayes, W. D., and Probstein, R. F., *Hypersonic Flow Theory*, Academic Press, Inc., New York, 1959.

[9] Vidal, R. J., *Model Instrumentation Techniques for Heat Transfer and Force Measurements in a Hypersonic Shock Tunnel*, WADC TN 56-315, February, 1956.

[10] Vidal, R. J., *A Resistance Thermometer for Transient Surface Temperature Measurements*, presented at the American Rocket Society Meeting, Buffalo, New York, September 24–26, 1956 (Preprint No. 327-56).

[11] Rose, Peter H., and Stark, William I., *Stagnation Point Heat Transfer Measurements in Dissociated Air*, Journal of the Aeronautical Sciences, Vol. 25, No. 2, pp. 86–97, February, 1958 (also Avco-Everett Research Laboratory RR 3, April 1957).

[12] Probstein, R. F., and Lin, C. C., *A Study of the Transition to Turbulence of the Laminar Boundary Layer at Supersonic Speeds*, presented at the 24th Annual Meeting of the Institute of the Aeronautical Sciences, January 23–26, 1956.

[13] Kemp, N. H., Rose, P. H., and Detra, R. W., *Laminar Heat Transfer Around Blunt Bodies in Dissociated Air*, Avco-Everett Research Laboratory RR 15, May, 1958.

[14] Fay, J. A., and Riddell, F. R., *Theory of Stagnation Point Heat Transfer in Dissociated Air*, Journal of the Aeronautical Sciences, Vol. 25, No. 2, pp 73–85, February, 1958 (also Avco-Everett Research Laboratory RR 1, April, 1957).

[15] Ferri, A., and Vaglio-Laurin, R., *A Note on the Effect of Centrifugal Forces and Accelerated Motion on the Instability of the Laminar Boundary Layer About Highly Cooled Bodies*, Polytechnic Institute of Brooklyn, PIBAL Report 313 (AFOSR No. TN 56-579), December, 1956.

[16] Lees, Lester, *Note on the Stabilizing Effect of Centrifugal Forces on the Laminar Boundary Layer Over Convex Surfaces*, Journal of the Aeronautical Sciences, Vol. 25, No. 6, pp 407–408, June, 1958 (also Ramo-Wooldridge Report No. GM-TR-118, December 14, 1956).

[17] Kuethe, A. M., *On the Character of the Instability of the Laminar Boundary Layer Near the Nose of a Blunt Body*, Journal of the Aeronautical Sciences, Vol. 25, No. 5, pp 338–339, May, 1958.

[18] Kuethe, A. M., *On the Stability of Flow in the Boundary Layer Near the Nose of a Blunt Body*, Rand RM-1972, August, 1957.

[19] Jack, J. R., *Effect of Favorable Pressure Gradients on Transition for Several Bodies of Revolution at Mach 3.12*, NACA TN 4313, July, 1958.

[20] Feldman, Saul, *Hypersonic Gas Dyanamic Charts for Equilibrium Air*, Avco-Everett Research Laboratory, January, 1957.

A Reprint

Journal of the Aeronautical Sciences

Now entitled Journal of the Aero/Space Sciences

Available

Volumes 1–5, 1934–1937/1938, paper bound set.....$140.00
Volumes 1–2, 1934–1935, single volumes, paper bound..... 20.00
Volumes 3–5, 1935/1936–1937/1938, single volumes, paper bound..... 35.00

In Preparation

Volumes 6–8, 1938/1939–1940/1941

(Reproduced with the permission of the original publisher, Institute of the Aeronautical Sciences, Inc.)

Please address orders and inquiries to:

Johnson Reprint Corporation
111 Fifth Avenue, New York 3, N.Y.

Change of Address

Since the Post Office Department does not as a rule forward magazines to forwarding addresses, it is important that the Institute be notified of changes in address 30 days in advance of publishing date to ensure receipt of every issue of the JOURNAL and AERO/SPACE ENGINEERING.

Notices should be printed legibly and sent directly to:

Subscription Department
Institute of the Aeronautical Sciences, Inc.
2 East 64th Street, New York 21, N.Y.

Transition in a Separated Laminar Boundary Layer

B. H. LOCHTENBERG*

Imperial Chemical Industries of Australia and New Zealand Limited

Symbols

x = distance along plate from trailing edge of step (step describes short plate attached to main plate)
y = distance above step surface measured normal to the surface
δ = boundary-layer thickness ($U/U_0 = 0.99$)
δ^* = boundary-layer displacement thickness
δ_s = boundary-layer thickness at separation
δ_1 = separated layer displacement thickness
h = step height
k = h/δ_s^*
u = instantaneous x component of fluctuation velocity
u' = root mean square value of u
U = mean velocity at a point in the boundary layer
U_0 = mean velocity outside boundary layer
ν = kinematic viscosity
R = Reynolds Number
f = oscillation frequency
β_r = $2\pi f$
R^* = Reynolds Number *based* on δ_s^*

Introduction

PROGRESS in understanding the mechanism of transition from laminar to turbulent flow in a boundary layer has been largely confined to flow along a flat plate. The present investigation is concerned with transition in a separated laminar boundary layer. A hot wire investigation of flow near the short leading-edge bubble on a RAE-103 airfoil section led to a study of a boundary-layer transition in the flow past a step. The step investigation represented airfoil bubble conditions approximately and to a larger scale.

Apparatus and Tests

The investigation was made in the 18-in. by 12½-in. open circuit tunnel at the Oxford University Engineering Laboratory. Transition was studied with a hot wire anemometer using a constant resistance technique. The 0.0002-in. diameter hot wire was soldered to two steel needles embedded in an Araldite plastic probe. The probe was carried on a rod held by a micrometer transversing head which was clamped to the side of the tunnel. The micrometer head allowed a traverse of 1 in. along and normal to the flow, and this was found sufficient to study the development of transition.

Transition was investigated in the flow above a short leading-edge bubble on an airfoil, and in the flow past a step. The airfoil was a 10 per cent thick RAE-103 section with a 30-in. chord. The stepped plate was made up of a short forward plate (referred to subsequently as the step) attached to a 24-in. long, 1/4-in. plate (Fig. 1). The plate spanned the tunnel working section and was stiffened and held by longitudinal edge angles. Step lengths of 4, 6, and 8.4 in. were used in the investigation. By means of filler plates, the step height was adjustable to 1/8, 1/4, 3/8, and 1/2 in. All steps had a sharp leading edge formed by the intersection of 64-in. radius arcs, tangential to the surface 4 in. from the leading edge.

The stagnation point was brought to the top surface by attaching a 1/2-in. blockage angle to the plate trailing edge, resulting in a laminar boundary layer. Pressure distributions, obtained from 0.040-in. pressure holes let into the plate surface, showed a constant pressure in the region of transition investigation.

Hot wire trace records of transition in the flow past a step were obtained for the different step heights and lengths and at stream velocities of 26, 37, 53, 74, 91, and 105 ft./sec. Hot wire oscillograms were also obtained of artificial disturbances in the separated laminar boundary layer, produced by a spark at the step edge. The behavior of the separated layer was further investigated with a probe carrying two parallel hot wires.

The investigation of transition was made possible by a reasonably low level of tunnel turbulence. As a result of several modifications to the tunnel, the level of turbulence was reduced to approximately 0.05 per cent for most of the stream velocities investigated (see Fig. 2).

Since transition in the separated layer was always initiated by the onset of regular velocity fluctuations, vibration analyses were made on the tunnel, the stepped plate, and the hot wire probe. Dominant frequencies appearing in the vibration spectra were compared with the frequencies of the separated layer fluctuations. It

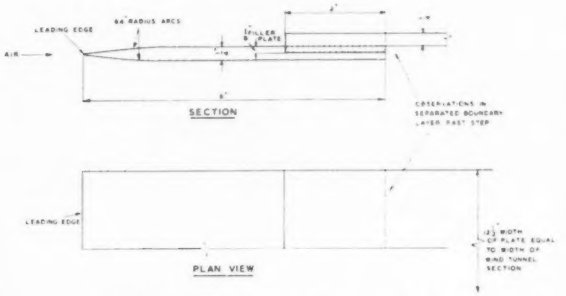

FIG. 1. Details of stepped plate showing 6-in. plate and 1/8-in. filler plate giving 1/4-in. step height.

Received March 18, 1958. Resubmitted June 11, 1959.
* Technical Engineering Department.

was found that the regular fluctuations in the separated layer were not caused by mechanical vibrations or disturbances external to the flow.

Results and Discussion

Leading-Edge Bubble on Airfoil

Hot wire records showed the development of regular waves in the separated boundary layer above the bubble. Immediately upstream of the separated layer reattachment point, bursts of erratic fluctuations characteristic of turbulence appeared in the separated layer. A typical example of a hot wire trace record showing bursts of turbulence is shown in Fig. 3. The regions of turbulence grew and rapidly formed a completely turbulent boundary layer further downstream. The significance of these observations was not appreciated

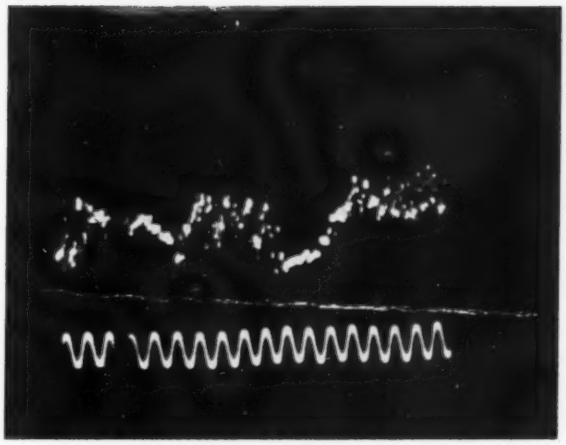

FIG. 3. Hot wire oscillogram of velocity fluctuations in transition region above bubble on the RAE-103 airfoil (time base = 500 cps).

until transition in the flow past the step had been studied.

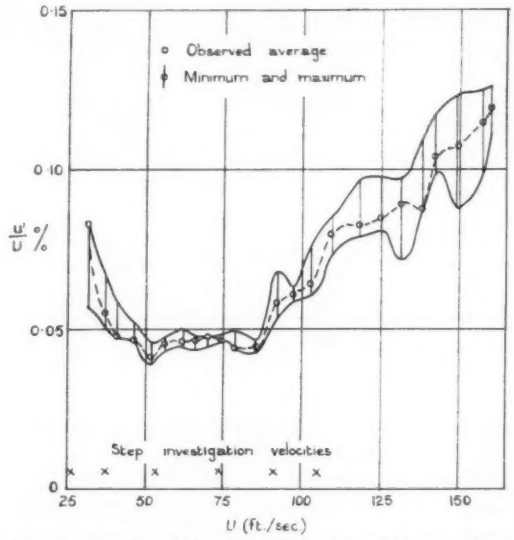

FIG. 2. Total turbulence level in the working section.

Original Figures

U Ft./Sec.	u'/U, per cent Max.	Ave.	Min.
31	0.083	0.083	0.057
37	0.067	0.055	0.051
40.5	0.059	0.048	0.048
46	0.052	0.047	0.047
51.5	0.046	0.041	0.039
56	0.047	0.045	0.043
62	0.050	0.046	0.044
66	0.048	0.047	0.043
70	0.048	0.048	0.044
74	0.049	0.046	0.046
78.5	0.050	0.044	0.044
85	0.047	0.044	0.042
92	0.068	0.058	0.053
97	0.063	0.061	0.059
102.5	0.075	0.064	0.060
109	0.085	0.080	0.073
118	0.096	0.083	0.079
125	0.098	0.085	0.081
131	0.097	0.089	0.072
138	0.109	0.088	0.088
142	0.117	0.104	0.099
149	0.123	0.108	0.089
157	0.125	0.115	0.097
160	0.127	0.119	0.111

Step Investigation Velocities
26, 37, 53, 74, 91, and 105 ft./sec.

Flow Past Step

Transition in the separated boundary layer past the step was observed to be initiated by the onset and growth of regular velocity fluctuations. Since the fluctuations were observed only in the separated layer immediately upstream of transition, they were considered to be Tollmien-Schlichting waves. Evidence that the regular waves were caused by the natural amplification of small disturbances was obtained by plotting the results of the investigation on Schlichting's neutral stability curve (Fig. 4). Values of R_{δ^*} were obtained by using the boundary-layer displacement thickness at the step separation. The error introduced by using this value instead of the displacement thickness at the point of instability in the separated layer is considered small. Plotted points lie about a line similar in shape to the arms of the neutral curve. The points represent the fluctuation frequencies observed in the separated layer. These frequencies are those which have undergone maximum amplification, and points therefore lie near the right-hand arm of a neutral curve. The scatter of points is partly caused by the range of step conditions in the investigation and also by the difficulty of obtaining accurate values of the critical frequency. This difficulty arose because of the scattered frequency values on the hot wire trace record.

A comparison of the envelope of fluctuation frequencies with Schlichting's neutral curve shows that instability develops more rapidly in a separated than in an attached boundary layer. The limit of stability or minimum critical value of R_{δ^*} below which all individual oscillations decay in flow along a flat plate is given as 420 by Tollmien, 575 by Schlichting[1] and 320 by Timman, Zaat, and Burgerhout.[3] Schubauer and Skramstad[2] obtained an experimental value for R_{δ^*} of about 425. From the plotted results in Fig. 4, the minimum value of R_{δ_1} may be estimated as 350. The criti-

cal value of R_{δ_1} for a separated layer is therefore less than 350.

The step investigation showed that transition in a separated laminar boundary layer is brought about by one of two alternative mechanisms of breakdown to turbulence. The first of these is the burst mechanism observed by Schubauer and Klebanoff in the boundary layer along a flat plate.[4] An initially regular velocity fluctuation becomes unstable and is suddenly "triggered" into a burst of turbulence. The burst is followed by an exponential decay back to laminar flow. The bursts of turbulence grow, merge and rapidly form a diffuse turbulent layer. In the second slower type of breakdown, the Tollmien-Schlichting waves grow in extent and amplitude until each wave becomes distorted and breaks into a fluctuation characteristic of turbulence. At no stage do the waves trigger to a burst.

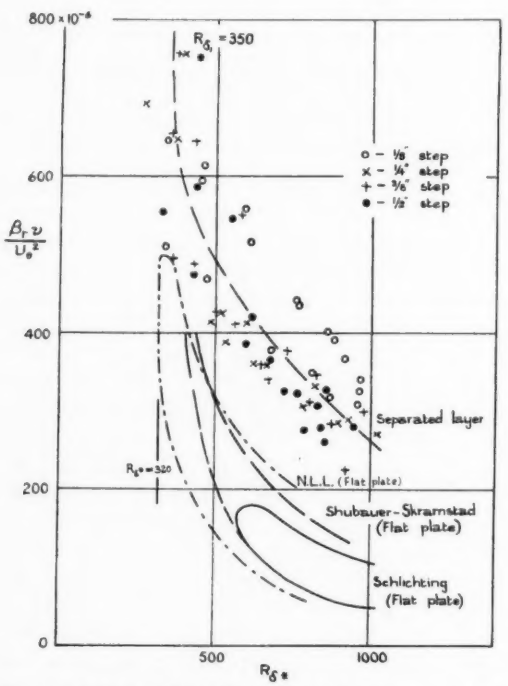

FIG. 4. Observed critical frequencies of regular waves in separated laminal layer (4, 6, and 8.4 in. steps) for separated layer assume critical $\delta_1 = \delta^*$ at separation.

1/8" Step		1/2" Step		3/8" Step		1/2" Step	
$\frac{\beta_T \nu}{U_0^2}$	R_{δ^*}	$\frac{\beta_T \nu}{U_0^2}$	R_{δ^*}	$\frac{\beta_T \nu}{U_0^2}$	R_{δ^*}	$\frac{\beta_T \nu}{U_0^2}$	R_{δ^*}
644	332	753	386	754	366	751	437
611	453	691	258	653	348	587	432
594	445	645	365	643	427	553	326
558	586	425	515	548	573	545	551
515	608	414	596	496	352	474	425
510	331	413	482	488	421	420	613
469	467	387	531	428	497	385	595
442	760	361	619	412	560	367	676
436	769	359	664	379	730	327	857
403	863	331	822	360	642	325	718
302	878	306	782	347	821	322	767
378	682	290	933	340	671	308	833
369	914	286	894	313	802	283	941
349	810	270	1020	300	978	281	835
341	963			285	873	276	785
326	962			224	922	264	840
319	865						
310	957						

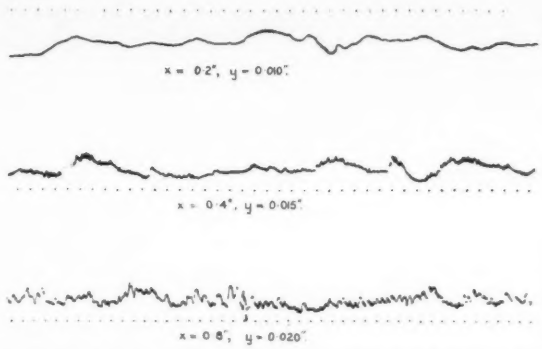

FIG. 5. Typical example of "burst" type breakdown to turbulence (step 1/2 in. to 8.4 in., U_0 = 74 ft./sec., time base = 400 cps).

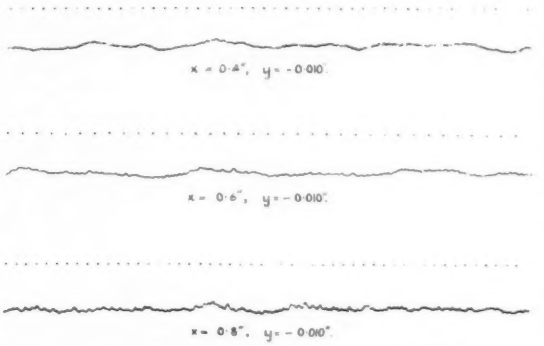

FIG. 6. Typical example of "wave" type breakdown to turbulence (step 1/4 in. to 6 in., U_0 = 53 ft./sec., time base = 400 cps).

Typical examples of the two types of transition are shown in Figs. 5 and 6.

Transition burst patterns were observed inside the separated layer. They were therefore regarded as natural breakdowns similar to those observed by Schubauer and Klebanoff, and not as the vortex, patterns of a surface of discontinuity springing from the step edge. Nor were the bursts caused by sudden incursions of the hot wire into regions of reduced velocity. Some of the trace records obtained with two parallel hot wires, both in the separated layer, showed a burst passing through the outer hot wire when no similar deflection was recorded by the hot wire nearer the plate. This was in contrast to frequent simultaneous recordings by both hot wires of low velocity regions due to waving of the separated layer.

Nearly all observations of transition in the flow past a step showed one or other of the two breakdown mechanisms. Artificial spots of turbulence produced by a spark showed that when transition was brought about by the wave breakdown the conditions were unable to support turbulent spots. Spots were damped as they passed downstream (Fig. 7). However, a few transition observations did show isolated bursts when transition due to a wave breakdown was well advanced.

Whether the Tollmien-Schlichting waves trigger to bursts or grow and gradually distort was found to be

dependent on the free-stream velocity (U_0), the step height (h) and the boundary-layer displacement thickness at separation (δ_s^*). From an analysis of the conditions supporting the wave or the burst transition mechanisms, a criterion emerged whose critical value separates the two types of breakdown. The form and critical value of the criterion is given by

$$(\delta_s^* h U_0^2/\nu^2)_{\text{crit.}} = 4.2 \times 10^6 \qquad (1)$$

The criterion may be expressed as the product of two Reynolds Numbers based on the step height and the boundary-layer displacement thickness at separation. Transition is brought about by a wave breakdown at values of the criterion less than the critical, and by the burst mechanism at values greater than the critical.

The critical value of the criterion was obtained by plotting transition observations according to wave or burst breakdowns. The distribution of ($\delta_s h U_0^2$) values from the step investigation is shown in Fig. 8, and the separated groupings of the two breakdown mechanisms is distinct.

An early attempt at distinguishing between the two types of transition was made by the author.[5] A criterion of the form δ_s/h was suggested, based on observations with the 6-in. step and step heights of 1/8, 3/8, and 1/2 in. The further experimental results available in this work show the δ_s/h relationship to be inapplicable as a criterion for type of breakdown mechanism.

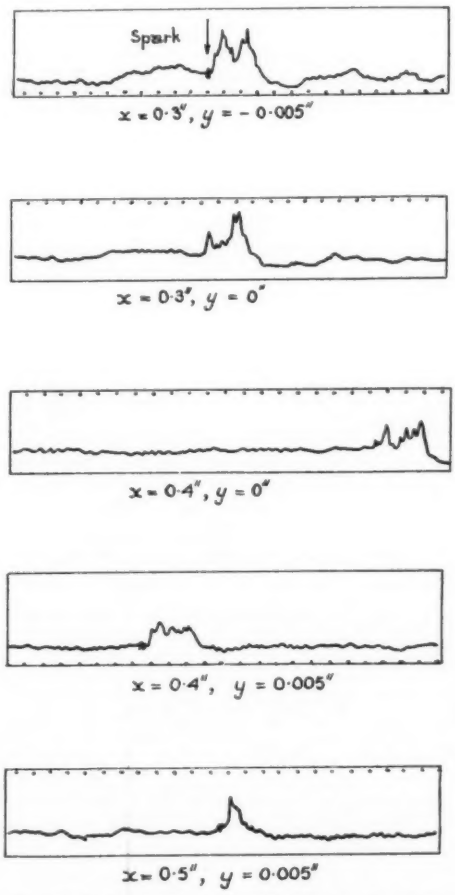

FIG. 7. Typical examples of artificially produced turbulent spots (step 1/4 in. to 6 in., U_0 = 53 ft./sec., time base = 400 cps).

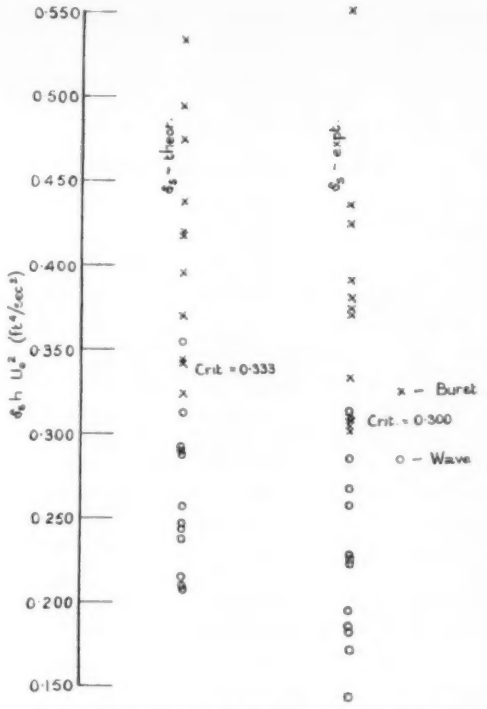

FIG. 8. Distribution of $\delta_s h U_0^2$ values for wave and burst type transitions.

Values of $\delta_s h U_0^2$

δ_s Theor.		δ_s Expt.	
Burst	Wave	Burst	Wave
533	355	550	313
494	323	435	284
474	292	423	266
438	290	391	258
420	288	380	228
		373	226
418	247	370	223
396	243	332	195
370	238	310	186
345	216	307	182
342	211	304	171
321	208	301	143

The criterion for type of transition in the separated layer past the step is compared with Owen's criterion for a long or short bubble.[6] Owen's criterion states that the bubble will be long or short according to R^* being less than or greater than a critical range of 400 to 500.

This bubble criterion is insufficient to determine reattachment, and it was therefore considered reasonable to modify its form so as to compare it with the criterion for transition. Squaring Owen's criterion and multiplying by k we have

$$k(\delta_s^* U_0/\nu)^2 = k(16 \text{ to } 25) \times 10^4$$

or

$$h\delta_s^* U_0^2/\nu^2 = k(16 \text{ to } 25) \times 10^4 \qquad (2)$$

Substituting the extreme upper and lower values of k found in the experiments we have approximately

$$(h\delta_s^* U_0^2/\nu^2)_{\text{crit.}} = (1.5 \text{ to } 5.7) \times 10^6 \quad (3)$$

which may be written

$$R_h R^*_{\text{crit.}} = (1.5 \text{ to } 5.7) \times 10^6 \quad (4)$$

To determine the behavior of separated flow on an airfoil it is suggested that the stability of both the separated boundary layer and the bubble must be considered. Owen's criterion determines the stability of the laminar boundary layer at separation. It is suggested that the stability of the bubble can be represented by a Reynolds Number based on the height of the bubble.

Eq. (4) is then an approximate criterion for flow separation on an airfoil. Since no value of bubble height was available, R_h (where h here described bubble height) was estimated by using values of k from the step investigation. The use of k makes the estimate of the critical value, (1.5 to 5.7)10^6, doubtful because of the different separation conditions over a step and preceding a bubble. An exploration of the behavior of a bubble on a large airfoil would be necessary to decide if the criterion is valid.

As a result of the close agreement between the critical values of the transition and bubble criteria in Eqs. (1) and (4), a theory for separated flow on an airfoil is put forward. It is suggested that a short bubble at the leading edge of an airfoil is the result of a burst type transition in the separated layer, and a long bubble is caused by a wave type breakdown. Investigations of transition in the flow past a step showed the burst mechanism to bring about transition more rapidly than the wave breakdown. On an airfoil, therefore, when transition is brought about by the burst mechanism, reattachment of the separated layer occurs near the separation point, and a short bubble is formed. For conditions of wave type breakdown the slower development of transition prevents a rapid reattachment of the separated layer, resulting in a long bubble. Owen, when describing leading-edge bubbles, spoke of a short bubble being the result of a "dynamic" instability and a long bubble resulting from a gradual transition.

The hot wire investigation of the short bubble on the RAE-103 airfoil section showed transition in the separated layer to be brought about by burst breakdowns. However, further evidence is needed to verify the proposed theory for separated flow on the airfoil.

Conclusions

The investigation of transition in the flow past a step, with special reference to the boundary-layer flow above airfoil bubbles, resulted in the following conclusions:

(1) Transition in a separated laminar boundary layer is initiated by the formation of Tollmien-Schlichting waves.

(2) Instability develops more rapidly in a separated than in an attached boundary layer. The minimum critical value of R_{δ_1} for the amplification of disturbances in a separated layer was estimated as being less than 350.

(3) The breakdown to turbulence in a separated layer is brought about by either a wave or a burst mechanism. The wave mechanism consists of the amplification, distortion, and breaking up of the Tollmien-Schlichting waves. The burst mechanism consists of the appearance and growth of spots of turbulence as observed by Schubauer and Klebanoff. Transition develops more rapidly with the burst than with the wave breakdown.

(4) The mechanism of breakdown in the transition region is dependent on the critical value of a criterion:

$$(\delta_s^* h U_0^2/\nu^2)_{\text{crit.}} = 4.2 \times 10^6$$

Wave breakdowns are observed at values less than the critical and burst mechanisms occur at values greater than the critical. The value of 4.2×10^6 applies to separated flow past a step.

(5) Owen's criterion for long or short bubbles is insufficient to determine reattachment. To determine the behavior of separated flow on an airfoil more fully, it is suggested that the criterion must be in the form of $R_h \cdot R^*$ where h here represents the bubble height. A critical value of the criterion must await further experimental investigations.

(6) It is suggested that a short bubble is the result of a burst type transition in the separated layer, and a long bubble is caused by the slower developing wave type transition.

References

[1] Schlichting, H., *Boundary Layer Theory*, McGraw-Hill Book Company, New York, 1955.

[2] Schubauer, G. B., and Skramstad, H. K., *Laminar Boundary Layer Oscillations and Transition on a Flat Plate*, NACA Report 909, 1948.

[3] Timman, R., Zaat, J. A., and Burgerhout, Th. J., *Stability Diagrams for Laminar Boundary Layer Flow*, N.L.L. Report F.184, 1956.

[4] Schubauer, G. B., and Klebanoff, P. S., *Contributions on the Mechanics of Boundary Layer Transition*, NACA TN 3489, September, 1955.

[5] Lochtenberg, B. H., *Some Studies of Transition in a Laminar Boundary Layer After Separation*, A.R.C. 17,972 - F.M. 2319, October, 1955.

[6] Owen, R. R., and Klanfer, L., *On the Laminar Boundary Layer Separation From the Leading Edge of an Aerofoil*, A.R.C. 16,576, C.P. 220, F.M. 2027, October, 1953.

Large Deflections of Structures Subjected to Heating and External Loads

M. J. TURNER,* E. H. DILL,†† H. C. MARTIN,‡ AND R. J. MELOSH**

Boeing Airplane Company and University of Washington

Summary

The method of direct formulation of the stiffness matrix[1–3] is extended to include the effects of nonuniform heating and large deflections. The purpose is to develop an analytical tool for the treatment of actual structures.

In the solution of aeroelastic problems the relations between forces and deflections must be determined. The usual stiffness matrix formulation of this relationship is limited to small temperature changes and small deflections. For large temperature changes additional terms are required. Also the problem becomes geometrically nonlinear when large deflections are involved. To overcome the inherent difficulties of the nonlinear problem for practical structures either an iterative or a step-by-step procedure must be used. The force-deformation relations necessary for this step-by-step or iterative approach are derived for an axially loaded member and for a plate element including the effects of thermal strains.

(I) Introduction

A NUMBER OF PROBLEMS in aeroelasticity and structural dynamics are likely to be encountered in the design of advanced vehicles and missiles which must operate within the sensible atmosphere at high supersonic and hypersonic speeds. In order to solve these problems it is necessary to be able to predict the internal stresses and structural deflections resulting from a combination of thermal gradients, inertia loads, and externally applied loads. Although the general principles of thermoelasticity are well established, and studies have been published on the behavior of simple structures when exposed to aerodynamic heating, there is still a great need to develop straightforward numerical procedures for analysis of complex practical structures.

In the nonuniform high-temperature environment which results from aerodynamic heating, classical linear methods of structural analysis do not adequately describe the behavior of the structure under loads. Temperature gradients in statically indeterminate structures result in a self-equilibrating system of internal forces, and deformation of the structure alters the directions of these initial internal forces. The components of force resulting from these changes in direction must be included in the equilibrium considerations, thereby introducing changes in the apparent or effective stiffnesses of the structure. It seems likely that the effects of internal thermal loads on structural stiffnesses and vibration characteristics will be of particular significance when there is a trend toward thermoelastic instability. There is an obvious analogy in the behavior of a column whose fundamental lateral frequency tends toward zero as the end load on the column approaches the critical buckling load. In the analysis of aeroelastic behavior of a complex structure we need to be able to establish trends in stiffness and in the natural frequencies and shapes of several of the lower order modes of vibration.

The experience which has been accumulated since reference 1 appeared has generally confirmed our belief that the stiffness method is particularly well suited for utilization with high-speed digital computers in the analysis of deflections of complex structures. The basic underlying principle is to subdivide the structure to be analyzed into elements (axially loaded members, beam segments, shell and plate elements, etc.) which are small enough to permit simple representations of their states of strain in terms of a small number of parameters. The procedure is quite general and appears adequate for the analysis of elastic deflections of a large variety of practical structures. It has been our intent in this present paper to indicate in a general way how the stiffness method can be extended to handle large deflections and initial stresses associated with temperature gradients.

(II) Some Important Aspects of the Problem

(1) *Simple Truss*

Force-deflection curves for the simple redundant truss of Fig. 1 are shown in Fig. 2. Straight lines in Fig. 2 represent the usual linear relationship; the nonlinear curves reflect the effect of geometry changes as the structure deflects under load. The behavior of this simple truss is illustrative of the more important thermoelastic phenomena associated with complex structures.

The initial stiffness, or slope of the force-deflection curve at zero external load, will be designated by K^0. When external loading is present the slope K is different from K^0 if nonlinear effects are taken into account.

Heating truss member 1–2 will induce compression in that member; at the same time the truss will remain

Presented at the Aeroelasticity Session, IAS 27th Annual Meeting, N.Y., Jan. 26–29, 1959. Revised and received July 10, 1959.

* Chief, Structural Research and Development Section, Aero-Space Division, Boeing Airplane Company.

†† Associate Professor of Aeronautical Engineering, University of Washington, Seattle.

‡ Professor and Chairman, Department of Aeronautical Engineering, University of Washington, Seattle.

** Research Engineer, Seattle Division, Boeing Airplane Company.

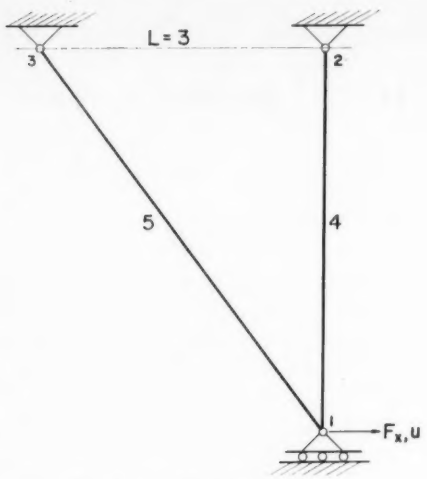

FIG. 1. Simple redundant truss.

undeflected. Subsequent application of load F_x will cause node 1 to displace and this will be augmented by the initial force in 1–2. As a result truss stiffness is reduced due to the action of the initial force induced by temperature gradient.

If temperature of 1–2 is increased to a critical value, T_{cr}, the truss will have zero stiffness against force F_x. Still further increase in temperature will then result in a negative value for K^0.

If, on the other hand, member 1–3 is heated, immediate displacement of node 1 will take place. This is represented by OB in Fig. 3. An alternative viewpoint is to assume node 1 constrained while member 1–3 is heated. This requires negative force F_{x_0} as shown in Fig. 3. After heating has been completed constraining force F_{x_0} can be relaxed. This will result in displacement of node 1 to point B as shown by AB, Fig. 3. This procedure simplifies thermodynamic considerations since individual members remain at constant temperature during the relaxation process and subsequent deflection due to application of external loading.

Simultaneous heating of both members 1–2 and 1–3 will result in immediate displacement of node 1. Equilibrium will eventually be established in a deflected configuration containing a system of self-equilibrating internal member forces.

In addition to the effects discussed above, material moduli E and G will decrease as temperature is increased. This will further reduce structural stiffness and must be taken into account. Reduced moduli will be represented by E_T and G_T, and these may be treated as constants for a given member when proceeding with calculations by relaxing the initially constrained structure as described above.

Behavior similar to that exhibited by the truss can also be experienced by the complex aircraft structure. Assume a wing symmetrical about a horizontal midplane to be heated uniformly through its depth. Vertical deflection will then only occur after external loading is applied to the wing structure. This is analogous to the truss when only member 1–2 is heated. Thermoelastic instability which may result under such conditions has been previously studied for simple wing-type structures.[4–7]

If heating is nonuniform through the wing depth vertical deflection will occur at once. This corresponds to heating member 1–3 of the truss.

For aeroelastic analyses it is assumed that the temperature distribution throughout the structure is fixed and known. Consider first a case in which a single force F_1 is applied and for which the corresponding deflection is w_1. About this point of static equilibrium additional deflections are now assumed to occur. These incremental deflections are related to corresponding force increments by the equation

$$\Delta F = K_1 \cdot \Delta w \tag{1}$$

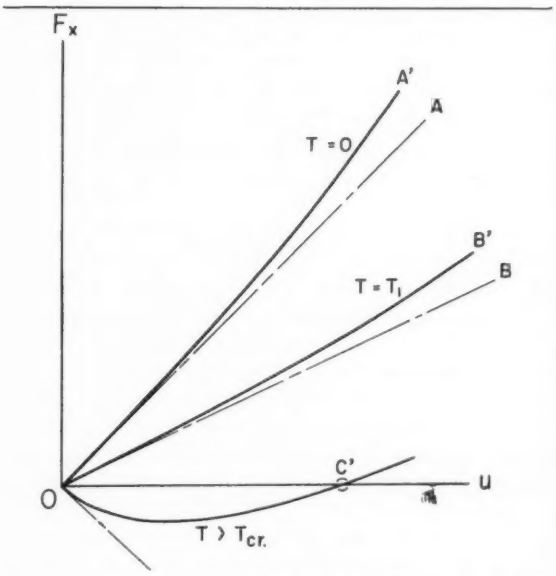

FIG. 2. Truss force-deflection curves (member 1–2 heated).

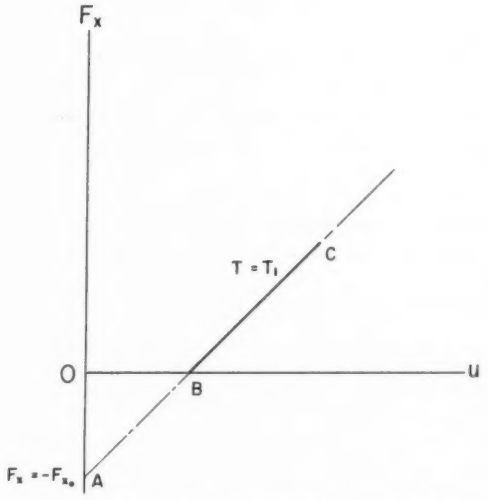

FIG. 3. Truss force-deflection curves (member 1–3 heated).

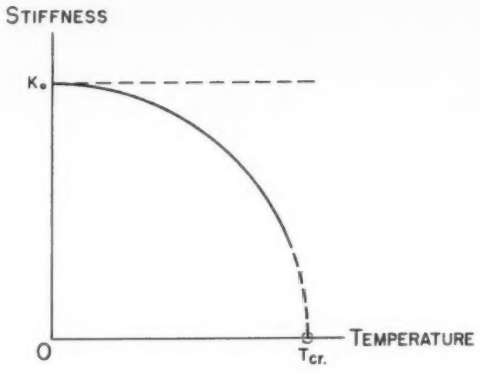

FIG. 4. Stiffness vs. temperature.

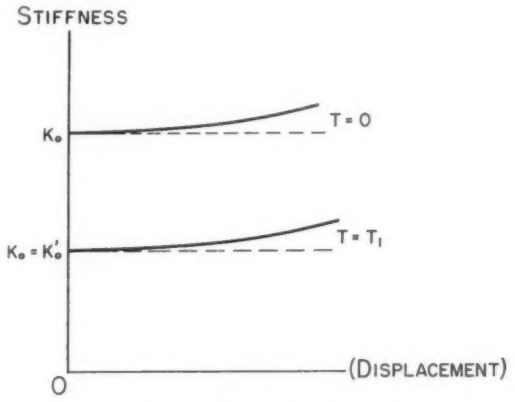

FIG. 5. Stiffness vs. displacement.

where $$K_1 = \left|\partial F/\partial w\right|_{w=w_1} \qquad (2)$$

and $$\Delta F = F - F_1, \quad \Delta w = w - w_1$$

In Eq. (1) K_1 is the stiffness at static equilibrium.

It will subsequently be seen that, in general, stiffness K of the heated structure is made up of two parts, $K^0 + K^1$. Furthermore, K^0 will be seen to depend on instantaneous geometry, while K^1 depends on initial member forces as well as the geometric configuration. Derivation of general stiffness matrices for heated structural members forms an important part of this paper.

(2) *Method of Solution*

The objective is to extend the methods of analysis presented in references 1 and 2 to provide a method of solution for the following problems: (1) to determine the effects of initial stresses (as due to temperature gradients) on structural stiffness, and (2) to determine the effects of large deflections on stiffness.

In order to accomplish these objectives, general stiffness matrices, including effects of initial internal stresses, are developed in subsequent portions of the paper. In this section it will be assumed that these stiffness matrices can be found. The purpose here will be to show why they are required and how they permit a solution to the actual nonlinear problem of the complex structure to be obtained.

For a typical aeroelastic problem the initial conditions for the structure will be expressed in terms of given distributions of external load and of internal temperature. The first step in solving such a problem is to determine the initial internal forces and the initial deflections. These define the initial equilibrium configuration. Due to the nonlinear character of the problem it is proposed that a step-by-step process or an iterative procedure be used in establishing the equilibrium state.

If structural instability occurs, or if the equilibrium state is not unique, then the remarks at the end of Section (III-2) apply. Here we are interested in well-defined, unique, and stable equilibrium configurations under the given loading and temperature conditions.

Fig. 6 illustrates the step-by-step procedure as applied to the truss of Fig. 1. It is assumed that member 1–2 has been heated to $T = T_1$. We then desire to determine both the deflection u due to an applied load F_x, and the stiffness K corresponding to the equilibrium configuration. For the simple truss having only a single degree of freedom, it would be a simple matter to calculate the required force F_{x_i} for several assumed deflections u_i. Plotting these would give points $A, B, C, \ldots$ of Fig. 6. In this way the specified load level F_x could be reached, at a corresponding deflection u. The required stiffness at D could then be calculated or determined graphically from the curve (slope at D).

An alternative step-by-step process may be used. This is illustrated by the broken line $OA'B' \ldots$ of Fig. 6. Since this process is immediately applicable to complex structures it is of interest to examine it in further detail.

First divide the load range F_x into a number of intervals given by F_{x_1}, F_{x_2}, etc. The initial stiffness K_0 is used to calculate u_1' as follows:

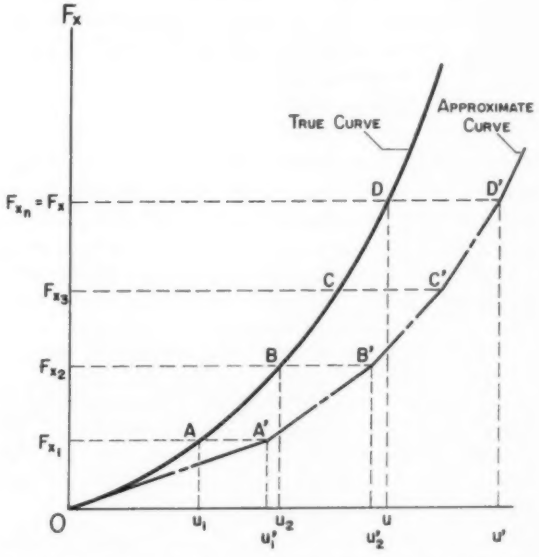

FIG. 6. Truss force-deflection curve; step-by-step approximation.

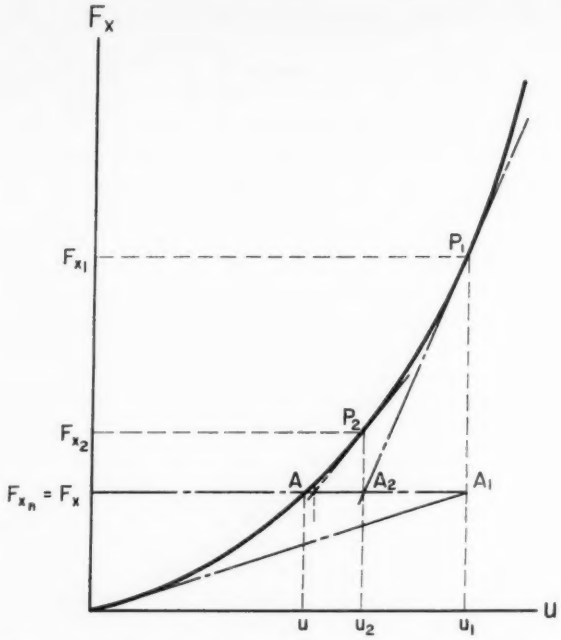

FIG. 7. Truss force-deflection curve; iteration procedure.

$$u_1' = (K_0)^{-1} F_{x_1} \tag{3a}$$

Taking account of the changes in member loads and in the structural geometry we can then calculate a new stiffness K_1. The next increment in deflection is then given by

$$u_2' - u_1' = (K_1)^{-1}(F_{x_2} - F_{x_1}) \tag{3b}$$

or, in general,

$$u'_{n+1} - u_n' = (K_n)^{-1}(F_{x_{n+1}} - F_{x_n}) \tag{3c}$$

The accuracy of this approximation can be increased to any desired level by increasing the number of steps.

In determining the equilibrium configuration of a complex structure the specified loading will be represented by a column matrix,

$$\{F\} = \bar{F}\{f\}$$

where $\{f\}$ is a column of constants specifying the distribution of external loads, while $\bar{F}$ is an intensity factor which may be increased stepwise from zero to the desired level, as in the preceding example of the simple truss. Thus, corresponding to Eq. (3c) we have (replacing u by w),

$$\{w_{n+1} - w_n\} = (F_{n+1} - F_n)[K_n]^{-1}\{f\} \tag{4}$$

The large amount of numerical work which may be involved in this process should not be overlooked. The matrices $[K_n]$ must be calculated and also inverted. However, it is expected that a small number of steps will suffice for many practical problems.

If only a single point on the true force deflection curve is required, plus the stiffness associated with that point, it is possible to use an iterative type solution. The process is illustrated by Fig. 7, again for the problem of the simple truss.

It is desired to determine stiffness K, associated with equilibrium point A, Fig. 7. Using K_0 and load F_{x_1} point A_1 can be established. This fixes displacement u_1. Knowing u_1, the true stiffness K_1 associated with point P_1 can be calculated. Applying load F_x and this stiffness gives point A_2 according to the equation,

$$u_2 = (K_1)^{-1}(F_x - F_{x_1}) + u_1 \tag{5}$$

Repeating the process will lead to convergence at point A. Stiffness calculated for u will be the true stiffness at A. Again it is repeated that difficulties will arise if instability occurs, or if the displacement is not a single valued function of F_x in the interval from $u = 0$ to u_1.

(III) Stringer Stiffness

(1) *Derivation*

A stringer is assumed to carry constant tension or compression. It may be thought of as the simplest load-carrying element appearing in the composite structure. Consequently, it is considered first in investigating the effect of initial stresses on stiffness.

The unloaded unheated stringer appears as L_0 in Fig. 8. After initial strains have developed (which may be due to heating) and consequent internal stresses have arisen (which may be due to inhibiting thermal expansion), the stringer appears as L in Fig. 8. Also node 1 is initially fixed at the origin, while node 2 is left unrestrained.

First, the stringer will be assumed to be heated to T°F. above the room temperature. The unit thermal expansion is then αT, where α = coefficient of thermal expansion (in./in./°F.). After heating has occurred force will be applied to the stringer sufficient to put it

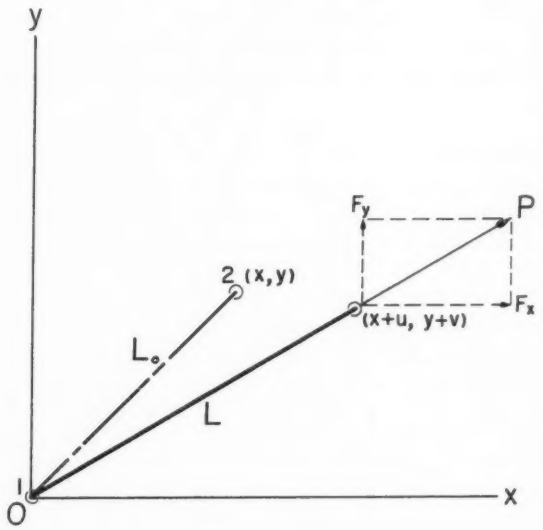

FIG. 8. Stringer.

in the final position, L, Fig. 8. Under this sequence of events the following equations apply:

$$\left.\begin{aligned} L_0 &= \sqrt{x^2 + y^2}, \quad L = \sqrt{(x+u)^2 + (y+v)^2} \\ \epsilon &= (L - L_0)/L_0 \\ \sigma &= E_T(\epsilon - \alpha T) \\ P &= A\sigma = AE_T(\epsilon - \alpha T) \\ F_x &= P\lambda, \quad F_y = P\mu \\ \lambda &= (x+u)/L, \quad \mu = (y+v)/L \end{aligned}\right\} \tag{6}$$

where E_T = modulus of elasticity at temperature, T, and A = cross-sectional area of stringer.

It should be noticed that, in the expression for P, the quantity αT could be replaced by an equivalent term arising from a source other than that of a temperature increase. Also it is seen that P is a nonlinear function of displacement components u and v.

We are now interested in the stiffness of the member with respect to incremental displacements from position L. To obtain the desired relation in linear form it is convenient to expand F_x and F_y in a Taylor's series as follows:

$$F_x(u + \Delta u, v + \Delta v) = F_x(u, v) + \left.\frac{\partial F_x}{\partial u}\right|_{u,\,v} \Delta u + \left.\frac{\partial F_x}{\partial v}\right|_{u,\,v} \Delta v + \ldots \tag{7}$$

A similar expression holds for F_y. By retaining all terms in the first derivatives, the complete expression for the stiffness will result. This is essential as previously pointed out in Section (II).

By using Eqs. (6), the terms on the right-hand side of the above equation can be determined. The result is

$$F_x(u + \Delta u, v + \Delta v) = P\lambda + [(P/L)(1 - \lambda^2) + (AE/L_0)\lambda^2]\Delta u + \{[(AE/L_0) - (P/L)]\lambda\mu\}\Delta v$$

and, similarly,

$$F_y(u + \Delta u, v + \Delta v) = P\mu + \{[(AE/L_0) - (P/L)]\lambda\mu\}\Delta u + [(P/L)(1 - \mu^2) + (AE/L_0)\mu^2]\Delta v$$

Now remove the restriction that node 1 remain at the origin by letting

$$\Delta u = u_2' - u_1', \quad \Delta v = v_2' - v_1'$$

where u_2' is a displacement component of node 2 from L position of the stringer, etc. Also impose equilibrium by requiring

$$F_{x_1} = -F_{x_2}, \quad F_{y_1} = -F_{y_2} \tag{8}$$

Then the equations for force components become

$$F_{x_2} = -F_{x_1} = P\lambda + [(P/L)(1 - \lambda^2) + (AE/L_0)\lambda^2](u_2' - u_1') + \{[(AE/L_0) - (P/L)]\lambda\mu\}(v_2' - v_1') \tag{9a}$$

$$F_{y_2} = -F_{y_1} = P\mu + \{[(AE/L_0) - (P/L)]\lambda\mu\}(u_2' - u_1') + [(P/L)(1 - \mu^2) + (AE/L_0)\mu^2](v_2' - v_1') \tag{9b}$$

These are most conveniently written as a single matrix equation as follows:

$$\begin{Bmatrix} F_{x_1} \\ F_{y_1} \\ F_{x_2} \\ F_{y_2} \end{Bmatrix} = -P\begin{Bmatrix} \lambda \\ \mu \\ -\lambda \\ -\mu \end{Bmatrix} + \frac{AE}{L_0}\begin{bmatrix} \lambda^2 & & \text{(Sym.)} & \\ \lambda\mu & \mu^2 & & \\ -\lambda^2 & -\lambda\mu & \lambda^2 & \\ -\lambda\mu & -\mu^2 & \lambda\mu & \mu^2 \end{bmatrix}\begin{Bmatrix} u_1' \\ v_1' \\ u_2' \\ v_2' \end{Bmatrix} + \frac{P}{L}\begin{bmatrix} 1 - \lambda^2 & & \text{(Sym.)} & \\ -\lambda\mu & 1 - \mu^2 & & \\ -(1 - \lambda^2) & \lambda\mu & 1 - \lambda^2 & \\ \lambda\mu & -(1 - \mu^2) & -\lambda\mu & 1 - \mu^2 \end{bmatrix}\begin{Bmatrix} u_1' \\ b_1' \\ u_2' \\ v_2' \end{Bmatrix} \tag{10}$$

or, in compact form,

$$\{F\} = \{F^1\} + ([K^0] + [K^1])\{\Delta\} \tag{11a}$$

$$= \{F^1\} + [K]\{\Delta\} \tag{11b}$$

Some pertinent facts pertaining to this last equation are now listed.

(a) $\{\Delta\}$ is the column matrix of incremental displacement components $u_1' \ldots$ etc., occurring from position L, in which initial force P is present.

(b) Terms having superscript 1 contain the initial force P.

(c) $[K^0]$ represents the conventional stiffness matrix for the stringer. It initially appeared as K in reference 1, Eq. (6).

(d) $[K^1]$ represents the contribution of initial forces to the stiffness. The sum of $[K^0]$ and $[K^1]$ is called $[K]$. This latter matrix represents the total correct stiffness at instantaneous configuration L and initial loading P.

(e) The generalization of Eq. (10) to three-dimensional space presents no new difficulty and hence need not be considered here.

(2) *Application to Truss*

In order to illustrate the application Eq. (10) the truss of Fig. 1 will be considered for the case in which member 1–2 is heated. It is emphasized that this example is introduced merely to illustrate basic concepts; the numerical results are not intended to have any practical significance.

The calculation is first made from elementary considerations. Assume $P = AE_T\alpha T$ (compression) to be developed in member 1–2 as a result of heating. Then submit node 1 to an arbitrary small displacement Δu. This will result in a component of P acting in the positive x direction of magnitude $AE_T\alpha T \cdot \Delta u/4$. At the same time member 1–3 will be elongated and the component of the tensile force thereby developed is $9AE \cdot \Delta u/125$. When $T = T_{cr}$ these two components are equal, yielding

$$T_{cr} = 36\ E/125\ E_T\alpha \tag{12}$$

The solution can also be found by forming the stiff-

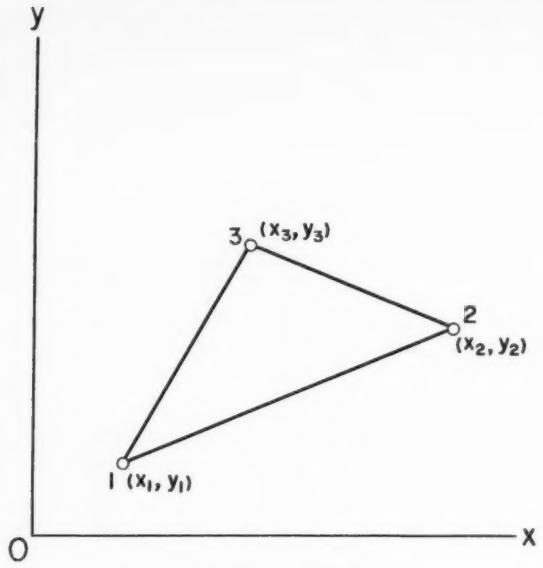

FIG. 9. Typical plate element.

ness matrix for the truss. (See reference 1 for a detailed explanation of this procedure.) Since all node displacements except u_1 are constrained to be zero, application of Eq. (10) to the truss will quickly reduce to the single equation,

$$\begin{aligned} 0 &= -P\lambda + [(AE/L_0)\lambda^2 + (P/L)(1-\lambda^2)]u_1' \\ &= -[(P\lambda)_{1-2} + (P\lambda)_{1-3}] + \\ &\qquad A[(E_T\lambda^2/L_0)_{1-2} + (E\lambda^2/L_0)_{1-3}]u_1' + \\ &\qquad [\{(P/L)(1-\lambda^2)\}_{1-2} + \{(P/L)(1-\lambda^2)\}_{1-3}]u_1' \\ &= -[P\cdot 0 + 0\cdot\lambda] + A[0 + (9/125)E]u_1' + \\ &\qquad [(P/4) + 0]u_1' \end{aligned}$$

Putting $P = -AE_T\alpha T_{cr}$ then leads to the same result as above for T_{cr}.

It is at once apparent that a trial and error type of solution will be required to find T_{cr} from Eq. (12). This is so because E_T is not known until the temperature in the corresponding member is specified.

For a complex structure, it will, of course, be necessary to calculate the eigenvalues of the stiffness matrix $K^0 + K^1$ in order to determine the thermoelastic instability modes. Due to the nonlinear nature of the problem the equilibrium condition may not be unique and instabilities may occur. (This also occurs for the truss of Fig. 1 if displacements in the negative x direction are considered.) In either case, difficulties will be encountered in seeking a solution. Generally, these difficulties can be overcome by carrying out equilibrium solutions at reduced values of load and/or temperature. In such cases a graph of some representative deflection versus load or temperature will show the trend toward instability. Since a general instability within the design envelope of the aircraft is unacceptable, we will mainly be interested in identifying such a state of affairs when it exists. We need not analyze in detail the behavior of the structure in the unstable range.

(3) *Castigliano's Theorem*

In the following section of the paper the plate stiffness matrix is derived by applying Castigliano's theorem. It is helpful to see the corresponding equations for the stringer. If U is defined as

$$U = (E_T/2)\int\int\int (\epsilon - 2\alpha T)\epsilon dv_0 = (E_T/2)AL_0(\epsilon^2 - 2\alpha T\epsilon) \quad (13)$$

where the integration is over the original volume of the undeformed stringer and σ has been taken from Eqs. (6). Then,

$$F_x = \partial U/\partial u = (\partial U/\partial\epsilon)(\partial\epsilon/\partial u) = AE_TL_0(\epsilon - \alpha T)(\partial\epsilon/\partial u)$$

Again using Eqs. (6) it is found that

$$\partial\epsilon/\partial u = \lambda/L_0$$

so that

$$F_x = AE_T(\epsilon - \alpha T)\lambda = P\lambda$$

This is the desired result.

It should be realized that some important thermodynamic questions have been omitted in the above discussion. Further information on these matters may be found in reference 8. For the purposes of the present paper the above procedure is considered adequate.

(IV) Stiffness Matrix for a Plate Element in Plane Stress

The derivation of the stiffness matrix for the plate element is closely parallel in principle to that for the stringer, although considerably more complicated in detail. As in reference 1 we shall employ a plate element of triangular shape as the basic unit for analyzing the behavior of flat panels. The principal reason for this selection is that the triangle provides the most convenient basis for representing polygonal panels, such as general quadrilaterals.

As noted earlier, it is intended to include within the scope of the analysis deformations in which the structural elements are subjected to strains that are small compared to unity; however, rotations are retained that may be large compared to the strains. This is the class of deformations involving "geometrical nonlinearities" as defined by Novozhilov in reference 9, pp. 143–144.

For the time being the triangular element is oriented with its middle surface parallel to the x–y plane, Fig. 9, and it is assumed further that the strain components and the temperature may be considered constant throughout an individual triangular element. In order to utilize the fundamental theory from reference 9 for the analysis of the heated structure, we shall imagine that the elements of the structure are first disconnected and allowed to expand freely during the heating process; temperatures are then held constant during the remainder of the analysis (permitting the use of constant elastic moduli). The elements are then forced back to their original shapes and reconnected to ad-

jacent elements; the structure is held momentarily in its original configuration by suitable constraints. Subsequent steps in the analysis consist in the determination of deflections resulting from the removal of constraints and application of external loads. For purposes of analysis the deformation will be subdivided into a series of steps, such that the rotations and the *changes* in displacement that occur in an element during any one step are small compared to unity. However, we must still admit the possibility that rotations may be large compared to strains.

For convenience, displacements are referred to the original configuration of the plate *before heating*; coordinates of a typical point in the middle surface of the plate are (x, y) and the displacement components are $u(x, y)$, $v(x, y)$, $w(x, y)$. Strain components are given by (cf. reference 9, Eqs. (I.22), p. 13, and (I.117), p. 52)

$$\left.\begin{aligned} \epsilon_{xx} &= e_{xx} + (1/2)(\omega_y^2 + \omega_z^2) + \\ &\qquad (1/2)(e_{xy}\omega_z - e_{xz}\omega_y) \\ \epsilon_{yy} &= e_{yy} + (1/2)(\omega_x^2 + \omega_z^2) + \\ &\qquad (1/2)(e_{yz}\omega_x - e_{xy}\omega_z) \\ \epsilon_{xy} &= e_{xy} - \omega_x\omega_y + (1/2)(e_{xz}\omega_x - e_{yz}\omega_y) + \\ &\qquad \omega_z(e_{yy} - e_{xx}) \end{aligned}\right\} \tag{14}$$

where

$$\left.\begin{aligned} e_{xx} &= \partial u/\partial x, \quad e_{yy} = \partial v/\partial y, \\ &\qquad e_{xy} = (\partial v/\partial x) + (\partial u/\partial y) \\ \omega_x &= (1/2)[(\partial w/\partial y) - (\partial v/\partial z)], \\ &\qquad \omega_y = (1/2)[(\partial u/\partial z) - (\partial w/\partial x)], \\ &\qquad \omega_z = (1/2)[(\partial v/\partial x) - (\partial u/\partial y)] \end{aligned}\right\} \tag{15}$$

in which

$$\partial u/\partial z \backsimeq \partial w/\partial x, \quad \partial v/\partial z = -(\partial w/\partial y)$$

The stress-strain relations and the strain energy for the heated plate will be expressed first in terms of displacements *from the heated stress-free state*. Coordinates of the typical point in the heated stress-free state are denoted by $(\bar{x}, \bar{y})$ and the displacements from that state are $\bar{u}$, $\bar{v}$, $\bar{w}$. The following relations then apply:

$$\left.\begin{aligned} \bar{x} &= x(1 + \alpha T), \quad \bar{y} = y(1 + \alpha T), \\ \bar{z} &= z(1 + \alpha T), \quad \bar{u} = u - \alpha T x, \\ \bar{v} &= v - \alpha T y, \quad \bar{w} = w - \alpha T z \end{aligned}\right\} \tag{16}$$

The strains $\bar{\epsilon}_{xx}$, $\bar{\epsilon}_{yy}$, and $\bar{\epsilon}_{xy}$ referred to the heated stress-free state are given by Eqs. (14). For example, the first of these is given by

$$\bar{\epsilon}_{xx} = \bar{e}_{xx} + (1/2)(\bar{\omega}_y^2 + \bar{\omega}_z^2) + (1/2)(\bar{e}_{xy}\bar{\omega}_z - \bar{e}_{xz}\bar{\omega}_y) \tag{17}$$

and similarly for the other two strain components. The terms in the above equation are found by substituting Eqs. (16) into Eqs. (15). For example,

$$\bar{e}_{xx} = \partial\bar{u}/\partial x = (\partial\bar{u}/\partial x)(\partial x/\partial\bar{x}) = [(\partial u/\partial x) - \alpha T][1/(1 + \alpha T)]$$

and since $\alpha T \ll 1$ and $\partial u/\partial x = e_{xx}$ this becomes

$$\bar{e}_{xx} = e_{xx} - \alpha T \tag{18a}$$

Similarly,

$$\bar{e}_{yy} = e_{yy} - \alpha T \tag{18b}$$

The remaining terms in Eq. (17) will be found to be unaffected by temperature and, therefore, by the transformation represented by Eqs. (16). As a result,

$$\bar{\epsilon}_{xx} = \epsilon_{xx} - \alpha T \tag{19}$$

and similarly for $\bar{\epsilon}_{yy}$. Other terms are unaffected.

The stresses satisfy the usual Hooke's Law relation,

$$\begin{Bmatrix} \sigma_{xx} \\ \sigma_{yy} \\ \sigma_{xy} \end{Bmatrix} = \frac{E_T}{1 - \nu^2} \begin{bmatrix} 1 & \nu & 0 \\ \nu & 1 & 0 \\ 0 & 0 & \lambda_1 \end{bmatrix} \begin{Bmatrix} \bar{\epsilon}_{xx} \\ \bar{\epsilon}_{yy} \\ \bar{\epsilon}_{xy} \end{Bmatrix} \tag{20}$$

where $\lambda_1 = (1 - \nu)/2$. However, as a consequence of Eqs. (17), the above equation may be rewritten as

$$\begin{Bmatrix} \sigma_{xx} \\ \sigma_{yy} \\ \sigma_{xy} \end{Bmatrix} = \frac{E_T}{1 - \nu^2} \begin{bmatrix} 1 & \nu & 0 \\ \nu & 1 & 0 \\ 0 & 0 & \lambda_1 \end{bmatrix} \begin{Bmatrix} \epsilon_{xx} \\ \epsilon_{yy} \\ \epsilon_{xy} \end{Bmatrix} - \frac{E_T\alpha T}{1 - \nu} \begin{Bmatrix} 1 \\ 1 \\ 0 \end{Bmatrix} \tag{21}$$

The strain energy for the heated plate is expressed as

$$U = (1/2)\int\int\int (\sigma_{xx}\bar{\epsilon}_{xx} + \sigma_{yy}\bar{\epsilon}_{yy} + \sigma_{xy}\bar{\epsilon}_{xy})dx\,dy\,dz \tag{22}$$

Carrying out the integration over the volume of the unheated and unstrained plate and replacing $\bar{\epsilon}_{xx}$ by Eq. (19), etc., there results

$$\begin{aligned} U &= (1/2)At[\sigma_{xx}\epsilon_{xx} + \sigma_{yy}\epsilon_{yy} + \sigma_{xy}\epsilon_{xy} - \alpha T(\sigma_{xx} + \sigma_{yy})] \\ &= \frac{AE_Tt}{2(1 - \nu^2)} [\epsilon_{xx}\ \epsilon_{yy}\ \epsilon_{xy}] \begin{bmatrix} 1 & \nu & 0 \\ \nu & 1 & 0 \\ 0 & 0 & \lambda_1 \end{bmatrix} \begin{Bmatrix} \epsilon_{xx} \\ \epsilon_{yy} \\ \epsilon_{xy} \end{Bmatrix} - \\ &\qquad \frac{AE_T\alpha Tt}{1 - \nu} (\epsilon_{xx} + \epsilon_{yy}) + F(T) \end{aligned} \tag{23}$$

where A is the corresponding plate area and t the plate thickness.

At the beginning of a typical intermediate step in the deformation process a typical plate element is in a state of initial strain with strain components ϵ^0_{xx}, ϵ^0_{yy}, ϵ^0_{xy}. Our present task is to derive general formulas for the changes in the components (with respect to fixed axes) of the node forces resulting from small additional displacements. In this development the total strain with respect to the undeformed state will be required. Therefore, we note first that the plate with small initial strains can be derived from a fictitious nearby configuration with zero strains by means of a linear transformation involving no rotations. To show this set

$$\omega_x^0 = \omega_y^0 = \omega_z^0 = 0 \tag{24}$$

in (14) with the result that

$$\begin{bmatrix} \epsilon^0_{xx} \\ \epsilon^0_{yy} \\ \epsilon^0_{xy} \end{bmatrix} = \begin{bmatrix} e^0_{xx} \\ e^0_{yy} \\ e^0_{xy} \end{bmatrix} = \begin{bmatrix} (\partial u^0/\partial x) \\ (\partial v^0/\partial y) \\ [(\partial v^0/\partial x) + (\partial u^0/\partial y)] \end{bmatrix} \tag{25}$$

The coordinates of a typical point in the middle surface of the *strained* element are now denoted by (x, y); the corresponding point of the unstrained element is (x^0, y^0) where

$$x = x^0 + u^0(x^0, y^0), \quad y = y^0 + v^0(x^0, y^0)$$

Expressions for u^0, v^0 in terms of the initial strains can be derived by integration of Eqs. (25) and imposing conditions of Eqs. (24); the resulting formulas are not presented explicitly however, since they will not be required in further developments. Since the strains are given by linear theory we shall not make any distinction between differentiation or integration with respect to x, y and the corresponding operations with respect to x^0, y^0. In fact, subsequent displacements will be regarded as functions of x, y, rather than x^0, y^0.

Additional displacements u', v', w' are now introduced so that total displacements from the hypothetical unstrained state become

$$u = u^0 + u', \quad v = v^0 + v', \quad w = w' \tag{26}$$

If it is assumed that additional strains and rotations are small compared to unity, but not necessarily of the same order of magnitude, then terms $e_{xy}'\omega_z'$, $e_{xx}'\omega_z'$, etc., may be neglected by comparison with the remaining terms, and the total strains are

$$\left.\begin{aligned} \epsilon_{xx} &= e^0{}_{xx} + e_{xx}' + (1/2)[(\omega_y')^2 + (\omega_z')^2] + (1/2)e^0{}_{xy}\omega_z', \\ \epsilon_{yy} &= \epsilon^0{}_{yy} + e_{yy}' + (1/2)[(\omega_x')^2 + (\omega_z')^2] - (1/2)e^0{}_{xy}\omega_z', \\ \epsilon_{xy} &= e^0{}_{xy} + e_{xy}' - \omega_x'\omega_y' + (e^0{}_{yy} - e^0{}_{xx})\omega_z' \end{aligned}\right\} \tag{27}$$

Recall that prior to the deflections u', v', w' the plate is situated with the middle surface in the x–y plane. We consider a triangular element, Fig. 9, with node points at (x_1, y_1), (x_2, y_2), (x_3, y_3). We assume that for small additional displacements u', v', w', it is sufficiently accurate to take

$$\left.\begin{aligned} u' &= a'x + b'y + c' \\ v' &= d'x + e'y + f' \\ w' &= g'x + h'y + k' \end{aligned}\right\} \tag{28}$$

where a', b', c', d', e', f', g', h', k' are constants which can be expressed in terms of the nodal displacements:

$$\left.\begin{aligned} u_1' &= a'x_1 + b'y_1 + c' \\ v_1' &= d'x_1 + e'y_1 + f' \\ w_1' &= g'x_1 + h'y_1 + k' \\ &\text{etc.} \end{aligned}\right\} \tag{29}$$

Therefore,

$$\begin{bmatrix} a' \\ b' \\ d' \\ e' \\ g' \\ h' \end{bmatrix} = \frac{1}{D} \begin{bmatrix} y_{31} & y_{12} & 0 & 0 & 0 & 0 \\ -x_{31} & -x_{12} & 0 & 0 & 0 & 0 \\ 0 & 0 & y_{31} & y_{12} & 0 & 0 \\ 0 & 0 & -x_{31} & -x_{12} & 0 & 0 \\ 0 & 0 & 0 & 0 & y_{31} & y_{12} \\ 0 & 0 & 0 & 0 & -x_{31} & -x_{12} \end{bmatrix} \begin{bmatrix} u_{21}' \\ u_{31}' \\ v_{21}' \\ v_{31}' \\ w_{21}' \\ w_{31}' \end{bmatrix} \tag{30}$$

where $u_{21}' = u_2' - u_1', \quad x_{21} = x_2 - x_1, \quad y_{21} = y_2 - y_1, \quad \text{etc.}$

and $D = x_{21}y_{31} - x_{31}y_{21} = 2A$

From Eqs. (14), (28), and (30),

$$\begin{bmatrix} e_{xx}' \\ e_{yy}' \\ e_{xy}' \\ 2\omega_x' \\ 2\omega_y' \\ 2\omega_z' \end{bmatrix} = \frac{1}{2A} \begin{bmatrix} y_{23} & y_{31} & y_{12} & 0 & 0 & 0 & 0 & 0 & 0 \\ 0 & 0 & 0 & -x_{23} & -x_{31} & -x_{12} & 0 & 0 & 0 \\ -x_{23} & -x_{31} & -x_{12} & y_{23} & y_{31} & y_{12} & 0 & 0 & 0 \\ 0 & 0 & 0 & 0 & 0 & 0 & -x_{24} & -x_{31} & -x_{12} \\ 0 & 0 & 0 & 0 & 0 & 0 & -y_{23} & -y_{31} & -y_{12} \\ x_{23} & x_{31} & x_{12} & y_{23} & y_{31} & y_{12} & 0 & 0 & 0 \end{bmatrix} \begin{bmatrix} u_1' \\ u_2' \\ u_3' \\ v_1' \\ v_2' \\ v_3' \\ w_1' \\ w_2' \\ w_3' \end{bmatrix} \tag{31}$$

Eqs. (31) and (27) express the strain in terms of the initial strains $\epsilon^0{}_{xx}$, $\epsilon^0{}_{yy}$, $\epsilon^0{}_{xy}$ and the node displacement u_1, v_1, w_1, etc. The corresponding node forces may be found from

$$Fx_i = \partial U/\partial u_i', \quad F_{yi} = \partial U/\partial v_i', \quad Fz_i = \partial U/\partial w_i', \quad i = 1, 2, 3 \tag{32}$$

where U is given by Eq. (23) with $F(T)$ omitted since it does not contribute to the forces as found from Eqs. (32).

Letting

$$\begin{bmatrix} 1 & \nu & 0 \\ \nu & 1 & 0 \\ 0 & 0 & \lambda_1 \end{bmatrix} = [B] \tag{33}$$

then substituting from Eq. (27) into Eq. (23) gives

$$U = \frac{AE_T t}{2(1-\nu^2)}\Bigg([e^0_{xx}, e^0_{yy}, e^0_{xy}][B]\begin{Bmatrix} e^0_{xx} \\ e^0_{yy} \\ e^0_{xy} \end{Bmatrix} + 2[e^0_{xx}, e^0_{yy}, e^0_{xy}][B]\begin{Bmatrix} e_{xx}' \\ e_{yy}' \\ e_{xy}' \end{Bmatrix} + 2\omega_z'[e^0_{xx}, e^0_{yy}, e^0_{xy}][B]\begin{Bmatrix} e^0_{xy}/2 \\ -e^0_{xy}/2 \\ e^0_{yy} - e^0_{xx} \end{Bmatrix} +$$

$$(\omega_z')^2[e^0_{xx}, e^0_{yy}, e^0_{xy}][B]\begin{Bmatrix} 1 \\ 1 \\ 0 \end{Bmatrix} + 2[e^0_{xx}, e^0_{yy}, e^0_{xy}][B]\begin{Bmatrix} (\omega_y')^2/2 \\ (\omega_x')^2/2 \\ -\omega_x'\omega_y' \end{Bmatrix} + [e_{xx}', e_{yy}', e_{xy}'][B]\begin{Bmatrix} e_{xx}' \\ e_{yy}' \\ e_{xy}' \end{Bmatrix} +$$

$$2\omega_z'[e_{xx}', e_{yy}', e_{xy}'][B]\begin{Bmatrix} e^0_{xy}/2 \\ -e^0_{xy}/2 \\ e^0_{yy} - e^0_{xx} \end{Bmatrix} + 2(\omega_z')^2[e_{xx}', e_{yy}', e_{xy}'][B]\begin{Bmatrix} 1 \\ 1 \\ 0 \end{Bmatrix} + 2[e_{xx}', e_{yy}', e_{xy}'][B]\begin{Bmatrix} (\omega_y')^2/2 \\ (\omega_x')^2/2 \\ -\omega_x'\omega_y' \end{Bmatrix} +$$

$$(\omega_z')^2[e^0_{xy}/2, e^0_{xy}/2, e^0_{yy} - e^0_{xx}][B]\begin{Bmatrix} e^0_{xy}/2 \\ -e^0_{xy}/2 \\ -e^0_{yy} - e^0_{xx} \end{Bmatrix} + 2(\omega_z')^2[e^0_{xy}/2, -e^0_{xy}/2, e^0_{yy} - e^0_{xx}][B]\begin{Bmatrix} 1 \\ 1 \\ 0 \end{Bmatrix} +$$

$$2\omega_z'[e^0_{xy}/2, -e^0_{xy}/2, e^0_{yy} - e^0_{xx}][B]\begin{Bmatrix} (\omega_y')^2/2 \\ (\omega_x')^2/2 \\ -\omega_x'\omega_y' \end{Bmatrix} + 2(1+\nu)(\omega_z')^4 +$$

$$2(\omega_z')^2[1+\nu, 1+\nu, 0]\begin{Bmatrix} (\omega_y')^2/2 \\ (\omega_x')^2/2 \\ -\omega_x'\omega_y' \end{Bmatrix} + [(\omega_y')^2/2, (\omega_x')^2/2, -\omega_x'\omega_y'][B]\begin{Bmatrix} (\omega_y')^2/2 \\ (\omega_x')^2/2 \\ -\omega_x'\omega_y' \end{Bmatrix}\Bigg) -$$

$$[AE_T\alpha t/(1-\nu)]\{e^0_{xx} + e^0_{yy} + e_{xx}' + e_{yy}' + (\omega_z')^2 + (\omega_x')^2/2 + (\omega_y')^2/2\} \quad (34)$$

In this last equation the third and tenth matrix multiplications yield only squares in the initial strains ($e^0_{xx}, \ldots$, etc.) They consequently can be neglected compared to the remaining terms.

Substituting Eq. (34) into Eq. (32) and retaining only those terms which are linear in the displacements,

$$\begin{Bmatrix} F_x \\ F_y \\ F_z \end{Bmatrix} = \frac{E_T t}{2(1-\nu^2)}\begin{bmatrix} \mathbf{Y} & \mathbf{0} & -\mathbf{X} \\ \mathbf{0} & -\mathbf{X} & \mathbf{Y} \\ \mathbf{0} & \mathbf{0} & \mathbf{0} \end{bmatrix}\begin{Bmatrix} e^0_{xx} + \nu e^0_{yy} \\ e^0_{yy} + \nu e^0_{xx} \\ \lambda_1 e^0_{xy} \end{Bmatrix} + \frac{E_T t}{4A(1-\nu^2)}\begin{bmatrix} \mathbf{Y} & \mathbf{0} & -\mathbf{X} \\ \mathbf{0} & -\mathbf{X} & \mathbf{Y} \\ \mathbf{0} & \mathbf{0} & \mathbf{0} \end{bmatrix}\begin{bmatrix} \mathbf{Y}' & -\nu\mathbf{X}' & \mathbf{0}' \\ \nu\mathbf{Y}' & -\mathbf{X}' & \mathbf{0}' \\ -\lambda_1\mathbf{X}' & \lambda_1\mathbf{Y}' & \mathbf{0}' \end{bmatrix}\begin{Bmatrix} u \\ v \\ w \end{Bmatrix} +$$

$$\frac{E_T t(e^0_{xx} + e^0_{yy})}{16A(1-\nu)}\begin{Bmatrix} \mathbf{X} \\ \mathbf{Y} \\ \mathbf{0} \end{Bmatrix}[\mathbf{X}', \mathbf{Y}', \mathbf{0}']\begin{Bmatrix} u' \\ v' \\ w' \end{Bmatrix} + \frac{E_T t e^0_{xy}}{16A(1+\nu)}\left(\begin{Bmatrix} \mathbf{X} \\ \mathbf{Y} \\ \mathbf{0} \end{Bmatrix}[\mathbf{Y}', \mathbf{X}', \mathbf{0}'] + \begin{Bmatrix} \mathbf{Y} \\ \mathbf{X} \\ \mathbf{0} \end{Bmatrix}[\mathbf{X}', \mathbf{Y}', \mathbf{0}']\right)\begin{Bmatrix} u' \\ v' \\ w' \end{Bmatrix} +$$

$$\frac{E_T t(e^0_{yy} - e^0_{xx})}{16A(1+\nu)}\left(\begin{Bmatrix} \mathbf{X} \\ \mathbf{Y} \\ \mathbf{0} \end{Bmatrix}[-\mathbf{X}', \mathbf{Y}', \mathbf{0}'] + \begin{Bmatrix} -\mathbf{X} \\ \mathbf{Y} \\ \mathbf{0} \end{Bmatrix}[\mathbf{X}', \mathbf{Y}', \mathbf{0}']\right)\begin{Bmatrix} u' \\ v' \\ w' \end{Bmatrix} + \frac{E_T t(e^0_{xx} + \nu e^0_{yy})}{4A(1-\nu^2)}\begin{Bmatrix} \mathbf{0} \\ \mathbf{0} \\ -\mathbf{Y} \end{Bmatrix}[\mathbf{0}', \mathbf{0}', -\mathbf{Y}']\begin{Bmatrix} u' \\ v' \\ w' \end{Bmatrix} +$$

$$\frac{E_T t(e^0_{yy} + \nu e^0_{xx})}{4A(1-\nu^2)}\begin{Bmatrix} \mathbf{0} \\ \mathbf{0} \\ -\mathbf{X} \end{Bmatrix}[\mathbf{0}', \mathbf{0}', -\mathbf{X}']\begin{Bmatrix} u' \\ v' \\ w' \end{Bmatrix} - \frac{E_T t e^0_{xy}}{8A(1+\nu)}\left(\begin{Bmatrix} \mathbf{0} \\ \mathbf{0} \\ -\mathbf{Y} \end{Bmatrix}[\mathbf{0}', \mathbf{0}', -\mathbf{X}'] + \begin{Bmatrix} \mathbf{0} \\ \mathbf{0} \\ -\mathbf{X} \end{Bmatrix}[\mathbf{0}', \mathbf{0}', -\mathbf{Y}']\right)\begin{Bmatrix} u' \\ v' \\ w' \end{Bmatrix} -$$

$$\frac{E_T\alpha T}{2(1-\nu)}\begin{Bmatrix} \mathbf{Y} \\ -\mathbf{X} \\ \mathbf{0} \end{Bmatrix} - \frac{E_T\alpha T}{8A(1-\nu)}\left(\begin{Bmatrix} \mathbf{X} \\ \mathbf{Y} \\ \mathbf{0} \end{Bmatrix}[\mathbf{X}', \mathbf{Y}', \mathbf{0}'] + 2\begin{Bmatrix} \mathbf{0} \\ \mathbf{0} \\ -\mathbf{X} \end{Bmatrix}[\mathbf{0}', \mathbf{0}', -\mathbf{X}'] + 2\begin{Bmatrix} \mathbf{0} \\ \mathbf{0} \\ \mathbf{Y} \end{Bmatrix}[\mathbf{0}', \mathbf{0}', -\mathbf{Y}']\right)\begin{Bmatrix} u' \\ v' \\ w' \end{Bmatrix} \quad (35)$$

in which

$$\mathbf{X} = \begin{Bmatrix} x_{23} \\ x_{31} \\ x_{12} \end{Bmatrix}, \quad \mathbf{Y} = \begin{Bmatrix} y_{23} \\ y_{31} \\ y_{12} \end{Bmatrix}, \quad \mathbf{0} = \begin{Bmatrix} 0 \\ 0 \\ 0 \end{Bmatrix} \quad (36)$$

and primes indicate the transpose of a matrix.

A partial check on the previous assumptions and lengthy calculations occurs in that the last equation may finally be expressed in the form,

$$\begin{Bmatrix} F_{x_1} \\ F_{x_2} \\ F_{x_3} \\ F_{y_1} \\ F_{y_2} \\ F_{y_3} \\ F_{z_1} \\ F_{z_2} \\ F_{z_3} \end{Bmatrix} = \{F^0\} + ([K^0] + [K^1])\begin{Bmatrix} u_1' \\ u_2' \\ u_3' \\ v_1' \\ v_2' \\ v_3' \\ w_1' \\ w_2' \\ w_3' \end{Bmatrix} \quad (37)$$

where

$$\{F^0\} = \frac{t}{2}\begin{bmatrix} \mathbf{Y} & \mathbf{0} & -\mathbf{X} \\ \mathbf{0} & -\mathbf{X} & \mathbf{Y} \\ \mathbf{0} & \mathbf{0} & \mathbf{0} \end{bmatrix} \begin{Bmatrix} \sigma^0_{xx} \\ \sigma^0_{yy} \\ \sigma^0_{xy} \end{Bmatrix} \tag{38}$$

$$[K^0] = \frac{E_T t}{4A(1-\nu^2)} \begin{bmatrix} \mathbf{S} + \lambda_1\mathbf{Q} & (\text{Sym.}) & \\ -\nu\mathbf{R} - \lambda_1\mathbf{R}' & \mathbf{Q} + \lambda_1\mathbf{S} & \\ \mathbf{0}_3 & \mathbf{0}_3 & \mathbf{0}_3 \end{bmatrix} \tag{39}$$

$$[K^1] = \frac{t\sigma^0_{xx}}{16A}\begin{bmatrix} 3\mathbf{Q} & (\text{Sym.}) & \\ \mathbf{R}' & -\mathbf{S} & \\ \mathbf{0}_3 & \mathbf{0}_3 & 4\mathbf{S} \end{bmatrix} + \frac{t\sigma^0_{yy}}{16A}\begin{bmatrix} -\mathbf{Q} & (\text{Sym.}) & \\ \mathbf{R}' & 3\mathbf{S} & \\ \mathbf{0}_3 & \mathbf{0}_3 & 4\mathbf{Q} \end{bmatrix} + \frac{t\sigma^0_{xy}}{8A}\begin{bmatrix} \mathbf{R} + \mathbf{R}' & (\text{Sym.}) & \\ \mathbf{Q} + \mathbf{S} & \mathbf{R} + \mathbf{R}' & \\ \mathbf{0}_3 & \mathbf{0}_3 & -2(\mathbf{R} + \mathbf{R}') \end{bmatrix} \tag{40}$$

and

$$\mathbf{Q} = \mathbf{X}\mathbf{X}', \quad \mathbf{R} = \mathbf{X}\mathbf{Y}', \quad \mathbf{S} = \mathbf{Y}\mathbf{Y}' \tag{41}$$

$$\mathbf{0}_3 = \begin{bmatrix} 0 & 0 & 0 \\ 0 & 0 & 0 \\ 0 & 0 & 0 \end{bmatrix} \tag{42}$$

Also σ^0_{xx}, σ^0_{yy}, and σ^0_{xy} are the initial stresses given by Eq. (21) as follows:

$$\begin{Bmatrix} \sigma^0_{xx} \\ \sigma^0_{yy} \\ \sigma^0_{xy} \end{Bmatrix} = \frac{E_T}{1-\nu^2}\begin{bmatrix} 1 & \nu & 0 \\ \nu & 1 & 0 \\ 0 & 0 & \lambda_1 \end{bmatrix} \begin{Bmatrix} \epsilon^0_{xx} \\ \epsilon^0_{yy} \\ \epsilon^0_{xy} \end{Bmatrix} - \frac{E_T\alpha T}{1-\nu}\begin{Bmatrix} 1 \\ 1 \\ 0 \end{Bmatrix} \tag{43}$$

It can now be observed that $[K^0]$ agrees with Eq. (B-3) of Reference 1 and $[K^1]$ is proportional to the initial stresses as in the case of the stringer (see Eq. 10).

(V) Concluding Remarks

It is believed that sufficient basic material has been presented here and in references 1 and 3 for carrying out the deflection analysis of complex composite structures. Such structures may, for example, consist of an assemblage of beams, ribs, trusses, and flat, or nearly flat, cover sheets carrying plane stresses (with or without directional stiffeners).

Although the stiffness matrix as presented for the triangular plate element assumes a special orientation in which the element is parallel to the x–y plane, a simple coordinate transformation can be introduced to derive the corresponding matrix form for the arbitrarily oriented element.

Also it is noted that a shell element with single curvature (portion of a developable, cylindrical, or conical shell) can be approximated by a series of flat plate elements. This makes it possible to use the results presented here, and in the preceding papers (references 1 and 3), for the analysis of elongated, slender bodies. Work is in progress to determine whether this is a satisfactory procedure, or if it might be preferable (because of a possible reduction in the number of required elements) to use matrix stiffness expressions which have been derived explicitly for shell elements possessing single curvature.

Also, some comment appears to be in order as to the probable importance of the bending stiffness of the cover plate elements. This has been omitted in the published results. Actually it is a relatively straightforward task to derive stiffness matrices for shell or plate elements subjected to simple modes of bending. These can then be introduced into the analysis of the composite structure. However, in the majority of practical wing structures it is believed that these contributions will prove to be negligible, relative to the wing stiffness as a whole. Of course, a plate type analysis would be recommended for solid or sandwich wing structures having full depth core. However, even for these types it has been found that direct calculation of the stiffness matrix is a practical procedure; in fact, in such cases the basic "building block" in the analysis is the stiffness matrix for the quadrilateral plate element.

It will be evident to the reader that inelastic effects and buckling instabilities of individual structural elements have been neglected in the foregoing developments. In principle, it would be possible to carry out a step-by-step or iterative analysis of a complex structure in which the load-deflection characteristics of individual elements are represented by nonlinear functions. However, the increase in computational labor would be considerable. In fact, the required functions would not even be single-valued in general since the sequential order is significant in applying large deformations.

In performing this work the authors have been particularly interested in applications to problems in structural dynamics—flutter, transient response to fluctuating loads, and dynamic load analysis. It is believed that the methods of elastic analysis presented in this paper will be useful for the solution of a large class of practical problems. These are of the type wherein it is necessary to analyze small amplitude vibrations of a structure containing initial thermally induced stresses plus a system of external loads.

References

[1] Turner, M. J., Clough, R. W., Martin, H. C., and Topp, L. J., *Stiffness and Deflection Analysis of Complex Structures*, Journal of the Aeronautical Sciences, Vol. 23, No. 9, pp. 805–823, 854, September, 1956.

[2] Levy, S., *Structural Analysis and Influence Coefficients for Delta Wings*, Journal of the Aeronautical Sciences, Vol. 20, No. 7, pp. 449–454, July, 1953.

(*Continued on page 127*)

Application of Power Spectral Methods in Airplane and Missile Design

KENNETH R. THORSON* AND QUENTIN R. BOHNE**

Boeing Airplane Company

Summary

This paper illustrates some applications of power-spectral methods in the determination of dynamic loadings and response for both airplanes and missiles subject to continuous turbulence. Input-transfer-function-output relationships are discussed and a procedure outlined whereby mission design load information may be obtained utilizing high-speed digital computing equipment. Where time rate of change of the atmospheric and aerodynamic characteristics is significant, a continuous analog simulation is suggested. Applications of these techniques to specific problem areas are shown. These include determination of design fin load for a representative high-performance airplane, an evaluation of crew station accelerations for low-level high-speed operation, and missile gust loads in a terminal dive condition.

Symbols

Ω	= spatial frequency, rad./ft.
$\Phi_0(\Omega)$	= output power spectrum, (load)²/(rad./ft.)
$T(i\Omega)$	= load frequency response function
$\Phi_I(\Omega)$	= input power spectrum, (ft./sec.)²/(rad./ft.)
σ_0	= root mean square load output
$N(\xi)$	= expected number of exceedances of a given load per foot of flight
N_0	= expected number of crossings of the zero load reference axis with positive slope per foot of flight
ξ	= load
σ_u	= root mean square gust velocity
$\Phi_{IN}(\Omega)$	= normalized input power spectrum
A^2	= integrated output power spectrum
$F(\sigma_{u_j})$	= fraction of total flight distance spent in turbulence with a root mean square level σ_{u_j}
$f(\sigma_u)$	= probability density function of σ_u
q	= generalized coordinate
q'	= first derivative of q with respect to τ
q''	= second derivative of q with respect to τ
$[M_1]$	= generalized inertia coefficient matrix
$[M_2]$	= coefficient matrix of damping terms not convoluted with unsteady lift
$[M_3]$	= structural stiffness coefficient matrix
$[M_4]$	= aerodynamic damping coefficient matrix
$[M_5]$	= aerodynamic stiffness coefficient matrix
$\{C_1\}$	= gust force coefficient matrix
V_g	= true gust velocity
$[A]$	= inertia load coefficient matrix
$[B]$, $[C]$, $[D]$	= coefficient matrices of aerodynamic loads due to the response
$\{E\}$	= gust load coefficient matrix
$*$	= symbol denoting convolution
$K(\tau)$	= Wagner unsteady lift function
$\psi(\tau)$	= Kussner unsteady lift function
τ	= aerodynamic time ($\tau = Vt/b$)
V	= true airspeed
t	= time, sec.
b	= semichord
ω	= reduced frequency, rad./semichords traveled
f	= frequency, rad./sec.
L	= scale length of turbulence
$R(\xi)$	= distance ratio: miles of flight per exceedance of ξ divided by miles of flight by Stratocruiser per exceedance of its limit load
D	= distance flown, ft.
Δn	= incremental load factor
$N_i(\Delta n)$	= number of exceedances of Δn in the ith altitude band
$N_i(\Delta n \mid \sigma_u)$	= number of exceedances of Δn in the ith altitude band for a given value of σ_u

Presented at the Meteorology Session, IAS 27th Annual Meeting, N.Y., Jan. 26-29, 1959. Revised and received June 3, 1959.

* Unit Chief, Dynamic Loads Unit.

** Research Engineer.

Appreciation is acknowledged to Bruce Clingan and Stanley Nanevicz in the preparation of this paper.

Introduction

IN THE PAST, existing gust load design criteria have proved adequate for those airplanes which have been designed by gust requirements. These design criteria are based on a load transfer concept. The maximum gust loads were measured on one family of airplanes, and, through use of a simplified gust load transfer function, a discrete design gust of a specified shape and magnitude was selected. For a new configuration the inverse process was used to determine the load for this design gust. If the new configuration was essentially similar to those on which the loads were measured, it could be expected that the gust load formula would satisfactorily predict the maximum gust load experience of the new configuration.

Present and future airplane and missile configurations may differ markedly from those on which the loads were measured, thus invalidating the existing semiempirical gust design criteria. Consequently, additional, more comprehensive design requirements and analysis techniques have been developed to meet the needs of these advanced configurations. It is the purpose of this paper to illustrate some applications of the newest of these techniques in the prediction of design gust loads—namely, the power spectral method. For background purposes earlier methods of gust load prediction will first be reviewed briefly.

Gust Load Formula

A number of gust load transfer functions have been used. Perhaps the most widely accepted formula was

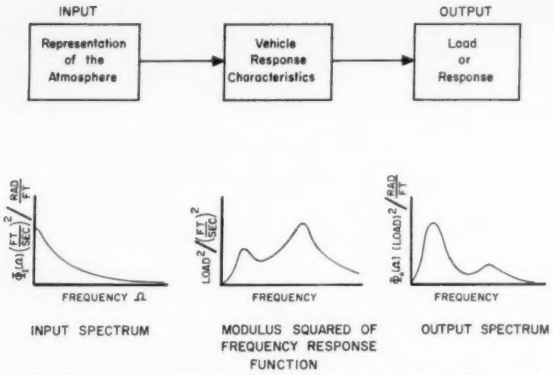

FIG. 1. Basic power spectral output to input relationship showing a typical input power spectrum, amplitude squared of the frequency response function, and output power spectrum.

given by Pratt,[1] which was essentially a formula for finding airplane vertical acceleration by dividing the lift due to the gust by the airplane mass. An alleviation factor was used to account for gradual build-up of lift, gust gradient, and alleviation due to the rising of the airplane with the gust. The assumptions upon which this simple mass-parameter gust load formula was based are:

(1) The airplane is rigid.
(2) The airplane is free to rise but not pitch.
(3) The airplane penetrates a discrete gust of (1−cos) shape and length equal to 25 wing chords.
(4) The gust is distributed uniformly across the span.

Dynamic Gust Analysis

With the advent of low load factor airplanes which were large and flexible, but still of a more or less conventional type, it became necessary to consider the influence of structural response to dynamic loading and the assumptions associated with the gust load formula. In particular, those specifying a rigid airplane and negligible pitch response were no longer valid. The simple gust load formula was replaced by a set of simultaneous integro-differential equations, the solution of which yielded the time history of airplane motions; further calculations then provided the load history.

The necessity for comprehensive dynamic analyses to account for dynamic loading effects increased the complexity of the gust load prediction problem by an order of magnitude. Treatment of the gust problem by these methods of dynamic analysis became practicable only with the advent of high-speed digital and analog computing equipment. Numerous authors contributed to the development of methods of dynamic gust analysis, including Goland,[2] Bisplinghoff, et al.,[3] and Houbolt.[4] The assumptions upon which these methods are commonly based are:

(1) The airplane is free to pitch, translate vertically and deform elastically.
(2) The airplane penetrates a gust of (1 − cos) shape. Unlike the mass parameter gust load formula the gust length is varied to produce critical phasing, thus yielding a maximum load at each load station on the airplane.
(3) The gust is distributed uniformly across the span.

Although this represented a significant advance toward a more rational method of gust load prediction, it was still limited to a rather arbitrary description of the gust input. The entire spectrum of continuous turbulence was still represented by a discrete gust of a given magnitude and of one-minus-cosine shape. In essence, this represented an extension of the load transfer concept to include the influence of airplane dynamics.

Studies by Press and Mazelsky[5] and by Richardson[6] indicated that, with even more marked variations in vehicle configuration shape, performance capability, and stability characteristics, consideration of the gust input as continuous rather than discrete was important. This was particularly true for those high-performance configurations which exhibited relatively poor damping characteristics. For such configurations, prediction of gust loads based on a discrete input could result in a serious underestimation of the gust loads. Under these conditions the applicability of the discrete gust load transfer concept is questionable, because of the wide differences between the measuring airplanes and those for which the loads are desired.

Power Spectral Methods

The development of more rational techniques for gust load prediction which are applicable to such configurations is a two-fold problem. The requirements are, first, the determination of adequate vehicle gust load response characteristics and, second, a more rational description of atmospheric turbulence as a continuous phenomenon. The vehicle response characteristics are given by the gust load frequency response function which is obtained by a minor extension of the previously described dynamic analysis for a discrete gust input. Clementson,[7] Liepmann,[8] and Press[9] have contributed to the definition of a continuous turbulence input based on application of the theory of generalized harmonic analysis. This general approach to the prediction of gust loads has been termed the power spectral method of gust load analysis and is described in some detail by Press and Houbolt.[10] In the remainder of this paper the authors will indicate some applications of the power spectral method in the determination of vehicle response and in prediction of design gust loads. First, however, a few comments will be made relative to the basic treatment of the gust problem by power spectral techniques. The procedure is essentially that defined by Press in reference 9.

Basic Power Spectral Relations

The basic elements of any gust analysis problem can be summarized as shown schematically in Fig. 1. They include an input disturbance, based on a representation of the atmosphere, a linear system defined by its response characteristics, and an output, defined in terms of

the load or response item of interest. For a power spectral analysis the input is characterized by the power spectrum of atmospheric turbulence. The response characteristics of the vehicle are defined by the output spectrum for the load item of interest.

A fundamental relationship which holds between output and input spectra for linear systems is given below.

$$\Phi_0(\Omega) = |T(i\Omega)|^2 \Phi_I(\Omega) \tag{1}$$

The output spectrum is obtained as the product of the input spectrum of gust velocity and the squared modulus of the vehicle frequency response function. Also, from the output spectrum, the mean square value or the variance of the load can be determined as

$$\sigma_0^2 = \int_0^\infty \Phi_0(\Omega) d\Omega \tag{2}$$

Further, if atmospheric turbulence can be considered as locally stationary and Gaussian, as suggested in reference 9, and if the input spectrum shape is invariant with the root mean square level of turbulence, it is possible to calculate the expected number of times that a given load is exceeded per unit time or distance flown. The expected number of exceedances $N(\xi)$, of load ξ, as derived by Rice[11] and extended by Press[9] is given by

$$N(\xi) = N_0 e^{-(\xi^2/2\sigma_0^2)} \tag{3}$$

where

$$N_0 = \frac{1}{2\pi}\left[\frac{\int_0^\infty \Omega^2 \Phi_0(\Omega) d\Omega}{\int_0^\infty \Phi_0(\Omega) d\Omega}\right]^{1/2} \tag{4}$$

N_0 defines the expected number of times per foot distance flown that ξ crosses the zero reference with a positive slope.

It is possible to rewrite Eq. (3) in terms of the frequency response characteristics of the vehicle and the root mean square level of the turbulence input by defining a normalized gust velocity input spectrum such that

$$\Phi_I(\Omega) = \sigma_u^2 \Phi_{I_N}(\Omega) \tag{5}$$

where $\Phi_{I_N}(\Omega)$ is the normalized gust input spectrum with a root mean square value of unity and σ_u is the root mean square level of the turbulence.

Substituting $\Phi_I(\Omega)$ from Eq. (5) into Eq. (1) yields the output spectrum $\Phi_0(\Omega)$ in terms of the normalized gust velocity input spectrum $\Phi_{I_N}(\Omega)$ and the root mean square level of the turbulence σ_u.

$$\Phi_0(\Omega) = |T(i\Omega)|^2 \Phi_{I_N}(\Omega) \sigma_u^2 \tag{1a}$$

Further substitution of $\Phi_0(\Omega)$ from Eq. (1a) into Eq. (2) yields

$$\sigma_0^2 = \sigma_u^2 \int_0^\infty |T(i\Omega)|^2 \Phi_{I_N}(\Omega) d\Omega \tag{2a}$$

Thus, by substitution of the above expression for σ_0^2 in Eq. (3), the expression for the expected number of exceedances of load ξ per unit distance flown may be rewritten as

$$N(\xi) = N_0 e^{-(\xi^2/2A^2\sigma_u^2)} \tag{6}$$

where

$$A^2 = \int_0^\infty |T(i\Omega)|^2 \Phi_{I_N}(\Omega) d\Omega \tag{7}$$

In a similar fashion N_0 may be rewritten

$$N_0 = \frac{1}{2\pi}\left[\frac{\int_0^\infty \Omega^2 |T(i\Omega)|^2 \Phi_{I_N}(\Omega) d\Omega}{\int_0^\infty |T(i\Omega)|^2 \Phi_{I_N}(\Omega) d\Omega}\right]^{1/2} \tag{8}$$

Under these conditions both A^2 and N_0 are functions only of the vehicle frequency response characteristics and a normalized gust velocity power spectrum shape.

Eq. (6) defines the expected number of exceedances of a given load level per foot traveled, for a given root mean square level of the gust input and for a stationary Gaussian process. Since over large space or time intervals the root mean square level of turbulence varies, the operational load history of an airplane arises as a summation of the fractional time exposure to turbulence of various root mean square levels. For turbulence defined in terms of several discrete root mean square levels, σ_{u_j}, Eq. (6) can be written

$$N(\xi) = N_0 \sum_j F(\sigma_{u_j}) e^{-(\xi^2/2A^2\sigma_{u_j}^2)} \tag{9}$$

where $F(\sigma_{u_j})$ is the fraction of the total flight time or distance spent in turbulence with a root mean square level σ_{u_j}. Eq. (9) has been extended to integral form

$$N(\xi) = N_0 \int_0^\infty f(\sigma_u) e^{-(\xi^2/2A^2\sigma_u^2)} d\sigma_u \tag{10}$$

where $f(\sigma_u)$ is the probability density function of σ_u. Press in reference 9 has presented several empirical expressions for $f(\sigma_u)$ as a function of altitude and weather condition obtained by fitting existing loads history data.

Eq. (10) is the basic equation used in the design gust load investigations. For a given scale length of turbulence the determination of A^2, N_0, and the evaluation of the integral given in Eq. (10) represents a relatively minor extension of the larger effort required to calculate the vehicle frequency response function. Some examples of application of power spectral methods will be discussed below.

Fin Loads Due to Turbulence

The first example illustrates an application of power spectral methods in the preliminary design examination of fin loads due to turbulence. The configuration under study was a relatively flexible manned bomber with a high-performance capability.

To cover the intended operational usage of the airplane, five different mission profiles were defined, including both training and tactical operation. To each of these was assigned a value representing the fraction of total life which the airplane was expected to spend in each mission. These are shown in Fig. 2.

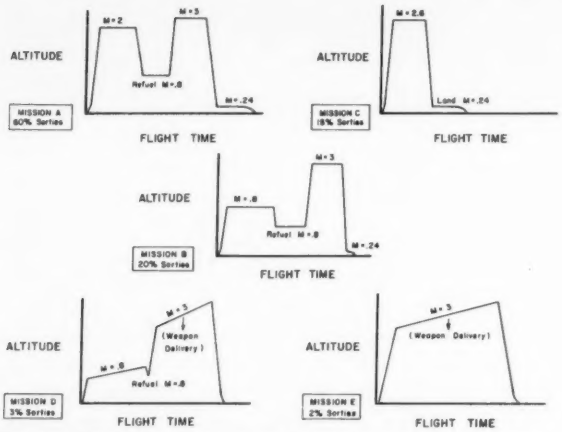

FIG. 2. Mission profiles used to define the operational usage of a high-performance manned bomber.

Each of the mission profiles was in turn subdivided into several weight-speed-altitude blocks. Within each block it is assumed that the vehicle mass and mass distribution, speed, and altitude are constant. Choice of the number of blocks to be considered is based on considerations of required accuracy and complexity of analysis. Consideration must be given not only to the differences in turbulence input in each altitude block but also to the change in the dynamic response characteristics resulting from fuel usage, speed changes, and change in atmospheric density with altitude.

The next step involved the derivation of equations of motion and load equations from which the vehicle response for each of the specified weight-speed-altitude blocks could be determined. The problem in the present example was a preliminary design investigation yielding fin gust load data. A study of the configuration indicated that the major features of the problem could be covered by considering the airplane response defined in terms of airplane yaw, roll, sideslip, and body side bending freedoms. Also included was the influence of a yaw axis artificial stability augmentation system. This system in the airplane was idealized by providing a rudder input which was linearly proportional to airplane yaw rate.

Matrix techniques utilizing high-speed digital computing equipment were applied in the derivation of the coefficients of the equations of motion for each of the defined weight-speed-altitude blocks. Further equations expressing the fin load in terms of the applied gust and vehicle response were derived for each of the weight-speed-altitude blocks. The solution for the load frequency response function involves determination of the steady-state load response amplitude to a unit sinusoidal gust applied to the fin as a function of the forcing frequency. In this preliminary design study it was considered sufficient to examine the effect of a lateral gust only. More rigorous studies would include the influence on fin load of the roll producing capability of the asymmetrical vertical gust components. Again high-speed digital computing equipment is used in the solution for the frequency response function. The equations of motion, loads equations, and a set of frequencies covering the range in which the frequency response function is desired are read into the computer. In practice the initial machine calculations are based on a relatively uniform spread of frequencies over the desired range. However, in order to define the frequency response function with sufficient accuracy in the vicinity of the response peaks it is usually necessary to recalculate the response function with closely spaced frequencies near these peaks. Theoretically, the frequency spectrum from zero to infinity should be covered. However, the frequency content of turbulence, as defined by existing gust spectra, is such that most of the energy is associated with the lower frequencies. A practical cut-off frequency appears to be one whose period corresponds to a distance traveled of one chord length or less. The response amplitude and phase angle for each of the supplied frequencies is computed by the machine.

The calculation procedure used in the program is given as follows. The equations of motion and an equation predicting the gust loads in terms of the response are written in matrix form as given below:

$$[M_1]\{q''\} + [M_2]\{q'\} + [M_3]\{q\} + [M_4]\{q'\}_* K(\tau) + [M_5]\{q\}_* K(\tau) = \{C_1\} V_{g*} \psi(\tau) \quad (11)$$

$$\{\xi\} = [A]\{q''\} + [B]\{q'\} + [C]\{q'\}_* K(\tau) + [D]\{q\}_* K(\tau) + \{E\} V_{g*} \psi(\tau) \quad (12)$$

where $\{q\}$ are the generalized coordinates defining the response in the rigid and elastic modes. $[M_1]$ is the generalized inertia matrix. $[M_2]$, $[M_3]$, $[M_4]$, and $[M_5]$ are matrices defining the aerodynamic and structural stiffness and damping characteristics of the vehicle. The asterisk denotes convolution with the Wagner and Kussner lift growth functions $K(\tau)$ and $\psi(\tau)$, respectively. The right-hand side of Eq. (11) is the forcing function due to the gust. The symbol τ denotes dimensionless aerodynamic time, Vt/b, which is measured in number of semichords traveled.

The loads equation, Eq. (12) is defined as a summation of the inertial and aerodynamic loads resulting from the vehicle response and the loads due to the gust itself. The matrix coefficients $[A]$, $[B]$, $[C]$, $[D]$, and $\{E\}$ define the load components in terms of the coordinate response and the gust.

The response for a unit sinusoidal gust input of frequency ω is found by taking the Laplace transform of each side of the above equation and substituting the variable $i\omega$ for the transform variable p.

$$\{(-[M_1]\omega^2 + [M_3] + i\omega[M_2]) + ([M_5] + i\omega[M_4])K(i\omega)\}\{q\} = \{C_1\}\psi(i\omega) \quad (13)$$

The digital program solves for the complex coordinate responses, $\{q\}$, in Eq. (13) by matrix algebra. Insertion of $\{q\}$, $i\omega\{q\}$, and $-\omega^2\{q\}$ in the loads equation, Eq. (12), results in the load response for the frequency ω.

This calculation is performed for each of the supplied frequencies, and a tabulation of the load amplitude and

phase angle is printed out. Shown in Fig. 3 is a plot of the amplitude squared of the fin load frequency response function for one of the weight-speed-altitude blocks of mission A shown in Fig. 2.

Although the problem is solved in terms of the reduced frequency $\omega = bf/v$, the frequency response function is normally plotted in terms of the frequency argument f in radians per second for the purpose of comparing peaks with the vehicle natural frequencies. However, the turbulence spectra are defined in terms of the spatial frequency Ω in radians per foot traveled. It is therefore necessary to rewrite the frequency response function in terms of Ω prior to determining the load output spectrum. This relationship is defined by

$$f = V\Omega \tag{14}$$

Having defined the load frequency response function, the next step is the definition of the normalized gust input spectrum. The normalized spectrum for vertical turbulence usually given in the literature[8, 9, 12] is

$$\Phi_{I_N}(\Omega) = (L/\pi)[(1 + 3L^2\Omega^2)/(1 + L^2\Omega^2)^2] \tag{15}$$

where L is the scale length of the turbulence. In this study we are concerned with turbulence velocity fluctuations in the lateral direction since the problem is one of predicting fin loads. The assumption has been made that the lateral and vertical spectra are equivalent. Further, a scale length of 1,000 ft. has been assumed. It is recognized that these assumptions are somewhat arbitrary in the light of recent evidence, particularly in the low-altitude regimes; however, they will serve for purposes of illustration.

Insertion of the normalized input spectrum and load frequency response function into Eqs. (7) and (8) will yield the parameters A^2 and N_0 which were described earlier.

In practice the conversion to spatial frequency Ω and the calculation of A^2 and N_0 for each weight-speed-altitude block are effected in the digital program previously described. The assumed normalized input spectrum is written into the digital program. Theoretically the integrations in Eqs. (7) and (8) should be extended over the entire frequency spectrum, but in practice good results are obtained with a cut-off frequency as described previously.

The expected number of exceedances of a given load per foot traveled in a given weight-speed-altitude block is obtained from Eq. (10).

As described earlier empirical expressions have been derived for $f(\sigma_u)$ for several altitude bands.

Using these expressions for $f(\sigma_u)$ and the values of A^2 and N_0 determined from Eqs. (7) and (8), it is possible to calculate by Eq. (10) the expected number of exceedances of a given fin load versus the load itself for each of the defined weight-speed-altitude blocks.

Choice of Design Criterion

Since the results obtained by the power spectral method are statistical, the task remains to choose for

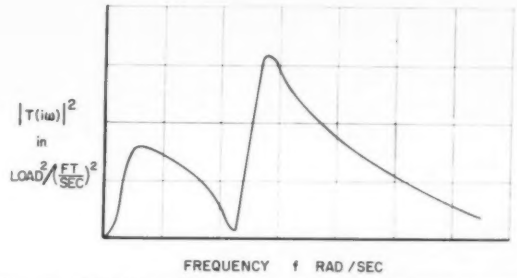

FIG. 3. Modulus squared of the fin load frequency response function for one of the weight-speed-altitude blocks of mission A.

design purposes an acceptable rate of encounter, as defined by the distance to fly to exceed a given load. A means of specifying an acceptable rate of encounter which is compatible with the past history of satisfactory operation is required. A comparative method of evaluation is outlined below which will lead to the selection of a design value on a rational basis.

If past airplanes, which were originally designed on the basis of gust rather than maneuver considerations, were re-examined by power spectral techniques it would be unreasonable to have a design criterion that would result in increased design gust loads in view of their proven satisfactory gust experience. Instead, the re-evaluation of past airplane gust loads on a power spectral basis should provide a criterion for selection of design loads on a more advanced configuration. One such criterion might be the selection of a design load on the basis of equal probability of exceeding limit load rather than equal design gust velocity. Under these conditions correspondence is established between the satisfactory, but somewhat arbitrary, gust criteria of the past and the more rational but untested power spectral approach. In the present example the predicted load experience of the configuration under study is defined relative to that predicted for the Boeing Stratocruiser. Thus, the curves which describe the expected distance flown to exceed a given fin load once, in each weight-speed-altitude block, are ratioed to the predicted distance to be flown by the Stratocruiser to exceed its design limit fin load once. This distance ratio is denoted as $R(\xi)$. The distance which the Stratocruiser must fly to exceed its design fin load was determined from a gust power spectral analysis of the Stratocruiser based on representative North Atlantic and transcontinental operation.

In Figs. 4, 5, and 6 are shown the results of the example study. Fig. 4 describes the relative distance to fly to exceed a given load for each of the various segments of mission A shown in Fig. 2. The load corresponding to a value of unity for the distance ratio $R(\xi)$ for each segment is the limit fin design load which should yield a gust load risk level, on the airplane under study, which is comparable to that for the Stratocruiser assuming the airplane spent its entire life in that segment. Curves of this type for each mission indicate clearly the relative significance of the various segments of the mission.

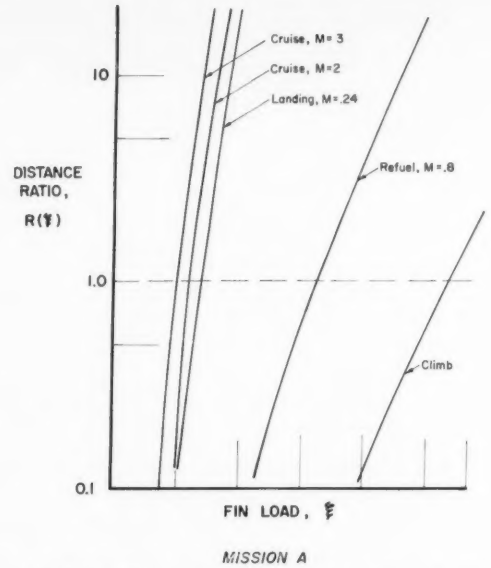

FIG. 4. Relative distance to fly to exceed a given fin load for each of the various segments of mission A.

Fig. 5 describes the relative distance to fly to exceed a given load for each of the five missions. These curves are weighted to account for the fraction of the total distance flown in each segment of a given mission.

Let $R(\xi)$ be defined as the distance ratio shown as the ordinate in the Figures.

Then, for mission A,

$$R(\xi)_A = (D_A/D_s)\left[1 \Big/ \sum_{j=1}^{n} N_j(\xi)D_j\right] \qquad (16)$$

where n is the total number of segments in mission A, D_s is the distance in feet which the Stratocruiser flies to exceed its limit fin load once, D_j are the distances flown in the j segments of mission A, D_A is the tot a distance flown in mission A, and $N_j(\xi)$ is the number of exceedances of load (ξ) per foot traveled in segment j.

Again a value of unity for the distance ratio $R(\xi)$ denotes for each mission the limit fin load for that mission which would yield a risk level comparable to the Stratocruiser.

Similarly, Fig. 6 shows a single curve which represents a weighted average of the curves for all of the missions. The weighting factor depends on the anticipated ratio of distance flown in each mission to the total distance for all missions. These ratios are based on the assumed operational usage of the airplane given in Fig. 2.

Choice of a limit design fin load associated with a unit value of the distance ratio $R(\xi)$ should yield a fin gust load experience comparable to that for the Stratocruiser, including the influences of the various operational usages of the vehicle. Further information can be obtained from these curves such as the relative risk, defined in terms of the distance ratio $R(\xi)$, for any chosen fin design load. Probably the greatest value lies in the ability to assess the relative importance of the various segments of each mission and the various missions which make up the operational life of the vehicle. It can also be seen that the values of the exceedances derived for each weight-speed-altitude block can be used as building blocks in estimating the effect on fin gust load of changes in the operational usage of the airplane.

Crew Station Accelerations Due to Random Turbulence

In certain types of missions operational limits may be dictated by the influence of turbulence on crew efficiency

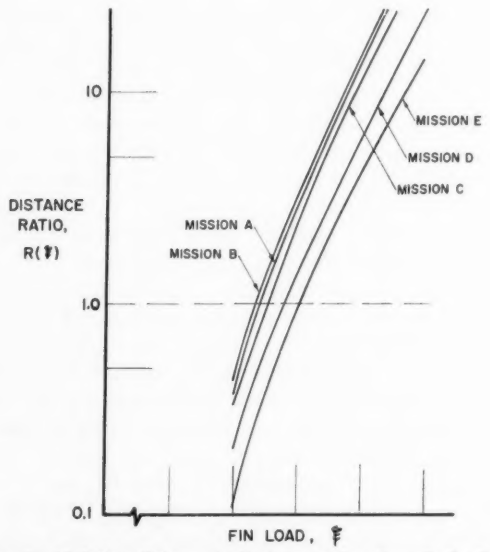

FIG. 5. Relative distance to fly to exceed a given fin load for each of the five missions comprising the operational usage of the airplane.

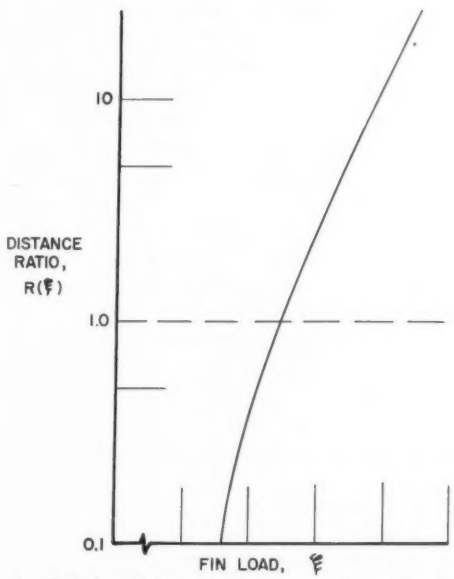

FIG. 6. Relative distance to fly to exceed a given fin load considering all five missions and the fraction of total distance flown in each.

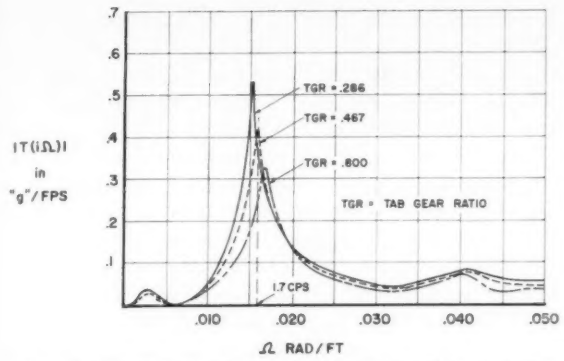

FIG. 7. Frequency response functions of tail gunner crew station accelerations for various values of mechanical yaw damper tab gear ratio (TGR).

and flight precision rather than structural limitations. In particular, it has been found that in high-speed low-altitude missions the range and speed of the airplane is apt to be limited by the acceleration environment induced at the crew station by excessive turbulence. Since this limitation results from a continuous exposure to turbulence, it follows that the problem should be studied from a power spectral approach rather than a discrete loading approach. The problem is twofold in that the crew station environment must be determined and human tolerance levels for the mission must be defined.

The crew station environment is defined statistically by power spectral methods. By this technique the important parameters relative to crew tolerance can be determined—namely, amplitude, vibration frequency, and time duration of acceleration.

The definition of human tolerance levels for airplane operation is not well established at this time. Whereas some standards are available which give acceleration as a function of frequency for various sensation levels,[13] more research is necessary to determine the length of time that these levels can be endured and to establish a definition of "damage" in the human fatigue sense including consideration of the function which the crew member must perform. In defining the concept of damage it must be recognized that more effort and concentration are required to fly an airplane at low altitude than at normal high altitude. In the recent work of Mozell and White[14] an evaluation has been made of the effects of vibration on visual acuity and the ability to perform a manual task. Their study was in a frequency range above the fundamental structural modes, however, and did not include the effects of prolonged exposure.

As an illustration, a study has been made predicting the lateral acceleration environment at the tail gunner's station during high-speed low-altitude operation of a manned subsonic bomber. This is usually the most critical crew station location with respect to turbulence excitation.

The input used in this study is again that given in reference 9 for the zero to 10,000 ft. altitude band. It is recognized that this information is not strictly applicable at extremely low altitudes. Unpublished data indicate a probable decrease in the scale length of the turbulence and an increase in the intensity, particularly on the horizontal plane, at altitudes from zero to 500 ft. For illustrative purposes, however, the data of reference 9 should suffice.

The basic block diagram of Fig. 1 requires two elements in the transfer function determination. The first is the determination of the crew station environment in terms of frequencies, magnitude, and duration of loads. Since the ultimate answer required is a measure of crew efficiency, the second element of the transfer function must transform crew station loads into crew damage by evaluating factors associated with crew tolerance. In this example primary emphasis is placed on the former determination. The loads thus obtained can be applied by the human factors engineer to the crew member through a given seat-suspension system to determine crew damage.

The degrees of freedom included in the study were sideslip, yaw, roll, body side bending, body torsion rudder deflection, and stability tab deflection. The output information was lateral acceleration at the tail gunner station. Studies were made for low-altitude high-speed flight considering the influence of variations in the yaw damper configuration.

Results of the study are shown in Figs. 7 and 8. For illustrative purposes the acceleration frequency response functions for different yaw damper configurations are given in Fig. 7. The parameter which is varied is the ratio of the stability tab deflection to the bob weight deflection in a mechanical yaw damper system, or it might be considered as a gain in an electronic yaw damper. Although the values of such parameters are

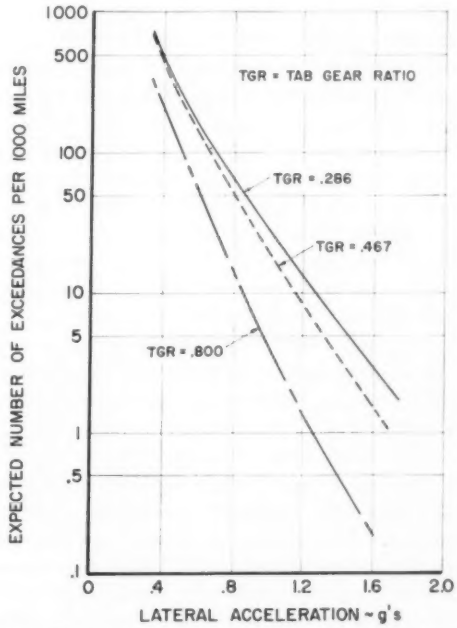

FIG. 8. Expected number of exceedances of lateral acceleration levels at the tail gunner crew station computed for various tab gear ratios.

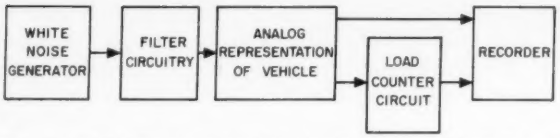

FIG. 9. Block diagram of analog simulation of terminal dive of boost-glide vehicle.

usually dictated by other conditions, it can be seen in Fig. 8 that these relatively simple changes may have a large effect on the expected number of exceedances of the various acceleration levels.

It is also evident from Fig. 7 that most of load will be experienced at the body side bending frequency of 1.7 c.p.s. Hence, for preliminary work it might be assumed that all of the acceleration occurs at that frequency, and tolerance factors could be determined for this frequency. It should be pointed out that the structural loads such as fin load are most critical at the lower yaw-roll frequency, although the crew accelerations occur predominantly at the body bending frequency. Thus, corrective measures, such as yaw stability augmentation, might be beneficial in reducing fin loads, whereas they would have little effect on crew station accelerations.

Continuous Analog Simulation

Although the previously described methods of power spectral analysis provide a convenient tool in determining the gust loads of airplanes and missiles, there are certain limitations which must be considered. One such limitation is the assumption that the physical characteristics of the vehicle are invariant within the time duration of interest defined by the time within a given weight-speed-altitude block. Under this assumption the governing equations become a set of simultaneous integro-differential equations with constant coefficients similar to those shown in Eq. (11) which are amenable to the described digital solution procedures. However, for missiles with high vertical velocities during boost and terminal dive, important parameters such as mass, velocity, Mach Number and dynamic pressure may vary quite rapidly over rather wide ranges. Under these conditions the coefficients of the equations of motion may no longer be considered constant. The methods described earlier may not therefore be applicable.

In the example described here we are interested in determining the gust loads in the terminal dive phase of a boost-glide missile. The vehicle initiates the terminal dive at Mach 4 at an altitude of 84,000 ft. and impacts at Mach 2 at sea level. The desired result is the expected number of exceedances, per dive, of any given normal load factor versus the load factor. From this information a design gust load factor may be based on the selection of an acceptable risk level, in terms of expected number of flights to exceed the design load factor.

In order to account for the influence on gust loads of these rate effects a continuous analog simulation technique is suggested. The basic elements of this analog simulation are shown in the block diagram given in Fig. 9. Mazelsky and Amey[15] have described in some detail the analog simulation of random excitations and vehicle response characteristics.

The simulation of the atmospheric turbulence, which is applied as an input to the analog representation of the vehicle, is accomplished by means of a "white noise" generator and a filter circuit. The "white noise" generator produces a random time varying voltage output with a flat power spectrum and a desired probability distribution. The filter circuit is used to tailor the spectrum shape to the desired form without altering the probability distribution of the noise input. In designing the filter circuit it was necessary to rely on atmospheric turbulence data obtained from airplanes in essentially horizontal flight. However, in the case considered here the missile flight path is near vertical. Two problems arise in this process. The first deals with the shape of the gust spectrum. Press and Steiner[16] have indicated that there is a serious question as to the applicability of gust spectra determined from airplanes with essentially horizontal flight paths to configurations with near vertical paths. However, since no adequate spectral descriptions exist for the vertical flight case, the filter circuit was adjusted to produce a spectral shape matching that given in Eq. (15) for horizontal flight. The second problem deals with the assumption of the continuous nature of the turbulence input. Since the vertical dimension of turbulent areas is often small compared to the horizontal dimension, it is possible that the time required for the high-speed missile to traverse the turbulent area is not large compared to the missile response times. In this case, the assumption of a locally stationary process described earlier would not be valid and a different atmospheric turbulence representation would be required. In this example the continuous turbulence input was assumed, although for future applications the validity of the assumption should be examined in terms of specific missile velocity, flight path angle, response frequencies, and typical dimensions of turbulent areas.

The equations of motion of the vehicle are wired in the analog. The variations in the time-dependent parameters are simulated by means of function generators. In this example the vehicle response could be defined adequately in terms of a rigid body translational mode and a pitch mode. It was necessary, however, to include the effect of an artificial stability augmentation system. It was found that this could be represented with a simple linear, nonlagged control function.

The load factor output for each dive is fed into a counting device. The count appears as a random step function, a unit step being made each time a given load factor level is crossed with a positive slope.

A typical record for one dive illustrating the time variation of load factor and the count is shown in Fig. 10. This analog record represents the simulation of one dive of the missile from the maximum altitude to

impact at sea level. Fig. 10a describes the time history of load factor for this one dive where time zero corresponds to the initiation of the dive and the last time point corresponds to impact at sea level. Also indicated are the load factor bands in which the counts are made. Fig. 10b describes the output of the counter where $N(\Delta n_i)$ represents the number of crossings with positive slope of the ith band. Also shown are the altitude levels through which the missile passes in the dive.

From the counts of Fig. 10 it is possible to determine the average number of exceedances of various load factor increments for a single dive. To obtain the necessary degree of statistical reliability a number of dives must be made. In this study a total of twenty dives was considered sufficient, and the average number of exceedances of each load factor band for each dive was determined. These were collected in each altitude band. For a linear system, the load factor increment, Δn, is directly proportional to the root mean square intensity of the turbulence, σ_u. In this problem it was therefore only necessary to examine the case for one value of σ_u, and solutions for σ_u other than that considered are determined from a linear extrapolation.

As described earlier, atmospheric turbulence cannot be defined in terms of a constant value of σ_u. Again probability distributions of σ_u for several altitude bands are defined in reference 9. These probability distributions of σ_u may then be used to determine the expected number of exceedances in each altitude band accounting for the variation in σ_u. Thus,

$$N_i(\Delta n) = \int_0^\infty N_i(\Delta n \mid \sigma_u) f(\sigma_u) d\sigma_u \qquad (17)$$

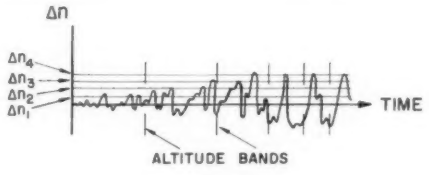

FIG. 10a

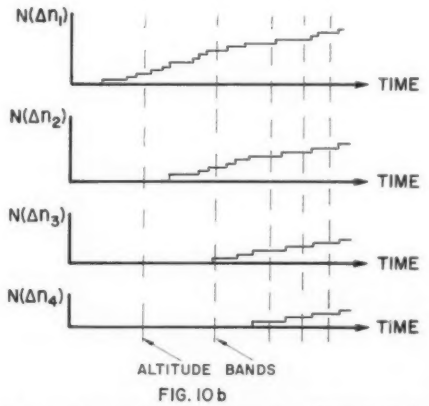

FIG. 10b

FIG. 10. Typical record for one dive illustrating the time variation of load factor and the counts of exceedances of various load factor levels.

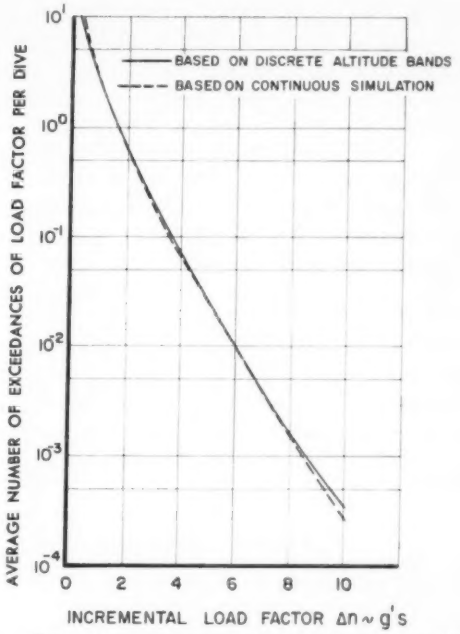
BASED ON DISCRETE ALTITUDE BANDS
BASED ON CONTINUOUS SIMULATION
AVERAGE NUMBER OF EXCEEDANCES OF LOAD FACTOR PER DIVE
INCREMENTAL LOAD FACTOR Δn ~ g's

FIG. 11. Comparison of power spectral solution and continuous analog simulation results.

where $N_i(\Delta n)$ is the number of exceedances of Δn in the ith altitude band.

$N_i(\Delta n \mid \sigma_u)$ is the number of exceedances of Δn in the ith altitude band for a given value of σ_u. $N_i(\Delta n \mid \sigma_u)$ is determined from the counts of Fig. 10. The actual integration of Eq. (17) has been carried out numerically.

The expected number of exceedances for each dive can be determined by simply summing those within each altitude band. The final results are then presented in the form of expected number of exceedances per dive of any given incremental load factor. These results are shown in Fig. 11.

The procedure described here is applicable to those cases where the effects of rapid time variation of the system parameters may be important. In order to evaluate the importance of this rate effect for this configuration a conventional power spectral solution was also made. The procedure is essentially the same as that described in the first example. The terminal dive phase of the flight was divided into 15 altitude bands. The time varying coefficients in the equations of motion were assumed to be held constant in each band at a value defined by the midpoint of the band. The gust load transfer function was then determined for each band as well as values for the parameters A^2 and N_0 given by Eqs. (7) and (8).

Using Eq. (10), it was then possible to calculate the expected number of exceedances, in each altitude band, of the various load factor levels. These were then summed, after introducing weighting factors proportional to the distance traveled in each band, to yield the expected number of exceedances versus load factor level for each dive. The results of this analysis are shown together with the results of the continuous simulation

in Fig. 11. As can be seen, for this example at least, there is little difference between the results of the conventional power spectral solution and the continuous simulation. Thus, for this example, rate effects are not significant. It is anticipated, however, that rate effects may be important for boost conditions where there is a rapid change in mass and mass distribution and for vehicles with poor stability characteristics.

From this curve the design load factor corresponding to a specified risk level may be selected. For example, the limit gust load factor which would be exceeded once, on the average in 100 dives, is 6 g's.

For simplicity we have considered here only one facet of the missile structural design problem. In a rational treatment of this problem consideration should be given on a similar probability basis to the effects of other load producing phenomena such as wind shear and maneuver.

Concluding Remarks

Some illustrations have been given on the application of power spectral methods in the prediction of design gust load information and system response in continuous turbulence. In these illustrations a statistical design load philosophy has been presented which considers the intended operational usage of the airplane including a rational approach to the problem of establishing an acceptable rate of load encounter. This criterion is based on a comparative evaluation of the configuration under study with an airplane which has a proven satisfactory gust experience.

Power spectral methods have also been demonstrated as an effective means of evaluating the influence of system parameter and flight condition changes as they affect the acceleration environment to which the crew is subjected. In particular it is shown that relatively minor variations in the gain of artificial damping systems may have significant effects on the statistical description of crew station accelerations.

In certain missile configurations, particularly during boost and terminal dive, the rapid time rate of change of the system parameters may be significant in the prediction of gust loads. Under these conditions the power spectral approach based on description of the system frequency response function within given weight-speed-altitude blocks may not be valid. For those cases where rate effects are significant a continuous analog simulation technique is suggested, utilizing power spectral concepts in the synthesis of atmospheric turbulence as an input to the computer. Limitations on the applicability of this spectral description of atmospheric turbulence are also described. Application of this technique to the prediction of gust loads on a representative missile in the terminal dive condition is discussed.

References

[1] Pratt, K. G., and Walker, W. G., *A Revised Gust Load Formula and a Re-Evaluation of V-G Data Taken on Civil Transport Airplanes From 1933 to 1950*, NACA Report 1206, 1954.

[2] Goland, M., Luke, Y. L., and Kahn, E. A., *Prediction of Wing Loads Due to Gusts Including Aeroelastic Effects*, Midwest Research Institute Report 1-536-E-9, 1947.

[3] Bisplinghoff, R. L., Isakson, G., Pian, T. H. H., Flomenhoft, H. I., and O'Brien, T. F., *An Investigation of Stresses in Aircraft Structures Under Dynamic Loading*, M.I.T., Aeroelastic and Structures Research Laboratory Report, January, 1949.

[4] Houbolt, J. C., *A Recurrence Matrix Solution for the Dynamic Response of Aircraft in Gusts*, NACA TN 2060, March, 1950.

[5] Press, H., and Mazelsky, B., *Study of Application of Power Spectral Methods of Generalized Harmonic Analysis to Gust Loads on Airplanes*, NACA TN 2853, 1953.

[6] Richardson, A. S., Jr., *Theoretical and Experimental Investigation of Random Gust Loads. Part II—Theoretical Formulation of Atmospheric Gust Response Problem*, NACA TN 3879, May, 1957.

[7] Clementson, Gerhardt C., *An Investigation of the Power Spectral Density of Atmospheric Turbulence*, Sc.D. Thesis, M.I.T., 1950.

[8] Liepmann, H. W., *On the Application of Statistical Concepts to the Buffeting Problem*, Journal of the Aeronautical Sciences, Vol. 19, No. 12, pp. 793–800, 822, December, 1952.

[9] Press, H., Meadows, M. T., and Hadlock, I., *A Reevaluation of Data on Atmospheric Turbulence and Airplane Gust Loads for Application in Spectral Calculations*, NACA Report 1272, 1956.

[10] Press, H., and Houbolt, J. C., *Some Applications of Generalized Harmonic Analysis to Gust Loads on Airplanes*, Journal of the Aeronautical Sciences, Vol. 22, No. 1, pp. 17–26, 60, January, 1955.

[11] Rice, S. O., *Mathematical Analysis of Random Noise, Parts I and II*, Bell System Technical Journal, Vol. XXIII, No. 3, July, 1944; *Parts III and IV*, Vol. XXIV, No. 1, January, 1945.

[12] Fung, Y. C., *Statistical Aspects of Dynamic Loads*, Journal of the Aeronautical Sciences, Vol. 20, No. 5, pp. 317–330, May, 1953.

[13] Lippert, S., *Limitations to Noise and Vibration Control*, Proc. Symp. on Frontiers of Man Controlled Flight, Inst. of Transportation and Traffic Engineering, University of California, Los Angeles, April, 1953.

[14] Mozell, Maxwell M., and White, David C., *Behavior Effects of Whole Body Vibration*, Journal of Aviation Medicine, October, 1958.

[15] Mazelsky, B., and Amey, H. B., Jr., *On the Simulation of Random Excitations for Airplane Response Investigations on Analog Computers*, Journal of the Aeronautical Sciences, Vol. 24, No. 9, pp. 633–649, 712, September, 1957.

[16] Press, H., and Steiner, R., *An Approach to the Problem of Estimating Severe and Repeated Gust Loads for Missile Operations*, NACA TN 4332, September, 1958.

Microcards for Volumes 1–5 Available

Microcards for Volumes 3–5 of the JOURNAL are now available (Vols. 1 and 2 were republished in this form earlier). All five volumes are priced at $5.50 each, and are obtainable through:

J. S. Canner & Company, Inc.
Boston, Roxbury 20, Mass.

Propagation of Weak Disturbances in a Gas Subject to Relaxation Effects†

FRANKLIN K. MOORE* AND WALTER E. GIBSON**

Cornell Aeronautical Laboratory, Inc.

Summary

A generalized wave equation is derived for sound disturbances in a gas when relaxation effects connected with, for example, molecular vibration or dissociation are important. Solutions involving discontinuous wave fronts are presented, and it is shown that, under certain assumptions, the complete wave equation reduces to a variant of the telegraph equation. Detailed solutions are presented for disturbance fields produced by a wavy wall in subsonic and supersonic flow and a simple wedge in supersonic flow. This study is viewed as a step in the development of a theory of small disturbances of a high-temperature gas, as is found behind the shock in hypersonic flight.

Symbols

A = constant, Eq. (44)
a = inclination of wave front, Eq. (46) and Fig. 3
a_e = equilibrium sound speed, Eq. (17)
a_f = frozen sound speed, Eq. (16)
b = wave attenuation, Eq. (46)
C = transformation factor, Eqs. (35) and (39)
D = quantity defined in Eq. (18c)
E = internal energy per unit mass
f = slope of surface as function of ξ
f^* = slope of surface as function of X
I_0 = Bessel function of the first kind, of an imaginary argument
K = function of k and M, Eq. (22)
k = ratio of sound speed, a_e/a_f
M = Mach Number based on frozen sound speed, $\tilde{u}/a_f$
p = static pressure
q = heat of dissociation per unit mass
R = gas constant
s = inclination of discontinuous wave front
T = translational temperature
t = time
u = velocity in x direction
v = velocity in y direction
X = transformed x coordinate, Eq. (21)
x = coordinate (in stream direction for steady flow)
Y = transformed y coordinate, Eq. (21)
y = coordinate (normal to stream direction)
α = fraction of diatomic molecules dissociated
β = quantity subject to relaxation (either α or ϑ)
γ_f = ratio of specific heats for frozen process
δ = amplitude of wavy wall
ϵ = related to difference of sound speeds $[= (1 - K^2)/2]$
η = transformed Y coordinate, Eqs. (35)
Θ = wedge angle
ϑ = vibrational temperature
λ = wavelength of wavy wall
ν = dimensionless frequency, Eq. (42)
ξ = coordinate measured normal to frozen waves
σ = quantity defined in Eq. (18d)
τ = relaxation time for constant ρ and T
τ^* = relaxation time for adiabatic process
ϕ = velocity potential
ω = variable of integration

Subscripts

Subscript notation is used for partial differentiation
d pertains to dissociative relaxation
e = equilibrium conditions
f = frozen conditions
v pertains to vibrational relaxation
w = evaluation at a surface
r denotes distance at which β effectively reaches equilibrium

Superscripts

Primes denote perturbation quantities [except X', Y', Eqs. (24)]
Bars denote the undisturbed uniform gas flow
(0), (1), (2), . . . successive terms in expansion of ϕ, Eq. (34).

Introduction

THE CLASSICAL THEORY of aerial vibrations, upon which nonviscous small-perturbation theories of aerodynamics are based, applies when these degrees of freedom of the constituent gas molecules which happen to be excited are either in a state of complete equilibrium at each instant during the motion, or remain unchanged (frozen) during the motion. In air at ordinary temperatures and densities, molecular translation and rotation are the only excited degrees of freedom, and the relaxation times for these degrees of freedom are very short compared with ordinary acoustic periods. In such cases, equilibrium acoustic propagation may be assumed.

During hypersonic flight at high altitude, however, the air behind the leading shock wave is generally at very high temperature, and may be at low density. These circumstances tend strongly to excite the additional degrees of freedom of molecular vibration and dissociation of diatomic molecules. These "inert" degrees of freedom have longer relaxation times than the "active" processes of translation and rotation. Fig. 1 summarizes available information[1–4] concerning the variation of the various relaxation times with temperature for the constituents of air. The results presented are referred to sea-level density. At high altitudes, the times are much longer, being inversely proportional to density.

Presented at the Aerodynamics—IV Session, IAS 27th Annual Meeting, N.Y., Jan. 26–29, 1959.

† This research was supported by the USAF through the Mechanics Division of the Office of Scientific Research, ARDC.

* Director, Aerodynamics Division.

** Associate Physicist.

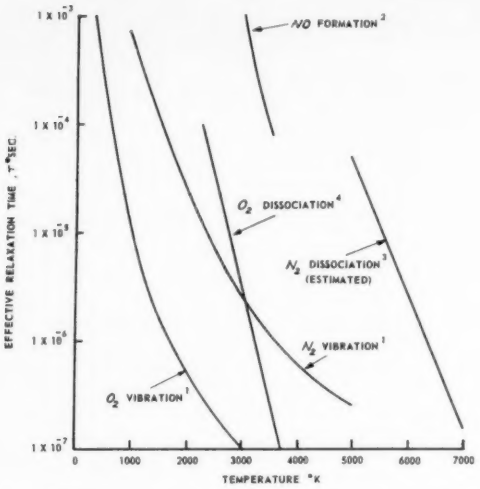

FIG. 1. Relaxation times for air, referred to a density of 1 atm.

In many problems of hypersonic flight, therefore, one may expect that the relaxation times of the excited degrees of freedom are comparable with the times for the passage of a gas particle over the flying object. In such cases, aerodynamic theory should include consideration of relaxation effects. In the present paper, we shall be concerned with the necessary modifications of the small disturbance, or acoustic, theories of aerodynamics. Fig. 1 indicates that, except near certain temperatures at which the relaxation time curves cross, the various relaxation times differ by factors of the order of 10. Thus, in a problem for which relaxation of a certain degree of freedom is important, other processes would have either much shorter relaxation times, and hence tend to be in equilibrium, or have much longer relaxation times, and hence tend to be frozen. Therefore, in a wide variety of cases involving air, relaxation of each degree of freedom may be considered separately.

Wave propagation in a relaxing gas is complicated by the fact that the speed of propagation of a sound wave depends on whether the propagation occurs by an equilibrium process or a frozen process. This fact is prominent in the extensive literature of ultrasonic absorption.[5] The wave speed which applies when the acoustic period is shorter than the vibrational relaxation time is greater than that which applies for long periods. Further, for those intermediate periods which are comparable to vibrational relaxation time, acoustic energy is absorbed.

Fig. 2 shows calculations[6] of the variation of sound speed with dissociation level for oxygen. The propagation speed is largest when both vibration and dissociation are frozen, and is smallest when both these processes proceed in equilibrium. An intermediate wave speed occurs when vibration is in equilibrium but dissociation remains frozen. It is noteworthy that if, in the spirit of the previous discussion of relaxation times, only one degree of freedom is considered at a time, the frozen and equilibrium sound speed do not greatly differ. For oxygen, the difference would not exceed 10 per cent. A similar set of curves to which the same conclusions apply may be calculated for nitrogen.

Wood and Kirkwood,[7] Chu,[8] and Resler[9] have studied the propagation of waves in a gas which possess the various degrees of freedom discussed above. These authors were chiefly concerned with the formulation of a proper method of characteristics to be used in numerical solution of nonlinear problems. Chu[8] also presents an analysis of certain aspects of the acoustic wave pattern produced by a piston suddenly set in motion. The present paper deals only with the theory of small disturbances, and begins with the development of a single differential equation to replace the classical wave equation under circumstances when relaxation effects are important.[10] This general equation will be found to be the same as that previously derived by Morrison[11] for the propagation of elastic waves in a solid material for which a time lag exists between the application of stress and the appearance of strain. In some cases, this generalized wave equation may be solved in closed form in certain important regions of a small-disturbance flow field.† Making proper use of the observation that the frozen and equilibrium sound speeds are not greatly different permits a reduction of the general differential equation to a variant of the telegraph equation and, for this equation, solutions in closed form for an entire flow field may be derived.

The purpose of the present paper is to contribute to the extension of aerodynamic theory to flows involving relaxation phenomena. Therefore, boundary conditions which are related to problems of aerodynamic interest will be emphasized, though the theory may readily be applied to problems of unsteady wave propagation. The particular examples chosen for this study are the wavy wall in both subsonic and supersonic flow, and the supersonic flow over a simple wedge. Finally, brief consideration will be given to the connection between

† A detailed account of this and other topics covered in this paper is provided in reference 12.

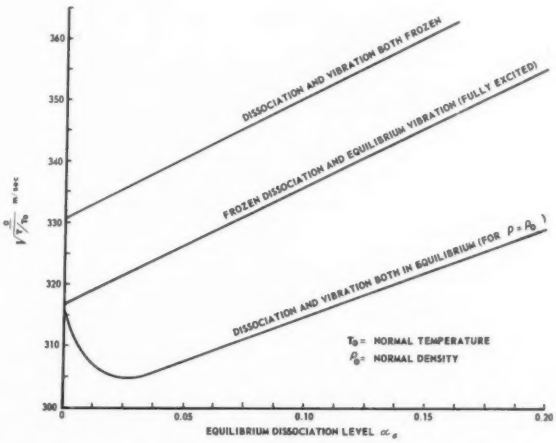
DISSOCIATION AND VIBRATION BOTH FROZEN
FROZEN DISSOCIATION AND EQUILIBRIUM VIBRATION (FULLY EXCITED)
DISSOCIATION AND VIBRATION BOTH IN EQUILIBRIUM (FOR $\rho = \rho_0$)
T_0 = NORMAL TEMPERATURE
ρ_0 = NORMAL DENSITY
EQUILIBRIUM DISSOCIATION LEVEL α_e

FIG. 2. Speed of sound in oxygen (from reference 6).

the present theory and the theory of dispersing nonlinear waves.[14]

The Wave Equation

Basic Equations for a Weak Disturbance

In order to derive a wave equation for small disturbances of a gas subject to relaxation processes, we may first write the equations expressing the conservation of momentum, mass, and energy as follows, neglecting viscosity, heat conduction, and diffusion:

$$\bar{\rho}u_t + \nabla p' = 0 \tag{1}$$

$$\rho_t' + \bar{\rho}\nabla\cdot u = 0 \tag{2}$$

$$\bar{\rho}E_t' + \bar{p}\nabla\cdot u = 0 \tag{3}$$

Apart from the disturbance field, the gas is assumed to be at rest, though in a state of vibrational or dissociative excitation. Each variable of state is described by a small deviation (ρ', for example) about a mean state ($\bar{\rho}$).

The necessary set of disturbance equations is completed by adding a real-gas definition of E (the internal energy), an equation of state, and a rate equation for the relaxation process.

The state equation

$$p = (1 + \alpha)\rho RT \tag{4a}$$

where α is the fraction of original molecules dissociated, may be written in the linearized form

$$p'/\bar{p} = [\alpha'/(1 + \bar{\alpha})] + (\rho'/\bar{\rho}) + (T'/\bar{T}) \tag{4b}$$

The internal energy may be written as

$$E = [(5 + \alpha)/2]RT + (1 - \alpha)E\vartheta + \alpha q \tag{5a}$$

where ϑ is the vibrational temperature, and is equal to the translational temperature T for the special case of fully excited vibration, and q denotes the heat required to dissociate a unit mass of diatomic molecules. Eq. (5a) may be linearized as follows:

$$E' = [(5 + \bar{\alpha})/2]RT' + (1 - \bar{\alpha})R\vartheta' + [q + (R\bar{T}/2) - R\bar{\vartheta}]\alpha' \tag{5b}$$

It is assumed that translation and rotation are in equilibrium, and that either vibration (ϑ) or dissociation (α) is subject to relaxation. We write the rate equation in a form suitable for consideration of small disturbances,

$$-(D\beta/Dt) = (1/\tau)[\beta - \beta_e(\rho, T)] \tag{6a}$$

which states that the Lagrangian rate of change of β (used here to denote ϑ or α, whichever is applicable) is proportional at each instant to the difference between the actual β and the value β_e which would apply if equilibrium prevailed at the existing level of density and temperature. The constant of proportionality $(1/\tau)$ is a reciprocal relaxation time. The function β_e is presumed to be known from equilibrium gas theory or experiment.

Eq. (6a) may be justified in general terms by the following argument: The quantity β changes as a consequence of an imbalance of forward and reverse reaction rates related to the occurrence of molecular collisions in the gas. In general, these rates depend on the populations of the interacting species—e.g., an excess of atoms would favor recombination. Thus, assuming that the reaction rates are regular functions of population (β), the net production of β may be expanded in a Taylor series in $(\beta - \beta_e)$. The right side of Eq. (6a) is the first term in such an expansion and is valid only when $\beta - \beta_e$ is small.

In order to make a consistent linearization of Eq. (6a), we may write β_e in the form

$$\beta_e = \bar{\beta} + \beta_{e_T}T' + \beta_{e_\rho}\rho' \tag{6b}$$

Linearizing the Lagrangian derivative, and writing $\beta = \bar{\beta} + \beta'$, Eq. (6a) then becomes

$$-\beta_t' = (1/\tau)(\beta' - \beta_{e_T}T' - \beta_{e_\rho}\rho') \tag{6c}$$

Eqs. (1)–(3), (4b), (5b), and (6c) constitute the complete set of small-disturbance equations which will, after introduction of a velocity potential, be combined to yield a single equation of acoustic propagation.

Derivation of the Acoustic Equation

Taking the curl of Eq. (1) shows that the vorticity at any point in the gas remains constant for small perturbations. Since we are concerned with waves in a gas initially at rest, it follows that the flow is irrotational. Therefore, a velocity potential may be defined:

$$u \equiv \nabla\phi \tag{7}$$

and, from Eqs. (1) and (2),

$$p' = -\bar{\rho}\phi_t \tag{8}$$

$$\rho_t' = -\bar{\rho}\nabla^2\phi \tag{9}$$

Next, we may observe that, for wave motions in a gas initially at rest, Eqs. (2) and (3) provide that

$$E' - (\bar{p}/\bar{\rho}^2)\rho' = 0 \tag{10}$$

Eq. (10) states that the flow process is adiabatic. If the gas remains either in the equilibrium or the frozen state, the process is also reversible, and the flow is isentropic. If we are concerned with vibrational relaxation, dissociation will be assumed frozen, so that Eqs. (5b) and (10) give

$$(\bar{p}/\bar{\rho}^2)\rho' = [(5 + \bar{\alpha})/2]RT' + (1 - \bar{\alpha})R\vartheta' \tag{11a}$$

If we are concerned with dissociation relaxation, $\vartheta = \vartheta_e(T)$, and Eq. (11a) is replaced by

$$(\bar{p}/\bar{\rho}^2)\rho' = \{[(5 + \bar{\alpha})/2] + (1 - \bar{\alpha})\vartheta_{e_T}\}T' + [q + (R\bar{T}/2) - R\vartheta_e]\alpha' \tag{11b}$$

In these two cases, the rate Eq. (6c) becomes

$$-\vartheta_t' = (1/\tau_v)(\vartheta' - \vartheta_{e_T}T') \tag{12a}$$

for vibrational relaxation (and frozen dissociation), or

$$-\alpha_t' = (1/\tau_d)(\alpha' - \alpha_{e_T}T' - \alpha_{e_\rho}\rho') \quad (12b)$$

for dissociative relaxation (and equilibrium vibration). Corresponding to Eqs. (11a) and (12a), the state Eq. (4b) is simply

$$p'/\bar{p} = (\rho'/\bar{\rho}) + (T'/\bar{T}) \quad (13)$$

while, corresponding to Eqs. (11b) and (12b), Eq. (4b) applies directly.

The differential equation for ϕ may now be determined by the following process, which we will trace for the case of dissociative relaxation: Eqs. (11b) and (4b) yield two independent expressions for α' in terms of p', T', and ρ'. These two expressions may be substituted into Eq. (12b), yielding two equations connecting p', T', and ρ'. Between these two equations, T' may be eliminated. Then Eqs. (8) and (9) may be introduced into the resulting equation connecting p' and ρ', yielding a single differential equation for ϕ. An equivalent procedure applies in the vibration case. In either case, the result may be expressed in the form

$$(\tau^*\partial/\partial t)(\phi_{tt} - a_f{}^2\nabla^2\phi) + \phi_{tt} - a_e{}^2\nabla^2\phi = 0 \quad (14)$$

This is the required generalized acoustic equation† which, it may be shown, also governs each of the other dependent variables of the problem.‡ The new quantities τ^* (effective relaxation time), a_f and a_e (frozen and equilibrium sound speeds, respectively) appearing in Eq. (14) are defined as follows:

$$\tau^*/\tau \equiv 1/[1 + D(\gamma_f - 1)\beta_{e_T}] \quad (15)$$

$$a_f{}^2 \equiv \gamma_f(\bar{p}/\bar{\rho}) \quad (16)$$

$$a_e{}^2 \equiv \frac{\gamma_f + \sigma(\gamma_f - 1)D\beta_{e_T} - (\gamma_f - \sigma)D\beta_{e_\rho}}{1 + (\gamma_f - 1)D\beta_{e_T}} \quad (17)$$

in terms of the following expressions:

	Vibration	Dissociation	
$\beta \equiv$	$\vartheta'/\bar{T}$	$\alpha'/(1 + \bar{\alpha})$	(18a)
$\gamma_f \equiv$	$\dfrac{7 + 3\bar{\alpha}}{5 + \bar{\alpha}}$	$\dfrac{7 + 3\bar{\alpha} + 2(1 - \bar{\alpha})\vartheta_{e_T}}{5 + \bar{\alpha} + 2(1 - \bar{\alpha})\vartheta_{e_T}}$	(18b)
$D \equiv$	$\dfrac{1 - \bar{\alpha}}{1 + \bar{\alpha}}$	$\dfrac{1}{2} + \dfrac{q}{R\bar{T}} - \dfrac{\bar{\vartheta}}{\bar{T}}$	(18c)
$\sigma \equiv$	1	$1 + (1/D)$	(18d)

The expressions listed above are the result of the manipulations leading to Eq. (14). The identification of a_f and a_e as frozen and equilibrium sound speeds can be justified in two ways: First, from basic acoustic theory, we know that the speed of sound is given by

$$a^2 = dp/d\rho \quad (19)$$

evaluated for the particular thermodynamic process which applies. For frozen flow, $\beta' = 0$, and elimination of T' between Eqs. (11a) and (13) [or between Eqs. (11b) and (4b)] yields an expression for $dp/d\rho = p'/\rho'$ identical with that listed as $a_f{}^2$ in Eq. (16). For equilibrium flow, $\beta - \beta_e = 0$ or, from Eq. (6c), $\beta' - \beta_{e_T}T' - \beta_{e_\rho}\rho' = 0$. Carrying out the elimination of β' and T' between this equation and Eqs. (11a) and (13) [or Eqs. (11b) and (4b)] yields an expression for p'/ρ' identical with that identified as $a_e{}^2$ in Eq. (17). A second means of identification of a_f and a_e is provided by the new Eq. (14) itself: If $\tau^* \to 0$, we must have equilibrium motion, and the second wave operator, which would dominate the motion, must be identical with the equilibrium wave operator, so that a_e is the equilibrium sound speed. Conversely, if we have a frozen process, the first operator dominates, and a_f must be the frozen sound speed. A more complete account of the derivation of Eq. (14) and the identification of sound speeds appears in reference 12.

In effect, therefore, Eq. (14) involves a combination of the two wave operators, frozen and equilibrium, one of which would be equated to zero separately if the process were purely frozen or purely equilibrium. If the relaxation time is long, the frozen operator will dominate Eq. (14), while in the opposite case, the equilibrium wave operator will govern the motion. It will be found that the latter state of affairs usually applies when a time long compared with the relaxation time has elapsed since the initiation of the wave.

The presence of the extra time derivative applied to the frozen operator implies that, during a given periodic disturbance, the frozen and equilibrium operators must be out of phase, so that both absorption and dispersion are present. Thus, a mechanism for the distortion of the wave form is apparent even in this linear approximation, suggesting the known decay of a wave packet.[5] In general, any given wave packet would include both low and high frequency components. The high frequency components are associated with the wave front and, as we shall see later, they propagate with the frozen speed of sound.

While the foregoing aspects of wave propagation in a relaxing gas are not in themselves new, it is interesting that they follow directly from the differential equation, Eq. (14). In the present formulation, the perturbations away from a uniform state may be of any degree of "frozenness." This is, the wave motions may involve all the wave speeds and absorption coefficients of a complete frequency spectrum.

For the special purpose of the present paper, we may write Eq. (14) in the following form, for steady two-dimensional flow with an undisturbed velocity $\bar{u}$:

$$(\phi_{XX} - \phi_{YY})_X + \phi_{XX} - K^2\phi_{VV} = 0 \quad (20)$$

where

$$\left.\begin{aligned} X &\equiv [(M^2 - k^2)/(M^2 - 1)](x/\bar{u}\tau^*) \\ Y &\equiv [(M^2 - k^2)/\sqrt{M^2 - 1}](y/\bar{u}\tau^*) \end{aligned}\right\} \quad (21)$$

and

† Identical in form to that derived by Morrison[11] for propagation of elastic waves in a material for which Hooke's law is subject to relaxation, in effect.

‡ See reference 10, in which Eq. (14) is shown to govern a temperature disturbance in a relaxing gas.

$$K^2 \equiv [(M^2 - 1)/(M^2 - k^2)]k^2; \quad k \equiv a_e/a_f; \quad M \equiv \bar{u}/a_f \tag{22}$$

Eq. (20) is, in effect, the two-dimensional Ackeret equation generalized to include the effect of relaxation, and applies when $\bar{u} > a_f$. The corresponding Prandtl-Glauert equation for subsonic steady two-dimensional flow ($\bar{u} < a_e$) is

$$(\phi_{X'X'} + \phi_{Y'Y})_{X'} + \phi_{X'X'} + K^2\phi_{Y'Y'} = 0 \tag{23}$$

where

$$X' \equiv X; \quad Y' \equiv [(k^2 - M^2)/\sqrt{1 - M^2}](y/\bar{u}\tau^*) \tag{24}$$

By manipulation of the basic Eqs. (4b), (8), (9), (11) and (12) together with the acoustic Eq. (20), one may relate the potential to the physical quantities of interest:

Expression of Flow Quantities in Terms of ϕ

$$u'/\bar{u} = \phi_X \tag{25}$$

$$v'/\bar{u} = \sqrt{M^2 - 1}\phi_Y \quad (\text{or } \sqrt{1 - M^2}\phi_{Y'}) \tag{26}$$

$$p'/\bar{p}^2\bar{u} = -\phi_X \tag{27}$$

$$\rho'/\bar{\rho} = -\{\phi_X + [(M^2 - 1)/K^2](\phi_{XX} - \phi_{YY} + \phi_X)\} \tag{28}$$

$$\beta' = -[\gamma_f/D(\gamma_f - \sigma)][(M^2 - 1)/K^2] \times [(1 - K^2)\phi_X + \phi_{XX} - \phi_{YY}] \tag{29}$$

$$T'/\bar{T} = -\frac{1}{(\gamma_f - \sigma)C_{v_f}}\left\{\left[\gamma_f M^2 - \sigma \times \left(1 + \frac{M^2 - 1}{K^2}\right)\right]\phi_X - \sigma\frac{M^2 - 1}{K^2}(\phi_{XX} - \phi_{YY})\right\} \tag{30}$$

The Telegraph Equation

Decay of a Discontinuous Wave Front

The solutions of Eqs. (20) and (21) may be investigated in certain circumstances to be described subsequently. However, being of third order, these equations are difficult to solve in general terms. Accordingly, it would seem desirable to effect a reduction in order of Eqs. (20) and (21). This may be done by making proper use of the observation, made in the Introduction, that, for a given process, a_e and a_f are nearly equal.

First, we may observe that if a_e and a_f are simply assumed equal, Eq. (20) may be integrated once to give

$$\phi_{XX} - \phi_{YY} = (\text{const.})e^{-X} \tag{31}$$

In order that reasonable boundary conditions may be applied at $x = -\infty$, the constant in Eq. (31) must be set equal to zero, and we recover the classical Ackeret equation. This result is degenerate, yielding no information concerning decay processes. It may also be shown that Eq. (31) is not a suitable basis for an iteration process. Nevertheless, it is obvious that, in some sense, we should have nearly the Ackeret theory for $1 - k \ll 1$.

In order to see how the approximation should properly be made, consider the propagation of a discontinuous wave in one-dimensional unsteady flow. A priori, we do not know what propagation velocities are permitted for a discontinuous wave. Therefore, we assume the head of the wave to be given by $X - sY = 0$, and determine s in the course of the analysis. If Eq. (14) is put into coordinates $X - sY$, $X + sY$, and integrated twice across the postulated discontinuity at $X + sY$, assuming that derivatives with respect to $X - sY$ are small compared to those with respect to $X + sY$, the second integration yields

$$s = 1 \quad (\text{or, } y/x = \sqrt{M^2 - 1}) \tag{32}$$

Thus, since $M \equiv \bar{u}/a_f$, any discontinuous wave front must propagate with frozen speed of sound[7,8] (in the acoustic approximation). The first integration yields the decay of the jump in normal velocity

$$\Delta[\partial\phi/\partial(X - Y)] \propto 1(X - Y)e^{-[(1-K^2)/2]Y} \tag{33}$$

Eq. (33) shows clearly that when $1 - K \ll 1$, the rate of decay is very slow, but that the solution is not uniformly convergent as $K \to 1$, $Y \to \infty$. However, Eq. (33) does suggest a scheme of successive approximations for one-dimensional unsteady or two-dimensional steady flows.

Derivation of the Telegraph Equation

We write

$$\phi(\xi, \eta) = \phi^{(0)}(\xi, \eta) + \epsilon\phi^{(1)}(\xi, \eta) + \epsilon^2\phi^{(2)}(\xi, \eta) + \ldots \tag{34}$$

where, by analogy with Eq. (33), for the supersonic case

$$\xi \equiv C(X - Y); \quad \eta \equiv \epsilon Y; \quad \epsilon \equiv (1 - K^2)/2 \tag{35}$$

and C is a constant of order one to be selected subsequently. Thus, we assume that the flow consists of waves starting at $Y = 0$, forming a pattern which may be described in terms of the single variable ξ (as in the Ackeret classical theory) together with a weak dependence on distance from the starting point. In terms of the variables defined in Eqs. (35), Eq. (20) may be given the form

$$\left(\frac{\partial}{\partial\xi} - \frac{\epsilon}{2C}\frac{\partial}{\partial\eta}\right)(\phi_{\xi\eta} + \phi_{\xi} + \phi_{\eta}) = \frac{\epsilon^2}{2C}\frac{\partial}{\partial\eta}\left[\frac{1 - C - 2\epsilon}{C\epsilon}\phi_{\eta} + \frac{3\epsilon - 2(1 - C)}{\epsilon^2}\phi_{\xi}\right] \tag{36}$$

Now, it is clear that C may be selected in terms of ϵ in such a way that the right-hand side of Eq. (36) is of order ϵ^2. For this purpose it is sufficient to specify that

$$C = 1 - (3/2)\epsilon + 0(\epsilon^2) \tag{37}$$

If the expansion Eq. (34) is substituted into Eq. (36), we find the simple equation

$$\phi_{\xi\eta}^{(0)} + \phi_{\xi}^{(0)} + \phi_{\eta}^{(0)} = 0 \tag{38}$$

apart from a function of η alone, which should be discarded for wave motions. The choice of C made in Eq. (37) provides that $\phi^{(1)}$ must also satisfy Eq. (38), and

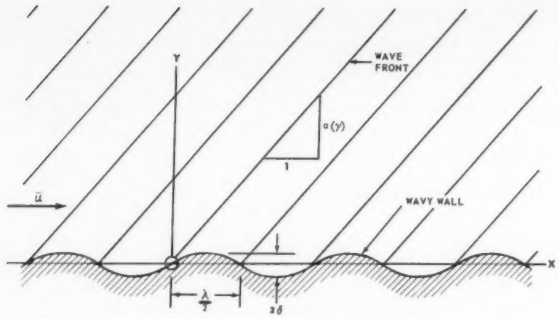

FIG. 3. Supersonic flow over an infinite wavy wall.

may be set equal to zero, provided the boundary conditions are satisfied by $\phi^{(0)}$ with sufficient accuracy. The first correction to $\phi^{(0)}$ is then given by $\phi^{(2)}$, and $\phi^{(0)}$ therefore represents ϕ with an error of order ϵ^2. Even this error may be made uniformly small in the whole flow field by a more complete specification of C. Specifically, it will later prove advantageous to make the selection [consistent, of course, with Eq. (37)]:

$$C \equiv (1/2)(1 - 2\epsilon + \sqrt{1 - 2\epsilon}) = (1/2)K(1 + K) \quad (39)$$

Eq. (38) is a variant of the telegraph equation which governs a class of wave motions in which absorption and dispersion takes place (electric waves, water waves, etc.). Returning to X, Y coordinates, Eq. (38) is

$$\phi_{XX}^{(0)} + \phi_{XY}^{(0)} + [(1 + K)/2]\,(\phi_X^{(0)} + K\phi_Y^{(0)}) = 0 \quad (40)$$

For the subsonic case, we may note that Eqs. (23) and (24) are obtained from Eqs. (20) and (21) by the formal substitution $Y = \pm iY$. With this change, Eq. (38) governs the solution

$$\phi = \Re\{\phi^{(0)}(X' \pm iY',\ \pm i\epsilon Y')\} + 0[\epsilon^2] \quad (41)$$

We may now summarize the assumptions by which Eq. (20) is reduced to Eq. (38) as follows: (1) the flow is in two dimensions (one of which may be time); (2) the wave pattern consists essentially of one family, i.e., without relaxation, $\phi = \phi(\xi)$; and (3) the decay process is slow, owing to the closeness of the frozen and equilibrium sound speeds. On this account, the Y coordinate is contracted by the factor ϵ. The $(X - Y)$ coordinate is also contracted, by the factor C, in order to enhance the accuracy of Eq. (38). In the following sections we shall discuss certain particular flow problems chosen to illustrate the application of Eq. (38).

The Wavy Wall

Supersonic Case

A classical application of Ackeret theory concerns the supersonic flow over a wavy wall of infinite extent (Fig. 3). A harmonic wave pattern of constant strength is produced, inclined downstream at the Mach angle. Relaxation affects the wave inclination and introduces a decay of the wave as they proceed outward. We may anticipate that the solution has the form

$$\phi = A \exp\left(i\nu\{X - [Y/a(\nu)]\} - b(\nu)Y\right) \quad (42)$$

where $a(\nu)$ is the (unknown) slope of the wave pattern, and $b(\nu)$ is the decay rate.

At the wall ($Y = 0$), the normal velocity is proportional to

$$[b + i(\nu/a)]^{-1}(\phi_Y)_w = -Ae^{i\nu X} \quad (43)$$

If the wall has a wavelength λ and a height δ, reference to Eqs. (21) shows that

$$\left.\begin{aligned} \nu &= 2\pi[(M^2 - 1)/(M^2 - k^2)](\bar{u}\tau^*/\lambda) \\ A &= -(2\pi\delta/\lambda)/\{\sqrt{M^2 - 1}[(\nu/a) - ib]\} \end{aligned}\right\} \quad (44)$$

Substitution of Eq. (42) into Eq. (20) yields a complex equation from which $a(\nu)$ and $b(\nu)$ may be determined:

$$b(\nu) + i[\nu/a(\nu)] = i\nu\sqrt{(1 + i\nu)/(K^2 + i\nu)} \quad (45)$$

This is the "exact" solution of the problem, and corresponds to the Kneser theory of the ultrasonic absorption.[5,14] If, instead, we use the "telegraph" Eq. (40), we find

$$\left.\begin{aligned} a(\nu) &= \frac{4\nu^2 + K^2(1 + K)^2}{4\nu^2 + K(1 + K)^2} \\ b(\nu) &= \frac{1 - K^2}{2}\,\frac{4\nu^2}{4\nu^2 + K^2(1 + K)^2} \end{aligned}\right\} \quad (46)$$

Comparing Eqs. (45) and (46) gives an evaluation of the success of the telegraph approximation. We may note that, in the frozen limit ($\nu \to \infty$), both sets of equations agree:

$$a(\infty) = 1;\ b(\infty) = (1 - K^2)/2 \quad (47)$$

which means that the waves are inclined at the frozen Mach angle, and the decay rate is the same as for a discontinuous wave front [Eq. (33)]. In the equilibrium limit ($\nu \to 0$), both equations give

$$a(0) = K \quad (48)$$

which, through Eqs. (20) and (21), may be shown to describe the equilibrium wave inclination. The agreement as to $b(\nu)$ {actually, $\lim_{\nu \to 0}[b(\nu)/\nu^2]$} is complete to order ϵ.

We may recall here that a precise specification of the constant C was made in Eq. (39) in order to fix the coordinate transformation leading to the telegraph equation. It may be shown that the selection made is the only one of the class satisfying Eq. (37) which provides exact agreement between Eqs. (45) and (46) as to the inclination of an equilibrium wave. In fact, it may be shown that this selection of C provides that the right-hand side of Eq. (36) vanishes for an equilibrium wave. Thus, in summary, the "telegraph approximation" is correct to order ϵ in general, is made exact in the frozen limit by the choice of ϵ [Eq. (35)], and made exact as to wave inclination in the equilibrium limit by the choice of C [Eq. (39)]. The agreement between Eqs. (45)

and (46) has been calculated as a function of ν for $\epsilon = 0.3$. The maximum discrepancy between the a's is about 1 per cent, and between the b's, $2^1/_2$ per cent.

From Eq. (27), the drag coefficient for one wavelength of the wavy wall is

$$\text{Drag}/(1/2)\bar{\rho}\bar{u}^2\lambda = (a/\sqrt{M^2-1})[2\pi(\delta/\lambda)]^2\{1/[1+(ab/\nu)^2]\} \quad (49)$$

which differs from the classical Ackeret result by the last factor which has a minimum value of $4K/(1+K)^2$ when

$$\lambda/\bar{u}\tau^* = 4\pi\sqrt{K}/k^2(1+K) \quad (50)$$

The effect is small for reasonable values of K. For example, if $k = 0.8$ and $M = 1.2$, then $K \approx 0.6$, and the maximum effect of dispersion is to diminish the drag by 7 per cent when $\lambda = (7.7)\bar{u}\tau^*$.

Subsonic Case

We may immediately write down the telegraph solution for the case when a subsonic flow exists over the wavy wall by changing Y to $-iY'$ in Eq. (42):

$$\phi = A\exp\left(i\nu\{X' + [b(\nu)/\nu]Y'\} - [\nu/a(\nu)]Y'\right) \quad (51)$$

Eqs. (44) still apply, making the identification $\sqrt{M^2-1} = -i\sqrt{1-M^2}$. The telegraph solution yields Eqs. (46) as before. Now, however, the roles of a and b are reversed. In the classical case, $a = 1$ and $b = 0$. Thus, a modifies the classical potential decay, while b tends to introduce a tilt of the "wave front" which, in the classical case, is perpendicular to the wall.

An interesting consequence of this inclination is that the wavy wall experiences drag owing to relaxation, as shown previously by Ackeret[13] for the special case of vibrational relaxation. Per unit wave length,

$$\frac{\text{Drag}}{(1/2)\bar{\rho}\bar{u}^2\lambda} = \frac{1}{\sqrt{1-M^2}}\left(2\pi\frac{\delta}{\lambda}\right)^2\left[\frac{-(ab/\nu)}{1+(ab/\nu)^2}a\right] \quad (52)$$

This drag vanishes in the two limits $\nu \to 0$ and $\nu \to \infty$, and has a maximum value governed by the maximum absolute value which ab/ν can attain. (We note that, while $K < 1$ in the supersonic case, in the subsonic case $K > 1$, and thus $b < 0$.) When $k = 0.8$ and $M = 0.6$, then $K = 1.2$, and, in these circumstances, the largest value of the square bracket in Eq. (52) is about 0.1, occurring when $\lambda \approx (13)\bar{u}\tau^*$. The variation of the square bracket with $\lambda/\bar{u}\tau^*$ is shown in Fig. 4. It is remarkable that the drag coefficient is near its largest value when λ is so large compared with $\bar{u}\tau^*$ that purely equilibrium conditions would perhaps be expected.

Finally, we may note that in the limit $M \to 0$, Eq. (22) shows that $K \to 1$ for all k, so that $a \to 1$ and $b \to 0$, whatever the value of ν. Thus, when the Mach Number vanishes, the classical solution applies. On the other hand, the present analysis suggests a particularly powerful effect of relaxation in the transonic regime, where $K \to \infty$ from the subsonic side and $K \to 0$ from the supersonic side. This type of problem is beyond the scope of the present linearized analysis, however.

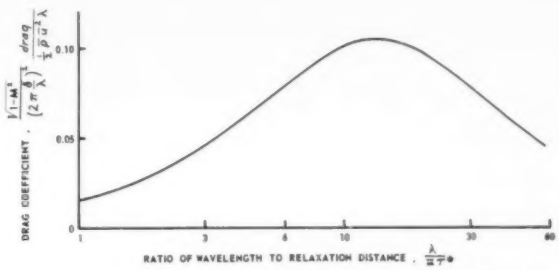

FIG. 4. Drag coefficient of wavy wall in subsonic flow, $k = 0.8$, $M = 0.6$.

The Supersonic Airfoil

General Telegraph Solution for an Airfoil

We consider now the more general problem of weak disturbances produced in a gas subject to relaxation flowing supersonically over a surface having slight changes in slope—in effect, the two-dimensional Ackeret problem. The solutions to be described also apply, in different coordinates, to the unsteady one-dimensional motion produced by the movement of a piston face.

If the local slope of the surface is given by $f(\xi)$, then the linearized boundary condition to be applied at the plane $Y = 0$ is

$$(v/\bar{u})_w = \sqrt{M^2-1}(\phi_Y)_w = f(\xi) \quad (53)$$

If the configuration has a leading edge, there will be a frozen wave emanating from that point, and upstream of this wave, the gas is to be at rest. The solution of Eq. (38) subject to these boundary conditions is

$$\sqrt{M^2-1}\,\phi_Y = e^{-(\xi+\eta)}(\partial/\partial\xi) \times \int_0^\xi I_0[2\sqrt{\eta(\xi-\omega)}]\,e^{\omega}f(\omega)d\omega \quad (54)$$

Eq. (54) may be obtained by application of the method of Laplace transformation to Eq. (38). The previous supersonic solution for a wavy wall [Eq. (42)] could, of course, be derived from Eq. (54) by selecting $f(\omega)$ to be a harmonic wave.

The dependence of Eq. (54) on η is a measure of the effect of relaxation. We may recover the Ackeret solution by formally setting $\eta = 0$. Then, since $I_0(0) = 1$, Eq. (54) would give $\sqrt{M^2-1}\,\phi_Y = f(\xi)$, which is the classical result. The leading-edge frozen wave is obtained by taking the limit of Eq. (54) as $\xi \to 0$, with the result

$$\lim_{\xi\to 0_+}(\sqrt{M^2-1}\,\phi_Y) = e^{-\eta}f(0) \quad (55)$$

which is exactly Eq. (33) describing the decay of a discontinuous wave front.

Evaluation of ϕ_X and $\phi_{XX} - \phi_{YY}$

In order to use Eq. (54) to give a full description of the flow, we must have expressions for ϕ_X and $\phi_{XX} - \phi_{YY}$ appearing in Eqs. (25)–(30). Manipulation of Eq. (40) together with Eq. (54) yields the results

$$\phi_X = -\phi_Y + \epsilon\int_Y^X e^{-[(1+K)/2](X-\omega)}\,\phi_Y(\omega, Y)d\omega \quad (56)$$

$$[2/\epsilon(1+K)(\phi_{XX}-\phi_{YY}) = [4\phi_Y/(1+K)] - \int_0^X [e^{-[(1+K)/2](X-\omega)} + Ke^{-[K(1+K)/2](X-\omega)}]\phi_Y d\omega + \int_0^Y \{Ke^{-[K(1+K)/2](X-\omega)} + (1-K)e^{-[(1+K)/2](X-\omega)} + Ke^{-[(1+K)/2][KX+(1-K)Y-\omega]}\}\phi_Y d\omega \quad (57)$$

Generally, it would be desired to evaluate Eqs. (25)–(30) on the airfoil. For this purpose we set $Y = 0$ in Eqs. (56), (57):

$$\sqrt{M^2-1}\,(\phi_X)_w = -f^*(X) + \epsilon\int_0^X e^{-[(1+K)/2]}f^*(\omega)d\omega \quad (58)$$

$$[2\sqrt{M^2-1}/\epsilon(1+K)](\phi_{XX}-\phi_{YY})_w = [4/(1+K)]f^*(X) - \int_0^X [e^{-[(1+K)/2](X-\omega)} + Ke^{-[K(1+K)/2](X-\omega)}]f^*(\omega)d\omega \quad (59)$$

where, at the same X, $f^*(X) = f(\xi)$.

In reference 12, a study of the exact Eq. (20) is made, and, while a general solution corresponding to Eqs. (54) and (56), (57) is not found, it is possible to derive the solution at the airfoil surface. Comparison of these results with Eqs. (58), (59) thus gives a measure of the accuracy of the telegraph equation. The exact expressions are in the same form as Eqs. (58), (59), with somewhat different integrands. It is found that the maximum error of the integrand in Eq. (58) is about 2 per cent, while the maximum error of the integrand in Eq. (59) is about 5 per cent. Generally, the errors are much less than these extremes; in fact, the errors integrated over the infinite range of X are both zero.

Solution for a Simple Wedge

Let us now apply the solution, Eq. (54), to the case of a simple wedge, for which

$$f^*(X) = f(\xi) = \Theta 1(\xi)$$

where Θ is the constant semiangle of the wedge and $1(\xi)$ is the unit step function. Eq. (54) becomes

$$(\sqrt{M^2-1}/\Theta)\phi_Y = e^{-(\xi+\eta)}(\partial/\partial\xi)\int_0^\xi I_0[2\sqrt{(\eta\xi-\omega)}]e^{\omega}d\omega \quad (60)$$

When $Y = 0$, of course, $\phi_Y = \Theta/\sqrt{M^2-1}$, and, from Eq. (55), the frozen wave from the leading edge gives a discontinuous jump in ϕ_Y from zero to $\Theta(M^2-1)^{-1/2}e^{-\eta}$. These features are illustrated in Fig. 5. Although the frozen discontinuity decays with distance, it does not follow that the entire flow disturbance vanishes at infinity. Rather, the disturbance develops into a dispersed wave centered on the equilibrium Mach wave from the leading edge. Specifically, a study of the asymptotic behavior of Eq. (54) for large η shows that, for the wedge,

$$\phi_Y \overset{a}{=} (\Theta/\sqrt{M^2-1})(1/\sqrt{\pi}) \times \int_{-\infty}^{[(1+K)/4][(KX-Y)/\sqrt{\epsilon Y}]} e^{-\omega^2}d\omega \quad (61)$$

when $\eta = \epsilon Y$ is large, but $KX - Y$ is finite. Thus, Eq. (61) applies near the equilibrium Mach line, for which $KX - Y = 0$. Eq. (61) represents a rise in ϕ_Y from an initial value of 0 to a final value of $\Theta(M^2-1)^{-1/2}$, accomplished over a distance, measured along a streamline, proportional to $\sqrt{\epsilon Y}$. This parabolic dispersion of the equilibrium wave which takes over, so to speak, from the decaying frozen wave is illustrated in Fig. 5. This feature of wedge flow also appears in the analogous unsteady case of a piston started impulsively from rest.[8]

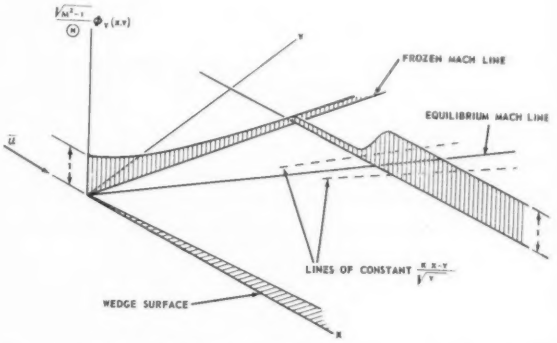

FIG. 5. Variation of normal velocity along the frozen Mach line and a line Y = constant far from the wedge surface.

From Eq. (20), an exact expression may be derived for the asymptotic behavior of wedge flow. Comparison with Eq. (61) provides a further check on the accuracy of the telegraph equation. In reference 12, it is shown that the exact asymptotic formula differs from Eq. (61) only in that the quantity $(1/4)(1+K)$ appearing in the upper limit should be replaced by $(1/2)\sqrt{K}$. The ratio of the former quantity to the latter is greater than one by the small quantity $\epsilon^2/8$, to a first approximation. Thus, the telegraph solution gives a rate of equilibrium wave dispersion very slightly greater than the exact value. For $\epsilon = 0.3$, the error is about 1 per cent.

Other Flow Quantities for the Wedge

The foregoing discussion deals only with the normal velocity field. We may complete the description of the flow by application of Eqs. (25)–(30) and (56), (57), or (58), (59). The results on the wedge surface may conveniently be expressed as follows:

$$p' = p_e' + (p_f' - p_e')e^{-[(1+K)/2]X} \quad (62)$$

$$\rho' = \rho_e' + (1/2)(\rho_f' - \rho_e')[e^{-[(1+K)/2]X} + e^{-[K(1+K)/2]X}] \quad (63)$$

$$\beta' = \beta_e'\{1 - (1/2)[e^{-[(1+K)/2]X} + e^{-[K(1+K)/2]X}]\} \quad (64)$$

$$T' = T_e' + (1/2)(T_f' - T_e')[e^{-[(1+K)/2]X} + e^{-[K(1+K)/2]X}] \quad (65)$$

where the subscripts f and e denote the values which would apply if the flow were purely frozen or purely equilibrium. In each case, near the leading edge ($X = 0$) frozen values apply ($\beta_f = 0$, of course), and far from the leading edge ($X \to \infty$), equilibrium values apply. These values are, in present notation,

$$p_e' = Kp_f' = \bar{p}K\gamma_f(\Theta M^2/\sqrt{M^2 - 1}) \quad (66)$$

$$\left.\begin{aligned}\rho_e' &= \bar{\rho}\{1 + [(M^2 - 1)/K^2]\}(K\Theta/\sqrt{M^2 - 1}) \\ \rho_f' &= T_f'/(\gamma_f - 1) = M^2\Theta/\sqrt{M^2 - 1}\end{aligned}\right\} \quad (67)$$

$$\beta_e' = [\gamma_f/D(\gamma_f - \sigma)][(1 - K^2)/K]\Theta\sqrt{M^2 - 1} \quad (68)$$

$$T_e' = [(\gamma_f - 1)/(\gamma_f - \sigma)]\{(\gamma_f M^2 - \sigma\{1 + [(M^2 - 1)/K^2]\})(K\Theta/\sqrt{M^2 - 1}) \quad (69)$$

In Eqs. (62)–(65) the coefficients of the exponentials are given to zero order in ϵ. Actually, we are entitled to keep terms of first order. However, it may be shown that, in these formulas, the terms of order ϵ are very small. The exponents are written "exactly," however, inasmuch as they can embody errors only of order ϵ^2, and comparison with the exact solution has shown these errors to be extremely small.

In order to evaluate flow properties in the flow field, the direct procedure would be to use Eqs. (56), (57). However, recalling that all flow properties satisfy the same differential equation (20) and hence (38), it is simpler to re-solve Eq. (38) with boundary conditions specified, in turn, by Eqs. (62)–(65). In each of these, constant terms are linearly combined with exponential terms of the types

$$\exp\{-[(1 + K)/2]X\} = e^{-\xi/K}$$

$$\exp\{[K(1 + K)/2]X\} = e^{-\xi}$$

Corresponding to the constant terms, the solution already calculated for ϕ_Y [Eq. (60)] may be adapted by inserting the proper constant. Now, the telegraph solution for a boundary value of $f(\xi) = e^{-\xi/K}$ is, from Eq. (54),

$$e^{-\xi+\eta}(\partial/\partial\xi)\int_0^\xi I_0[2\sqrt{\eta(\xi - \omega)}]e^{[1-(1/K)]\omega}d\omega \quad (70)$$

For boundary values $e^{-\xi}$, Eq. (54) yields the simple solution

$$e^{-(\xi+\eta)}I_0[2\sqrt{\eta\xi}] \quad (71)$$

Fig. 6 presents calculations for $v/\bar{u}$, β'/β_e', and p'/p_f' carried out by forming the appropriate linear combinations of Eqs. (60), (70), and (71).

Discussion of Results for Wedge Flow

The Relaxation Distance

It is interesting to relate the calculated relaxation of β' to the effective relaxation time τ^*. From Eq. (64), we see that the surface value of β' reaches its equilibrium value in a distance which we may characterize by the "displacement integral"

$$X_\tau = \int_0^\infty [1 - (\beta'/\beta_e')]dX = 1/K \quad (72)$$

Introducing definitions (15) to (16), (21), (22),

$$x_\tau/\bar{u}\tau^* = (1/k)\sqrt{(M^2 - 1)/(M^2 - k^2)} \quad (73)$$

Thus, except when M is near 1, the relaxation distance $x_\tau \approx \bar{u}\tau^*$, which is the distance traveled by the stream during the effective relaxation time. However, as $M \to 1$, the relaxation distance becomes shorter compared with $\bar{u}\tau^*$. Thus, the present linearized study suggests the possibility of a pronounced tendency of transonic flows of a relaxing gas to remain in equilibrium. A nonlinear analysis would be required to make this point more definite.

The distinction between τ and τ^* should perhaps be clarified at this point. In a gas at constant density and temperature, τ as defined in Eq. (6a) governs the relaxation rate. In the adiabatic process described in this study, the effective relaxation time τ^* is shorter than τ by an amount depending on the exchange of energy between the relaxing degree of freedom and the various other excited modes. In the case of vibrational relaxation, estimates of the terms in Eq. (15) suggest that $0.7 < \tau^*/\tau < 1$. Similar estimates suggest that τ^*/τ is very small for dissociation relaxation—of the order of 0.1. Finally, it may be remarked that relaxation times measured by shock-tube methods would correspond more closely to the present τ^* than to τ.

Application to a Sequence of Relaxation Processes

Figs. 5 and 6 provide a picture of how the wave produced by a simple wedge has first a frozen character

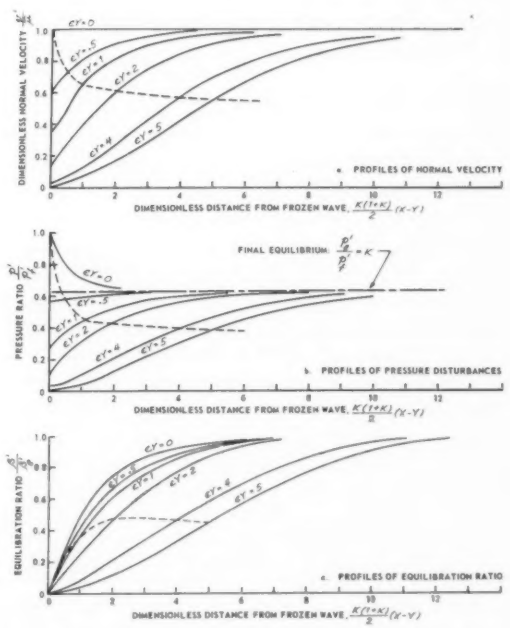

FIG. 6. Profiles of flow quantities along streamlines of supersonic flow over a simple wedge, $K^2 = 0.4$. Dashed lines represent location of equilibrium Mach line.

and subsequently changes to a dispersed equilibrium wave. Here, "frozen" and "equilibrium" refer to a chosen degree of freedom, others being assumed to be either completely frozen or in complete equilibrium. Since the wedge has no geometrical length, the foregoing point of view has meaning only in reference to an assumed scale of observation. Thus, if we state that Fig. 5 applies for dissociation relaxation, then, if we magnify the vicinity of the leading edge, we must see the same pattern appear again with reference to vibrational relaxation.

In other words, the vibrationally frozen Mach wave decays over a very short distance, a dispersed wave in vibrational equilibrium appears, and this latter wave decays over a much longer distance as a chemically frozen wave. In a gas with a number of degrees of freedom with widely different relaxation times, it is easy to imagine this sort of repetition of Fig. 5 at successively larger scale.

One point, however, needs to be established in order that the foregoing description be valid. We know that an equilibrium wave spreads parabolically—can we regard this spreading wave as a discontinuity on the larger scale of the next, slower, relaxation process? From Eqs. (61) and (21), the spatial width of a wave in vibrational equilibrium is proportional to $\sqrt{\bar{u}\tau_v{}^* y\epsilon_v}$. This distance is to be compared with the basic distance involved in dissociative relaxation, $\bar{u}\tau_d{}^*$. The appropriate ratio of distances is

$$\sqrt{\bar{u}\tau_v{}^* y\epsilon_v}/\bar{u}\tau_d{}^* = \sqrt{(\tau_v{}^*/\tau_d{}^*)(\epsilon_v/\epsilon_d)\eta} \qquad (74)$$

where η is based on dissociation. Now, the wave in question will be essentially decayed when η reaches 2 or 3. Thus, since ϵ_v/ϵ_d is of order 1, the thickness is always much less than $\bar{u}\tau_d{}^*$ if $\sqrt{\tau_v{}^*/\tau_d{}^*} \ll 1$. This, of course, is the assumption we have made throughout this study.

Connection With Viscous Dispersion

In the flow field produced by a wedge in a gas subject to relaxation, an analogy holds between the ultimate equilibrium wave (Fig. 5) which spreads parabolically and the effect of normal viscous stresses in spreading a sound wave. This analogy can be formalized by the definition of an equivalent viscosity in terms of the sound-speed difference ϵ. It should be emphasized that the analogy applies only in a near-equilibrium flow[14] and not to an entire field of disturbance produced in a relaxing gas.

This point may be clarified by reference to the "Burgers equation" adopted by Lighthill[14] to study viscous dispersion of one-dimensional sound waves. If this equation is linearized it has the form

$$\phi_{\zeta\zeta} - \phi_t = 0 \qquad (75)$$

where ζ is a suitably nondimensionalized distance measured normal to the wave front. The analogous equation from the present study is the telegraph equation for one-dimensional unsteady motion, which is formally identical with Eq. (40) if X is replaced by a dimensionless time. If a change of variables is introduced so that distance ζ is measured normal to a wave front traveling at equilibrium speed, the telegraph equation reads approximately

$$\phi_{\zeta\zeta} - \phi_t + \phi_{\zeta t} = 0 \qquad (76)$$

Eqs. (75) and (76) are fundamentally different, and, hence, no strict analogy exists between the effects of viscosity and relaxation. However, the dispersed wave

$$\phi = \int_{-\infty}^{\zeta/2\sqrt{t}} e^{-\omega^2} d\omega \qquad (77)$$

which satisfies Eq. (75) exactly is also the asymptotic solution of Eq. (76) for large t [compare Eq. (61)]. Thus, there is a strict equivalence for the ultimate equilibrium wave.

Remarks on Wave Steepening

In the classical Ackeret theory for a wedge, a discontinuous leading-edge wave extending to infinity provides at least a qualitatively correct picture of the oblique shock which actually occurs. In the acoustic approximation for a gas subject to relaxation, the discontinuous (frozen) wave decays and the remaining equilibrium pattern disperses. Thus, in the linear theory, there is no possible qualitative representation of an oblique shock in the usual sense.

A shock wave is, of course, the result of a balance between nonlinear wave steepening and viscous dispersion. The classical acoustic theory accounts for neither of these effects, while the present theory considers dispersion (owing to relaxation rather than viscosity), but neglects nonlinear steepening. Thus, it is natural that the ultimate wave pattern is quite unlike an oblique shock.

This state of affairs is realistic for weak waves. As Lighthill[14] has shown, a permanent type of shock satisfying a set of Rankine-Hugoniot conditions cannot exist unless the wave has sufficient strength, and hence shock velocity, to keep pace with, or overtake, waves propagating at the frozen sound speed.

Concluding Remarks

The chief purpose of the present paper has been to show how the problem of small disturbances of a gas subject to relaxation may be approached by the method, traditional in fluid mechanics, of setting up a single differential equation which can satisfactorily represent a variety of phenomena. Many specific phenomena described here have been separately described by previous investigators.[5, 7, 8, 14]

In view of the aerodynamic interest in flows involving vibrational or chemical excitation, we have chosen to emphasize formulation of the theory for steady flow. The same approach, and, in fact, the same differential equation for ϕ, applies in unsteady flow with one less dimension. It should be pointed out that the small perturbation theory as presented does not have the

ready applicability to problems of hypersonic flight that the corresponding Ackeret theory has had in supersonics. The basic flow in the present theory cannot be identified as a free stream in the usual aerodynamic sense, but rather as a steady uniform flow produced behind a strong shock, for example.

In connection with external aerodynamics of hypersonic high-altitude flight, the present theory might be applicable to certain control surface problems. Certain internal aerodynamic problems in propulsive flows of highly excited gases would be amenable to the present approach. A further application may be cited in connection with experimental research: the behavior of sound waves in a flow field produced in a shock tube[15] or tunnel may, subject to theoretical interpretation, provide a means of determining either the state of a gas or basic information concerning relaxation times.

A final general observation may be made from the results of the present study. The flow distance required to effect equilibration is related to the product of velocity and relaxation time only as to order of magnitude, in general. Significantly shorter equilibration distances may be found in near-transonic flow, while on the other hand, the drag of a wavy wall can be most strongly affected when the wave length is many times longer than the product of velocity and relaxation time. In other words, the equilibration process is strongly dependent on the particular flow in which relaxation occurs.

References

[1] Blackman, V. H., *Vibration Relaxation in O_2 and N_2*, Technical Report II-20, Princeton University, May, 1955.

[2] Glick, H. S., Klein, J. J., and Squire, W., *Single Pulse Shock Tube Studies of the Kinetics of the Reaction $N_2 + O_2 \rightleftharpoons 2\ NO$ Between 2,000–3,000°K.*, J. Chem. Phys., Vol. 27, No. 4, p. 850–857, October, 1957.

[3] Logan, J. G., Jr., *Relaxation Phenomena in Hypersonic Aerodynamics*, Presented at the IAS 25th Annual Meeting, New York, January 28–31, 1957.

[4] Byron, S. R., *Interferometric Measurement of the Rate of Dissociation of Oxygen Heated by Strong Shock Waves*, Cornell University Graduate School of Aeronautical Engineering Report Contract N401(25). See also Glick, H. S., and Wurster, W. H., *A Shock Tube Study of Dissociation Relaxation in Oxygen*, J. Chem. Phys., Vol. 27, No. 5, p. 1224–1226, November, 1957.

[5] Herzfeld, K. F., *Thermodynamics and Physics of Matter* Princeton Series, Section H, "Relaxation Phenomena in Gases," p. 646–735, 1955.

[6] Treanor, C. E., and Logan, J. G., *Tables of Thermodynamic Properties of Air from 3,000° K. to 10,000°K.*, C.A.L. Report No. AD-1052-A-2, AFOSR TN 56-243, AD 95219, June, 1956.

[7] Wood, W. W., and Kirkwood, J. G., *Characteristic Equations for Reactive Flow*, J. Chem. Phys., Vol. 27, No. 2, p. 596, 1957.

[8] Chu, B.-T., *Wave Propagation and the Method of Characteristics in Reacting Gas Mixtures with Applications to Hypersonic Flow*, Brown University, WADC TN-57-213, AD 118350, May, 1957.

[9] Resler, E. L., Jr., *Characteristics and Sound Speed in Nonisentropic Gas With Nonequilibrium Thermodynamic States*, Journal of the Aeronautical Sciences, Vol. 24, No. 11, p. 785–791, November, 1957.

[10] Moore, F. K., *Propagation of Weak Waves in a Dissociate Gas*, Readers' Forum, Journal of the Aero/Space Sciences, Vol. 25, No. 4, p. 279–80, April, 1958.

[11] Morrison, J. A., *Wave Propagation in Rods of Voigt Material and Visco Elastic Materials with Three Parameter Models*, Quart. Appl. Math., Vol. 14, pp. 153–169, 1956–57.

[12] Gibson, W. E., and Moore, F. K., *Acoustic Propagation in a Diatomic Gas Subject to Thermal or Chemical Relaxation*, C.A.L. Report No. HF-1056-A-2, AF OSR TN 58-1057, AD 205988, October, 1958.

[13] Ackeret, J., *Über Widerstände die Durch Gasdynamische Relaxation Hervorgerufen Werden*, Zeitschr. für Flugwiss. 4, Heft 1/2, pp. 14–17, 1956.

[14] Lighthill, M. J., *Survey in Mechanics and Applied Mathematics*, "Viscosity Effects in Sound Waves of Finite Amplitude," Cambridge University Press, p. 250–351, 1956.

[15] Camac, M., Camm, J., Feldman, S., Keck, J., and Petty, C., *Chemical Relaxation in Air, Oxygen, and Nitrogen*, paper presented at the IAS 26th Annual Meeting, New York, January 27–30, 1958.

Large Deflections of Structures

(*Continued from page 106*)

[3] Melosh, R. J., and Merritt, R. G., *Evaluation of Spar Matrices or Stiffness Analyses*, Journal of the Aeronautical Sciences, Vol. 25, No. 9, pp. 537–543, September, 1958.

[4] Bisplinghoff, R. L., *Some Structural and Aeroelastic Considerations of High Speed Flight*, Journal of the Aeronautical Sciences, Vol. 23, No. 4, pp. 289–329, 367, April, 1956.

[5] Kochanski, S. L., and Argyris, J. H., *Some Effects of Kinetic Heating on the Stiffness of Thin Wings*, Aircraft Engineering, Vol. 29, No. 344, October, 1957 (and subsequent issues).

[6] Singer, J., and Hoff, N. J., *Effect of the Change in Thermal Stresses Due to Large Deflections on the Torsional Rigidity of Wings*, Readers' Forum, Journal of the Aeronautical Sciences, Vol. 24, No. 4, p. 310, April, 1957.

[7] Bisplinghoff, R. L., *The Finite Twisting and Bending of Heated Elastic Lifting Surfaces*, Ph.D. Thesis, The Swiss Federal Institute of Technology, Zurich, Switzerland, 1957.

[8] Hemp, W. S., *Fundamental Principles and Theorems of Thermo-Elasticity*, The Aeronautical Quarterly, Vol. VII, Part 3, August, 1956.

[9] Novozhilov, V. V., *Foundations of the Nonlinear Theory of Elasticity*, Graylock Press, Rochester, New York, 1953.

A Statistically Averaged Error Criterion for Feedback-System Synthesis

JOHN ZABORSZKY* AND JOHN W. DIESEL**

McDonnell Aircraft Corporation

Summary

A performance criterion for feedback control systems is introduced based on the averaging of penalized error values over such times when the output is actually utilized. This is accomplished by assigning a probability to the time of output utilization. The criterion is a suitable starting point of design since it unifies in one summary the various specifications normally used to describe special aspects of performance. Where the penalty is proportional to the squared error, mathematical methods are developed for two roles: (1) evaluating the criterion for a given system operating in a known environment, and (2) designing the optimum time-invariant linear system, in the sense of giving the smallest average-penalized-error criterion value operating in a known input environment. An illustrative example is given.

Survey of Performance Criteria

AUTOMATIC CONTROL is, in one sense, at least as old as the first governors applied on early steam engines and, in another sense, as recent as World War II. As a field of engineering analysis and design, automatic control, feedback control, and servomechanisms were developed in the years around the beginning of World War II as a specialty of electrical engineering. Considering that the major portion of most systems controlled is nonelectrical, the predominance of electrical engineers in the early developing field of controls seems to be surprising. The reasons for this predominance are threefold. Among the members of the engineering fraternity electrical engineers were equipped with some intuition in transient phenomena. Electrical engineers had tools available for the analysis of feedback devices—that is, amplifiers. The necessary corrective devices were synthesized in the form of electric networks with the least difficulty in hardware and in theory of design.

Performance criteria were from the beginning the guiding factors in the development of the field, and their gradual refinement simultaneously served as an index of the state of the art.

The first criteria were characteristically indirect in nature. Since the early analysis and synthesis methods were borrowed from the field of feedback amplifiers, the performance criteria were based on frequency response considerations;[1–3] notably, sharpness and frequency location of resonance peaks were specified in addition to rough indices of stability (Nyquist, Nichols, Bode criteria). This was done with the realization that the actual operating input environment of control systems is not one of steady sinusoidal inputs, but rather a sequence of arbitrary changes followed by transient adjustments. However, it was found that semiquantitative relationships exist between frequency and transient responses so that a system of certain resonance characteristics will exhibit satisfactory transient response features, of which "stability" is one aspect. This line of development led through refinements of the relationships between transient and frequency response. These relations follow from the fact that both responses are determined by the location of poles and zeros in the Laplace transforms of the system impulse responses, called transfer functions. Methods[4–7] emerged to actually locate these poles and zeros. Simultaneously the emphasis in performance criteria shifted toward direct consideration of the transient response[8, 9] by specifying peak overshoot, rise time, settling time, steady-state error, etc., with specified step or ramp inputs. This type of criterion was extended in recent years into the area of nonlinear control.[10–13]

As far as performance criteria are concerned, this line of development at present culminates in efforts[14–18] to condense in a single index of performance the various aspects of the transient response. These criteria usually take the form of the general integral error criterion

$$\text{Index of performance} = \int_0^\infty F(e)\, w(t)\, dt \qquad (1)$$

with $w(t)$ defined as an arbitrary weighting function. Specifically $w(t) = t$ and $w(t) = t^2$ were investigated.[15, 16] The resulting index of performance has no clear meaning but its reduction is supposed to signal an improvement in the transient response. The selection of the $w(t)$ weighting function has been described as an art.[17] The argument for selecting a specific $w(t)$ function customarily is that it leads (through cut-and-try) to optimum systems (pinpointed by minima of the index of performance) which exhibit transient responses that are "very good" as a designer would view them, or superior to those produced by some other criterion. Standard systems of varying orders were established by cut-and-try on the analog computer on the basis of such criteria, but no direct synthesis technique was developed on this basis previously.

The penalty function $F(e)$ in Eq. (1) is usually

Received December 22, 1958. Revised and received October 5, 1959.

* Consultant. Also, Professor of Electrical Engineering at Washington University.

** Dynamics Engineer.

simply e^2, the square of the error, although $|e|$ has also been used. Recently it has been proposed[19, 20] to use an $F(e)$, which is a linear combination of the squares of the error and its various derivatives (or some other system variables) as well as the square of some quantity (such as m, the driving torque requirement) which is to be limited. That is

$$F(e) = \sum_n a_n(d^n e/dt^n)^2 + bm^2 \qquad (2)$$

with a_n and b constants.

This form of the criterion is ideally suited for the design[20] of a special class of control systems called "dead beat," that is, systems which come to complete equilibrium after a finite time following a step disturbance. If n in Eq. (2) covers a range equal to the order of the system, then clearly zero value of the index of performance in Eq. (1) is the criterion of equilibrium, that is, the accomplished dead beat response. Non-dead-beat solutions[19, 21] for specific input functions have also been proposed on the basis of penalty functions per Eq. (2) by the use of dynamic programing, a specially organized scanning operation to search for minima of the index of performance. When applied in this fashion the meaning of the criterion of Eq. (1) based on Eq. (2) is not too clear. Worse, the penalizing of rates, accelerations, and higher derivatives of the error naturally leads to sluggish response.[21]

In a sense the field of automatic control exhibits a "split personality" since a parallel line of development has accompanied the already described "main" line from the earliest times on.

The differences between the two lines of development stem from the different views of the input environment of the system which they represent. The large majority of control systems operate in input environments which consist of a random sequence of more or less abrupt jumps and continuous changes. Further, part of the input signals received by the control system are reference signals which it should follow as exactly as possible and part are spurious noise signals which it should disregard as completely as possible.

Now the main line of development focuses its attention on the abruptness of the individual jumps in the input environment and the accompanying transient response of the control system. This approach is all but powerless to deal with the problem of the noise.

The second line of development views the entire input environment as a whole, focusing its attention on the nature of the randomness of the changes as described by the methods of statistics. The noise problem becomes an integral part of this approach in a natural way.

Because of larger theoretical difficulties the second line of development has taken a somewhat secondary role in terms of the extent of application to actual design. However, the second line is more wholesome in its outlook and accordingly its relative importance tends to increase.

The nature of the performance criteria used by the two lines of development are in keeping with the nature of the lines themselves.

As has been discussed, the main line of development tends to utilize a set of specific criteria like overshoot or encirclement of the -1 point in the s plane. Only relatively recently have efforts[14–17] been made to unify these into a single index of performance which is defined in a completely arbitrary fashion.

The comprehensive nature of the second line of development, on the other hand, is conducive to the use of comprehensive performance criteria such as mean square error.

The fundamental work[22] launching the second line of development was based on the assumption that reference signal and noise are both "stationary" in some sense—that is, that the statistical description of these signals is unchanged over long time intervals or from application to application. Under these circumstances the average of some penalized error is a most logical performance index. Of these, for reasons of mathematical expediency, the mean square error was selected.

The mean square error can be defined for input number n

$$\overline{e_n^2} = \lim_{T=\infty} (1/2T) \int_{-T}^{+T} e_n^2(t)\, dt \qquad (3)$$

or an average indicated by the wavy line can be taken over the ensemble of inputs for some time, t,

$$\widetilde{e^2(t)} = \lim_{N=\infty} (1/N) \sum_{n=1}^{N} e_n^2\,(t) \qquad (4)$$

where $e_n^2(t)$ is the square at t of the error produced by input number n. An ensemble of inputs simply means the set of individual inputs occurring in individual repeated applications of the identical control system. For instance, input number n might be the angular motions of the beam in the number n flight of a beam-riding missile. For stationary input environments

$$\overline{e_n^2} = \widetilde{e^2(t)} \qquad (5)$$

The system producing the minimum root mean square error, which is then "optimum" in a clearly defined sense, is the solution of the well-known Weiner-Hopf integral equation

$$\int_0^\infty k(t_1)\, \psi_{rr}'(t - t_1)dt_1 - \psi_{ri}'(t) = 0, \quad t > 0 \qquad (6)$$

Here ψ_{rr}', the autocorrelation of the input, is a function of $t - t_1$ only. As a result, a closed solution is possible for this equation by the spectrum factorization method of Wiener. The finding of closed optimum solutions seems to be characteristic in the second line of development while cut-and-try is predominant in the main line of development. Mean square error studies of nonlinear, multi-input, etc., systems in stationary random environments were carried out recently.[23–25]

Wiener's work was eventually also extended to various types of nonstationary conditions.[26–29] When signals are nonstationary, averages taken over time do

not agree any more with averages taken over the ensemble and the latter will be functions of time—that is, the statistics of the signals changes in time. This opens the way for different possible interpretations of the mean square error and a mean square error criterion.

Seemingly the most direct way is to define an ensemble average mean square error which then is a function of time. If now this is to be stated as a criterion there are two possibilities. If the output is of interest at only one instant—as it would be in some armament applications—then the performance criterion is simply that the ensemble average root mean square error be minimum at that instant. Optimum systems under this criterion are known as final value systems.[26, 30–32] A different optimum system results for different final times. When applicable this performance criterion is useful and effective, resulting in explicit solutions for optimum systems.

The second possibility is to require more generally that the mean square error be minimum at all times.[26] Unfortunately then the optimum system is defined by the integral equation

$$\int_0^\infty dt_1 k(t - t_2, t)\psi_{rr}'(t - t_1, t - t_2) - \psi_{ir}(t - t_2, t) = 0, \quad t > 0 \quad (7)$$

Solutions of this equation would represent in a sense the ultimate of optimization; in fact, they would be time-varying systems which also produce minimum "end-sigma" (s) error among all linear systems. (s is the end sigma, the form of the letter sigma used at the end of Greek words.) However, even if solutions for the general case were obtainable from Eq. (7) these would be realizable only in terms of digital computers of excessive speed and memory or time-varying distributed-constant analogs. Actually solutions were only obtained[33] for a special class when the kernel ψ_{rr} can be split into two factors, each a function of one variable only.

Instead of requiring that the ensemble mean square error be minimum at all times, the criterion can be stated to require the time average of the ensemble mean to be minimum.[27]

This requires averaging over both time and members of the ensemble. (This could be contrasted to the stationary case where averaging either on time or an ensemble is adequate since both give the same result.) Sometimes, rather than averaging in time, simply the time integral of the mean square error is taken, the so-called integral error.[28]

$$I = \int_0^\infty e(t)^2\, dt \quad (8)$$

This, when finite, can desirably replace the time average which is then zero. For certain input conditions, systems with optimum transient response can be obtained under the criterion of Eq. (8) simply by solving a Wiener-Hopf integral equation.[28]

This is one instance where a technique evolving from the second line of development yields an organic solution to a problem of the main line; a problem the main line of development is able to handle only by cut-and-try and only without clear theoretical basis. There are other such instances indicating that the two lines of development in control system theory are destined to merge combining the split personality into a single healthy individual engineering field.

Introduction of the "end-sigma" (s) criterion of the present paper represents a step forward in this direction. It is not uniquely tied to either the transient or the random-signal approach but can deal with either. It eliminates much of the arbitrariness of the general integral-error criterion [Eq. (1) and its special form of Eq. (8)] for transient conditions. Optimum solutions are obtainable and realizable in terms of invariant linear systems for combinations of nonstationary random and transient environments. The s error is finite and nonzero for any stable control system in a practical input environment and even for nonstable systems when the output is utilized over finite time intervals only.

The accompanying bibliography strives to be representative rather than complete in order to keep its size within reason. In some instances the most pertinent references were used rather than the ones with the clearest claim to priority. It should also be remembered that in its present size the preceding summary must be sketchy and oversimplified in some respects. It is hoped, however, that it will make clear the salient events and trends in the development of performance criteria and the place of the s criterion in this development.

The Proposed Criterion

The following equation produces a statistical average of the weighted error of a control system:

$$s = \int_0^\infty \overline{F[e(t),\ t,\ V_1,\ \ldots,\ V_R]p(t)}dt \quad (9)$$

where $p(t)$ is the probability distribution of all times when the system output is utilized, assuming excitation by one given type of input on the same control systems or on identical systems. The wavy line indicates averaging over an ensemble of inputs of different type. Function $F[e(t), r, V_1, \ldots, V_R]$ represents the weight or penalty which is put on the size of the error, $e(t)$, to express its undesirability. This penalty, as indicated in Eq. (9), can be dependent on the time, t, when the error occurs and on assorted parameters, $V_1, V_2, \ldots, V_R$.

As an example, for a homing missile $p(t)$ can be the probability distribution of time elapsing from the instant of firing to explosion. A common type of penalty function is

$$F[e(t), t, V_1, \ldots, V_R] = e^2 \quad (10)$$

in which case Eq. (9) yields the average square error for all such times when the output is actually utilized.

The studies in this paper are generally based on the penalty function of Eq. (10).

Control systems are built to convert some input into a desired output which may or may not be identical to the input. The error is any deviation from this desired output, but error values are only significant when the output is actually utilized. Eq. (9) weights and averages such significant error values and so produces an overall one figure description of the performance which truly summarizes the performance. This criterion is also universal in the sense that it unifies in one single concept all the varied aspects of system performance such as transient and steady state, peak time and overshoot, etc. Each of these is part of the criterion but neither is overemphasized; each gets its proper share in determining the criterion number.

Evaluating the Criterion

The error, e, of a linear time-invariant control system at rest prior to $t = 0$ is defined by convolution in the time domain as

$$e(t) = i(t) - \int_0^\infty k(t_1)r(t - t_1)dt_1 \tag{11}$$

where $i(t)$ is the desired output, $r(t)$ is the input, and $k(t)$ is the weighting function or impulsive response of the control system. For realizable systems

$$k(t) = 0 \quad \text{if} \quad t < 0$$

Substituting Eq. (11) into Eq. (9) and assuming that $p(t)$ is independent of the input,

$$\mathfrak{s} = \psi_{ii}(0, 0) - 2\int_0^\infty dt_1 k(t_1)\psi_{ir}(0, -t_1) + \int_0^\infty dt_3 k(t_3) \int_0^\infty dt_1 k(t_1)\psi_{rr}(t_3, t_3 - t_1) \tag{12}$$

where the following definitions apply:

$$\psi_{rr}(t, \tau) = \int_0^\infty dt_2 \overline{p(t_2 + t)r(t_2)r(t_2 + \tau)} \tag{13}$$

$$\psi_{ii}(t, \tau) = \int_0^\infty dt_2 \overline{p(t_2 + t)i(t_2)i(t_2 + \tau)} \tag{14}$$

$$\psi_{ir}(t, \tau) = \int_0^\infty dt_2 \overline{p(t_2 + t)i(t_2)r(t_2 + \tau)} \tag{15}$$

The wavy line denotes averaging over the ensemble of inputs.

Eqs. (12)–(15), as is readily seen, represent modified definitions which unite the auto- and cross-correlation functions used[22] in describing stationary input environments and the auto- and cross-translation functions which are used[28] for the study of transient or nonstationary input environments. With the proposed definitions no distinction need be made between these two special cases. Furthermore, these are not the only ones within the definition, which actually includes an infinitude of special cases depending on the specific $p(t)$ probability distribution. It is frequently convenient to expand the functions occurring in Eq. (12) in Fourier series like

$$p(\theta) = \sum_\alpha p_\alpha \phi_\alpha{}^{\mathrm{I}}(\theta) \tag{16}$$

$$r(\theta) = \sum_\beta r_\beta \phi_\beta{}^{\mathrm{II}}(\theta) \tag{17}$$

$$i(\theta) = \sum_\delta i_\delta \phi_\delta{}^{\mathrm{III}}(\theta) \tag{18}$$

$$k(\theta) = \sum_n k_n \phi_n{}^{\mathrm{IV}}(\theta) \tag{19}$$

where $\phi_\alpha{}^{\mathrm{I}}(\theta)$, $\phi_\beta{}^{\mathrm{II}}(\theta)$, $\phi_\delta{}^{\mathrm{III}}(\theta)$, and $\phi_n{}^{\mathrm{IV}}(\theta)$, respectively, form complete normalized orthogonal sets of functions over the interval 0 to ∞ (or 0 to T if the upper limits of the integrals in Eq. (12) are finite as they would be for a weighting function, $k(t)$ with finite memory or a probability function which is zero past $t = T$). These four sets of orthogonal functions may be the same but this is not required. In fact, the following considerations are valid even if $\phi_\alpha{}^{\mathrm{I}}$, $\phi_\beta{}^{\mathrm{II}}$, $\phi_\delta{}^{\mathrm{III}}$ and $\phi_n{}^{\mathrm{IV}}$ are not orthogonal sets, only linearly independent. Of course, orthogonality has the advantage of facilitating the determination of p_α, r_β, i_δ, and k_n which are then the Fourier coefficients. For instance,

$$p_\alpha = \int_0^\infty p(\theta)\phi_\alpha{}^{\mathrm{I}}(\theta)d\theta \tag{20}$$

On the other hand, if input $r(t)$ is given, for instance, as a polynomial in time, $\phi_\alpha(t)$ can simply be t^α, the successive powers of time. The variation of accuracy with the number of terms in Fourier and Taylor series is well established in the literature.[34] Substituting Eqs. (16)–(19) into Eqs. (12)–(15),

$$\mathfrak{s} = \sum_\alpha \sum_\delta \sum_\epsilon \Psi_{\alpha\delta\epsilon}{}^{\mathrm{II}} G_{\alpha\delta\epsilon} - 2\sum_m k_m \sum_\alpha \sum_\beta \sum_\delta \times \Psi_{\alpha\beta\delta}{}^{\mathrm{I}} G_{\alpha\beta\delta m} + \sum_m \sum_n k_m k_n \sum_\alpha \sum_\beta \sum_\gamma \Psi_{\alpha\beta\gamma} G_{\alpha\beta\gamma mn} \tag{21}$$

where

$$\Psi_{\alpha\beta\gamma} = \overline{p_\alpha r_\beta r_\gamma} \tag{22}$$

$$\Psi_{\alpha\beta\delta}{}^{\mathrm{I}} = \overline{p_\alpha r_\beta i_\delta} \tag{23}$$

$$\Psi_{\alpha\delta\epsilon}{}^{\mathrm{II}} = \overline{p_\alpha i_\delta i_\epsilon} \tag{24}$$

$$G_{\alpha\beta\gamma mn} = \int_0^T dt_3 \phi_m{}^{\mathrm{IV}}(t_3) \int_0^T dt_2 \phi_n{}^{\mathrm{IV}}(t_2)\Phi_{\alpha\beta\gamma}(t_2, t_3) \tag{25}$$

$$G_{\alpha\beta\delta m} = \int_0^T dt_3 \phi_m{}^{\mathrm{IV}}(t_3)\Phi_{\alpha\beta\delta}{}^{\mathrm{I}}(t_3) \tag{26}$$

$$G_{\alpha\delta\epsilon} = \Phi_{\alpha\delta\epsilon}{}^{\mathrm{II}} \tag{27}$$

$$\Phi_{\alpha\beta\gamma}(t, \tau) = \begin{cases} \displaystyle\int_\tau^T dt_1 \phi_\alpha{}^{\mathrm{I}}(t_1)\phi_\beta{}^{\mathrm{II}}(t_1 - \tau) \times \phi_\gamma{}^{\mathrm{III}}(t_1 - t) & t \le \tau \\ \displaystyle\int_t^T dt_1 \phi_\alpha{}^{\mathrm{I}}(t_1)\phi_\beta{}^{\mathrm{II}}(t_1 - t) \times \phi_\gamma{}^{\mathrm{III}}(t_1 - \tau) & t \ge \tau \end{cases} \tag{28}$$

$$\Phi_{\alpha\beta\delta}{}^{\mathrm{I}}(\tau) = \int_\tau^T \phi_\alpha{}^{\mathrm{I}}(t_1)\phi_\beta{}^{\mathrm{II}}(t_1 - \tau)\phi_\delta{}^{\mathrm{III}}(t_1)dt_1 \tag{29}$$

$$\Phi_{\alpha\delta\epsilon}{}^{\mathrm{II}} = \int_0^T \phi_\alpha{}^{\mathrm{I}}(t_1)\,\phi_\delta{}^{\mathrm{III}}(t_1)\phi_\epsilon{}^{\mathrm{III}}(t_1)dt_1 \tag{30}$$

The upper limit in these integrals can be $T = \infty$ if in Eq. (12) the interval is infinite as shown.

The advantage of the form given in Eq. (21) over that given in Eq. (12) is that once the orthogonal sets are specified, the quantities defined in Eqs. (25)–(30) can be precalculated. Then Eq. (21) can be readily evaluated, for instance, by a digital computer, without the need of carrying out the integrations of Eq. (12) for the individual case. An even more decisive advantage of the form given in Eq. (21) will be discovered below in facilitating the solution of the integral equation which defines the optimum weighing function.

Finding the Optimum System Under the Criterion

The s criterion can be evaluated from Eq. (12) or (21) for a given system with a known impulsive response, $k(t)$. Frequently, however, the objective of the design is just the determination of $k(t)$ in some optimum way. If optimum is defined as the system giving the smallest value of the s error of Eq. (12), then by simple use of the calculus of variations the following integral equation of the first kind results as a necessary and sufficient definition of the optimum $k(t)$:

$$\int_0^T dt_1 k(t_1)\psi_{rr}(t, t - t_1) - \psi_{ir}(0, -t) = 0, \quad T > t > 0 \tag{31}$$

where T can be infinity.

Applying the definitions of Eqs. (16)–(30), Eq. (31) can be modified into

$$\sum_n k_n f_n(\tau) = f(\tau) \tag{32}$$

where

$$f_n(\tau) = \int_0^T dt_1 \phi_n{}^{IV}(t_1)\psi_{rr}(\tau, \tau - t_1) = \sum_\alpha \sum_\beta \sum_\gamma \Psi_{\alpha\beta\gamma} \int_0^T \Phi_{\alpha\beta\gamma}(t_2, \tau)\phi_n{}^{IV}(t_2)dt_2 \tag{33}$$

$$f(\tau) = \psi_{ir}(0, -\tau) = \sum_\alpha \sum_\beta \sum_\delta \Psi_{\alpha\beta\delta}{}^{I}\phi_{\alpha\beta\delta}{}^{I}(\tau) \tag{34}$$

Let $\phi_m{}^{V}(\theta)$ be a complete normalized orthogonal set of functions on the interval $0 < t < T$. Then by Fourier expansion

$$f_n(\theta) = \sum_m f_{mn}\phi_m{}^{V}(\theta) \tag{35}$$

$$f(\theta) = \sum_m f_m \phi_m{}^{V}(\theta) \tag{36}$$

where, of course,

$$f_{mn} = \int_0^T f_n(\tau)\phi_m{}^{V}(\tau)d\tau = \sum_\alpha \sum_\beta \sum_\gamma \Psi_{\alpha\beta\gamma} F_{\alpha\beta\gamma mn} \tag{37}$$

$$f_m = \int_0^T f(\tau)\, \phi_m{}^{V}(\tau)d\tau = \sum_\alpha \sum_\beta \sum_\delta \Psi_{\alpha\beta\delta}{}^{I}\, F_{\alpha\beta\delta m} \tag{38}$$

with reference to Eqs. (22), (23), (28), and (29). Further,

$$F_{\alpha\beta\gamma mn} = \int_0^T dt_3 \phi_m{}^{V}(t_3) \int_0^T dt_2 \phi_n{}^{IV}(t_2)\Phi_{\alpha\beta\gamma}(t_2, t_3) \tag{39}$$

$$F_{\alpha\beta\delta m} = \int_0^T dt_3 \phi_m{}^{V}(t_3)\Phi_{\alpha\beta\delta}{}^{I}(t_3) \tag{40}$$

Now Eq. (32) takes the form

$$\sum_n k_n \sum_m f_{mn}\phi_m{}^{V}(\tau) = \sum_m f_m \phi_m{}^{V}(\tau) \tag{41}$$

which can only be satisfied identically over $0 < \tau < T$ if

$$\sum_n f_{mn}k_n = f_m \quad \text{for all } 0 < m < L \tag{42}$$

where the largest value of m has been limited to the finite L, as any practical Fourier series must have a finite length.

In an alternate matrix notation,

$$[f_{mn}]\, k_n] = f_m] \tag{43}$$

or

$$k_n] = [f_{mn}]^{-1} f_m] \tag{44}$$

This gives the Fourier coefficients of the weighting function of the optimum system up to order L. Eq. (19) then determines the approximate optimum weighing function and Eq. (21) determines the s criterion value for the optimum weighting function. For the optimum system, if $\phi_m{}^{IV}$ and $\phi_n{}^{V}$ are chosen to be the same orthogonal set, Eq. (21) for evaluating the optimum s simplifies to

$$s = f - \sum_m k_m f_m = \sum_\alpha \sum_\delta \sum_\epsilon \Psi_{\alpha\delta\epsilon}{}^{11}G_{\alpha\delta\epsilon} - \sum_m k_m f_m \tag{45}$$

Some Aspects of the Design

The above equations establish a design process leading to the impulsive response of a control system which is optimum in the sense that it has the smallest true average error or s value among all time-invariant linear systems in a given input environment. Once the impulsive response is known it is still necessary for the designer to find a physical system to fit the impulsive response. Of course, the impulsive response can be converted into a frequency response for the fitting. In either case, standard methods of network synthesis can be used.

One advantage of the above derived process is that, once the particular sets of orthogonal functions are selected, most of the working equations as well as the design program can be precomputed and programed for a digital computer since these working equations [specifically, Eqs. (25)–(30), (39), and (40)] depend only on the selection of the orthogonal sets and not on the specific input and output conditions. All that is needed then is to expand the input, output, and probability distribution over the selected orthogonal sets in accordance with Eqs. (16)–(19) and feed the coefficients into the program.

For cases where the upper limits of integration in Eq. (12) are infinite, an exponential polynominal orthogonal set of functions[29] can be used.

Where the interval is finite, upper limit T, either a

trigonometric orthogonal set or Legendre polynominals can be used to advantage, the latter mainly where the input is given in the form of a polynominal in t, which is a rather common case. Finite upper limit of the integrals in Eq. (12) may be an expression of either (but not both) of two situations. Either the probability density $p(t)$ is zero for $t > T$, meaning that T is the longest time within which the output is utilized, or $k(t) = 0$ for $t > T$, which would be the case for a system of finite memory, a system which bases its output on information not older than T. In either of these two cases the solution will lead to a $k(t)$ defined for $0 < t < T$. The difference is that for a finite memory system $k(t)$ will be known to be zero for $t > T$. On the other hand, for a system where the $p(t)$ function is zero beyond T, $k(t)$ will be undefined for $t > T$; also it will be inconsequential what $k(t)$ is for $t > T$ since this part of the response is never used. This latter indefiniteness is an additional degree of freedom in searching for a physical system to fit the optimum $k(t)$ weighting function—the last step of the design. For the aforementioned three orthogonal sets, complete details of the working equations for digital computer programing are now in the process of being derived. The aim of the present paper is to explain the mathematical theory of the solution and the philosophical basis of the criterion and also to demonstrate that it is possible to base a workable design process on the criterion.

A highly simplified example follows, which is intended to illustrate the steps of solution in a simplified way.

Illustrative Example

Design an optimum system under the criterion for an input

$$r(t) = u(t)[1 + 0.5t + 2t^2]$$

and a desired output which is a prediction of the input 1 sec. from the present time

$$i(t) = r(t + 1) = u(t)[3.5 + 4.5t + 2t^2]$$

assuming that the output is utilized with uniform probability between $t = 1$ sec. and $t = 6$ sec.; that is,

$$p(t) = (1/5)[u(t - 1) - u(t - 6)]$$

where $u(t)$ is the unit step function at $t = 0$. Because of the simplicity of this problem, Eqs. (13)–(15) can be evaluated directly—that is, without recourse to expansions of the type given in Eqs. (16)–(18).

$$\psi_{rr}(t, t - t_1) = \int_0^\infty (1/5)[u(t_2 - 1) - u(t_2 - 6)] \times u(t_2 - t)[1 + 0.5(t_2 - t) + 2(t_2 - t)^2] \cdot u(t_2 - t_1) \times [1 + 0.5(t_2 - t_1)^2] dt_2$$

$$\Psi_{ir}(0, -t) = \int_0^\infty (1/5)[u(t_1 - 1) - u(t_1 - 6)] \times u(t_1 - t)[1 + 0.5(t_1 - t) + 2(t_1 - t)^2] \times [3.5 + 4.5t_1 + 2t_1^2]\, dt_1$$

So, with reference to Eq. (32),

$$\sum_{n=0}^{2} k_n f_n(\tau) = f(\tau)$$

Using the first form of Eqs. (33) and (34), and $\phi_n{}^{IV}(\theta) = \sqrt{(2n + 1)/6}\, \mathcal{P}_n\left((\theta/3) - 1\right)$ where $\mathcal{P}_n(x)$ is the nth Legendre polynomial

$$f_n(\tau) = \int_0^6 dt_1 \mathcal{P}_n(t_1) \Psi_{rr}(\tau, \tau - t_1)$$

$$= \int_0^6 \mathcal{P}_n(t_1) \left\{ \int_1^6 (1/5) u(t_2 - \tau) \times [1 + 0.5(t_2 - \tau) + 2(t_2 - \tau)^2] \cdot u(t_2 - t_1) \times [1 + 0.5(t_2 - t_1) + 2(t_2 - t_1)^2] dt_2 \right\} dt_1$$

$$f(\tau) = \Psi_{ir}(0, -\tau)$$

$$= \int_0^6 (1/5) u(t_1 - \tau)[1 + 0.5(t_1 - \tau) + 2(t_1 - \tau)^2] \cdot [3.5 + 4.5t_1 + 2t_1^2]\, dt_1$$

Now, expanding $f_n(\tau)$ and $f(\tau)$ according to Eqs. (35)–(36) on the functions $\phi_n{}^{V}(\theta) = \sqrt{(2n + 1)/6}\, \mathcal{P}_n\left((\theta/3) - 1\right)$ on the interval $0 \leq \theta \leq 6$

$$f_n(\theta) = f_{0n}\sqrt{1/6} + f_{1n}\sqrt{3/16}[(\theta/3) - 1] + f_{2n}\sqrt{5/6}[(\theta^2/6) - \theta + 1]$$

$$f(\theta) = f_0\sqrt{1/6} + f_1\sqrt{3/6}[(\theta/3) - 1] + f_2\sqrt{5/6}[(\theta^2/6) - \theta + 1]$$

Only three Legendre polynomials are used to preserve the brevity of the example, of course at the expense of the refinement of the solution.

The matrix equation (43) can now be set up

$$\begin{bmatrix} 4{,}392.06 & -4{,}165.43 & 1{,}412.35 \\ -15{,}206.65 & 13{,}815.24 & -4{,}543.13 \\ 3{,}538.83 & -3{,}188.88 & 1{,}335.96 \end{bmatrix} \begin{bmatrix} k_0 \\ k_1 \\ k_2 \end{bmatrix} = \begin{bmatrix} 8{,}829.85 \\ -29{,}021.61 \\ 7{,}912.02 \end{bmatrix}$$

Solving this matrix equation for k_0, k_1, k_2,

$$k(t) = k_0\phi_0{}^{IV}(t) + k_1\phi_1{}^{IV}(t) + k_2\phi_2{}^{IV}(t)$$

$$= (0.5075)\sqrt{1/6} + (-0.1702)\sqrt{3/6} \times [(t/3) - 1] + (4.1716)\sqrt{5/6}[(t^2/6) - t + 1]$$

$$= 4.136 - 3.848t + 0.635t^2$$

This optimum impulsive response is shown in Fig. 1.

The response of the optimum system can be computed by convolution

$$c(t) = \int_0^t k(\tau) r(t - \tau) d\tau$$

$$= 4.13\,6t - 0.890t^2 + 2.648t^3 - 0.614t^4 + 0.042t^5$$

The optimum s error can now be computed directly from Eq. (16).

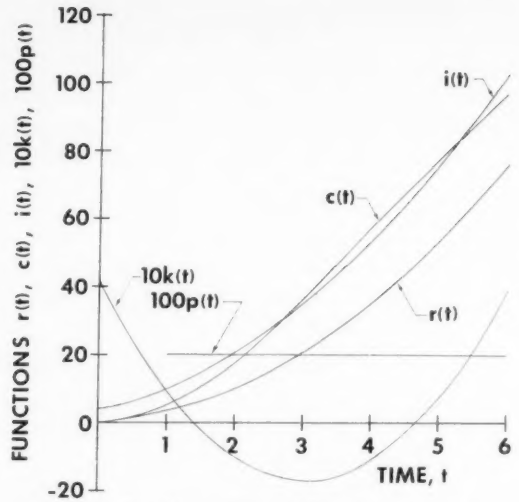

FIG. 1. Graphic summary of illustrative example.

$$s = 11.01$$

In interpreting this example it should not be forgotten that the approximation of the optimum impulsive response has been limited to a second-order parabola by selecting an approximation by only the first three Legendre polynomials. Therefore, the approximation is necessarily crude. Nevertheless, the way $c(t)$ is oscillating around $i(t)$ suggests an optimum fit by limited means. The aim of the example was to illustrate direct use of the general solutions without deriving final working equations from Eqs. (39) and (40) for the Legendre polynomials in general. It could be expected, however, that such derivation would substantially increase the power of the method.

Conclusion

A performance criterion is defined for feedback control systems which has a clear physical meaning as the average value of the penalized error for such times when the output is utilized. The criterion provides a summary of system performance which unifies other techniques devised for special aspects of performance.

It is demonstrated that tractable mathematical procedures can be based on this criterion both for evaluating the criterion and for designing systems which are optimum under this criterion. A simple illustrative example of optimization is included.

A subsequent publication will put the equations derived here into a form suitable for "production" type digital computer solution.

References

[1] Brown, G. S., and Campbell, D. P., *Principles of Servomechanisms*, John Wiley and Sons, Inc., New York, 1948.

[2] Chestnut, Harold, and Mayer, R. W., *Servomechanisms and Regulating System Design*, John Wiley and Sons, Inc., New York, 1951.

[3] James, H. M., Nichols, N. B., and Philips, R. S., *Theory of Servomechanisms*, McGraw-Hill Book Co., Inc., New York, 1947.

[4] Evans, W. R., *Control System Dynamics*, McGraw-Hill Book Co., Inc., New York, 1954.

[5] Tustin, A., (Ed.), *Automatic and Manual Control*, Symposium, Kusters, N. L., and Moore, W. J. M., *Generalization of the Frequency Response Method for Study of Feedback Control Systems*, Academic Press, Inc., New York, 1952.

[6] Biernson, G., *Quick Methods of Evaluating the Closed-Loop Poles of Feedback Control Systems*, Trans. AIEE, Part II, p. 53, 1953.

[7] Russel, D. W., and Weaver, C. H., *Synthesis of Closed Loop Systems Using Curvilinear Squares to Predict Root Location*, Trans. AIEE, Part II, p. 95, 1952.

[8] Chu, Yaohan, *Correlation Between Frequency and Transient Responses of Feedback Control Systems*, Trans. AIEE, Part II, p. 81, 1953.

[9] Truxal, J. G., *Automatic Feedback Control System Synthesis*, McGraw-Hill Book Co., Inc., New York, 1955.

[10] McDonald, D., *Non-Linear Techniques for Improving Servo Performance*, Proceedings, National Electronics Conference, Vol. 6, p. 400, 1950.

[11] Hopkin, A. M., *A Phase Plane Approach to the Compensation of Saturating Servomechanisms*, Trans. AIEE, Part I, p. 631, 1951.

[12] Neiswander, R. S., and MacNeal, R. H., *Optimization of Non-Linear Control Systems by Means of Non-Linear Feedbacks*, Trans. AIEE, Part II, p. 262, 1953.

[13] Bogner, I., and Kazda, L. F., *An Investigation of the Switching Criteria for Higher Order Contactor Servomechanisms*, Trans. AIEE, p. 118, Part II, 1954.

[14] Nims, Paul T., *Some Design Criteria for Automatic Control*, Trans. AIEE, Vol. 70, Part I, p. 606, 1951.

[15] Graham, D., and Lathrop, R. C., *The Synthesis of "Optimum Transient Response:" Criteria and Standard Forms*, Trans. AIEE, Vol. 72, Part II, p. 273, 1953.

[16] Crow, Jack, *An Integral Criterion for Optimizing Duplicator Systems on the Basis of Transient Response*, Doctoral Dissertation, Washington University, St. Louis, Mo., 1956.

[17] Schulz, W. C., and Rideout, V. C., *The Selection and Use of Servo Performance Criteria*, Trans. AIEE, Vol. 76, Part II, p. 383, 1957.

[18] Schulz, W. C., and Rideout, V. C., *A General Criterion for Servo Performance*, Proceedings, National Electronics Conference, Vol. 13, pp. 549–560, 1957.

[19] Bellman, R., *On the Application of the Theory of Dynamic Programming to the Study of Control Processes*, Proceedings of the Symposium on Nonlinear Circuit Analysis, Polytechnic Institute of Brooklyn, Vol. VI, New York, 1956.

[20] Kalman, R. E., and Bertram, J. E., *General Synthesis Procedure for Computer Control of Single-Loop and Multiloop Linear Systems*, Trans. AIEE, Part II, pp. 602–608, January, 1959.

[21] Kalman, R. E., and Koepcke, R. W., *Optimal Synthesis of Linear Sampling Control Systems Using Generalized Performance Indexes*, Trans. ASME, Vol. 80, pp. 1820–1825, November, 1958.

[22] Wiener, N., *Extrapolation, Interpolation, and Smoothing of Stationary Time Series*, John Wiley and Sons, Inc., New York, 1949.

[23] Hopkin, A. M., and Wang, P. K. C., *A Relay-Type Feedback Control System Designed for Random Inputs*, Trans. AIEE, Part II, 1958.

[24] Chuang, K., and Kazda, L. F., *A Study of Nonlinear Systems With Random Inputs*, Trans. AIEE, Part II, 1959.

[25] Amara, R. C., *The Linear Least Squares Synthesis of Multivariable Control Systems*, Trans. AIEE, Part II, 1959.

[26] Booton, R. C., Jr., *An Optimization Theory for Time-Varying Linear Systems With Non-Stationary Statistical Inputs*, Proceedings, Institute of Radio Engineers, New York, Vol. 40, p. 977, August, 1952.

[27] Zadeh, L. A., and Ragazzini, J. R., *An Extension of Wiener's Theory of Prediction*, Journal of Applied Physics, Vol. 21, p. 645, 1950.

[28] Newton, G. C., Jr., Gould, L. A., and Kaiser, J. F., *Analytical Design of Linear Feedback Controls*, John Wiley and Sons, Inc., New York, 1957.

(*Continued on page 160*)

Readers' Forum

BRIEF REPORTS of investigations in the aerospace sciences and discussions of papers published in the JOURNAL are presented in this special department. Entries must be restricted to a maximum of 1,300 words or the equivalent of one JOURNAL page including formulas and illustrations. Publication is completed as soon as possible after receipt of the material. The Editorial Committee does not hold itself responsible for the opinions expressed by the correspondents.

Contents

The Effect of Shock-Generated Vorticity, Surface Slip, and Temperature Jump on Stagnation-Point Heat-Transfer Rates ..... H. HOSHIZAKI 135
The Pitot and Static Tubes—Condensed Sources of General Fundamentals and Applications ..... JAY W. STUART, JR. 136
The Influence of Panel Deformations on Wing Flutter ..... D. J. JOHNS 137
A Simplified Expression for the Period of Nonlinear Oscillations of Curved and Flat Panels ..... JOSHUA E. GREENSPON 138
On Magnetohydrodynamic Channel Flow ..... J. E. MCCUNE AND W. R. SEARS 139
The Stagnation-Point Ablation of Telflon During Hypersonic Flight ..... S. M. SCALA AND N. S. DIACONIS 140
A Multiple Hot-Wire Array for Measurements of Downwash Integrals ..... KENT KRESA AND ERIK MOLLÖ-CHRISTENSEN 141
An Exact Calculation of Some Steady, Diabatic, Two-Dimensional Fields of Compressible Flow ..... BRUCE L. HICKS AND DONALD R. CHENOWETH 142
On an Exact Solution of Laminar Mixing of Two Different Gases ..... LUIGI G. NAPOLITANO 144
Erratum—"Note on the Turbulent Shear Stress Near A Wall" ..... H. G. ELROD 145
Minimizing the Mass of Thin Radiating Fins ..... J. ERNEST WILKINS, JR. 145
The Minimum-Weight Straight Fin of Triangular Profile Radiating to Space ..... EDWIN N. NILSON AND RICHARD CURRY 146
Relaxation Effects on the Interpretation of Impact-Probe Measurements ..... WILLIAM F. VAN TASSELL AND EUGENE E. COVERT 147
The Hydraulic Analogy for External Flow ..... R. A. A. BRYANT 148
Improvement of a Pressure Pickup for the Measurements of Turbulence Characteristics ..... V. KOBASHI, N. KONO, AND T. NISHI 149
A Simple Numerical Solution of the Supersonic Blunt-Body Problem for Real Gases ..... G. A. BIRD 151
Periodic Temperature Distribution in a Two-Layer Composite Slab ..... THOMAS E. STONECYPHER 152
Comment on "On a Class of Variational Problems in Rocket Flight" ..... G. LEITMANN 153
The Response of Linear Systems to Non-Gaussian Random Inputs ..... STEPHEN H. CRANDALL, WILLIAM H. SIEBERT, AND BERNARD P. HOQUETIS 154
On the Structure of Vortical Layers in Supersonic and Hypersonic Flows ..... HSIEN K. CHENG 155
Similar Solutions for Boundary Layers in Constant-Temperature Magneto-Gasdynamic Channel Flow ..... JACK L. KERREBROCK 156
Heat Transfer at a Corner ..... VICTOR ZAKKAY 157
A Graphical Solution for Normal Shock Waves in Real Gases ..... CHARLES E. TREANOR 158
An Approximation for Subsonic Flow Through an Orifice ..... P. G. MORGAN 160

The Effect of Shock-Generated Vorticity, Surface Slip, and Temperature Jump on Stagnation-Point Heat-Transfer Rates

H. Hoshizaki
Senior Scientist, Thermodynamics, Missiles and Space Division, Lockheed Aircraft Corporation, Sunnyvale, Calif.

October 16, 1959

SYMBOLS

Pr	=	Prandtl Number
$q_{B.L.}$	=	boundary-layer-theory heat-transfer rate
$q_{S.L.}$	=	shock-layer-theory heat-transfer rate
r	=	normal distance
r_w	=	body radius
Re	=	Reynolds Number
T_f	=	fluid temperature at body surface
T_w	=	surface temperature
V_∞	=	free-stream velocity
v_w	=	tangential surface velocity
α	=	accommodation coefficient
γ	=	isentropic exponent
λ_w	=	molecular mean free path at the wall
ν_s	=	kinematic viscosity behind shock
ϵ	=	ratio of free-stream density to density behind shock

IT WAS SHOWN in references 1 and 2 that stagnation-point heat-transfer rates on spherically capped bodies traveling at hypersonic velocities and moderately low Reynolds Numbers [$Re \sim 0(10^3)$] are considerable higher than the values predicted by boundary-layer theory. This increase is attributed to the vorticity generated by the curved bow shock. In these analyses, the incompressible Navier-Stokes equations were applied to the flow region between the bow shock and the body—i.e., to the shock layer. The shock layer was assumed to be completely viscous, and no boundary-layer approximations were made. Boundary conditions were applied immediately behind the shock and at the body surface. The shock boundary conditions

Contributors Please Note

Readers' Forum items must be confined to the equivalent of one page in the *Journal*. Contributions that exceed this limit will be returned to the authors for condensation and rewrite. To avoid inconvenience and delay, please adhere to the following specifications:

(1) Five, double-spaced, typewritten, manuscript pages ($8^1/_2$ by 11 in.), including wide margins, formulas, and headings, equal one printed page.

(2) For every illustration, deduct at least one-half or as much as one manuscript page, depending on the size of the illustration.

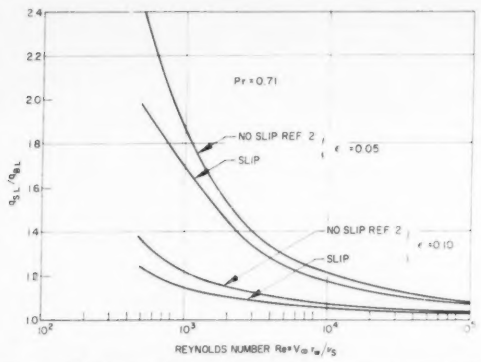

FIG. 1. Shock-layer-theory to boundary-layer-theory heat-transfer ratio.

were obtained from the normal-shock relations, whereas, on the surface, the usual no-slip conditions were employed.

It is the purpose of this note to show how surface slip and temperature jump affect the results of references 1 and 2. The surface-slip velocity and temperature jump are given approximately by[3]

$$v_w = \lambda_w(\partial v/\partial r)_w \tag{1}$$

$$T_f = T_w + [(2-\alpha)/\alpha]\,[2\gamma/(\gamma+1)](\lambda_w/Pr)(\partial T_f/\partial r) \tag{2}$$

The incompressible Navier-Stokes equations were solved numerically, using the normal-shock relations as the outer boundary condition and the slip boundary condition at the surface given by Eq. (1). The heat-transfer rates were then obtained from the energy equation using the temperature-jump expression, Eq. (2). Details of the numerical method employed are given in reference 2.

The results of these computations are shown in Fig. 1, where shock-layer to boundary-layer heat-transfer ratios are presented as a function of Reynolds Number with density ratio across the shock, ϵ, as a parameter. This ratio gives essentially the increase in heat-transfer rates due to shock-generated vorticity over the values predicted by boundary-layer theory. The boundary-layer heat-transfer rates were obtained from references 4 and 5. The Reynolds Number is based on the free-stream velocity V_∞, the body radius r_w, and on fluid properties behind the shock. The slip boundary conditions are seen to reduce the heat-transfer rates as expected. The effect of the slip boundary conditions relative to shock-generated vorticity effects increases as the shock strength decreases (ϵ increasing). The reason for this is that the shock-generated vorticity effect varies approximately as $(\epsilon)^{-2}$ (Fig. 1) whereas the slip boundary conditions are proportional to $(\epsilon)^{-1/2}$. It should be noted that these computations are restricted by the incompressible assumption to cases where the heat-transfer rates are low. The slip boundary conditions will have a smaller effect when the heat-transfer rates are high (cold wall), as was shown by Hayes and Probstein.[6]

In the Reynolds Number range between 500 and 3,000, the results shown in Fig. 1 for $\epsilon = 0.10$ can be approximated by

$$q_{S.L.}/q_{B.L.} = 1 + (14.8/Re^{0.60}) - (14.5/Re^{0.77}) \tag{3}$$

The second term in the above equation represents the increase in heat transfer resulting from shock-generated vorticity whereas the last term represents the counteracting effect of the slip boundary conditions. Hence, for the above conditions, the effect of slip boundary conditions on stagnation-point heat transfer is of the same order of magnitude as the effect of shock-generated vorticity.

REFERENCES

[1] Probstein, R. F., *Continuum Theory and Rarefied Hypersonic Aerodynamics*, Brown University, WADC TN 58-145, AD-155-587.

[2] Hoshizaki, H., *Shock-Generated Vorticity Effects at Low Reynolds Numbers*, Lockheed Missile and Space Division, LMSD-48381, (ASTIA No. 210 401) Sunnyvale, Calif., January, 1959.

[3] Kennard, E. H., *Kinetic Theory of Gases*, p. 291, McGraw-Hill Book Co., Inc., New York, 1938.

[4] Sibulkin, M., *Heat Transfer Near the Forward Stagnation Point of a Body of Revolution*, Journal of the Aeronautical Sciences, Vol. 19, No. 8, p. 570, August, 1952.

[5] Lighthill, *Dynamics of a Dissociating Gas. Part 1—Equilibrium Flow*, J. Fluid Mech., Vol. 2, No. 1, January, 1957.

[6] Hayes, W. D., and Probstein, R. F., *Hypersonic Flow Theory*, p. 375, Academic Press, New York, 1959.

The Pitot and Static Tubes—Condensed Sources of General Fundamentals and Applications

Jay W. Stuart, Jr.
Engineering Specialist, Aero Sciences, Norair, a Division of Northrop Corporation, Hawthorne, Calif.
September 18, 1959

SOME SUBJECTS, even though they constitute a well-developed portion of a field, have realized no complete, unified exposition. Thus, only a very few experts, workers who exercise a continuing, exhaustive interest in a subject, possess such knowledge. Hence, when the need arises, the nonexpert must hastily survey the field with such resources as are at hand. This note is presented to ease this task by briefly describing a condensed collection of papers which fill the void for the subject of pitot and static tubes, their origin, principles, theory, evolution, performance, and modern modifications and applications.

The author became aware of this need while being associated with a survey of the methods of measuring free-stream stagnation and static pressures,[1] experimentally developing his concept of sensing the free-stream static pressure by aerodynamic compensation,[2] and conducting a survey of attitude sensing,[3] each with pressure sensors in high-speed flows. These papers should complement the others discussed below in high-speed, modern aircraft applications. They rely heavily on all these papers or their predecessors, except references 9, 10, and 11. Reference 11 is very exemplary in fulfilling the described need and is the stimulus for this note.

Reference 4 is an especially complete treatment of the pressure sensing of altitude and speed for subsonic operational flight. Reference 5 is an extended, summarizing compilation of particularly obscured classical and World War II investigations of the entire subject. Reference 6 is a valuable, thorough treatment of the contemporary status of many geometries of the pitot tube and their performance, including large incidence to the flow. Likewise, reference 7 compiles most of the pertinent information about practical static-pressure installations on aircraft, including details about orifice configurations. Furthermore, extending aircraft applications into the transonic regime, reference 8 gathers the information of subfields investigated by each of its authors into a general treatment of the transonic behavior of the forward "pressure-field error." Reference 9 reports analytical prediction and experimental verification of the nose-boom shape perturbation for an aerodynamically simplified aircraft configuration. This provides for the accurate sensing of free-stream pressure and Mach Number by aerodynamic compensation or nullification of the "pressure-field error" according to the concept of reference 2, empirically adapted therein to a more complex configuration. Finally, reference 10 briefly reviews the significance of material in references 7, 8, and 9 to the restricted field of flight, especially projected transport flight, in the transonic speed regime.

Now we come to the basic review Reference 11 is Professor Folsom's "Review of the Pitot Tube," a compendious synopsis of precisely that subject which has been lacking in the literature as described It was published concurrently with references 6 and 8 and the references of the author and was, therefore, unknown at that time. It commendably condenses, discusses, docu-

ments, illustrates, and evaluates only that material of value in history, principle, theory, applications, and design without becoming burdened with details. Though crossing all applicable disciplines—e.g., homogeneous and heterogeneous liquids and gases and their mixtures, it exhibits special interest in none. This work is evidently the result of long, broad, intimate experience and is highly recommended by this author.

It is further suggested that the combination of these eleven references provides a valuable start of a coverage of the field and its application to flight as the first step before attacking the frontiers.

References

[1] Korkegi, R. H., and Mannes, R. L., *Investigation of Free-Stream Pressure and Stagnation Pressure Measurement from Transonic and Supersonic Aircraft— Phase I—Survey and Analysis*, USCEC R 33-201, WADC TR 55-238, March, 1955.

[2] Mannes, R. L., and Stuart, J. W., Jr., *Investigation of Free-Stream Pressure and Stagnation Pressure Measurement from Transonic and Supersonic Aircraft—Interim Phase Report II—Experimental*, USCEC R 33-202, WADC TR 55-238, July, 1956.

[3] Smetana, F. O., and Stuart, J. W., Jr., *A Study of Angle-of-Attack Angle-of-Sideslip Pitot-Static Probes*, USCEC, WADC TR 57-234, AD 118 209, January, 1957.

[4] Huston, W. B., *Accuracy of Airspeed Measurement and Flight Calibration*, NACA R 919, 1948.

[5] Bäuerle, H., *D₂., II., 3. Measuring Instruments for Pressure, Velocity, and Directional Measurements*, British R-T 951, MAP Volkenrode-VG-251, March 15, 1947.

[6] Gracey, W. B., *Wind-Tunnel Investigation of a Number of Total-Pressure Tubes at High Angles of Attack. Subsonic, Transonic and Supersonic Speeds*, NACA R 1303, (supersedes TN 3641), 1957.

[7] Gracey, W. B., *Measurement of Static Pressure on Aircraft*, NACA R 1364, (supersedes TN 4184 and RM L57A09), 1958.

[8] O'Bryan, Thomas C., Danforth, Edward C. B., and Johnston, J. Ford, *Error in Airspeed Measurement Due to the Static-Pressure Field Ahead of an Airplane at Transonic Speeds*, NACA R 1239, (supersedes RM L9C25, L50L28, and L52A17), 1955.

[9] Ritchie, Virgil S., *Several Methods for Aerodynamic Reduction of Static-Pressure Sensing Errors for Aircraft at Subsonic, Near-Sonic, and Low Supersonic Speeds*, NASA R 18 (adv. copy), 1959.

[10] Gracey, William, and Ritchie, Virgil S., *Review of Aircraft Altitude Errors Due to Static-Pressure Source and Description of Nose-Boom Installations for Aerodynamic Compensation of Error*, NASA Memo 5-10-59L, 1959.

[11] Folsom, R. G., *Review of the Pitot Tube*, Trans. ASME, pp. 1447–1460, October, 1956.

The Influence of Panel Deformations on Wing Flutter

D. J. Johns

Lecturer, The College of Aeronautics, Cranfield, England

September 29, 1959

Symbols

a	=	panel chord
A	=	panel-bending generalized coordinate
c	=	speed of sound
h	=	panel thickness
m	=	mass/unit area; m_T = whole wing; m_p = two panels
M	=	Mach Number
n	=	number of panel chords—i.e., na = wing chord (n is odd)
p	=	aerodynamic pressure
Q_α, Q_A	=	generalized aerodynamic forces
R	=	$[2\rho c/m_p\omega_A]$
t	=	time
U	=	velocity of supersonic stream
w	=	velocity of air normal to surface
$Z(x, t)$	=	displacement function
α	=	wing twist
ω	=	flutter frequency
ω_A, ω_α	=	fundamental frequencies in panel bending and wing twist
θ	=	ω_A/ω_α
λ	=	m_T/m_p
ρ	=	density of undisturbed supersonic stream
σ	=	density of panel material

THE PROBLEM of panel flutter has received considerable attention in recent years, and the phenomenon is now fairly well understood.[1–3] Similarly, investigations into flutter at high Mach Numbers of complete wings have been made which illustrate the effects of various parameters.[4, 5]

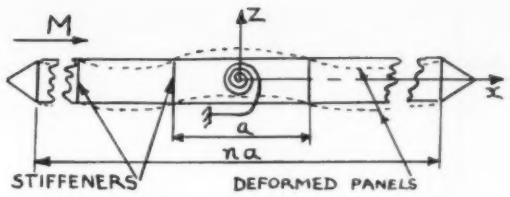

FIG. 1. Multipanel wing.

However, the question arises as to whether significant couplings can occur between the panel-bending modes and the deformation modes of the entire lifting body or surface—e.g., a wing. A brief investigation has been made of the simplified configuration shown in Fig. 1 and is reported in this note. Although this configuration may not be very representative—e.g., only spanwise stiffeners are shown—it should suffice for the purposes of the note. The various assumptions made are as follows:

(a) Wing elastic axis at midchord.
(b) Aerodynamic forces given by piston theory and acting only on the panels.
(c) Upper and lower panels have simply supported edges and deform similarly.
(d) Uniform mass distribution over wing.
(e) Zero structural damping.
(f) The motion is simple harmonic.

For the coupled modes of wing twist and fundamental panel bending (streamwise), the displacement function Z is given by

$$Z = x\alpha \text{ for the wing structure}$$

$$Z = x\alpha + aA\cos(\pi x/a) \text{ for the panels}$$

The total kinetic energy, per unit width spanwise, is given by

$$K.E. = \int_{-na/2}^{na/2} (1/2)m\dot{Z}^2\,dx$$

$$\therefore \quad \text{K.E.} = (1/2)m_T(n^2a^2/12)\dot{\alpha}^2 + (1/2)m_p(na^2/2)\dot{A}^2 \qquad (1)$$

and, hence, the strain energy can be written

$$\text{S.E.} = (1/2)m_T(n^2a^2/12)\omega_\alpha^2\alpha^2 + (1/2)m_p(na^2/2)\omega_A^2A^2 \quad (2)$$

The aerodynamic pressure, as given by linear piston theory, is $p = \rho cw$ where

$$w = U(dZ/dx) + (dZ/dt)$$

Therefore, the generalized aerodynamic forces are given by

$$\left.\begin{aligned} Q_\alpha &= 2\rho c[(\dot{\alpha}a^2n^2/12) - (\pm)(2Ua^2A/\pi)] \\ Q_A &= 2\rho c[\pm(2Ua^2\alpha/\pi) + (n\dot{A}a^2/2)] \end{aligned}\right\} \qquad (3)$$

where $\pm$ sign depends upon whether $(n + 1)/2$ is odd or even, and, by using Lagrange's equation, the final flutter equation obtained is

$$[\omega_\alpha^2 - \omega^2 + (2\rho ci\omega/m_T)] \times [\omega_A^2 - \omega^2 + (2\rho ci\omega/m_p)] + (96/\pi^2) \times [(2\rho cU/an^2)]^2(1/m_Tm_p) = 0 \quad (4)$$

If Eq. (4) is separated into its real and imaginary parts, one obtains

$$(\omega/\omega_\alpha)^2 = [(\theta^2 + \lambda)/(1 + \lambda)] \qquad (5)$$

and

$$(96/\pi^2)[U/a\omega_An^2]^2 = [(\theta^2 + \lambda)/(1 + \lambda)](1/\theta^2) + [\lambda/(1 + \lambda)]^2 \times [(\theta^2 - 1)/\theta^2]^2(1/R^2) \quad (6)$$

where

$$\lambda = m_T/m_p, \quad \theta = \omega_A/\omega_\alpha, \quad R = 2\rho c/m_p\omega_A \qquad (7)$$

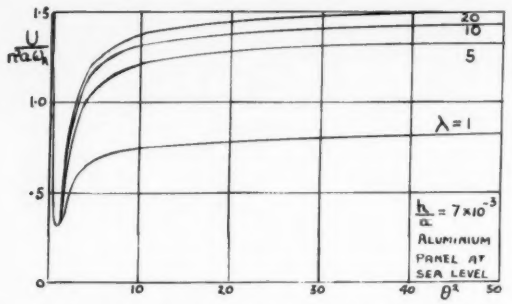

FIG. 2. Wing-panel critical flutter speed ($a\omega_A$ = 346 ft./sec.).

This latter term is a measure of the aerodynamic damping forces and depends upon altitude, panel material, and thickness-chord ratio.[6]

As an example, aluminum panels: $h/a = 7 \times 10^{-3}$ at sea level. Therefore, $R = 0.2$ and $a\omega_A = 5\rho ca/\sigma h$ = const. = 4,150 in./sec.—i.e., if $a = 10$ in., $\omega_A = 415$ rad./sec.

From Eq. (6), Fig. 2 shows the variation of $[U/n^2 a\omega_A]$ with θ^2 for various values of λ. It is seen from Fig. 2 that, as $\theta^2 \to \infty$ and $\lambda \to \infty$, for $R = 0.2$, the value of $[U/n^2 a\omega_A]$ tends to a maximum—i.e., 1.6.

Hence, the corresponding maximum value of U is (for $n = 1$)

$$U = 1.6 \times 4{,}150/12 \text{ ft./sec.}$$
$$\doteq 550 \text{ ft./sec.} \quad (8)$$

Although this result is meaningless since piston theory is inapplicable at subsonic speeds, it indicates that flutter in the modes considered here is more critical than in the pure panel-flutter problem, where, from reference 3, for an aluminum panel at sea level with $h/a = 7 \times 10^{-3}$, $M_{crit.} \doteq 4.5$. However, for $n = 3$, $U_{crit.} = 4{,}950$ ft./sec., which is equal to $M_{crit.} = 4.5$ (approx.).

Although a possibly pessimistic configuration has been considered in this analysis, the results still indicate the possible importance of wing-panel coupling. While the present result is not necessarily fully realistic, it would suggest that a coupling of the type considered in this note might be critical on certain practical designs. Obviously, the problem merits further study.

REFERENCES

[1] Hedgepeth, J. M., *Flutter of Rectangular Simply Supported Panels at High Supersonic Speeds*, Journal of the Aeronautical Sciences, Vol. 24, No. 8, pp. 563–573, 586, August, 1957.

[2] Houbolt, J. C., *A Study of Several Aerothermoelastic Problems of Aircraft Structures in High Speed Flight*, Inst. Flug. und Leicht, Mitt. 5, 1958.

[3] Johns, D. J., *Some Panel Flutter Studies Using Piston Theory*, Journal of the Aero/Space Sciences, Vol. 25, No. 11, pp. 679–684, November, 1958.

[4] Chawla, J. P., *Aeroelastic Instability at High Mach Number*, Journal of the Aero/Space Sciences, Vol. 25, No. 4, pp. 246–258, April, 1958.

[5] Morgan, H. G., Runyan, H. L., and Huckel, V., *Theoretical Considerations of Flutter at High Mach Numbers*, Journal of the Aero/Space Sciences, Vol. 25, No. 6, pp. 371–381, June, 1958.

[6] Johns, D. J., and Parks, P. C., *The Effect of Structural Damping on Panel Flutter*, to be published in Aircraft Engineering.

A Simplified Expression for the Period of Nonlinear Oscillations of Curved and Flat Panels

Joshua E. Greenspon
J G Engineering Research Associates, Baltimore, Md.

August 13, 1959

A PANEL undergoing large deformations acts like a nonlinear spring with cubic nonlinearity.[1, 6] The equation of motion of such a panel is

$$\ddot{w} + (\alpha w + \beta w^3) = 0$$

where α is connected with the linear portion of the restoring force and β is connected with the nonlinear part of the restoring force; α and β can be determined as outlined in reference 1.* Such a system has a period of oscillation dependent on the amplitude of the oscillation. The expression for the period is as follows:[2]

$$T = 4\sqrt{2} \int_0^{\pi/2} d\theta / \sqrt{2\alpha + \beta A^2 + \beta A^2 \sin^2 \theta} \quad (1)$$

where A is the amplitude of the motion and T is the period. A simplified expression for the period is derived below. First write the expression for the period in the following form:

$$T = 4\sqrt{2}/\sqrt{2\alpha + \beta A^2} \int_0^{\pi/2} d\theta / \sqrt{1 + k^2 \sin^2 \theta} \quad (2)$$

where

$$k^2 = \beta A^2/(2\alpha + \beta A^2); \quad \text{thus } k < 1$$

[for the linear case where $\beta = 0$, $T = (4\sqrt{2}/\sqrt{2}\sqrt{\alpha}) \times (\pi/2) = 2\pi/\sqrt{\alpha}$.] Now, referring to reference 1, it is seen that for a flat rectangular plate

$$\beta = D\delta/\rho h^3 b^4, \quad \alpha = D\gamma/\rho h b^4$$

where $D = Eh^3/[12(1 - \nu^2)]$, the plate modulus; h = plate thickness; ρ = mass density of plate material; b = one half the length of the shorter side of the plate; and δ and γ are obtained from the restoring-force curve.

$$F = \gamma(w/h) + \delta(w/h)^3$$

F being a nondimensional force function. So,

$$k^2 = (1/2)(\delta/\gamma)(A^2/h^2)/[1 + (1/2)(\delta/\gamma)(A^2/h^2)]$$

If the denominator in expression (2) is expanded into a series and the integration carried out,† we obtain

$$T = (2\pi/\sqrt{\alpha})\sqrt{1/[1 + (1/2)(\delta/\gamma)(A^2/h^2)]} \times [1 - (k^2/4) + (9k^4/64) - (225k^6/2304) \ldots]$$

so that the ratio of the period of oscillation to the linear period is

$$T/(2\pi/\sqrt{\alpha})$$

* For an initially flat panel, $\beta > 0$, corresponding to a hard spring; for an initially curved panel, $\beta < 0$, corresponding to a soft spring.

† Such a technique is employed by Malkin.[5]

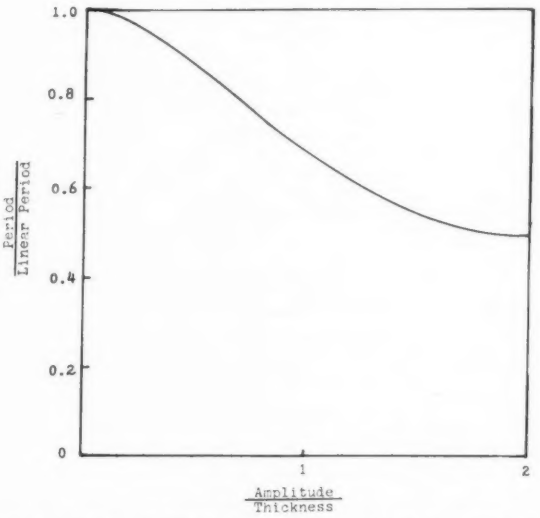

FIG. 1. Nonlinear period for a simply supported square plate.

As an example, take a clamped square plate. For this case, $\delta = 35$ and $\gamma = 45$, so $\delta/\gamma = 0.775$ (see reference 1). So,

$$T/Te = \sqrt{1/[1 + 0.388(A^2/h^2)]} \times [1 - (k^2/4) + (9k^4/64) - (225k^6/2304) \ldots]$$

where

$$k^2 = [0.388(A^2/h^2)]/[1 + 0.388(A^2/h^2)]$$

The curve of T/Te is given in Fig. 1 for a simply supported square plate[3] where

$$F = qa^4/Eh^3 = 1.37\, w_0 + 1.94(w_0^3/h^2)$$

or

$$qa^4/Dh = 12(1 - \nu^2) \times 1.37(w_0/h) + 12(1 - \nu^2) \times 1.94(w_0^3/h^3)$$

Therefore,

$$\gamma = 12(1 - \nu^2) \times 1.37; \quad \delta = 12(1 - \nu^2) \times 1.94$$

so

$$\delta/\gamma = 1.42$$

and

$$T/Te = \sqrt{1/[1 + 0.71(A^2/h^2)]}[1 - (k^2/4) + \ldots]$$

if

$$A/h = 1, \quad T/Te = 0.70$$

Chu and Herrmann[4] obtain 0.71 as a result of their more exact analysis.

REFERENCES

[1] Kirchman, E. J., and Greenspon, J. E., *Nonlinear Response of Aircraft Panels to Acoustic Noise*, J. Acoustical Soc. Am., Vol. 29, No. 7, pp. 854–857, July, 1957.

[2] Stoker, J. J., *Nonlinear Vibrations*, 1st Ed., Chap. II, p. 21, Interscience Publications, Inc., New York, 1950.

[3] Timoshenko, S., *Theory of Plates and Shells*, 1st Ed., Chap. IX, p. 350, McGraw-Hill Book Co., Inc., New York, 1940.

[4] Chu, H., and Herrmann, G., *Influence of Large Amplitudes on Free Flexural Vibrations of Rectangular Elastic Plates*, J. Appl. Mech., Vol. 23, No. 4, pp. 532–540, December, 1956.

[5] Malkin, I., *Certain Problems in the Theory of Nonlinear Oscillations* (in Russian), 1st Ed., Chap. I, p. 36, State Tech. and Theor. Lit. Press, Moscow, 1956.

[6] Lassiter, Leslie W., Hess, Robert W., and Hubbard, Harvey H., *An Experimental Study of the Response of Simple Panels to Intense Acoustic Loading*, Journal of the Aeronautical Sciences, Vol. 24, No. 1, pp. 19–24, January, 1957.

On Magnetohydrodynamic Channel Flow†

J. E. McCune* and W. R. Sears**
Cornell University, Ithaca, N.Y.

August 7, 1959

IN REFERENCES 1 AND 2, the flow of electrically conducting gases in channels, under the influence of crossed electric and magnetic fields, was treated in the quasi-one-dimensional approximation of gasdynamics. The present note is intended to clear up certain confusion which we believe exists concerning the approximations of that investigation and to present the results of an extension of the work.

(1) The first point is raised by certain published reviews[5] of the Resler-Sears paper and by a number of comments we have received privately in the same vein. The impression seems to exist that the perturbations of the applied magnetic field due to

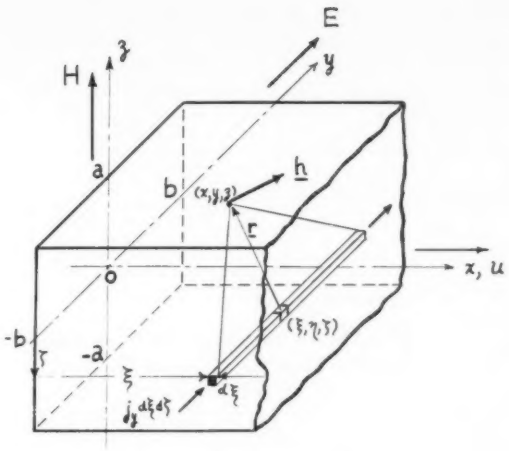

FIG. 1. Coordinate system and notation.

motion of the fluid have been neglected and, therefore, that the theory pertains only to flows of small conductivity, or, more precisely, small magnetic Reynolds Numbers. This is not correct. The applied field is, in general, grossly distorted by the motion, but this distortion does not appear explicitly in the channel-flow equations.

In references 1 and 2, the approximation was described as "the familiar methods of one-dimensional channel flow;" and the variables $p(x)$, $u(x)$, etc., were defined as average values of pressure, velocity, etc., for the cross section at x. Thus, the current $j_y(x)$ is also the average value, and $j_y H_z$ the average body force at x (see Fig. 1). Eqs. (38)–(40) are relations among such average values. Maxwell's equations are not needed here, since the effects they describe do not enter explicitly in determining the above average quantities. The average value $H_z(x)$ is the same as the boundary value—i.e., the field strength at the walls of the channel. The whole affair is quite analogous to the treatment of channel flow with viscosity, found in many textbooks. Although one works with an average speed $u(x)$, one also introduces wall friction in terms of a friction coefficient and thus surely recognizes that the profile of velocity $u(x, y)$ is not uniform in y but involves shear.

The actual approximation made in references 1 and 2 is to neglect the induced part of the boundary values $H_z(x)$ mentioned above—i.e., to take these values to be just the field strengths *applied* externally by magnets. This is valid for nearly uniform slender channels, as will be elucidated below; and for sufficiently slow variations of properties along the channel it is valid for any magnetic Reynolds Number. It becomes exact for an infinitely long uniform channel (e.g., Hartmann flow), where the field distortion, although gross, is the same for all x and the induced part of H_z is zero.

(2) Maxwell's equations (in particular, Ampère's law) are needed within the quasi-one-dimensional approximation described above only to calculate the induced part of the fields. Their use allows us to determine, for example, how much of the assumed boundary value $H_z(x)$ must actually be supplied by external magnets. This is the extension of references 1 and 2 mentioned above.

If the local value of the curl of **H**, given by $4\pi\mathbf{j}(x, y, z)$, were known everywhere, the corresponding values of **H** itself could be computed using the classical calculation of Biot-Savart. In the present case, we are interested only in that part of **H** associated with the currents *in the gas;* the fields arising from external circuitry, including the return circuits for the gas currents, are all considered "applied." The theory of references 1 and 2 provides the *average* current density in the y direction, $j_y(x)$. Associated with this component of current are the induced components of

† Part of this work was carried out by Dr. McCune as consultant to Thompson Ramo Wooldridge, Inc.

* Formerly, Instructor in Aeronautical Engineering. Now, Associate Consultant, Aeronautical Research Associates of Princeton.

** Director, Graduate School of Aeronautical Engineering.

magnetic field, h_x and h_z. As outlined below, if we replace the local value $j_y(x, y, z)$ in the Biot-Savart law by its average, $j_y(x)$, we can obtain a useful approximation to h_x and h_z.

From the Biot-Savart law, we have in general

$$\mathbf{h} = \iiint_{\substack{\text{all currents}\\ \text{in gas}}} [(\mathbf{j} \times \mathbf{r})/r^3] d\tau \tag{1}$$

where $\mathbf{r}$ is the vector displacement from the current element to the field point in question. Referring to the geometry illustrated in Fig. 1 and using the approximations outlined above, we may write for the plane $y = 0$

$$h_z(x, 0, z) = 2b \int_0^L j_y(\xi)(\xi - x) d\xi \int_{-a}^{a} \frac{d\zeta}{[(x-\xi)^2 + (z-\zeta)^2]\sqrt{b^2 + (x-\xi)^2 + (z-\zeta)^2}} \tag{2}$$

Here L is the total length of the channel. Generalization to arbitrary y is straightforward but tedious.

The inner integral in Eq. (2) has an elementary expression which when evaluated at the limits $\pm a$ gives

$$h_z(x, 0, z) = \int_0^L \frac{j_y(\xi)(\xi - x) d\xi}{|x - \xi|} \left\{ \cos^{-1}\left(\frac{(x-\xi)^2 + \{(a-z)^2[(x-\xi)^2 - b^2]/[(x-\xi)^2 + b^2]\}}{(x-\xi)^2 + (a-z)^2} \right) + \cos^{-1}\left(\frac{(x-\xi)^2 + \{(a+z)^2[(x-\xi)^2 - b^2]/[(x-\xi)^2 + b^2]\}}{(x-\xi)^2 + (a+z)^2} \right) \right\} \tag{3}$$

This expression can be used for direct computational purposes to obtain h_z corresponding to the currents *in the gas* for any solution obtained from the theory of references 1 and 2. More importantly, it can be used as a means of estimating the order of magnitude of h_z for various channel geometries in order to clarify the nature of the channel-flow approximation.

A particularly interesting limit of Eq. (3) arises when $b/L \to \infty$, i.e., the channel is two-dimensional, and $a/L \to 0$ such that the product aj_y remains finite. One then obtains, for $z = \pm a$,

$$h_z(x) \to -2 \int\!\!\!\!\!\!\diagup_0^L I(\xi) d\xi/(x - \xi) \tag{4}$$

where

$$I(\xi) = \lim_{a \to 0} 2aj_y(\xi)$$

This is the classical expression for the component of magnetic field normal to a current sheet. It is well known that, while h_z is continuous through such a sheet, h_x is discontinuous; this certainly suggests that $\partial h_x/\partial z$ is the dominant term in the expression for j_y, as will be confirmed below.

In most channels of interest, both a and b will be small compared with the channel length, L. Consider the upper edge of the channel, $z = a$, where only the second term in the brackets in Eq. (3) plays a role. The $\cos^{-1}$ has its maximum value of π at $x = \xi$ and contributes $O(\pi)$ over the range of integration for which $|x - \xi| = O(b)$ when a is also small. Thus, at the ends of the duct ($x = 0$ or L), the z component of the induced field is order $\pi j_y(x = 0, L)b$. On the other hand, since the integrand is discontinuous in sign at $x = \xi$, the above contribution to h_z cancels out in the range $b < x < L - b$; expansion of the integrand then shows that $h_z = O(j_y ab/L)$ over the middle portions of the duct. The approximation made in references 1 and 2, mentioned above, is to neglect terms of this order in comparison with the applied $H_z(x)$; this is seen to be justified if L is sufficiently large.

By contrast, the component h_x is $O(j_y a)$ according to Ampère's law; no approximation was made in references 1 and 2 regarding this component. It is now clear, moreover, that except near the ends of the duct the correct approximation for the slender channels of references 1 and 2 is

$$4\pi j_y \approx \partial h_x/\partial z \tag{5}$$

in e.m.u. This formula, incidentally, provides a simple means of computing the "pinch effect" for channel flows of this kind.

References

[1] Resler, E. L., Jr., and Sears, W. R., *The Prospects for Magneto-Aerodynamics*, Journal of the Aeronautical Sciences, Vol. 25, pp. 235–245, 258, April, 1958.

[2] Resler, E. L., Jr., and Sears, W. R., *Magneto-Gasdynamic Channel Flow*, ZAMP, Vol. 9b, Jako Ackeret Festschrift, pp. 509–518, 1958.

[3] Naze, J., Reviews of references 1 and 2 published in Mathematical Reviews, Vol. 19, p. 1226, 1958, and Vol. 20, p. 99, 1959.

The Stagnation-Point Ablation of Teflon During Hypersonic Flight†

S. M. Scala* and N. S. Diaconis**
General Electric Company, M.S.V.D., Philadelphia, Pa.

August 10, 1959

Symbols

h = enthalpy
Q^* = effective heat of ablation

Subscripts

e = outer edge of boundary layer, stagnation
w = wall
air = evaluated as if the gas is air

(1) Introduction

Although a cursory analysis seems to indicate that one can predict the thermal behavior of polytetrafluoroethylene (Teflon) by means of a simple energy balance,[1] a more complete understanding of the thermal response of this material requires that the chemical-kinetic and gas-dynamic aspects of the problem be considered, as well as the purely thermodynamic factors. In this note, we will compare several recent theoretical predictions,[1–3] with the most recent experimental results available,[1, 4] on the ablation of Teflon during exposure to the stagnation enthalpy and pressure levels encountered during hypersonic flight.

(2) Analysis

During severe heating, Teflon polymer $(C_2F_4)_n$, undergoes a rate-controlled pyrolysis process in which the solid gasifies primarily to the monomer C_2F_4. The early work of Madorsky, et al.,[5] and Siegle and Muus[6] concentrated on the experimental determination of the kinetics of the depolymerization process. More recently, Friedman[7] re-examined the earlier work and established new kinetic equations for the pyrolysis mechanism.

However, in order to predict the ablation rate of this material during hypersonic flight, it is also necessary to consider the effect of diffusion and combustion within the boundary layer, since a diffusion-controlled combustion process occurs in which part of the injected mass of C_2F_4 combusts to form COF_2.

† This note is based in part upon work performed under the auspices of the USAF, Ballistic Missiles Division, Contract No. AF 04(647)-269.

* Manager, High Altitude Aerodynamics.

** Specialist, Aerodynamics.

The authors wish to acknowledge the assistance of Mr. Leon Gilbert who performed the calculations and drew the graph.

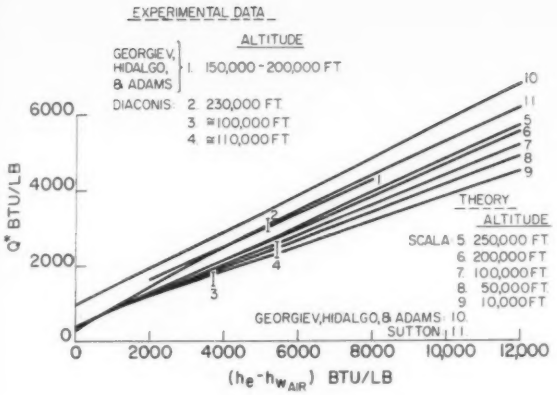

FIG. 1. Effective heat of ablation for Teflon.

(3) DISCUSSION

For this discussion, refer to Fig. 1. The experimental data of reference 1, which cover a broad range of stagnation enthalpies and which were taken within narrow pressure limits, are shown. In the theoretical calculations of reference 1 (also shown), the effects of combustion were assumed to be negligible, and in addition it was assumed that the surface temperature was some known constant—i.e., the "ablation temperature". As shown in Fig. 1, agreement between theory and experiment is fair.

Upon retaining the assumption of constant wall temperature, but including combustion effects, Sutton[2] independently calculated the variation of Q^* with stagnation enthalpy, and his result appears to coincide somewhat more closely with the experimental data of reference 1 than does the theory of reference 1.

The major shortcoming of each of these theories,[1, 2] however, is that the assumption of a constant surface temperature precludes the appearance of a pressure or altitude effect.

When the assumption of constant wall temperature is relaxed—i.e., making the latter an unknown to be obtained during the solution of the problem, Scala[3] found that the surface temperature correlated linearly with the logarithm of the stagnation pressure; and, moreover, a significant altitude effect appeared in the magnitude of the effective heat of ablation, Q^*. Scala's theoretical prediction has been confirmed in part by Diaconis who performed ablation tests on Teflon in a 60-kw. air-arc test facility. Diaconis[4] found that, in agreement with the theory, (a) at constant altitude, the effective heat of ablation of Teflon increases with stagnation enthalpy, and (b) at constant stagnation enthalpy, the effective heat of ablation of Teflon increases with altitude (see Fig. 1).

(4) CONCLUSIONS

The foregoing analysis and discussion serves to emphasize that extreme care must be exercised in analyzing the effects of the mass transfer of chemically reacting species whose molecular weight differs appreciably from that of air molecules.

The significance of the effect of altitude upon the assessment of surface temperature should not be overlooked; and further, the use of an "ablation temperature," while a useful expedient, is an artificial concept.

In order to establish the thermal response of ablating materials experimentally, good data are required at high stagnation pressures.

REFERENCES

[1] Georgiev, S., Hidalgo, H., and Adams, M. C., *On Ablation for the Recovery of Satellites*, Heat Transfer and Fluid Mechanics Institute, Stanford University Press, pp. 171–180, June, 1959.

[2] Sutton, G. W., private communication.

[3] Scala, S. M., *A Study of Hypersonic Ablation*, Tenth International Astronautical Federation Congress, London, England, August 30–September 5, 1959. Springer Verlag.

[4] Diaconis, N. S., Fanucci, J. B., and Sutton, G. W., *The Heat Protection Potential of Several Ablation Materials for Satellite and Ballistic Re-entry Into the Earth's Atmosphere*, G. E. Co., M.S.V.D., TIS No. R59 SD 423, August, 1959.

[5] Madorsky, S. L., Hart, V. E., Straus, S., and Sedlak, V. A., *Thermal Degradation of Tetrafluoroethylene and Hydrofluoroethylene Polymers in a Vacuum*, J. Res., N.B.S., Vol. 51, pp. 327–333, 1953.

[6] Siegle, J. C., and Muus, L. T., *Pyrolysis of Polytetrafluoroethylene*, address to Amer. Chem. Soc. Meeting, September 17, 1956.

[7] Friedman, H., *The Mechanism of Polytetrafluoroethylene Pyrolysis*, G. E. Co., M.S.V.D., TIS No. R59SD385, June 19, 1959. Address to Amer. Chem. Soc. Meeting, September, 1959.

A Multiple Hot-Wire Array for Measurements of Downwash Integrals

Kent Kresa* and Erik Mollö-Christensen
Student and Associate Professor, Respectively, Department of Aeronautics and Astronautics, Massachusetts Institute of Technology, Cambridge, Mass.
September 8, 1959

AT TIMES, a direct measurement of a momentum integral may facilitate our understanding of an unsteady flow process. This is especially the case where the quantity of immediate interest is very difficult to measure, such as the mean drag of an oscillating body or the lift on a heavy body in unsteady flow.

As a first attempt at direct measurement of an instantaneous momentum integral, an array of 26 hot wires was constructed and used for measurement of downwash in a Kármán vortex street.

(1) ZIG-ZAG HOT-WIRE ARRAY

The multiple array of hot wires is shown in Fig. 1. It consists of 26 wires, mounted on pins which are inserted in thermocouple

* Now with Avco, Burlington, Mass.

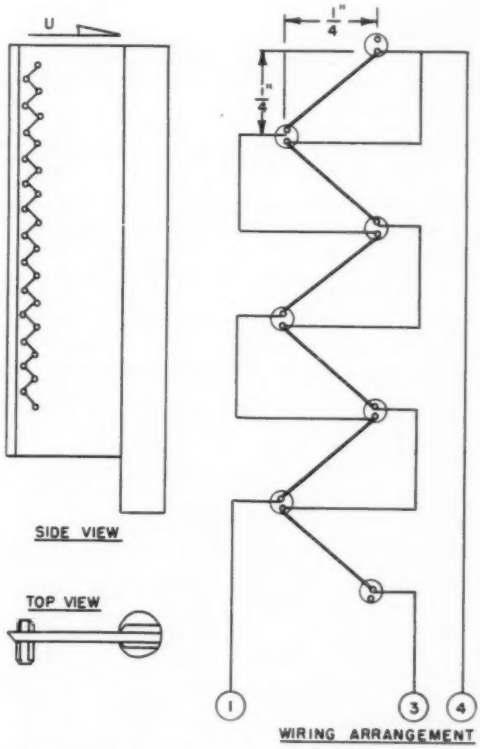

FIG. 1. Sketch and diagram of "zig-zag" hot wire.

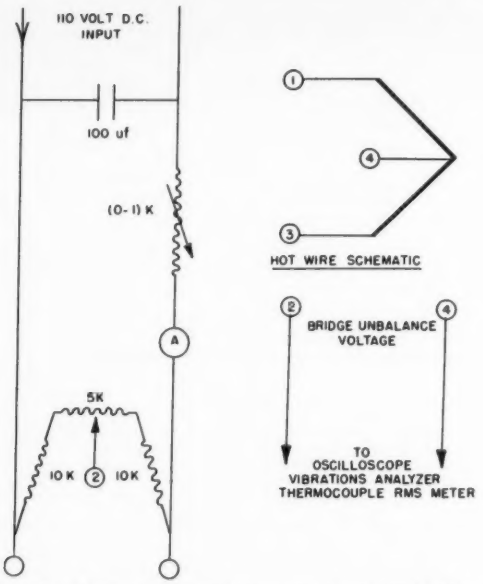

FIG. 2. Schematic of heating-current circuit and bridge.

tubing. The tubing is mounted in a steel-reinforced micarta wedge.

The wires are connected so as to form one half of a Wheatstone bridge, with all the "zigs" connected in series and all the "zags" connected in series, as shown in Fig. 2. The wire used is 0.001 in. diameter platinum wire.

The unbalance of the bridge is approximately proportional to

$$\int_{-h}^{+h} (v dy/U)$$

where v is the velocity along the array and U the velocity normal to the array.

A plot of bridge output vs. flow inclination is shown in Fig. 3.

The hot-wire bridge was found to need no compensation for time lag in the frequency range of 0–200 cps and could be used without any amplifiers.

(2) Measurement of Downwash in a Kármán Vortex Street

As a first application of the zig-zag hot wire, it was used to measure average streamwise flux of lateral momentum in the wake behind a cylinder.

The hot-wire output is proportional to

$$\int_{-h}^{+h} \{[v(y,\ t)]/U\}\ dy$$

The power spectral density $\varphi(\omega)$ of this quantity was measured

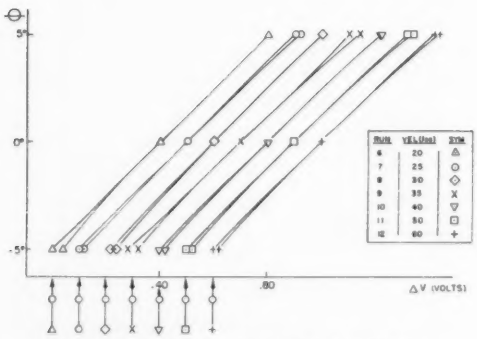

FIG. 3. Bridge output vs. flow inclination.

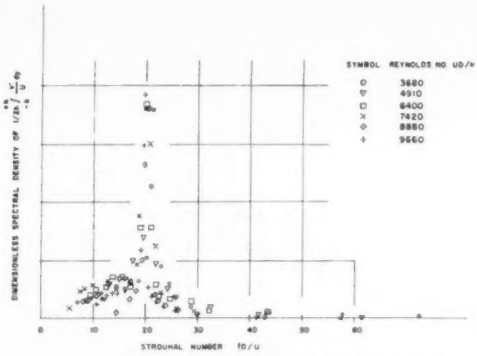

FIG. 4. Dimensionless power spectral density of $(1/2)\int_{-h}^{+h} (v'/U)dy$ vs. fD/U

and made dimensionless by multiplication by U/D, U being the free-stream velocity and D the diameter of the circular cylinder. The result was plotted against reduced frequency $\omega D/2\pi U$ and is shown in Fig. 4.

Although this result is interesting, we shall not attempt to interpret it here but merely exhibit it as a sample result of a measurement performed using a hot-wire rake.

References

[1] Kresa, K., *The Determination of Time-Varying Lift on a Cylinder Utilizing Hot-Wire Anemometry*, S.B. Thesis, Massachusetts Institute of Technology, May, 1959.

An Exact Calculation of Some Steady, Diabatic, Two-Dimensional Fields of Compressible Flow

Bruce L. Hicks* and Donald R. Chenoweth**
University of Illinois, Urbana, Illinois
August 12, 1959

Incomplete solutions of complex compressible flow problems can often be illuminated by comparison with exact solutions of elementary problems. We describe here a simple diabatic flow that can be constructed exactly by an inverse method applied to a restricted class of flow fields.

We characterize a steady, diabatic, flow field by the (irrotational) vector $\mathbf{N} = \nabla\phi_N$ where the (rotational) velocity vector $\mathbf{V} = \mathbf{N}[g(N)RT]^{1/2}$; R and T are the gas constant and the absolute temperature, respectively; $N = |\mathbf{N}|$; and the scalar $g(N)$ is a function of N only.[1] We describe the rate of heat addition by a coefficient

$$q_\Phi = (Q/2c_p)(RT^2)^{-1/2}$$

where Q is the heat added to the flow per unit mass and time, and q_Φ is, at the outset, an unknown function of position. We further characterize the types of flows considered here by a series of three restrictions.

Restriction 1. The partial differential equation satisfied by ϕ_N is of the elliptic type with determinant identically equal to one. Then, $g(N) = 2(1 - N^2)^{-1}$. In this case, an exact transformation on the dependent variable $\phi_N \rightarrow \Phi_1$, suggested by Dr. Bernard Dimsdale,[2] leads to the linear differential equation

$$\nabla^2\Phi_1 = (1/2)(\Lambda\Phi_1 - 4\alpha) \qquad (1)$$

where $\alpha = 0$ if $\Lambda \neq 0$. The fundamental solutions of this equation have already been discussed briefly.[2]

* Associate Professor, Department of Aeronautical Engineering.
** Graduate Student, Department of Aeronautical Engineering.

Restriction 2. $\Lambda \equiv 0$. In this case

$$\nabla^2\Phi_1 = -2\alpha, \text{ a constant} \tag{2a}$$

$$\Phi = \Phi_1 - \Phi_0 = \alpha(\phi_N + \phi_0)^2 \tag{2b}$$

where ϕ_0 and Φ_0 are integration constants. We shall use the function Φ to represent the flow field. In fact, most important characteristics of the flow can be expressed explicitly in terms of Φ. Thus,

$$\left.\begin{aligned}
&N^2 = |\nabla\phi_N|^2 = [(\nabla\Phi)^2]/4\alpha\Phi \\
&\gamma M^2 = gN^2 = [2P_0(\nabla\Phi)^2]/p \\
&p = P_0[4\alpha\Phi - (\nabla\Phi)^2] \\
&q_\Phi = (\pm\sqrt{2}/2\gamma)(P_0/p)^{3/2} \times \\
&\qquad \{4\alpha[4\alpha\Phi - p(\gamma+1)/P_0] - [\beta\eta + \zeta\chi]\} \\
&\mathbf{N}\cdot\nabla \ln T = \mathbf{N}\cdot\nabla \ln (p/\Phi) - \{p/[P_0(\nabla\Phi)^2]\}\mathbf{N}\cdot\nabla \ln \Phi \\
&\mathbf{N} = (1/2)(\alpha\Phi)^{-(1/2)}(\beta i + \zeta j) \\
&\beta = \partial\Phi/\partial x_2, \quad \zeta = \partial\Phi/\partial y_2 \\
&\eta = \partial(\nabla\Phi)^2/\partial x_2, \quad \chi = \partial(\nabla\Phi)^2/\partial y_2
\end{aligned}\right\} \tag{3}$$

where p, M, and γ are the pressure, the local Mach Number, and the specific heat ratio, respectively, and P_0 is an integration constant appearing in the pressure equation. Any second-degree algebraic function of x and y satisfies Eq. (2a). Furthermore, any appropriate boundary conditions can be satisfied by adding harmonic functions to these fundamental solutions, yielding, therefore, a great variety of calculable diabatic flow fields. We have classified in some detail the corresponding flow patterns of which there are many different types and will describe here only the simplest pattern, specified by the next restriction.

Restriction 3. The equipotential curves are parabolas. We may orient the parabolas symmetrically with respect to the y axis and write

$$\Phi = (e^2/4a)(x^2 + 2y) \tag{4}$$

where we have made the scale changes

$$x_2 = ex/2a, \quad y_2 = ey/2a \tag{5}$$

We can also express the other flow properties of interest as explicit functions of x and y:

$$\left.\begin{aligned}
&\Psi = (ex/2a)\exp(-y) \\
&\gamma M^2 = -2(x^2+1)(2x^2+2y+1)^{-1} \\
&p = -P_0e^2(2x^2+2y+1) \\
&q_\Phi = \pm\{[(\gamma+1)2a\sqrt{-2}]/e\gamma\}\{2x^2 + \\
&\qquad [2\gamma/(\gamma+1)]y+1\}[2x^2+2y+1]^{-(3/2)} \\
&\mathbf{N}\cdot\nabla \ln T = \mathbf{N}\cdot\nabla \ln [(2x^2+2y+1)/(x^2+2y)] + \\
&\qquad [(2x^2+2y+1)/(x^2+1)]\mathbf{N}\cdot\nabla \ln (x^2+2y) \\
&\mathbf{N} = [-(x^2+2y)]^{-(1/2)}(xi+j)
\end{aligned}\right\} \tag{6}$$

The quantity Ψ is not a stream function but is a parameter labeling the different streamlines.

Under the restrictions that we have imposed, the constant-pressure curves, the curve for zero rate of heat addition, and the sonic line are parabolas symmetric about the y axis (see Fig. 1). The parabola of zero pressure is a limit line, and real flow exists only within this parabola. We notice that the sonic parabola lies within the parabola of zero rate of heat addition and that this parabola in turn lies within the limit line.

If the streamlines are diverging at the sonic condition, then heat is being added continuously to the flow.[3, 4] For upward or nozzle flow, for example, heat is therefore being added to the fluid inside the parabola of zero rate of heat addition. The choice of signs in the fourth of Eqs. (6) must be in accordance with this principle and with the direction of the flow.

The streamlines are exponential curves (see Fig. 1). It is thus possible to simulate a particular diabatic nozzle flow. The thrust F_y per unit of exit diameter is found to be

$$F_{y/\text{ unit dia.}} = P_0e^2[(2/3)(2a\Psi/e)^2\exp(2y) + 2y + 1]_{y<y_{p=0}} \tag{7}$$

The exit of the nozzle is located at y, and the divergence of the nozzle is specified by the magnitude of $a\Psi/e$.

Corresponding to the equations above, the axis of symmetry of the nozzle is the zero streamline. Along this line, the differential equation for the temperature can be integrated, giving explicit relations between the flow properties and y and M:

$$\left.\begin{aligned}
&(p/p_*)_{x=0} = (-\gamma/2)(2y+1) = (1/M^2) \\
&(T/T_*)_{x=0} = (1/M^2)\exp\{(2/\gamma)[1-(1/M^2)]\} \\
&(T_t/T_{t*})_{x=0} = [2/(\gamma+1)]\{(1/M^2) + \\
&\qquad [(\gamma-1)/2]\}\exp\{(2/\gamma)[1-(1/M^2)]\} \\
&(V/V_*)_{x=0} = \exp\{(1/\gamma)[1-(1/M^2)]\} \\
&(Q/Q_*)_{x=0} = [(2/M^2)-1]\exp\{(3/\gamma)[1-(1/M^2)]\}
\end{aligned}\right\} \tag{8}$$

Some of these relations are plotted in Fig. 2. The subscripts t and $*$ denote the stagnation and the sonic conditions, respectively.

When the flow is supersonic, the flow properties vary with Mach Number in a fashion very similar to their variation in the

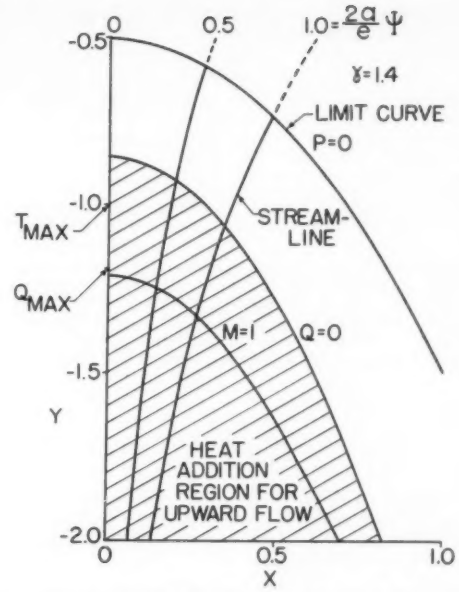

FIG. 1. Flow field when the equipotential curves are parabolas.

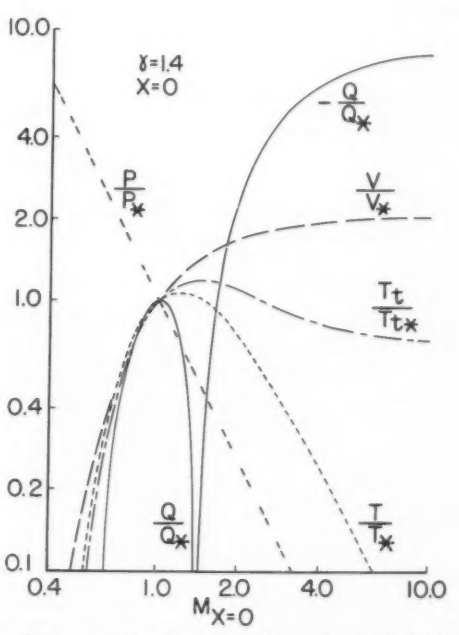

FIG. 2. Zero streamline flow properties vs. local Mach Number.

case of constant-area diabatic flow.[5, 6] In the subsonic flow, this similarity no longer obtains.

REFERENCES

[1] Hicks, B. L., *On the Characterization of Fields of Diabatic Flow*, Q. Appl. Math., Vol. 6, No. 4, pp. 405–416, January, 1949.

[2] Hicks, B. L., Hebrank, W. H., and Kravitz, S., *On the Characterization of Fields of Diabatic Flow*, Report No. 720, Ballistic Research Laboratories, Aberdeen Proving Ground, July, 1950.

[3] Hicks, B. L., Montgomery, D. J., and Wasserman, R. H., *On the One-Dimensional Theory of Steady Compressible Fluid Flow in Ducts with Friction and Heat Addition*, J. Appl. Phys., Vol. 18, No. 10, pp. 891–902, October, 1947.

[4] Hicks, B. L., *Diabatic Flow of a Compressible Fluid*, Q. Appl. Math., Vol. 6, No. 3, pp. 221–237, October, 1948.

[5] Hicks, B. L., *Addition of Heat to a Compressible Fluid in Motion*, NACA Wartime Report E-88 (originally issued as ACE No. E5 A29 in 1945).

[6] Shapiro, A. H., *The Dynamics and Thermodynamics of Compressible Fluid Flow*, Vol. 1, p. 196, Ronald Press Company, New York, 1953.

On an Exact Solution of Laminar Mixing of Two Different Gases†

Luigi G. Napolitano

Associate Professor of Aerodynamics, Instituto di Aeronautica, University of Naples, Naples, Italy

August 25, 1959

IN THE PRESENT NOTE, an exact solution of isovel laminar mixing of two different gases is presented.

Consider the interaction of two semi-infinite streams. The state, diffusion, and energy equations for the subject problem can be written as:[1, 2]

$$\rho T/m = \text{const.}, \quad 1/m = (W/m_2) + [(1 - W)/m_1],$$
$$\rho u W_x + \rho v W_y = (D_{12}\rho W_y)_y$$
$$\rho u T_x + \rho v T_y = (1/C_p)(\lambda T_y)_y + \rho D_{12} W_y T_y (c_{p_2} - c_{p_1})/C_p \quad (1)$$

where W is the mass-density ratio for gas number 2, m is the molecular weight of the mixture, $C_p = W c_{p_2} + (1 - W)c_{p_1}$, and subscripts 1 and 2 refer to streams 1 and 2. All other symbols have conventional meanings. Assume that similarity conditions prevail and that the diffusion coefficient D_{12} is proportional to T^2. It is then easy to verify that the velocity field is described by a stream function of the form

$$\psi = \rho_{1e}[2u_1(D_{12})_1 x]^{1/2}\sigma$$

where the similarity variable is defined by:

$$\sigma = \{u_1/[2x(D_{12})_1]\}^{1/2}\int_0^y (\rho/\rho_{1e})dy \quad (2)$$

Herein, ρ_{1e} is the density of stream 1, and ρ is that of the gas mixture. By letting $G = G(\sigma) = m/m_1$ and $(\theta) = T/T_1$, Eqs. (1) are reduced to

$$G^2 G''' + \sigma G' = 0 \quad (3)$$

$$(1/Le)(c_{p_1}/C_p)(G\theta')' + G\theta'\{(\sigma/G) + [(c_{p_1} - c_{p_2})GW']/C_p\} \quad (4)$$

where Le is the Lewis Number referred to the conditions of stream 1. The diffusion Eq. (3) results uncoupled from the energy equation and can be solved in closed form. By introducing the following new dependent and independent variables

$$dG/d\sigma = -U^{-1}(\alpha) \quad (5)$$

$$2^{-(1/2)}\alpha = U^{-1} + \sigma G^{-1}, \quad [d\alpha = 2^{-(1/2)}U^{-1}d\sigma] \quad (6)$$

Eq. (3) becomes

$$dU - 2\alpha U d\alpha = -2^{1/2}d\alpha \quad (7)$$

Integrating this equation results in

$$U^{-1} = dG/d\sigma = -2\pi^{-(1/2)}e^{-\alpha^2}(2\pi^{-(1/2)}C_1 - 2^{1/2}\,\text{erf}\,\alpha)^{-1} \quad (8)$$

The solution G can be determined by properly combining Eqs. (5), (6), and (7). Integrating the resulting equation with the boundary conditions, $G(+\infty) = 1$ and $G(-\infty) = m_2/m_1$, results in

$$2G = 2m/m_1 = [1 + (m_2/m_1)] + [1 - (m_2/m_1)]\,\text{erf}\,\alpha \quad (9)$$

Thus, the value of the molecular weight of the mixture at $\alpha = 0$ is equal to the arithmetic mean of the values of the two streams, and the corresponding nondimensional profile is simply expressed by the error function in the α plane.

To revert back to the physical plane, one must solve the energy equation first. It is interesting to note, however, that Eqs. (2) and (6) yield

$$dy = 2\{[x(D_{12})_1]/u_1\}^{1/2}(T/T_1)d\alpha$$

That is, the α plane is the transform of the physical plane according to the temperature ratio T_1/T and thus coincides with the physical plane itself if the mixing process is also isothermal. This feature could be exploited, for instance, to measure the diffusion coefficient D_{12}. Indeed, for isothermal mixing, the molecular weight is proportional to the density; and, therefore, experimentally determined density profiles at several stations x will make it possible to determine D_{12}.

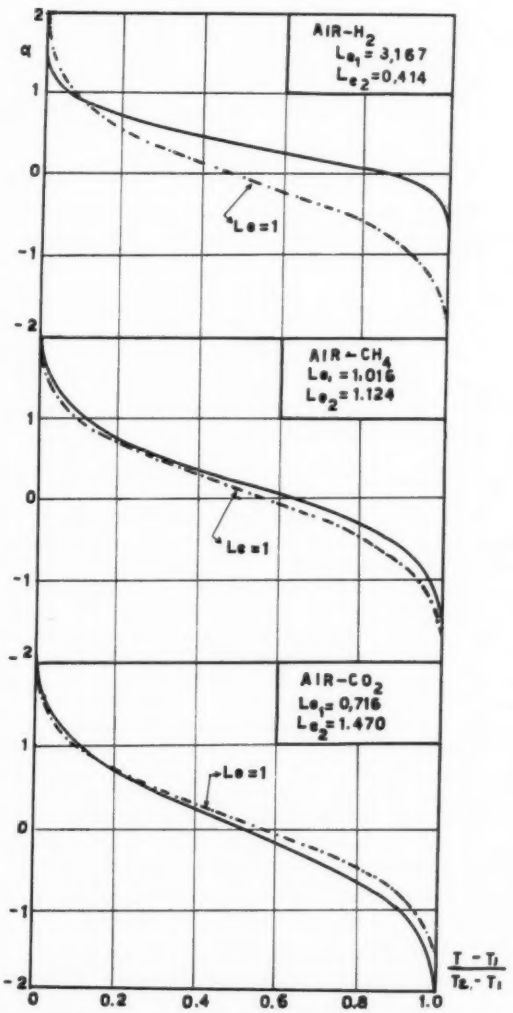

FIG. 1. Comparison of temperature profiles.

† The work presented in this paper was carried out under the sponsorship and the support of contract AF 61(052)-160, administered by the European Office of the ARDC.

The solution of the energy equation (Eq. 4) is obtained by simple quadratures and is given by

$$T - T_1 = (T_2 - T_1)[S(\alpha)/S(-\infty)]$$

with

$$S(\alpha) = \int_{\alpha}^{+\infty} G^{[Le(c_{p2} - c_{p1})m_2][c_{p2}(m_1 - m_2)]^{-1}} \times \exp\left[-2^{1/2}\int_0^{\alpha} \sigma(C_p/c_{p1})Led\alpha\right]d\alpha$$

wherein the variable σ is to be expressed in terms of α through Eqs. (9) and (6), as

$$\sigma = 2^{1/2}\{\alpha + [(m_1 - m_2)i(\alpha)]/2m_1\}$$

Herein, $i(\alpha)$ is the first integral of the complementary error function. The values of $i(\alpha)$ for positive values of the argument are tabulated in reference 3, and the formulas necessary to evaluate $i(-\alpha)$ in terms of $i(\alpha)$ are presented in reference 4.

Since an exact solution is now available, it might prove of interest to determine the effects of the often made simplifying assumption of a Lewis Number constant and equal to one. The static enthalpy in this case is a linear function of the mass density ratio W, so that the temperature profiles are simply given by

$$T - T_1 = (T_2 - T_1)(c_{p2}W/C_p)$$

Comparison between these temperature profiles and those obtained from the exact solution is made in Fig. 1 for the following three cases: Air-H_2; Air-CH_4; and Air-CO_2. It is seen that the hypothesis Le = const. = 1 introduces errors already of the order of 10 per cent, even when the values of the Lewis Number of the two free streams are not too different from one. The size of the error increases so as to make the solutions with $Le = 1$ devoid of any practical meaning when the Lewis Numbers of the two free streams are sensibly different from one (cf., for instance, the case Air-H_2).

The present exact solution can be extended to other geometries of interest in mixing problems and can be used, when the mixing is not isovel, to devise an iteration procedure which is rapidly convergent. This development will be presented in a forthcoming publication.

References

[1] Pai, S. I., *Fluid Dynamics of Jets*, D. Van Nostrand Co., Inc., New York, 1954.

[2] Napolitano, L. G., *La gasdinamica delle miscele nell'approssimazione dello strato limite*, L'Aerotecnica, Vol. No. 2, p. 36, March, 1957.

[3] Kaye, J., A Table of the First Eleven Repeated Integrals of the Error Function, J. Math. & Phys., Vol. 34, No. 2, pp. 119–125, July, 1955.

[4] Napolitano, L. G., *The Blasius Equation with Three-Point Boundary Conditions*, Quart. Appl. Math., Vol. 16, No. 4, pp. 338–408, January, 1959.

Erratum—"Note on the Turbulent Shear Stress Near a Wall"*

H. G. Elrod
Professor, Dept. of Mechanical Engineering, Columbia University, N.Y.

November 30, 1959

Professor Stanley Corrsin has kindly pointed out the oversight of this writer in concluding that the last integral of Eq. (5), reference 1, vanishes on grounds of symmetry. Accordingly, we cannot conclude on the basis of analytical arguments so far advanced that the turbulent shear stress vanishes faster than the cube of distance from a wall bounding a two-dimensional, established flow of incompressible fluid.

* Journal of the Aero/Space Sciences, Vol. 24, No. 6, p. 468, June, 1957.

Minimizing the Mass of Thin Radiating Fins*

J. Ernest Wilkins, Jr.
Nuclear Development Corporation of America, White Plains, N.Y.

October 19, 1959

Since mass is at a premium on space vehicles, we present here some observations on the possible reductions in the mass of fins used in space radiators by taking advantage of the freedom to choose the fin profile. Restricting attention to thin rectangular fins with an insulated tip designed to transfer heat from a base material at temperature $T_0(°R)$ by radiation to surroundings at $0°R$ at the rate q_0 (B.t.u./hr.-ft. of length of fin), Bartas and Sellers[1] have presented a graph from which it can be inferred that the straight fin with minimum mass has dimensions and profile area

$$w = 0.884\, q_0/\epsilon\sigma T_0^4$$
$$2\delta = 1.848\, q_0^2/k\epsilon\sigma T_0^5$$
$$A_p = 1.635\, q_0^3/k\epsilon^3\sigma^2 T_0^9$$

Here, w and 2δ are the fin height and base, ϵ is the emissivity of the fin material, and σ is the Stefan-Boltzmann constant. We wish to consider fins with not necessarily straight profiles $y = Y(x)$.

If we assume a temperature variation

$$T = T_0(x/w)^{\alpha}, \quad \alpha > 0$$

it is easy to see by an integration of the differential equations

$$q = 2kY(dT/dx), \quad dq/dx = 2\epsilon\sigma T^4, \quad (0 < x < w) \tag{1}$$

with the boundary conditions

$$x = 0, q = 0; x = w, q = q_0, T = T_0 \tag{2}$$

that

$$q = q_0(x/w)^{4\alpha+1}$$
$$Y = [(4\alpha + 1)q_0^2/4\alpha k\epsilon\sigma T_0^5](x/w)^{3\alpha+2}$$
$$w = (4\alpha + 1)q_0/2\epsilon\sigma T_0^4$$

and, hence, that the profile area is

$$A_p = 2\int_0^w Y(x)dx = [(4\alpha + 1)^2/12\alpha(\alpha + 1)](q_0^3/k\epsilon^3\sigma^2 T_0^9)$$

This profile area is least when $\alpha = 1/2$, when it has the value $q_0^3/k\epsilon^3\sigma^2 T_0^9$. It follows that a penalty of 63.5 per cent in mass is paid by using the best straight fin instead of the fin with profile

$$Y = (3q_0^2/2k\epsilon\sigma T_0^5)(x/w)^{7/2}, \quad 0 \leqq x \leqq w = 3q_0/2\epsilon\sigma T_0^4 \tag{3}$$

It can actually be shown[2] that the fin profile, Eq. (3), furnishes a minimum profile area in the class of all profiles (which transfer heat q_0 from a base at T_0) and not just in the class of profiles for which the temperature varies as x^{α}.

The optimum fin profile has a very sharp point where $x = 0$ (in fact, the profile $Y(x)$ for an arbitrary α is sharper than a parabola), and so it may be worthwhile to pay some penalty in mass in order to avoid this. Accordingly, we now assume a triangular profile $Y(x) = \delta x/w$. The differential system, Eqs. (1) and (2), then reduces to

$$(d/dx)[x(dT/dx)] = (\epsilon\sigma w/k\delta)T^4, \quad 0 < x < w$$
$$x = 0, x(dT/dx) = 0; x = w, T = T_0, q = q_0 \tag{4}$$

To solve this system, consider first the system

$$(d/du)[u(dv/du)] = v^4, \quad v(0) = 1$$

The solution of this system is

$$v = 1 + u + u^2 + (10u^3/9) + (23u^4/18) + (337u^5/225) + (7199u^6/4050) + (211144u^7/99225) + (814067u^8/317520) + \ldots \tag{5}$$

* The advice received from Professor Fred Landis of New York University in connection with the subject matter of this paper is gratefully acknowledged.

Although we have not determined the precise radius of convergence of the power series, Eq. (5), it is not difficult to show that it may be at least 1/2. The function $T = \gamma v(\beta x/w)$ will satisfy the system, Eq. (4), provided the constants β and γ are such that

$$\begin{aligned} \gamma &= T_0/v(\beta) \\ \epsilon\sigma w^2 T_0^3/k\delta &= \beta v^3(\beta) \\ wq_0/2k\delta T_0 &= \beta v'(\beta)/v(\beta) \end{aligned}$$

Hence, a one-parameter family of triangular fins exists which transfers heat at the rate q_0 from a base at temperature T_0. These fins have dimensions

$$\begin{aligned} w &= (q_0/\epsilon\sigma T_0^4)[v^4(\beta)/2v'(\beta)] \\ \delta &= (q_0^2/k\epsilon\sigma T_0^5)\{v^5(\beta)/4\beta[v'(\beta)]^2\} \end{aligned}$$

and, hence, have the profile area

$$A_p = w\delta = (q_0^3/k\epsilon^2\sigma^2 T_0^9)\{v^9(\beta)/8\beta[v'(\beta)]^3\}$$

With the help of Eq. (5), the minimum value of the factor

$$v^9(\beta)/8\beta[v'(\beta)]^3$$

is found to be 1.1030, attained when $\beta = 0.2866$, $v(\beta) = 1.4089$, $v'(\beta) = 2.053$. Therefore, the mass penalty paid by using the best triangular fin instead of the best fin, Eq. (3), is only 10.3 per cent.

The fin profile, temperature profile, heat-transfer rate profile, and fin effectiveness for this optimum triangular fin are

$$\begin{aligned} Y &= (1.1493q_0^2/k\epsilon\sigma T_0^5)(x/w), \quad 0 \le x \le w = 0.9598q_0/\epsilon\sigma T_0^4 \\ T &= T_0 v(0.2866x/w)/1.4089 \\ q &= q_0(x/w)v'(0.2866x/w)/2.053 \\ \eta &= q_0/2\epsilon\sigma T_0^4 w = 0.5210 \end{aligned}$$

REFERENCES

[1] Bartas, J. G., and Sellers, W. H., *Radiation Fin Effectiveness*, paper 59-HT-17 presented at the ASME-AIChE Heat Transfer Conference, Storrs, Conn., August 9–12, 1959.

[2] Wilkins, J. Ernest, Jr., *Minimum Mass Thin Fins Which Transfer Heat Only by Radiation to Surroundings at Absolute Zero*, submitted for publication to the J. Soc. Ind. & Appl. Math.

The Minimum-Weight Straight Fin of Triangular Profile Radiating to Space

Edwin N. Nilson and Richard Curry
Project Engineer and Assistant Project Engineer, Respectively, Pratt and Whitney Aircraft, East Hartford, Conn.

October 22, 1959

Introduction

JAKOB[1] gives the solution of the problem of determining the triangular fin of optimum shape for discharging heat by convection. The corresponding problem in radiation is of considerable interest with regard to waste-heat dissipation from spacecraft. The differential equation expressing the heat flow is now nonlinear, but a basic property of the equation yields a method of solution which is an extension of Jakob's.

Equation in the Temperature

Consider the straight fin of triangular profile shown in Fig. 1 with base temperature $\theta = \theta_0$. Employing the assumptions of reference 1, the heat flow q per unit length of base moving in the x-direction is

$$q = -k(2y)(d\theta/dx)$$

where k is the conductivity. By continuity, the difference between the heat-flow rates q and $q + dq$ at the two faces of the element shown is accounted for by radiation:

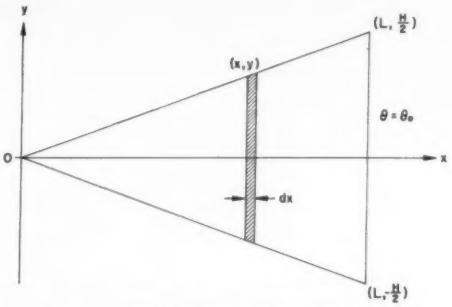

FIG. 1. Straight fin of triangular profile.

$$-dq = \sigma\theta^4 dx$$

where it is assumed that the fin is radiating to surroundings at zero temperature.* Since $y = Hx/2L$, it follows that

$$(d/dw)[w(d\theta/dw)] - \theta^4 = 0 \tag{1}$$

where

$$w = (\sigma L/KH)x$$

Now, if $\theta = f(w)$ is a solution of Eq. (1), then $\theta = \lambda f(w\lambda^3)$ is also a solution. For, if $\theta = \lambda f$ and $w = v/\lambda^3$ in Eq. (1), there results

$$(d/dv)[v(df/dv)] - f^4 = 0$$

The solution of Eq. (1) is restricted to be regular at $w = 0$. If Eq. (1) is written as

$$w\theta''' + \theta' - \theta^4 = 0 \tag{2}$$

it is seen that it is necessary and sufficient that $\theta' = \theta^4$ at $w = 0$. Let $f(w)$ be such a regular solution of Eq. (1) and take

$$\theta = \lambda f(w\lambda^3) \tag{3}$$

The condition that the base temperature be θ_0 gives

$$\theta_0 = \lambda f(w_L\lambda^3) \tag{4}$$

where

$$w_L = \sigma L^2/kH \tag{5}$$

Note that $1/(9w)^{1/3}$ is a solution of the differential equation but is of no interest here.

Optimization of Fin

The heat-flow rate per unit length along the base radiated from the surface is taken to be

$$Q = \sigma\int_{x=0}^{L}\theta^4 dx = (kH/L)\int_{w=0}^{w_L}\theta^4 dw = (kH/L)[w(d\theta/dw)]\Big|_{w=0}^{w_L}$$

so that, in virtue of the requirement of regularity,

$$Q = (kH/L)w_L(d\theta/dw)_{w_L}$$

If a_L is the profile area of the fin section, $a_L = HL/2$ and

$$L = (2ka_L w_L/\sigma)^{1/2} \tag{6}$$

$$H = (4a_L^2\sigma/kw_L)^{1/2} \tag{7}$$

Then, since $d\theta/dw = \lambda^4 f'(w\lambda^3)$,

$$Q = (2\sigma^2 ka_L)^{1/2} w_L^{1/2}\lambda^4 f'(w_L\lambda^3) \tag{8}$$

It is desired to maximize Q for a given area a_L with w_L and λ related by Eq. (4). From Eq. (4),

$$f(w_L\lambda^3)(d\lambda/dw_L) + \lambda f'(w_L\lambda^3)[3\lambda^2 w_L(d\lambda/dw_L) + \lambda^3] = 0 \tag{9}$$

Differentiate Eq. (8) with a_L held fixed:

* Here $\sigma/2$ is emissivity times Stefan-Boltzmann constant.

$$(1/Q)(dQ/dw_L) = (1/3w_L) + (4/\lambda)(d\lambda/dw_L) + [f''(w_L\lambda^3)/f'(w_L\lambda^3)]\,[\lambda^3 + 3\lambda^2 w_L(d\lambda/dw_L)] \quad (10)$$

Since

$$d^2\theta/dw_L^2 = \lambda^7 f''(w_L\lambda^3)$$

it is seen by Eq. (2) that

$$f''(w_L\lambda^3) = \{[f(w_L\lambda^3)]^4 - f'(w_L\lambda^3)\}/w_L\lambda^3$$

Let $\xi = w_L\lambda^3$. Set $dQ/dw_L = 0$ and replace $d\lambda/dw_L$ by its value from Eq. (9). There results

$$(1/3)[f(\xi) + 3\xi f'(\xi)] - 4\xi f'(\xi) + \{[f(\xi)]^4 - f'(\xi)\}[f(\xi)/f'(\xi)] = 0$$

or, alternatively,

$$3\xi[f'(\xi)/f(\xi)]^2 + (2/3)[f'(\xi)/f(\xi)] - [f(\xi)]^3 = 0 \quad (11)$$

The number $w_L = \xi/\lambda^3$ is independent of the particular function f chosen, as may easily be shown. Further, the optimum configuration as given by this value of ξ is independent of a_L, as in the convection case.

Numerical Solution

Eq. (1) was integrated by the Runge-Kutta method on an IBM 704 computer taking the solution for which $f'(0) = [f(0)]^4 = 1$. The value of $f''(0)$ needed to start the solution is obtained by l'Hospital's rule ($v = \lambda^3 w$):

$$\lim_{v\to 0} f''(v) = \lim_{v\to 0}\left(\{-f'(v) + [f(v)]^4\}/v\right) = \lim_{v\to 0}\{-f''(v) - 4[f(v)]^3 f'(v)\}$$

whence $f''(0) = 2$. The equation is integrated out to the point at which Eq. (11) is satisfied. Table 1 presents the necessary information about the solution. Note that

$$x/L = w/w_L$$

$$\theta/\theta_0 = [\lambda f(w\lambda^3)]/[\lambda f(w_L\lambda^3)] = f(v)/f(\xi)$$

Let $F(v)$ be the left-hand member of Eq. (11). Integration was carried out using $\Delta v = \xi/50$, and every fifth point is here given. The value of ξ is 0.28483, $f(\xi) = 1.40566$, and $f'(\xi) = 2.04456$.

Table 1

x/L	v	$f(v)$	$f'(v)$	$F(v)$	$\theta/\theta_0 = f(v)/f(\xi)$
0	0	1.0000	1.0000	−0.333333	0.7114
0.1	0.02848	1.02937	1.05989	−0.313736	0.7323
0.2	0.05696	1.06055	1.12602	−0.292429	0.7545
0.3	0.08544	1.09372	1.19930	−0.269103	0.7781
0.4	0.11393	1.12910	1.28085	−0.243359	0.8032
0.5	0.14241	1.16694	1.37200	−0.214709	0.8302
0.6	0.17089	1.20755	1.47439	−0.182543	0.8590
0.7	0.19938	1.25127	1.59002	−0.146099	0.8902
0.8	0.22786	1.29851	1.72138	−0.104410	0.9238
0.9	0.25634	1.34978	1.87158	−0.056236	0.9602
1.0	0.28483	1.40566	2.04456	+0.000027	1.0000

The quantity λ is now obtained from Eq. (4)

$$\lambda = \theta_0/f(\xi) = 0.71141$$

while

$$w_L = \xi/\lambda^3 = 0.79109/\theta_0^3$$

For prescribed values Q, θ_0, σ, and k, therefore,

$$a_L = Q^3/2\sigma^2 k\lambda^3\xi[f'(\xi)]^3 = 4.40055\,(Q^3/\sigma^2 k\theta_0^9)$$
$$L = Q/\sigma\lambda^4 f'(\xi) = 1.90951\,(Q/\sigma\theta_0^4)$$
$$H = Q^2/k\xi\sigma\lambda^5[f'(\xi)]^2 = 4.60910\,(Q^2/k\sigma\theta_0^5)$$

It is of interest to note that the tip temperature is 71 per cent of the base temperature.

Reference

[1] Jakob, Max., *Heat Transfer*, Vol. I, pp. 225 ff., Wiley, New York, 1949.

Relaxation Effects on the Interpretation of Impact-Probe Measurements

William F. Van Tassell* and Eugene E. Covert**
Massachusetts Institute of Technology, Cambridge, Mass.
August 20, 1959

When a blunt body has a supersonic speed in a dense atmosphere, a shock wave forms in front of the body. In general, this standoff distance is proportional to the diameter of the body; as the body becomes smaller, the shock wave approaches the body. With a relatively large diameter impact probe, the shock standoff distance is great enough to allow complete re-establishment of equilibrium flow behind the shock wave. As the probe diameter is decreased, the gas has less and less time to re-establish equilibrium. Eventually, with a small enough probe, it should be possible to measure a gas that effectively has its vibrational mode unexcited—i.e., "frozen." Measurements made with this small probe should then correspond to values as predicted by perfect fluid theory. By comparing equilibrium measurements and "frozen" measurements, the departure from equilibrium can be established. This departure from equilibrium as a function of the test parameters will make accurate interpretation of the probe data possible.

The purpose of this report is to present the results of some preliminary experiments designed to aid in the interpretation of impact-tube measurements. The departure from equilibrium has been related to relaxation of the internal degrees of freedom in the molecules comprising the flow field. One method of measuring this departure from equilibrium is through the use of impact probes, as pointed out by Kantrowitz.[1]

The experimental data presented here were taken at a Mach Number 4.8 in the hypersonic wind tunnel at the Naval Supersonic Laboratory. The hypersonic wind tunnel (HWT) is an open-circuit, heated tunnel. The heaters have a capacity of heating 1 lb. of air per sec. to 1,000 °F. The cycle timers allow control of stagnation temperature to within ±1°F. Data were taken at stagnation temperatures of 600°F., 925°F., and 1,000 °F. Stagnation pressures were varied between 5 and 100 psia. The raw data are tabulated in reference 2.

It should be noted that during all the tests the shock position was held fixed with respect to the nozzle as the probe size varied.

The impact probes used in this experiment are shown in Fig. 1. The probe geometries are listed in Table 1 in inches. All outside diameters were measured on either a micrometer or a cathetometer.

In addition to the nonequilibrium effects that are present in the data, there are two additional effects. These are: (1) the effect of the probe Reynolds Number on the probe reading and (2) the slight dependence of the tunnel Mach Number on the operating pressure. The latter effects were removed by handling the data at constant total pressure.

* Formerly, Research Assistant, M.I.T., Naval Supersonic Laboratory, Cambridge, Mass. Now, with AVCO, Wilmington, Mass.
** Staff Member, M.I.T., Naval Supersonic Laboratory, Cambridge, Mass.

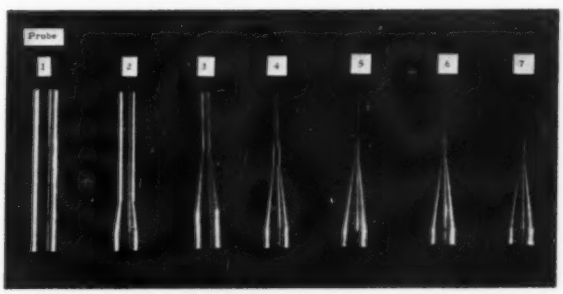

Fig. 1. Photograph of experimental probes.

TABLE 1

Probe No.	Outside Dia.	Inside Dia.	Length of Probe to Support
1	0.7514	0.3750	$3^3/_4$ in.
2	0.5150	0.2500	$2^1/_2$ in.
3	0.2517	0.1250	$1^1/_4$ in.
4	0.1235	0.0622	1 in.
5	0.0645	0.0311	1 in.
6	0.0307	0.0118	1 in.
7	0.0201	0.0072	1 in.

It was anticipated that the former effect would be small, since in the primary experiments the total-pressure range was from 25 psia to 100 psia. The Reynolds Number of the smallest probe at the lowest pressure was 435, based on free-stream conditions and the perfect-gas results of reference 3. At this Reynolds Number, the probe correction was indicated to be less than one-half per cent,[4] which is inside the experimental error. Since there were small differences in probe geometry between these probes and those discussed in reference 4, a supplementary set of experiments was conducted at a total temperature of 600°F., over a total-pressure range of 5 psia to 100 psia. These data were assumed to be independent of vibrational lag and spanned the Reynolds Number range of the primary tests. The results indicated that the effects of low Reynolds Number were inside the experimental error for these tests, as expected.

The following parameter was used to calculate the departure from equilibrium at each total-pressure level.

$$\alpha = \frac{(P_0'/P_{01})_{\text{measured}} - (P_{02}/P_{01})_{\text{frozen}}}{(P_{02}/P_{01})_{\text{equilibrium}} - (P_{02}/P_{01})_{\text{frozen}}}$$

The number-seven probe was assumed to give the frozen values of P_{02}/P_{01} while the number-one and -two probes were assumed to give equilibrium values. Note that α varies from zero to unity. The former indicates frozen flow, and the latter corresponds to equilibrium flow.

The factor α was related to the probe geometry by a dimensionless parameter, κ. This parameter is made up as follows: $p/\sqrt{T}$ is proportional to the collision frequency; $\exp \lambda/T^{1/3}$ is proportional to the number of collisions required to reach equilibrium; and d/U is a measure of the time that is available for a particle traversing the distance between the bow shock and the stagnation point. This factor can be generalized to include the gas properties, and, since this is an impact-point experiment, it can be written in terms of equilibrium impact properties.

In engineering units,

$$\kappa = (36.5\, p_0' d/\sqrt{T_0} U)\, \sqrt{m_{\text{air}}/m}\, \exp\left\{-30(m/m_{\text{air}}) \times [(\nu/10^{13})/T]^2\right\}^{1/3}$$

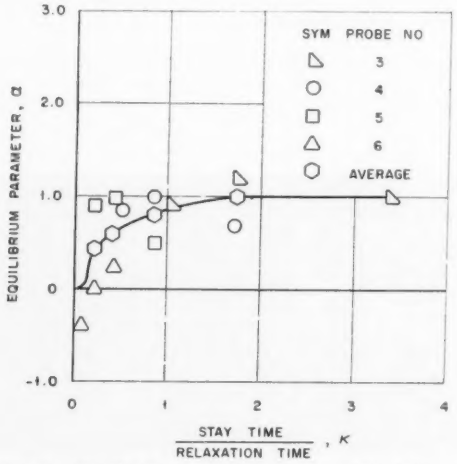

FIG. 2. Equilibrium parameter vs. normalized time.

where now m is the molecular weight; p_0' is in psia; T_0 is in degrees Rankine; ν is the state frequency of the molecule; and ν_{air} is taken to be 10^{13}. d and U are in consistent units for this experiment, and U is computed at a Mach Number of 4.75 and a T_0 of 1,000°F.

The scale of κ is such that when κ is of order of unity, the stay time between the shock and the stagnation point in terms of free-stream velocity is about equal to the relaxation time. When κ is very small, the relaxation time is large compared to the stay time; and when κ is large, the relaxation time is small compared to the stay time. Thus, a small κ corresponds to frozen flow while a large κ corresponds to equilibrium flow.

Now the plot of α vs. κ can be determined experimentally (see Fig. 2). The curve of α vs. κ is shown for average values of α, together with the probable error in α. It is estimated that a 1 per cent error in probe readings would result in roughly ± 50 per cent error in α. The pressure data were read to an accuracy of $\pm 1/2$ per cent, and hence a ± 25 per cent error in α can be expected.

Fig. 2 can be considered as a calibration curve for the probes described above at the given Mach Number and temperature, in that the reading of a given probe (hence κ and thus α) can be related to the calculated frozen and equilibrium flows.

It should be noted that the relaxation effects on the impact-tube readings are generally of the order of a few per cent at most. Consequently, the fact that the shock separation distance is slightly dependent upon the entropy rise, as well as being dependent on the probe geometry and flight Mach Number, should not introduce too much overall error.

It should be noted that dissociation and ionization have similar effects upon impact-tube reading. Consequently, for accurate interpretation of data, these effects must be allowed.

REFERENCES

[1] Kantrowitz, A., *Effect of Heat Capacity Lag in Gas Dynamics*, NACA WR L-457, January, 1944. (Also J. Chem. Phys., Vol. 10, p. 145, February, 1942.)

[2] Van Tassel, William F., *Relaxation Probe Effects on Impact Probe Measurements*, B. Sc. Thesis, Massachusetts Institute of Technology, Department of Aeronautics and Astronautics, May, 1959.

[3] Ames Research Staff, *Equations, Tables and Charts for Compressible Flow*, NACA TR 1135, 1953.

[4] Hill, J. A. F., Baron, J. R., Schindel, L. H., and Markham, J., *Mach Number Measurements in High Speed Wind Tunnels*, Agardograph 22, 1956.

The Hydraulic Analogy for External Flow

R. A. A. Bryant
Senior Lecturer in Mechanical Engineering, The University of New South Wales, Kensington, Australia
August 1, 1959

SYMBOLS

s = specific entropy
Z = cy^n = vertical locus of channel cross section
c = channel size factor
n = channel shape factor
h = $h(x, y, t)$ = local water depth
δ = $h + Z$ = height of free surface measured from bottom of channel
u, v, w = velocity components in x, y, z directions, respectively
U = ρgz = body force potential

IT IS GRATIFYING to see the results of Dr. W. H. T. Loh's research on the one-dimensional hydraulic analogy published.[1] After a period of thirteen years, his original work[2] stands as a significant contribution to the development of hydraulic analogy methods. At the same time, there still appears to be some doubt concerning possible types of basic analogy. This is evident from Loh's reference to the "generalized" analogy.[3]

The present author has already mentioned[4] that there are two types of analogy pertinent to gasdynamics. (See the references

of reference 4 for details.) Actually, there are *only* two. Loh's analogy is one; it is useful only for "inside" problems which can be considered one-dimensional. When external—i.e., two-dimensional, flow is considered there is just one other possible analogy; and this involves the use of a rectangular tank. The same applies to two-dimensional internal flows.

To demonstrate the above statement, consider pseudo two-dimensional shallow water flow in a channel having a horizontal bottom, $(y, z) = (0, 0)$, with a vertical cross section defined by $Z = cy^n$. (Symbols used are those of Loh,[1] except as noted above.)

Following the usual assumptions we can write

$$u = u(x, y, t), \quad v = v(x, y, t), \quad p = -\rho g(z - \delta), \quad h = h(x, y, t), \quad \delta = \delta(x, y, t) = h + Z$$

with

$$w = w(x, y, z, t)$$

and

$$dw/dt = [(\partial/\partial t) + u(\partial/\partial x) + v(\partial/\partial y) + w(\partial/\partial z)]w$$

both of negligible magnitude.

For a channel of fixed shape, it is clear that we can also write

$$\partial Z/\partial t = 0, \ \partial Z/\partial x = 0, \ \partial Z/\partial y = nZ/y \text{ for } n > 0, \ \partial h/\partial x = \partial \delta/\partial x, \ \partial h/\partial y = (\partial \delta/\partial y) - (\partial Z/\partial y), \ \partial h/\partial t = \partial \delta/\partial t$$

Now, by continuity, we have for any (x, y, t),

$$[\partial(hu)/\partial x] + [\partial(hv)/\partial y] + (\partial h/\partial t) = 0 \tag{1}$$

into which we can introduce the channel boundary conditions to find

$$h(\partial u/\partial x) + u(\partial \delta/\partial x) + h(\partial v/\partial y) + v[(\partial \delta/\partial y) - (\partial Z/\partial y)] + (\partial h/\partial t) = 0 \tag{2}$$

Furthermore, the existence of a gravitational body force potential $U = \rho g z$ enables us to write Eulerian equations of motion:

$$-g(\partial \delta/\partial x) = (\partial u/\partial t) + u(\partial u/\partial x) + v(\partial u/\partial y) \tag{3}$$

$$-g(\partial \delta/\partial y) = (\partial v/\partial t) + u(\partial v/\partial x) + v(\partial v/\partial y) \tag{4}$$

wherein $\delta = h + Z$.

Thus, we find

$$-g(\partial h/\partial x) = (\partial u/\partial t) + u(\partial u/\partial x) + v(\partial u/\partial y) \tag{5}$$

$$-g[(\partial h/\partial y) + (\partial Z/\partial y)] = (\partial v/\partial t) + u(\partial v/\partial x) + v(\partial v/\partial y) \tag{6}$$

We now ask under what conditions will Eqs. (2), (5), and (6) be analogous to the equations of two-dimensional flow of a perfect gas. For such flow we know that

$$[\partial(\rho u)/\partial x] + [\partial(\rho v)/\partial y] + (\partial \delta/\partial t) = 0 \tag{7}$$

$$-(\partial p/\partial x) = \rho[(\partial u/\partial t) + u(\partial u/\partial x) + v(\partial u/\partial y)] \tag{8}$$

$$-(\partial p/\partial y) = \rho[(\partial v/\partial t) + u(\partial v/\partial x) + v(\partial v/\partial y)] \tag{9}$$

where

$$\left.\begin{aligned} \rho &= \rho(p, s) \\ p &= p(\rho, s) \end{aligned}\right\} \tag{10}$$

By putting Eq. (7) into the same form as Eq. (2)—viz.,

$$\rho(\partial u/\partial x) + u(\partial \rho/\partial x) + \rho(\partial v/\partial y) + v(\partial \rho/\partial y) + (\partial \rho/\partial t) = 0 \tag{11}$$

it becomes evident that we can look for an analogous correspondence between ρ and h or ρ and δ, but then only if $\partial Z/\partial y = 0$. Thus, we could conclude immediately that Z must be independent of y and the channel rectangular with $\delta \equiv h$ at all points.

If we consider Eqs. (5), (6), (8), and (9), the position becomes even clearer. Using Eq. (10), we can rewrite Eqs. (8) and (9) as

$$-(\partial p/\partial \rho)_s(\partial \rho/\partial x) + (\partial p/\partial s)_\rho(\partial s/\partial x) = \rho[(\partial u/\partial t) + u(\partial u/\partial x) + v(\partial u/\partial y)] \tag{12}$$

$$-(\partial p/\partial \rho)_s(\partial \rho/\partial y) + (\partial p/\partial s)_\rho(\partial s/\partial y) = \rho[(\partial v/\partial t) + u(\partial v/\partial x) + v(\partial v/\partial y)] \tag{13}$$

These can be compared with Eqs. (5) and (6) rewritten:

$$-gh(\partial h/\partial x) = h[(\partial u/\partial t) + u(\partial u/\partial x) + v(\partial u/\partial y)] \tag{5a}$$

$$-gh[(\partial h/\partial y) + (\partial Z/\partial y)] = h[(\partial v/\partial t) + u(\partial v/\partial x) + v(\partial v/\partial y)] \tag{6a}$$

For ρ and h to be analogous, it is then quite clear that (i) the gas flow must be isentropic

$$\partial s/\partial x = 0, \quad \partial s/\partial y = 0$$

and (ii) the water channel must be of rectangular cross section

$$\partial Z/\partial y = 0$$

Under these conditions, the equations reduce to

$$-C^2(\partial \rho/\partial x) = \rho[(\partial u/\partial t) + u(\partial u/\partial x) + v(\partial u/\partial y)] \tag{14}$$

$$-C^2(\partial \rho/\partial y) = \rho[(\partial v/\partial t) + u(\partial v/\partial x) + v(\partial v/\partial y)] \tag{15}$$

$$-gh(\partial h/\partial x) = h[(\partial u/\partial t) + u(\partial u/\partial x) + v(\partial u/\partial y)] \tag{16}$$

$$-gh(\partial h/\partial y) = h[(\partial v/\partial t) + u(\partial v/\partial x) + v(\partial v/\partial y)] \tag{17}$$

and we can say that

$$\rho/\rho_0 = h/h_0 \tag{18}$$

$$C^2/C_0^2 = T/T_0 = h/h_0 \tag{19}$$

and easily demonstrate that

$$p/p_0 = (h/h_0)^2 \tag{20}$$

with $K = C_P/C_V = 2$.

It will be noticed that no restriction is placed on this analogy as far as vorticity is concerned. Consequently, for rotational flows the analogous prediction equations, Eqs. (18)–(20), can be applied along corresponding streamlines as long as the two flows are kinematically similar. Generally, it is necessary to assume a priori the existence of kinematic similarity. Loh's one-dimensional analogy, as would be expected, is limited to irrotational (isentropic) flow due to the assumptions involved in forming the one-dimensional equations.

References

[1] Loh, W. H. T., *Hydraulic Analogy for Two-Dimensional and One-Dimensional Flows*, Journal of the Aero/Space Sciences, Vol. 26, No. 6, pp. 389–391, June, 1959.

[2] Loh, W. H. T., *A Study of the Dynamics of the Induction and Exhaust Systems of a Four Stroke Engine by a Hydraulic Analogy*, Sc.D. Thesis, M.I.T., 1946.

[3] Szebehely, V. G., and Whicker, L. F., *Generalisation and Improvement of the Hydraulic Analogy*, pp. 893–901, Proc. 1st U.S. Natl. Congress Appl. Mech., 1951, Edwards Brothers, Inc., Ann Arbor, 1952.

[4] Bryant, R. A. A., *Use of the Hydraulic Analogy for "Inside" Problems*, Journal of the Aero/Space Sciences, Vol. 25, No. 8, p. 536, August, 1958.

Improvement of a Pressure Pickup for the Measurements of Turbulence Characteristics

Y. Kobashi,* N. Kono,** and T. Nishi***
National Aeronautical Laboratory of Japan and Hiroshima University, Hiroshima, Japan

August 26, 1959

Introduction

THE SENIOR AUTHOR formerly measured several turbulence characteristics in the wake of a cylinder by using a combination of a novel pressure pickup and an ordinary hot-wire anemometer.[1] The pickup was constructed from a condenser-type microphone as a transducer and a static tube as a probe; but the arrangement of the duct and a cavity volume of microphone gave rise to the Helmholtz resonance[2] and a loss of gain in high-frequency range, which obliged the author to use electronic compensation networks, a band-rejection filter, and a high-frequency booster.

* National Aeronautical Laboratory of Japan. Temporary Research Associate at the Polytechnic Institute of Brooklyn.
** Hiroshima University, Japan.
*** National Aeronautical Laboratory of Japan.

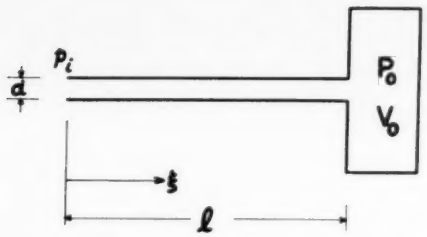

FIG. 1. Schematic arrangement of a duct-cavity combination.

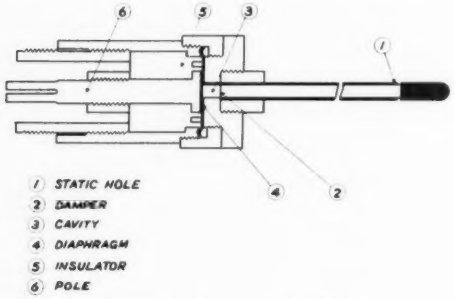

FIG. 2. Pressure pickup.

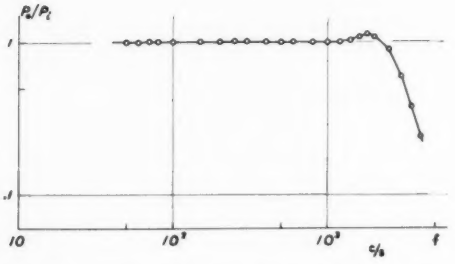

FIG. 3. Frequency response of the pressure pickup.

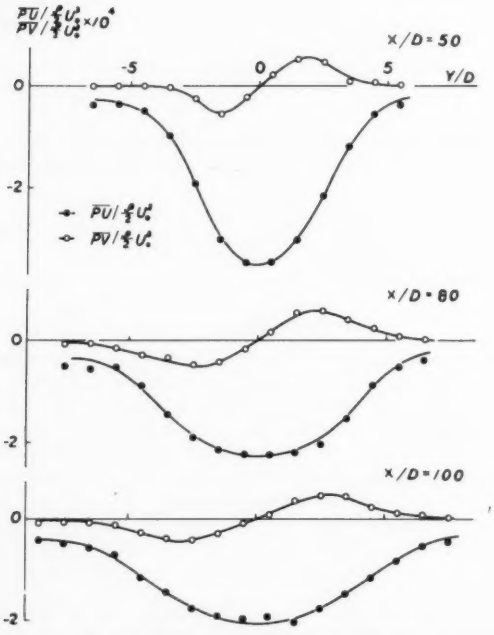

FIG. 4. Correlation between pressure and velocity at several cross sections downstream of the cylinder.

Afterwards, the authors tried to eliminate the Helmholtz resonance by choosing an adequate arrangement of the duct and microphone in which neither a band-rejection filter nor booster was needed. A new method of calibration of the apparatus was also developed, which enabled them to calibrate the characteristics of the pickup more accurately. The new apparatus was found to have a good response up to 2,500 cps, which was thought high enough for our present purpose. The application of the pickup to the measurements of the wake of a cylinder was carried out and showed satisfactory results, especially in determining the correlation of pressure and velocity components.

PRESSURE PICKUP

The motion of the medium in the duct-cavity combination, as is shown in Fig. 1, is given by the following equation:[3]

$$\rho\pi d^2 l(d^2\xi/dt^2) + (8\mu l/d^2)(\pi d^2)(d\xi/dt) + (\pi d^2)(p_0/V_0)(\pi d^2\xi) = p_i \cos \omega t(\pi d^2)$$

where p_0 is the pressure in the cavity volume and p_i the applied pressure.

By the aid of this equation, we estimated the effects of the variables such as diameter, length of the duct, and cavity volume. After a series of preliminary tests, we finally constructed a new pickup of the following dimensions:

static tube: 1 mm. inner dia., 35 mm. in length
cavity volume: 6 mm. dia., 0.1 mm. gap.

We also employed a damper in the duct, which was found to be very effective for eliminating the Helmholtz resonance peak value. The scheme of the newly developed pressure pickup is shown in Fig. 2.

For the calibration purpose, we adopted an acoustic method, "coupler method," which allowed us to make absolute calibration of the apparatus without any assumption about the applied pressure. In Fig. 3, the frequency response of the pressure

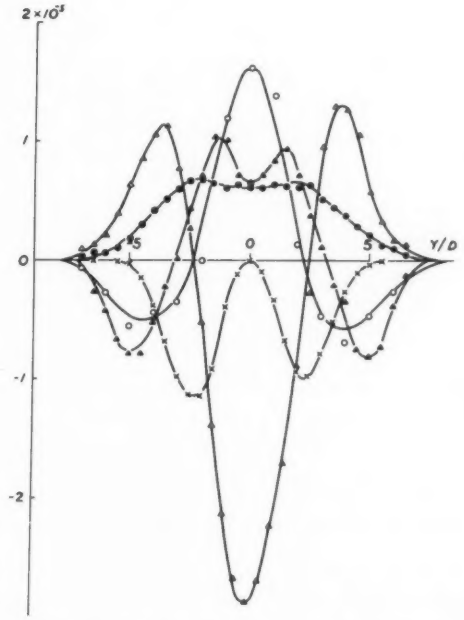

FIG. 5. Energy balance measured at the cross section, $x/D = 80$, in the wake of a cylinder.

- ● $15\,(\nu D/U3)\,(\partial U/\partial Y)^2$
- △ $(D/2U_0^3)\,(\partial/\partial X)\,(\overline{U}^2 + \overline{V}^2 + \overline{W}^2)$
- × $(\overline{UV}D/U_0^3)\,(\partial U/\partial Y)$
- ▲ $(D/2U_0^3)\,(\partial/\partial Y)\,(\overline{U^2V} + V^3 + \overline{W^2V})$
- ○ $(D/\rho U_0^3)\,(\partial/\partial Y)\,(PV)$

pickup is given, which shows a very flat response up to 2,500 cps.

Measurements of the Wake of a Cylinder

Our new pressure pickup, combined with the ordinary hot-wire anemometer, was applied for the measurement of the turbulence characteristics in the wake of a cylinder. The arrangement and the procedure were the same as those employed in the previous paper. Some of the most interesting results are shown in Figs. 4 and 5.

The results show important contributions of pressure fluctuations to the turbulence characteristics, especially in energy balancing mechanisms.

References

[1] Kobashi, Y., *Measurements of Pressure Fluctuation in the Wake of a Cylinder*, J. Phys. Soc. of Japan, Vol. 12, No. 5, pp. 533–543, May, 1957.

[2] Rayleigh, Lord (John William Strutt), *Theory of Sound*, MacMillan Company, New York, 1929.

[3] Takeda, S., *Transmission of Oscillatory Pressures Through Instrument Pipe Lines*, Technical College of Hosei University, Japan, Report 1, May, 1956.

A Simple Numerical Solution of the Supersonic Blunt-Body Problem for Real Gases*

G. A. Bird

Aerodynamics Division, Weapons Research Establishment, Salisbury, South Australia

August 31, 1959

Recently, several methods have been proposed—e.g., Van Dyke,[1] for obtaining a numerical solution of the inviscid flow behind the detached shock wave which is produced by the supersonic or hypersonic motion of a blunt body. The final forms of the equations of motion are usually so complex that a suitably programmed electronic computor is required to obtain a solution in a reasonable time and the methods cannot be applied easily to real gas problems. In this note, it is shown that a satisfactory hand solution of surprising accuracy may be obtained from a step-by-step method which makes use of only elementary forms of the equations of motion and which may, therefore, be based on realistic assumptions about the thermodynamic processes.

(1) Description of the Method

The solution is started from a prescribed plane or axisymmetric shock wave which is assumed to be symmetrical with respect to the x-axis. The flow is uniform in front of the shock, and all the flow properties immediately behind it may be found by applying the usual conservation laws. The present method constructs a network of streamlines and flow normals behind the shock, as illustrated in Fig. 1.

Part of this network is known, as the stagnation streamline lies along the x-axis. The first point chosen in the network (A in Fig. 1) lies immediately behind the shock and near the x-axis. The flow normal AB of the streamtube bounded by the origin O and A may then be constructed and the point B determined. Since the mean flow properties along OA are known and the mean entropy is constant along the streamtube, the usual one-dimensional isentropic relationships may be applied to find the mean value of pressure along AB. Now, the pressure at A and the mean pressure along AB are known, and the pressure gradient along the normal at B has to be zero, so that a curve can be constructed of pressure p against distance n along AB. This enables the pressure gradient dp/dn at A to be found, and the curvature K of the streamline through A is given by the centrifugal condition,

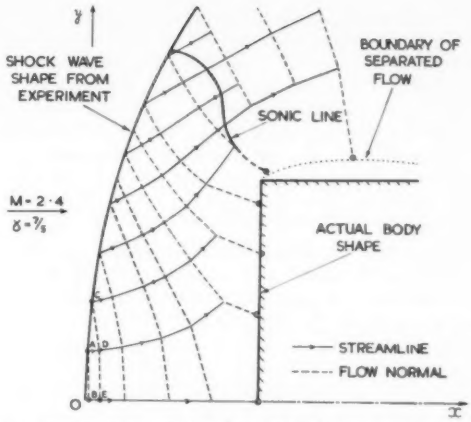

Fig. 1. Construction of the flow behind the shock wave produced by a flat nosed body of revolution.

$$K = -(dp/dn)/\rho q^2$$

where ρ is the density and q is the flow velocity. The streamline through A may then be constructed as far as the point D which is determined from the second point C, selected behind the shock. (For accurate work, the segment of streamline should be constructed using the mean values of slope and curvature between A and D, rather than the values at A, and this calls for an iteration procedure.) The changes in cross-sectional area of the streamtubes CD and DE are then measured and the one-dimensional flow relationships applied along them. A p-n curve is constructed for the normal CDE, and the procedure is continued.

The stagnation point on the body is found by extrapolating to zero a curve (which is very nearly linear) of velocity against distance along the stagnation streamline. A flow normal is eventually reached which must end on the body surface rather than on the stagnation streamline. The location of, and the pressure gradient at, the end point of this normal are not known in advance, but the p-n curve may be extrapolated to find the mean pressure in the streamtube adjacent to the body. A point on the body surface may then be found from continuity considerations, and the resulting body curvature provides a check on the accuracy of the extrapolation.

It may be shown that the method is unstable in subsonic flow, but this does not cause any difficulties as long as the mesh size is large. The solution given by the step-by-step process should be reviewed continuously for consistency of the flow properties and any discrepancies eliminated. As shown in Fig. 1, the cal-

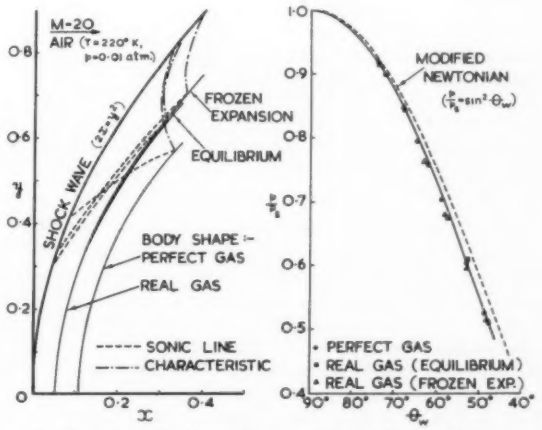

Fig. 2. Real gas effects on the axisymmetric flow behind a paraboloidal shock wave.

* Publication is made with the permission of the Chief Scientist, Australian Defence Scientific Service, Department of Supply, Melbourne.

culations along a particular streamline are stopped when the curvature becomes too large for the mesh size being used. A typical solution, with a total of about 50 mesh points, can be obtained in less than 40 man hours and requires only a desk calculator and basic compressible flow data. Reference 2 gives a detailed description of the procedure, and the method is shown to be able to reproduce existing solutions with an overall accuracy of several per cent.

(2) Application to Real Gases

Fig. 2 shows the results of the computation of the flow behind a paraboloidal shock wave ($M = 20$) for the three assumptions of air as a perfect gas, real gas in thermal equilibrium everywhere, and real gas with the composition frozen during expansion processes. The real-gas solutions are based on the thermodynamic data of Moeckel and Weston;[3] reference 2 outlines methods of deriving the required gasdynamic data in forms which are particularly suitable for the present method of solution of the blunt-body problem.

In the perfect-gas case, the body is nearly spherical and the ratio of the shock-separation distance to the radius of the body is 0.132, which compares very well with existing data.[1] The real-gas body shapes depart markedly from spherical, but the ratio of the separation distance to the nose curvature is about 0.066. It is noteworthy that the ratio of the real- to the perfect-gas shock-separation distance at the stagnation point is almost exactly equal to the ratio of the values of the density ratio across a normal shock wave of Mach Number 20. The ratio of the surface pressure p to the stagnation-point pressure p_s is shown in Fig. 2 as a function of the angle of inclination θ_w of the body surface. For a given θ_w, p/p_s is very nearly independent of the assumptions about the gas properties and lies just below the value given by modified Newtonian theory. In the equilibrium case, the specific-heat ratio of the gas behind the shock varied by less than one per cent in the subsonic region, but this variation increased to five per cent when the calculations were extended as far as the downstream characteristic through the sonic point on the body. Further details are given in reference 2.

References

[1] Van Dyke, M. D., *The Supersonic Blunt-Body Problem—Review and Extension*, Journal of the Aero/Space Sciences, Vol. 25, No. 8, pp. 485–496, August, 1958.

[2] Bird, G. A., *A Simple Numerical Method for Calculating the Flow around Blunt Bodies in a Supersonic Stream—with Applications to Real Gases*, Weapons Research Establishment, TN HSA 52, September, 1959.

[3] Moeckel, W. E., and Weston, K. C., *Composition and Thermodynamic Properties of Air in Chemical Equilibrium*, NACA TN 4265, April, 1958.

Periodic Temperature Distribution in a Two-Layer Composite Slab

Thomas E. Stonecypher

Rohm & Haas Company, Redstone Arsenal Research Division, Huntsville, Alabama

September 14, 1959

An investigation[1] to determine the feasibility of using an insulating thermal barrier to protect exposed solid-propellant motors from atmospheric or environmental temperature variations has recently been completed. In one portion of this study, a solution was developed for the periodic temperature distribution in a two-layer composite slab. One exposed surface of this composite slab was adiabatic, and the other exposed surface was subjected to a sinusoidal temperature variation. The technique used in the analysis was similar to that of Gröber.[2] In this note, pertinent features of the development of the solution are given.

The partial differential equation describing one-dimensional heat conduction in a rectangular coordinate system, assuming constant properties and no internal heat generation, is

$$\partial T(x, t)/\partial t = \alpha[\partial^2 T(x, t)/\partial x^2] \tag{1}$$

where T is temperature, t is time, and α is the thermal diffusivity of the conducting material.

The periodic solution to Eq. (1), found by using a separation of variables technique, is

$$T(x, t) = e^{i\lambda^2\alpha t}\{K_1 \cos[(1 - i)\lambda x/\sqrt{2}] + K_2 \sin[(1 - i)\lambda x/\sqrt{2}]\} \tag{2}$$

where i is the imaginary unit and λ, K_1, and K_2 are arbitrary constants to be determined from the statement of the problem. Substitution of the relations

$$e^{iu} = \cos(u) + i \sin(u) \tag{3}$$

$$\cos(1 - i)u = \cos(u) \cosh(u) + i \sin(u) \sinh(u) \tag{4}$$

$$\sin(1 - i)u = \sin(u) \cosh(u) - i \cos(u) \sinh(u) \tag{5}$$

$$f_{cc}(u) = \cos(u) \cosh(u) \tag{6}$$

$$f_{cs}(u) = \cos u \sinh(u) \tag{7}$$

$$f_{sc}(u) = \sin(u) \cosh(u) \tag{8}$$

$$f_{ss}(u) = \sin(u) \sinh(u) \tag{9}$$

into the solution given by Eq. (2) gives

$$\begin{aligned} T(x, t) = {} & \{\cos(\lambda^2\alpha t)[K_1 f_{cc}(\lambda x/\sqrt{2}) + K_2 f_{sc}(\lambda x/\sqrt{2})] + \\ & \sin(\lambda^2\alpha t)[-K_1 f_{ss}(\lambda x/\sqrt{2}) + K_2 f_{cs}(\lambda x/\sqrt{2})]\} + \\ & i\{\cos(\lambda^2\alpha t)[K_1 f_{cs}(\lambda x/\sqrt{2}) - K_2 f_{cc}(\lambda x/\sqrt{2})] + \\ & \sin(\lambda^2\alpha t)[K_1 f_{cc}(\lambda x/\sqrt{2}) + K_2 f_{sc}(\lambda x/\sqrt{2})]\} \end{aligned} \tag{10}$$

This form of the solution is composed of two terms, one of which is multiplied by the imaginary unit i.* Since each term is a solution of Eq. (1), the complete solution can be written in the form

$$\begin{aligned} T(x, t) = {} & \cos(\lambda^2\alpha t)[K_3 f_{cc}(\lambda x/\sqrt{2}) + K_4 f_{sc}(\lambda x/\sqrt{2}) + \\ & K_5 f_{ss}(\lambda x/\sqrt{2}) - K_6 f_{cs}(\lambda x/\sqrt{2})] + \\ & \sin(\lambda^2\alpha t)[-K_3 f_{ss}(\lambda x/\sqrt{2}) + K_4 f_{cs}(\lambda x/\sqrt{2}) + \\ & K_5 f_{cc}(\lambda x/\sqrt{2}) + K_6 f_{sc}(\lambda x/\sqrt{2})] \end{aligned} \tag{11}$$

where the K's are constants to be determined from the statement of the problem.

A particular solution of Eq. (11) was sought for the composite slab model, which consisted of two finite plane slabs in perfect thermal contact. The inner slab of the composite extended from $x = 0$ to $x = l$, and the outer slab extended from $x = l$ to $x = s$. The exposed surface of the inner slab ($x = 0$) was assumed to be adiabatic, and the exposed surface of the outer slab ($x = s$) was subjected to a sinusoidal surface temperature variation. Hence, the boundary conditions imposed on Eq. (11) are

$$T_2(x, t) = T_0 \cos(2\pi t/t_0), \quad x = s \tag{12}$$

$$T_1(x, t) = T_2(x, t), \quad x = l \tag{13}$$

$$k_1[\partial T_1(x, t)/\partial x] = k_2[\partial T_2(x, t)/\partial x], \quad x = l \tag{14}$$

$$\partial T_1(x, t)/\partial x = 0, \quad x = 0 \tag{15}$$

where T_0 is the surface-temperature amplitude, t_0 is the period of oscillation, k is thermal conductivity, and subscripts 1 and 2 refer to the inner and outer slabs, respectively. Since the temperature distribution in the model and its reflection is symmetric with respect to the $x = 0$ plane, the odd functions of argument $(\lambda x/\sqrt{2})$ in Eq. (11) do not appear in the corresponding equation for the temperature distribution in the inner slab, and the solution for the periodic temperature distribution in the composite is

$$\begin{aligned} T_1(x, t) = {} & \cos(\lambda_1^2\alpha_1 t)[C_1 f_{cc}(\lambda_1 x/\sqrt{2}) + C_2 f_{ss}(\lambda_1 x/\sqrt{2})] + \\ & \sin(\lambda_1^2\alpha_1 t)[-C_1 f_{ss}(\lambda_1 x/\sqrt{2}) + C_2 f_{cc}(\lambda_1 x/\sqrt{2})], \\ & 0 \le x \le l \end{aligned} \tag{16}$$

* The solution of Eq. (1), given by Eq. (2) or Eq. (10), can be used to obtain the solution to the problem under consideration, but extensive use of complex numbers is required. The note proceeds with a problem solution which avoids the use of complex numbers.

$$T_2(x,t) = \cos(\lambda_2^2\alpha_2 t)[C_3 f_{cc}(\lambda_2 x/\sqrt{2}) + C_4 f_{sc}(\lambda_2 x/\sqrt{2}) + C_5 f_{ss}(\lambda_2 x/\sqrt{2}) - C_6 f_{cs}(\lambda_2 x/\sqrt{2})] + \sin(\lambda_2^2\alpha_2 t)[-C_3 f_{sc}(\lambda_2 x/\sqrt{2}) + C_4 f_{cs}(\lambda_2 x/\sqrt{2}) + C_5 f_{cc}(\lambda_2 x/\sqrt{2}) + C_6 f_{sc}(\lambda_2 x/\sqrt{2})], \quad l \le x \le s \quad (17)$$

The constants appearing in the solution equations, Eqs. (16) and (17), are determined by the following relations resulting from the application of the boundary conditions

$$\lambda_1^2\alpha_1 = \lambda_2^2\alpha_2 = 2\pi/t_0 \quad (18)$$

$$T_0 = C_3 f_{cc}(\lambda_2 s/\sqrt{2}) + C_4 f_{sc}(\lambda_2 s/\sqrt{2}) + C_5 f_{ss}(\lambda_2 s/\sqrt{2}) - C_6 f_{cs}(\lambda_2 s/\sqrt{2}) \quad (19)$$

$$0 = -C_3 f_{ss}(\lambda_2 s/\sqrt{2}) + C_4 f_{cs}(\lambda_2 s/\sqrt{2}) + C_5 f_{sc}(\lambda_2 s/\sqrt{2}) + C_6 f_{ss}(\lambda_2 s/\sqrt{2}) \quad (20)$$

$$0 = -C_1 f_{cc}(\lambda_1 l/\sqrt{2}) - C_2 f_{ss}(\lambda_1 l/\sqrt{2}) + C_3 f_{cc}(\lambda_2 l/\sqrt{2}) + C_4 f_{sc}(\lambda_2 l/\sqrt{2}) + C_5 f_{ss}(\lambda_2 l/\sqrt{2}) - C_6 f_{cs}(\lambda_2 l/\sqrt{2}) \quad (21)$$

$$0 = C_1 f_{ss}(\lambda_1 l/\sqrt{2}) - C_2 f_{cc}(\lambda_1 l/\sqrt{2}) - C_3 f_{ss}(\lambda_2 l/\sqrt{2}) + C_4 f_{cs}(\lambda_2 l/\sqrt{2}) + C_5 f_{cc}(\lambda_2 l/\sqrt{2}) + C_6 f_{sc}(\lambda_2 l/\sqrt{2}) \quad (22)$$

$$0 = -C_1 k_1\lambda_1[f_{cs}(\lambda_1 l/\sqrt{2}) - f_{sc}(\lambda_1 l/\sqrt{2})] - C_2 k_1\lambda_1[f_{cs}(\lambda_1 l/\sqrt{2}) + f_{sc}(\lambda_1 l/\sqrt{2})] + C_3 k_2\lambda_2[f_{cs}(\lambda_2 l/\sqrt{2}) - f_{sc}(\lambda_2 l/\sqrt{2})] + C_4 k_2\lambda_2[f_{cc}(\lambda_2 l/\sqrt{2}) + f_{ss}(\lambda_2 l/\sqrt{2})] + C_5 k_2\lambda_2[f_{cs}(\lambda_2 l/\sqrt{2}) + f_{sc}(\lambda_2 l/\sqrt{2})] - C_6 k_2\lambda_2[f_{cc}(\lambda_2 l/\sqrt{2}) - f_{ss}(\lambda_2 l/\sqrt{2})] \quad (23)$$

and

$$0 = C_1 k_1\lambda_1[f_{cs}(\lambda_1 l/\sqrt{2}) + f_{sc}(\lambda_1 l/\sqrt{2})] - C_2 k_1\lambda_1[f_{cs}(\lambda_1 l/\sqrt{2}) - f_{sc}(\lambda_1 l/\sqrt{2})] - C_3 k_2\lambda_2[f_{cs}(\lambda_2 l/\sqrt{2}) + f_{sc}(\lambda_2 l/\sqrt{2})] + C_4 k_2\lambda_2[f_{cc}(\lambda_2 l/\sqrt{2}) - f_{ss}(\lambda_2 l/\sqrt{2})] + C_5 k_2\lambda_2[f_{cs}(\lambda_2 l/\sqrt{2}) - f_{sc}(\lambda_2 l/\sqrt{2})] + C_6 k_2\lambda_2[f_{cc}(\lambda_2 l/\sqrt{2}) + f_{ss}(\lambda_2 l/\sqrt{2})] \quad (24)$$

Eqs. (19)—(24) may be solved generally to give explicit relations for constants C_1 through C_6. However, it has been found more practical for a particular problem to evaluate the coefficients of constants C_1 through C_6 and then to solve the resulting equations by matrix methods.

References

[1] Quarterly Progress Report on Engineering Research, Report No. P-59-5, Rohm & Haas Company, Redstone Arsenal Research Division, Huntsville, Ala., April, 1959.

[2] Gröber, H., Erk, S., and Grigull, U., *Die Grundgesetze der Wärmeübertragung*, 3rd Ed., p. 79, Springer-Verlag, Berlin, 1955.

Comment on "On a Class of Variational Problems in Rocket Flight"

G. Leitmann*
Associate Professor, Engineering Science,
University of California, Berkeley, Calif.

September 14, 1959

In a recently published paper,[1] the optimization of the thrust direction and magnitude of a rocket traveling in a constant gravitational field was discussed. Properties of the extremal arc were investigated and criteria for its composition derived. Among other things, it was shown that the thrust direction angle may experience a discontinuous† jump of 180 degrees. The question has been raised whether or not such a jump could occur in a physically meaningful problem. It is the purpose of this note to present a problem, both simple and meaningful, in which a discontinuity in the thrust direction angle arises.

Consider the minimum time transfer of a given mass with prescribed fuel expenditure between two positions and velocities

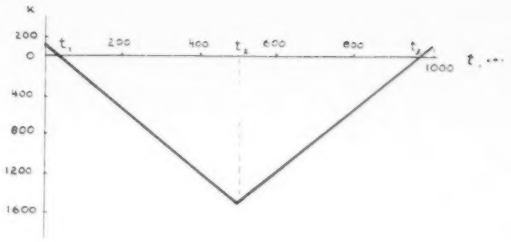

Fig. 1

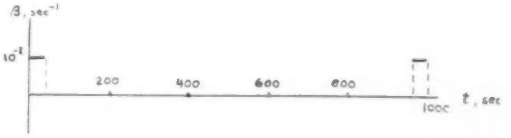

Fig. 2.

in field-free space. For the sake of simplicity, let the initial and final velocities be zero. That is, it is required to minimize[1]

$$G = t_f \quad (1)$$

subject to the equations of motion

$$\dot{p} = (c\beta/\mu)\cos\psi, \quad \dot{x} = p \quad (2)$$

and the constraint

$$\beta_l \le \beta \le \beta_u, \quad \beta_l \to 0 \quad (3)$$

where

$$\dot{\mu} = -\beta, \quad \mu = m/m_0 \quad (4)$$

The initial and final conditions are

$$t = 0 \begin{cases} x = 0 \\ p = 0, \\ \mu = 1 \end{cases} \quad t = t_f \begin{cases} x = x_f \\ p = 0 \\ \mu = \mu_f \end{cases} \quad (5)$$

The applicable Euler-Lagrange equations are

$$\cos\psi = \lambda_1/|\lambda_1| = \pm 1, \quad \lambda_1 = \lambda_{10} - \lambda_3 t \quad (6)$$
$$\dot{\lambda}_2 = 0, \quad \dot{\lambda}_3 = (c\beta/\mu^2)|\lambda_1|$$

Also,

$$\beta = \beta_u \text{ when } \kappa > 0 \quad (7)$$
$$\beta = \beta_l \text{ when } \kappa < 0$$

where

$$\kappa = (c/\mu)|\lambda_1| - \lambda_3 \quad (8)$$

Furthermore, the first integral becomes

$$1 = \beta\kappa + \lambda_2 p \quad (9)$$

so that, at $t = 0$ and $t = t_f$,

$$\beta\kappa > 0 \quad (10)$$

i.e., initial and final arcs are flown at maximum thrust. We expect that, in general, there will be an intervening coasting arc. In particular, because of the equality of initial and final velocities, one expects that the final arc be flown with decelerating thrust. According to Eq. (6), the jump in the thrust direction will take place when

$$\lambda_1 = 0, \quad (t = t_2) \quad (11)$$

During thrust-on periods, κ may be computed from Eq. (9). During coasting, κ is found from Eq. (8) with

$$\lambda_3 = \lambda_3(t_1) = \text{const.} \quad (12)$$

The instants of transition from full thrust to coast and back to full thrust, t_1 and t_3, are determined by Eq. (8) with

$$\kappa = 0 \quad (13)$$

To compute a trajectory, values of λ_{10} and λ_3 must be assumed

---

* Also, Research Scientist, LSMD.

† The rocket is treated as a point mass—i.e., as having zero moment of inertia.

such that the end values of p and μ are met when $x = x_f$. This calls for a two-parameter iteration process. It should be noted that the equations of motion in this simple example are integrable so that the multipliers can be expressed in terms of the boundary conditions obviating the iteration procedure.

To demonstrate this behavior, we consider a numerical example—e.g., let

$$x_f = 20.5 \times 10^4 \text{ ft} \cong 39 \text{ mi.}$$

$$\mu_f = 0.368$$

$$c = 10^4 \text{ ft./sec.}$$

$$\beta_u = 10^{-2} \frac{\text{slug/sec.}}{\text{slug}}$$

The behavior of κ and β is shown in Figs. 1 and 2. Transitions from full thrust to coast and back to full thrust take place at $t = t_1 = 39.4$ sec. and $t = t_2 = 960.6$ sec., respectively; and jump in thrust direction occurs halfway through coasting at $t = t_2 = 500.0$ sec. The minimum transfer time is $t_f = 1000.0$ sec. Of course, in a real situation, thrust reversal may take place any time during coasting.

REFERENCE

[1] Leitmann, G., *On a Class of Variational Problems in Rocket Flight*, Journal of the Aero/Space Sciences, Vol. 26, No. 9, p. 586, September, 1959.

The Response of Linear Systems to Non-Gaussian Random Inputs†

Stephen H. Crandall,* William H. Siebert,** and Bernard P. Hoquetis***

Massachusetts Institute of Technology, Cambridge, Mass.

September 14, 1959

IN A RECENT PAPER, Mazelsky[1] arrived at the result that, if a wide-band non-Gaussian stationary random process was impressed on a linear system with a narrow-band transfer function, the response would be a stationary random process with a probability distribution which is asymptotically Gaussian when the ratio of input bandwidth to system transfer bandwidth approaches infinity. The only restriction imposed was a relatively mild one on the skewness of the input process. This result is a strong statement of a widely held intuitive feeling that "filtering favors the Gaussian distribution." For very special non-Gaussian processes, rigorous proofs have been given[2, 3] that this is indeed the case. In an unrestricted random process, however, there is generally complete independence of the frequency distribution and the probability distribution. We give below a simple counterexample to show that Mazelsky's result cannot be valid in general.

We consider an input process consisting of a stationary Gaussian process of constant power spectral density s_0 and (wide) bandwidth B *plus* a sinusoid A sin $2\pi f_0 t$. The root mean square of the random process is $\sqrt{s_0 B}$. Let

$$a_i = A/\sqrt{s_0 B} \tag{1}$$

be a measure of the strength of the sinusoid in comparison with the Gaussian process in the input. Fig. 1 shows the probability density distribution for the resulting process for several values of a as computed by Rice.[4] Note that these distributions are symmetrical—i.e., there is no skewness at all, and hence these processes are admissible non-Gaussian inputs according to Mazelsky's criterion.

As a representative linear system, we consider the standard single-degree-of-freedom mass-spring-dashpot system with natural frequency $\omega_n = 2\pi f_n$ and damping ratio $\zeta = c/c_c$. The response of this system to the input above will consist of a Gaussian process with nonconstant spectral density *plus* a sinusoid. The root mean square of the Gaussian process is very nearly[5]

$$(s_0 f_n/8\zeta)^{1/2}$$

if f_n is within the bandwidth of the original process and ζ is small while the amplitude of the sinusoid is

$$A\{[1 - (f_0/f_n)^2]^2 + 4\zeta^2(f_0/f_n)^2\}^{-(1/2)}$$

The probability density distribution of the response will be of the same general character as the input, but the parameter a is now

$$a_r = \frac{2\sqrt{2}\, A\, \zeta^{1/2}}{\{[1 - (f_0/f_n)^2]^2 + 4\zeta^2(f_0/f_n)^2\}^{1/2}(\zeta f_n)^{1/2}} \tag{2}$$

so that

$$\frac{a_r}{a_i} = \left(\frac{B}{f_n}\right)^{1/2} \left(\frac{8\zeta}{[1 - (f_0/f_n)^2]^1 + 4\zeta^2(f_0/f_n)^2}\right)^{1/2} \tag{3}$$

Several conclusions can be drawn from Eqs. (2) and (3). For a fixed input (B, s_0, A, f_0 fixed) but with $f_0 \neq f_n$ sharpening, the filter—i.e., decreasing ζ, does *decrease* a_r which makes the response probability density function closer to Gaussian. However, if $f_0 = f_n$, sharpening the filter *increases* a_r, and the response probability density function becomes more nearly like that of the sinusoid. Finally, if the system is left unchanged (ζ, f_n fixed) while the bandwidth B of the Gaussian part of the input is increased, a_r remains essentially constant while the ratio a_r/a_i increases whether $f_0 = f_n$ or not—i.e., increasing the bandwidth of the input always tends to *decrease* the relative Gaussianness of the response in comparison with the input.

The use of a discrete component in the above counterexample makes for simple computation, but it is not an essential part of the argument. It is possible to imagine a random process of limited bandwidth as shown in Fig. 2(*a*) which would have a well-defined non-Gaussian probability density. If a Gaussian process were added to this with a spectral density as shown in Fig. 2(b), the combined process would have a uniform spectral density and a non-Gaussian probability density, although, if B were large compared to B_{ng}, the probability density might be quite close to

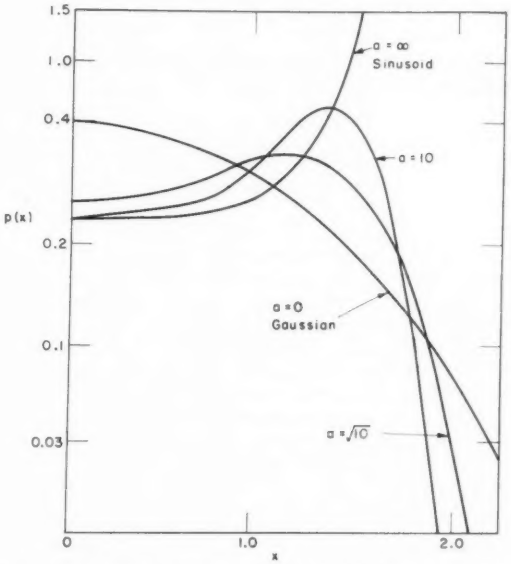

FIG. 1. Probability density of a sinusoid plus a Gaussian process for various values of the parameter a.

† This research was partially supported by the USAF through the AFOSR of the ARDC, under Contract No. AF 49(638)-564. Reproduction in whole or in part is permitted for any purpose of the United States Government.

* Professor of Mechanical Engineering.

** Associate Professor of Electrical Engineering.

*** Research Assistant.

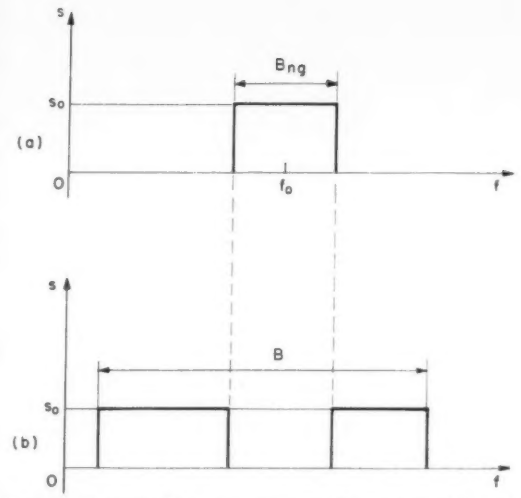

FIG. 2. Superposition of non-Gaussian process with limited bandwidth (a) and wide-band Gaussian process (b) to make combined process with uniform power spectral density.

Gaussian. If this input were applied to an ideal linear system with a bandwidth B_{ng} centered at $f = f_0$ and with a linear phase, the output would clearly contain a large proportion of non-Gaussian power. Thus, it cannot be true in general that filtering favors the Gaussian distribution.

REFERENCES

[1] Mazelsky, B., *Extension of Power Spectral Methods of Generalized Harmonic Analysis to Determine Non-Gaussian Probability Functions of Random Input Disturbances and Output Responses of Linear Systems*, Journal of the Aeronautical Sciences, Vol. 21, No. 3, pp. 145–153, March, 1954.

[2] Kac, M., and Siegert, A. J. F., *On the Theory of Noise in Radio Receivers with Square-Law Detectors*, J. Appl. Phys., Vol. 18, No. 4, pp. 383–397, April, 1957.

[3] Emerson, R. C., *First Probability Densities for Receivers with Square-Law Detectors*, J. Appl. Phys., Vol. 24, No. 9, pp. 1168–1176, September, 1953.

[4] Rice, S. O., *Statistical Properties of a Sine Wave Plus Random Noise*, Bell System Technical Journal, Vol. 27, pp. 109–157, January, 1948.

[5] Crandall, S. H., *Random Vibration*, p. 4–7, Technology Press, Cambridge, Mass., 1958.

On the Structure of Vortical Layers in Supersonic and Hypersonic Flows

Hsien K. Cheng
Cornell Aeronautical Laboratory, Inc., Buffalo, N.Y.
September 14, 1959

THE EXISTENCE of a "vortical layer" close to the surface of a slightly yawed cone in supersonic flow was first pointed out by Ferri.[1] This layer is characterized by the appearance of large entropy gradients and, hence, of strong vorticity. A treatment of the problem of supersonic flow over a yawed circular cone had been given previously by Stone[2] under the assumption of small yaw angle, with the corresponding computation having been carried out by Kopal.[3] Unfortunately, Stone's analysis, which is based on a small perturbation in the yaw angle, breaks down in the neighborhood of the cone surface and fails to account for the vortical layer.[1] A knowledge of the structure of the vortical layer, therefore, would be of basic importance not only for boundary-layer studies but also to insure the internal consistency of the Stone approximation.

As part of a study of hypersonic flow over yawed pointed bodies, to be published subsequently, a critical examination of the small-perturbation procedure used in the problem of a slightly yawed cone has been made and a new scheme found, giving a solution which is valid even at the surface. The first-order solution reveals the structure of the vortical layer. In this note, the main idea underlying the method of approximation will be described and the explicit formula for the entropy distribution presented.

Consider the problem of supersonic flow around a circular cone at small yaw angle, that is, $\sigma \equiv \sin\alpha/\sin\tau \ll 1$, where α is the yaw angle and τ the half-cone angle. The basic difficulty of the problem lies in the equation governing the entropy function $S \equiv p/\rho^\gamma$ of the conical-flow field. In terms of the spherical polar coordinates θ and ψ of reference 4, this equation is

$$[v\sin\theta(\partial/\partial\theta) + w(\partial/\partial\psi)]S = 0 \tag{1}$$

For small σ, the circumferential velocity w is proportional to the yaw parameter σ. In Stone's analysis, the term associated with w is always considered as a higher-order term when compared with the first term, and this leads to an invalid solution for S and the related quantities in the neighborhood of the surface. Here, it is essential to recognize that the small-perturbation procedure in Stone's theory overlooks the singular behavior of S, which results from the vanishing of the normal velocity v at the surface. This point may be made more evident by writing Eq. (1) in the form

$$[(\theta - \tau)(\partial/\partial\theta) - \sigma f(\theta, \psi; \sigma)(\partial/\partial\psi)]S = 0 \tag{2}$$

where the function f is defined as

$$f(\theta, \psi; \sigma) \equiv -(\sin\tau/\sin\theta)[(\theta - \tau)/v](w/\sin\alpha) \tag{3}$$

In view of the properties of v and w, the function f will generally be of unit order and nonvanishing, and the line $\theta = \tau$ is clearly a singularity. In order to account for the behavior of S in the neighborhood of the body and, hence, in the vortical layer, the higher-order term $\sigma f\,(\partial S/\partial\psi)$ must be retained. This term, however, is important only in the vicinity of the surface, insofar as the first-order yaw effect on S is concerned. Hence, in the present scheme, one uses only $f(\tau, \psi; o)$ instead of $f(\theta, \psi; \sigma)$ in Eq. (2). In determining this function, only the leading approximations for v and w at the surface are required. One may tentatively assume that the leading approximations for v and w are given correctly by Stone's analysis, which must then be verified a posteriori. Thus,

$$f(\tau, \psi; o) = A\sin\psi \tag{4}$$

where

$$A \equiv \left.\frac{z + 2x/\sin\tau}{\partial V/\partial\theta}\right|_{\theta=\tau}$$

with the same variables z, x, V given numerically by Kopal in reference 3.

Using the boundary condition behind the slightly perturbed shock and the simplification implicit in Eq. (4), Eq. (2) yields the following explicit formula for entropy distribution:

$$S/\bar{S} \approx 1 + \sigma B[(1 - \zeta^2)/(1 + \zeta^2)] \tag{5}$$

where

$$\zeta \equiv (\theta - \tau)^{A\sigma}\tan(\psi/2)$$

$\bar{S}$ is the unperturbed value of S given by the Taylor-Maccoll solution, and the constant B is related to the entropy jump across the strongest part of the shock and may be obtained for the present purpose from the variables $\eta/\bar{\rho}$ and $\xi/\bar{\rho}$ in reference 3 as

$$B \equiv \sin\tau[(\eta/\bar{\rho}) - \gamma(\xi/\bar{\rho})]\,|_{\theta=\delta_{sh}} \tag{6}$$

Eq. (5) exhibits all the features one may anticipate for the entropy field, and the structure of a vortical layer is clearly described by the characteristic variable ζ. On the body, $\theta = \tau$; the entropy is seen to be uniform; and, because $A\sigma$ is small, at a small distance from the surface, the entropy function becomes dependent only on ψ, as predicted by Stone's analysis. Using this formula and the data of reference 3, an example of the entropy field is given in Fig. 1 for a 30° cone at $M_\infty = 4.59$, with $\gamma = 1.405$, at 2° and 5° of yaw.

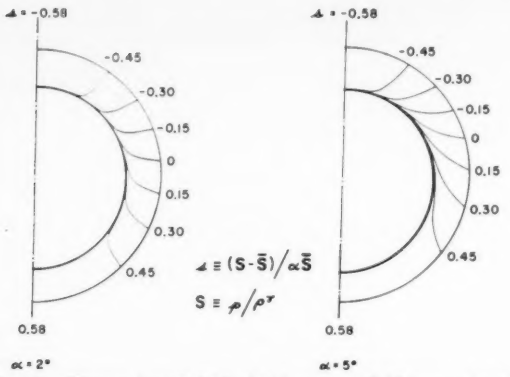

FIG. 1. Illustration of the inviscid entropy fields around a 30° (included angle) circular cone, at $M_\infty = 4.59$ with $\gamma = 1.405$, at 2° and 5° of yaw. Contours of constant s provide also the pattern of streamlines projected in the $\theta - \psi$ plane.

The first-order solution to the entire flow field, consistent with Eq. (5), can now be determined. To this approximation, the velocity components v and w and the pressure p are not affected by the vortical layer, as may be inferred from the governing equations on the basis of the entropy formula Eq. (5), and this confirms the conclusion reached previously by Ferri[1] and others.[4] Therefore, the assumption used in the determination of $f(\tau, \psi; o)$ is justified. However, in view of the existence of the "vortical layer," the density, temperature, and radial velocity are found to differ from the values given by Stone and Kopal and may be easily determined by applying Eq. (5) with the aid of the result of reference 3 for the pressure. It is important to note at this point that the results from the present scheme are self-consistent and can, in fact, be proved to be uniformly valid over the entire flow field within an error of order of σ^2, excluding perhaps the vicinity of the stagnation streamline on the lee side where a singularity of another nature arises.

It is seen from above that the lateral extent of the vortical layer depends on the parameter $A\sigma$. At higher Mach Numbers, the constant A will generally become smaller, as a study of the numerical data of reference 3 reveals. Thus, the vortical layer will be thin when the yaw angle is small and will be thinner if the Mach Number is also higher. This fact is, indeed, consistent with the result of a study based on the hypersonic shock-layer approximation which assumes a strong shock wave. This study, which will be published shortly elsewhere, reveals that, within the thin shock layer, there will exist a vortical sublayer, even at large degree of yaw. Recently Cole[5] and Gonor[6] have treated the problem of hypersonic flows over cone and bodies of revolution at yaw, using the shock-layer approach but not accounting for the behavior of the vortical layer.*

REFERENCES

[1] Ferri, A., *Supersonic Flow Around Circular Cones at Angle of Attack*, NACA TN 2236, November, 1950; NACA TR 1945, 1951.

[2] Stone, A. H., *On Supersonic Flow Past a Slightly Yawing Cone. Part I*, J. Math. and Phys., Vol. 27, pp. 67–81, 1948; Part II, J. Math. and Phys., Vol. 30, pp. 200–213, 1952.

[3] Staff of the Computing Section (under direction of Zdenek Kopal), *Tables of Supersonic Flow Around Yawing Cones*, M.I.T. Tech. Rpt. 3, 1947; *Tables of Supersonic Flow Around Cones of Large Yaw*, M.I.T. Tech. Rpt. 5, 1949.

[4] Roberts, R. C., and Riley, J. D., *A Guide to the Use of the M.I.T. Cone Tables*, Journal of the Aeronautical Sciences, Vol. 21, No. 5, pp. 336–342, May, 1954.

[5] Cole, J. D., *Lift of Slender Nose Shapes According to Newtonian Theory*, Rand Corp. Rpt. P-1270, April, 1958.

[6] Gonor, A. L., *Hypersonic Flow Around a Cone at an Angle of Attack*, Izvestiia, AN USSR, O.T.N., No. 7, pp. 102–105, 1958, English translation available from Morris D. Friedman, Inc., Needham Height, Mass.

* Readers may refer to a recent report by the author entitled *Hypersonic Shock-Layer Theory of a Yawed Cone and Other Three-Dimensional Pointed Bodies*, WADC TN 59-335. (Available also as Cornell Aero. Lab. Rpt. No. AF-1270-A-1, October, 1959.)

Similar Solutions for Boundary Layers in Constant-Temperature Magneto-Gasdynamic Channel Flow

Jack L. Kerrebrock
Daniel and Florence Guggenheim Jet Propulsion Center, California Institute of Technology, Pasadena, Calif.
September 17, 1959

ONE OF THE PROBLEMS that must be faced in the development of plasma accelerators is the growth of boundary layers upon the accelerator walls. The boundary-layer effects may be important not only from a heat-transfer standpoint, but because of the displacement effect on the main flow. For the steady-flow accelerator utilizing crossed electric and magnetic fields, such as that discussed by Resler and Sears, a very interesting situation may develop upon the walls that are perpendicular to the current flow. Since the wall must generally be cool, there is a tendency for the plasma conductivity near the wall to be lower than that in the relatively hot free stream. Consequently, the Joule heating associated with the continuous current will be highest in the neighborhood of the wall. This increased heating may produce an abnormal thermal boundary layer and, quite possibly, a severe heat-transfer condition.

The boundary-layer development may be analyzed, utilizing as free-stream conditions the simple, constant-temperature channel-flow solutions presented in a previous note.[1] It was shown in reference 1 that, if the free-stream velocity varies as a power of the streamwise coordinate, the pressure, current density, and flow area are also proportional to powers of the coordinate, as is the required magnetic-field strength, except for an additive constant. This simple behavior suggests that similar solutions, analogous to those of Falkner and Skan for the incompressible boundary layer, may exist for the boundary layer on the electrodes. It will be shown in the following paragraphs that such solutions do in fact exist, if the Mach Number is small. By utilizing the concept of local similarity, it may be possible to extend the results to nonzero Mach Numbers.

The usual boundary-layer equations must be modified by the inclusion of the electromagnetic body force in the momentum equation, and the electronic conduction and Joule heating in the energy equation. Thus, if j, σ, and B denote the current density, electrical conductivity, and magnetic-field strength, the equations are:

$$\text{continuity,} \quad [\partial(\rho u)/\partial x] + [\partial(\rho v)/\partial y] = 0 \tag{1}$$

$$\text{momentum,} \quad \rho[u(\partial u/\partial x) + v(\partial u/\partial y)] = (\partial/\partial y)[\mu(\partial u/\partial y)] - (dp/dx) + jB \tag{2}$$

$$\text{energy,} \quad \rho c_p[u(\partial T/\partial x) + v(\partial T/\partial y)] = (\partial/\partial y)[\lambda(\partial T/\partial y) + (5/2)(k/e)jT] + \mu[(\partial u/\partial y)]^2 + u(dp/dx) + (j^2/\sigma) \tag{3}$$

$$\text{and state,} \quad p = \rho RT$$

where k and e are Boltzmann's constant and the magnitude of the electronic charge, and the other notation is conventional.

It is assumed that the magnetic Reynolds Number is sufficiently low so that B may be regarded as a prescribed function of x. The current density is also assumed to be a function only of x, the form of which is determined by the free-stream flow. Thus, the electrical resistance of the boundary layer is considered a second-order correction to the free-stream resistance, just as the displacement thickness of a boundary layer is considered a small correction to the body contour.

In the channel-flow approximation, the momentum and energy equations for the free-stream flow are

$$\rho_\infty u_\infty(du_\infty/dx) = -(dp/dx) + jB$$

and

$$u_\infty(dp/dx) = -(j^2/\sigma_\infty)$$

With these relations, the boundary-layer momentum and energy

equations become

$$\rho[u(\partial u/\partial x) + v(\partial u/\partial y)] = (\partial/\partial y)[\mu(\partial u/\partial y)] + \rho_\infty u_\infty(du_\infty/dx) \quad (4)$$

and

$$\rho c_p[u(\partial T/\partial x) + v(\partial T/\partial y)] = (\partial/\partial y)[\lambda(\partial T/\partial y) + (5k/2e)jT] + \mu(\partial u/\partial y)^2 + (j^2/\sigma_\infty)[(\sigma_\infty/\sigma) - (u/u_\infty)] \quad (5)$$

Since the free-stream pressure varies while the free-stream temperature is constant, the following modification of the Stewartson transformation[3, 4]

$$\bar{y} = \int_0^y (\rho/\rho_0)dy, \quad \bar{x} = \int_0^x (p/p_0)dx \quad (6)$$

where the subscript 0 denotes values in the free stream at a reference point is convenient. It gives $\bar{u} = u$ and $\bar{v} = (p_0/p)[(\rho v/\rho_0) + u(\partial\bar{y}/\partial x)]$, where if μ and λ are proportional to T, as for Maxwellian molecules, $\bar{u}$ and $\bar{v}$ satisfy the transformed equations:

$$(\partial\bar{u}/\partial\bar{x}) + (\partial\bar{v}/\partial\bar{y}) = 0 \quad (7)$$

$$\bar{u}(\partial\bar{u}/\partial\bar{x}) + \bar{v}(\partial\bar{u}/\partial\bar{y}) = \nu_0(\partial^2\bar{u}/\partial\bar{y}^2) + \theta[\bar{u}_\infty(d\bar{u}_\infty/d\bar{x})] \quad (8)$$

The dimensionless temperature, $\theta \equiv T/T_0$, satisfies

$$\bar{u}(\partial\theta/\partial\bar{x}) + \bar{v}(\partial\theta/\partial\bar{y}) = (\nu_0/Pr)(\partial^2\theta/\partial\bar{y}^2) + (\nu_0/c_pT_0)(\partial\bar{u}/\partial\bar{y})^2 + (5kj/2ec_p\rho_0)(p_0/p)(\partial\theta/\partial\bar{y}) + (j^2/c_pT_0\sigma_0\rho_\infty)(p_0/p)\theta[(\sigma_\infty/\sigma) - (\bar{u}/\bar{u}_\infty)] \quad (9)$$

A simple solution for channel flow with constant temperature, conductivity, and electric field was given in reference 1. It was demonstrated that, if the velocity is of the form $u = \alpha x^n$, the current and pressure are given by

$$j = (\sigma_0 RT_0E/\alpha^2 n)(5n - 1)x^{-2n}$$

and

$$p = [\sigma_0(RT_0E)^2/\alpha^5][(5n - 1)/n^2]x^{1-5n}$$

where E is the constant electric field.

With this expression for the pressure, the transformation from x to $\bar{x}$ becomes

$$\bar{x} = Kx^{2-5n} \quad (10)$$

where

$$K \equiv [\sigma_0(RT_0E)^2/n^2\alpha^5p_0][(5n - 1)/(2 - 5n)] \quad (11)$$

and n must be less than 2/5.

Because of the simple power relation between x and $\bar{x}$, the transformed velocity, $\bar{u}_\infty$, varies as a simple power of $\bar{x}$. If we take $\bar{u}_\infty = \beta\bar{x}^m$, it follows that $\beta = \alpha/K^m$ and $m = n/(2 - 5n)$. With the transformed free-stream velocity in this form, the transformed momentum equation is that solved by Falkner and Skan, except that the factor θ has replaced unity in the last term.

Following Schlichting,[5] we define the coordinate η by

$$\eta \equiv \bar{y}\sqrt{[(m + 1)/2](\beta/\nu_0)}\bar{x}^{(m-1)/2}$$

and take the stream function as

$$\psi = \sqrt{[2\nu_0\beta/(m + 1)]}\bar{x}^{(m+1)/2}f(\eta)$$

whence $\bar{u} = \bar{u}_\infty f'(\eta)$, the prime denoting differentiation,

$$\bar{v} = -\sqrt{[2\nu_0\beta/(m + 1)]} \times [(m + 1)/2]\bar{x}^{(m-1)/2}\{f + [(m - 1)/(m + 1)]\eta f'\}$$

and the momentum equation reduces to

$$f''' + ff'' + [n/(1 - 2n)][\theta - (f')^2] = 0 \quad (12)$$

By utilizing the expressions for the current and pressure given by the channel flow, the energy equation may be put in the form

$$(1/Pr)(\partial^2\theta/\partial\eta^2) + f(\partial\theta/\partial\eta) = [2\bar{x}/(m + 1)]f'(\partial\theta/\partial\bar{x}) - (\gamma - 1)\bar{M}_\infty^2(f'')^2 - [(\gamma - 1)/\gamma][(5n - 1)/(1 - 2n)]^{1/2}(5kT_0/2e)(\sigma_0/\mu_0RT_0)^{1/2} \times (\partial\theta/\partial\eta) - [(\gamma - 1)/\gamma[(5n - 1)/(1 - 2n)] \times \theta[(\sigma_\infty/\sigma) - f'] \quad (13)$$

$\bar{x}$ does not occur in Eq. (12) and occurs in Eq. (13) only in the first and second terms on the right. If the Mach Number, which depends on $\bar{x}$, is small and the boundary conditions are independent of $\bar{x}$, solutions of Eqs. (12) and (13) exist such that f and θ depend only on η, since then the term proportional to $\partial\theta/\partial\bar{x}$ is zero. Thus, similar solutions exist for the thermal and viscous boundary layers if $\bar{M}_\infty^2$ is small and the wall temperature is constant.

It is worth noting that both the channel-flow solution and the boundary-layer transformation can be extended to include variations of the conductivity and electric field as powers of x. The momentum equation retains the form given above, as does the energy equation, except that the free-stream conductivity, which occurs in the coefficient of $\partial\theta/\partial\eta$, becomes a function of $\bar{x}$. Thus, exact similarity no longer exists for small $\bar{M}_\infty^2$ if σ_∞ varies with x.

Nevertheless, for many practical cases, the similarity may be nearly exact because the electronic conduction term is small compared to the Joule-heating term. As an example, for helium at 3,000°K., seeded to a conductivity of 100 mho/m, the coefficient of $\partial\theta/\partial\eta$ is 0.05, while that of $\theta(\sigma_\infty/\sigma - f')$ is 0.2, if $n = 1/4$.

The range of n which is physically interesting is limited by the channel-flow solution to positive values greater than 1/5, while the present transformation from x to $\bar{x}$ limits it to values below 2/5. Over the range of n from 1/5 to 2/5, m varies from 1/5 to ∞, so that boundary-layer flows with a very wide range of characteristics are described.

References

[1] Kerrebrock, J. L., and Marble, F. E., *Constant-Temperature Magneto-Gasdynamic Channel Flow*, Readers' Forum, Journal of the Aero/Space Sciences, Vol. 27, No. 1, p. 78, January, 1960.

[2] Falkner, V. M., and Skan, S. W., *Some Approximate Solutions of the Boundary Layer Equations*, Phil. Mag., Vol. 12, p. 865, 1931.

[3] Stewartson, K., *Correlated Incompressible and Compressible Boundary Layers*, J. Royal Society, A, Vol. 200, p. 84, 1931.

[4] Cohen, C. B., and Reshotko, Eli, *Similar Solutions for the Compressible Laminar Boundary Layer with Heat Transfer and Pressure Gradient*, NACA TN 3325, February, 1955.

[5] Schlichting, H., *Boundary Layer Theory*, p. 128, McGraw-Hill Book Company, Inc., New York, 1955.

Heat Transfer at a Corner*

Victor Zakkay

Research Assistant Professor, Aerodynamics Laboratory, Polytechnic Institute of Brooklyn, Freeport, N.Y.

September 25, 1959

THE HEAT TRANSFER about an arbitrary three-dimensional body may be estimated with good engineering accuracy, if the pressure distribution about the body is continuous. However, no simple heat-transfer analysis appears to be available for cases in which a discontinuity (a sharp change) in the pressure gradient occurs. A discontinuity of this type may occur at a conical-cylindrical junction, for example.

For the purpose of obtaining a rough estimate of the heat transfer downstream of the junction, a common procedure has been to balance the product of the momentum thickness and the dynamic pressure, before and after the discontinuity. This yields a reference length upon which local boundary-layer characteristics are based.

In order to investigate this, a program has been carried out at the Polytechnic Institute of Brooklyn Aerodynamics Laboratory in order to obtain some experimental information on this

* This contract is administered by the Aeronautical Research Laboratory of the ARDC and partially supported by the Air Force Ballistic Missile Division, Contract No. AF 33(616)-6118, Project No. 7064, Task No. 70169, under the supervision of Dr. Antonio Ferri.

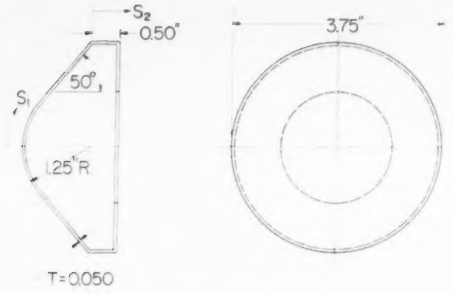

FIG. 1. Model configuration.

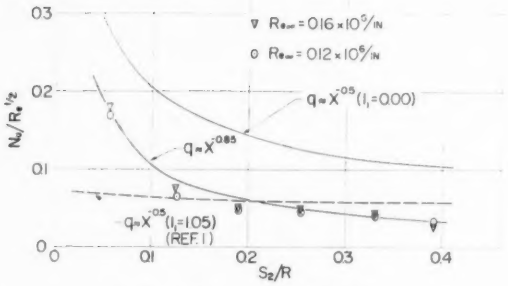

FIG. 2. Heat-transfer distribution.

problem. A blunt axially symmetric body with a 50° cone half-angle, followed by a cylindrical section (see Fig. 1), was chosen for this investigation.

Heat-transfer and pressure measurements were made at Mach 8 at a Reynolds Number per inch of 0.16×10^6 and 0.12×10^6, with a stagnation-to-wall temperature ratio of 2.3. A constant static pressure was obtained downstream of the corner. The heat-transfer results are presented in Fig. 2 in the form of a Nusselt Number divided by the square root of the Reynolds Number defined as

$$Nu/Re^{1/2} = (q\, C_{p_{s_e}}/K_{s_e})\sqrt{R\mu_{s_e}/\rho_{s_e}}\,(h_{s_e} - h_w)^{-1}\, h_{s_e}{}^{-(1/4)}$$

where

R = nose radius
q = local heat flux
h_{s_e} = stagnation enthalpy
S_e = stagnation conditions behind a normal shock
h_w = wall enthalpy
K = thermal conductivity of air

The results are compared with the usual flat-plate solution, choosing the junction as the starting length. Next, they are compared with the method presented in reference 1. The starting length in this case was estimated to be 1.05 in. The second method seems to compare fairly well with the experimental results far from the junction point; however, there is a large discrepancy close to the corner. The experimental results indicate that the heat-transfer parameter decreases like $S_2{}^{-0.85}$ rather than the usual $S_2{}^{-0.5}$ for laminar flow. A reason for this difference between the estimate of reference 1 and the experimental results may be related to the fact that the flow in the immediate vicinity of the corner cannot be treated by usual boundary-layer techniques. A somewhat different approach for treating the flow near a corner has been suggested by Dr. Antonio Ferri. In this method, it is assumed that the flow over the junction within a normal distance on the order of the boundary-layer thickness upstream of the discontinuity can be closely described by neglecting viscous effects. This is reasonable because of the short streamwise distance in the region of the corner, which reduces the importance of the viscous effects on the pressure and velocity. Therefore, the inviscid flow around the corner can be analyzed in two parts. The supersonic portion of the flow field may be analyzed by the method of characteristics, and the lower part of the flow field can probably be treated in a one-dimensional fashion by neglecting viscosity with the assumption that the pressure in this region is constant at each station along the streamline and the vorticity is conserved in the boundary layer. In this manner, the profile downstream of the corner may be obtained.

When the flow upstream of the corner is subsonic, the analysis requires very lengthy calculations. An analysis of this type is being conducted by Dr. Vaglio-Laurin. Additional information regarding this problem, where the flow upstream of the discontinuity is supersonic, will be published at a later date. The author wishes to thank Dr. Martin H. Bloom for initiating this investigation.

REFERENCE

[1] Romig, M. F., *Curves of Shock Waves, Expansion Waves, and Skin Friction Data for Hypersonic Speeds*, Convair Rpt. No. A-Atlas-103, December, 1954.

A Graphical Solution for Normal Shock Waves in Real Gases*

Charles E. Treanor
Cornell Aeronautical Laboratory, Inc., of Cornell University, Buffalo, N.Y.
October 1, 1959

THE SOLUTION of the equations for conditions behind a normal shock in a real gas usually represents a tedious and time-consuming part of shock-tube research. Even for gases for which the thermodynamic properties have been calculated completely, the simultaneous solution of the Rankine-Hugoniot equations using graphs or tables of thermodynamic properties presents a formidable amount of numerical work. For the important case of shocks in air, tables and graphs[1-3] of conditions behind shocks have been prepared for the range of initial temperatures which occur in the atmosphere and for a wide range of initial pressure and of Mach Number. A very general IBM 704 program solution for shock waves, including the effects of finite reaction rates for the chemical processes which occur, is also available.[4] There remains a need, however, for a simple but accurate method of obtaining solutions for shocks in real gases for which the thermodynamic properties are known, both for the case of air at high initial temperatures and for the many other gases of interest in current shock-tube research. In the present note, a rapid graphical method of obtaining such solutions is described. The accuracy is limited only by the accuracy of the graph available for the gas properties. No iterative procedure is involved, and the only machine or slide-rule calculations required are for factors having to do with the initial conditions of the gas and the speed of the shock wave. The method employs a universal curve, an auxiliary piece of graph paper, and a plot of the thermodynamic properties of the gas, where lines of constant enthalpy are plotted on a graph of density vs. pressure on log-log paper.† An extension for calculation of conditions behind a reflected shock is also described.

The equations of continuity through a shock wave can be written

* This work was supported by the USAF under Contract Nos. AF 18(603)-141 and AF 18(603)-19, monitored by the AFOSR of the ARDC.

† Graphs for N_2, O_2, NO, and air are available as Cornell Aeronautical Laboratory Rpt. No. AD 111 A-48.

$$\begin{aligned} \rho_1 V_1 &= \rho_2 V_2 \\ H_1 + (K/2)V_1^2 &= H_2 + (K/2)V_2^2 \\ P_1 + \rho_1 V_1^2 &= P_2 + \rho_2 V_2^2 \end{aligned} \qquad (1)$$

where ρ is the density, P the pressure, H the specific enthalpy, and V the velocity of the gas. K is either

$$2.389 \times 10^{-8}(\text{cal./gm.})/(\text{cm./sec.})^2$$

or

$$3.995 \times 10^{-5}\ \text{B.t.u./lb.}/(\text{ft./sec.})^2$$

depending on the units employed for H and V. Subscripts 1 and 2 are used for conditions ahead of and behind the shock, respectively. Velocities are measured relative to the shock wave, so that V_1 can also be considered as the velocity of the shock relative to the gas ahead of it. It will be assumed at present that all conditions 1 are known, and all conditions 2 are unknown. Eqs. (1) then give three relations for four unknowns, and it is assumed that the fourth relation, the thermodynamic properties of the gas, is given in graphical form as described above.

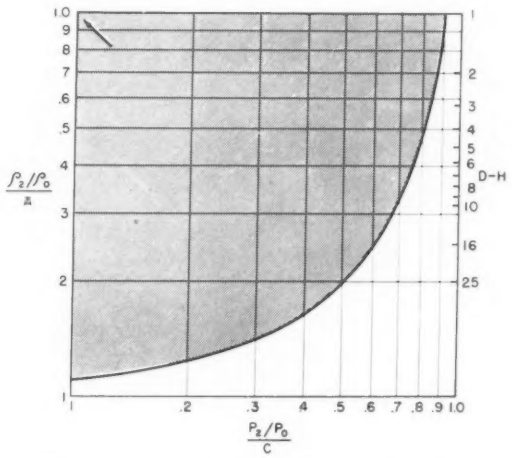

FIG. 1. Universal curve for template, Eq. (2).

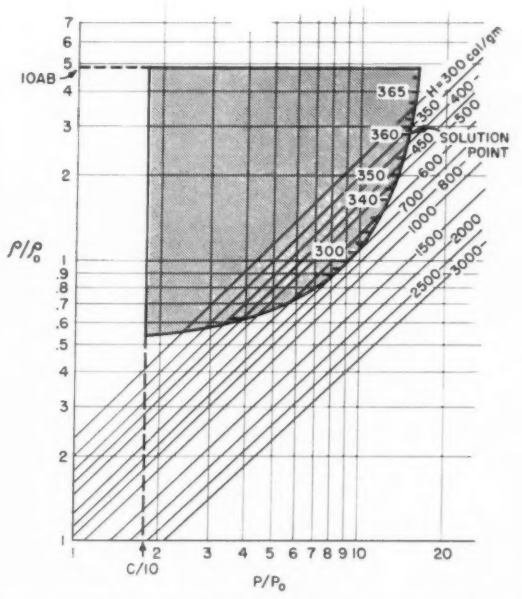

FIG. 2. Use of template for solution of the incident-shock equation.

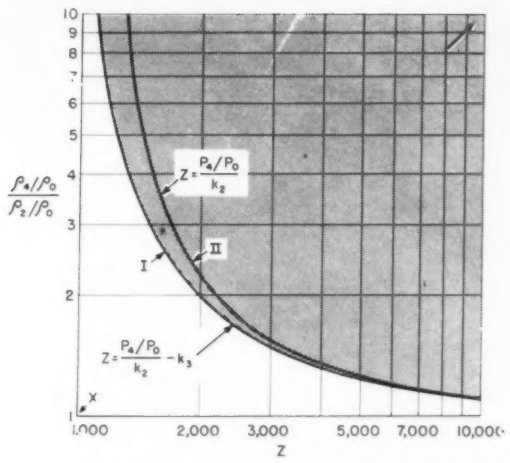

FIG. 3. Curve for solution of reflected-shock equations, Eqs. (4) and (5).

Eliminating V_2 from Eqs. (1), one obtains two equations in three unknowns

$$A/(\rho_2/\rho_0) = (1/B)\{1 - [(P_2/P_0)/C]\} = \sqrt{D - H} \qquad (2)$$

where A, B, C, and D are four terms having to do with conditions 1—viz.,

$$\begin{aligned} A &= \sqrt{K/2}(\rho_1/\rho_0)V_1 \\ B &= (2/K)(\rho_0/P_0)(A/C) \\ C &= (P_1/P_0) + (\rho_0/P_0)(\rho_1/\rho_0)V_1^2 \\ D &= H_1 + (K/2)V_1^2 \end{aligned} \qquad (3)$$

The quantities P_0 and ρ_0, the pressure and density at STP, have been introduced as usual. In the case where the gas ahead of the incident shock can be considered an ideal gas, the equations for the constants simplify still further.

A plot of $(\rho_2/\rho_0)/A$ vs. $(P_2/P_0)/C$, Eq. (2), on log-log paper is a universal curve whose position on the paper is determined by the value of B. The curve is shown in Fig. 1 for the case $B = 0.1$. The shaded region can conveniently be considered a template. For any other value of B, the template should be shifted vertically so that the point on the template marked with an arrow is at $(\rho_2/\rho_0)/A = 10B$. The quantity D-H, from Eq. (2), is universally related to $(\rho_2/\rho_0)/A$ and so is marked on the right vertical scale of the paper. From this scale, and knowing the value of D for a given problem, one can write the value of H at several convenient points on the template. The solution to the shock equations is now known to lie along this curve, no matter what the thermodynamic properties of the gas might be.

The gas properties are assumed available in the form of lines of constant enthalpy on a graph of ρ/ρ_0 vs. P/P_0 on log-log paper. This graph is used as a two-dimensional slide rule by placing the upper left corner of the template (arrow in Fig. 1) at the point $P/P_0 = 0.1\ C$, $\rho/\rho_0 = 10AB$ on the gas properties graph, with several values of H written on the template. The solution lies along the template at the point where the values of H agree, and this is the value of H_2. A typical positioning is shown in Fig. 2. The corresponding values of ρ_2/ρ_0 and P_2/P_0 can be read immediately from the graph (along with T_2, if lines of constant T have been included on the graph).

This graphical method of solution is of special interest in the problem which considers a gradual approach to equilibrium behind the shock wave. In this case, the values of pressure and density of the gas move along the curve as the shock passes through the gas (since Eqs. (1) are satisfied at all points behind the shock regardless of the degree of equilibration), finally arriv-

ing at the solution point described above when equilibrium is attained.

For a shock reflected from the closed end of a shock tube, the velocity of the reflected shock is usually unknown, and the method is more difficult to apply. Referring to conditions ahead of and behind the reflected shock with subscripts 3 and 4, the continuity equations are

$$k_1/[1 - (\rho_2/\rho_0)/(\rho_4/\rho_0)] = [(P_4/P_0)/k_2] - k_3 \quad (4)$$

$$H_4 = [(P_4/P_0)/k_2] + k_4 \quad (5)$$

where

$$k_1 = KV_1^2[1 - (\rho_1/\rho_2)]^2, \quad k_2 = (1/K)(\rho_C/P_0)(\rho_2/\rho_C) \quad (6)$$

$$k_3 = (P_2/P_0)/k_2, \qquad k_4 = H_2 - (1/2)k_1 - k_3$$

and the substitutions $P_3 = P_2$, $\rho_3 = \rho_2$, and $H_3 = H_2$ have been made. It is assumed that the gas is at rest behind the reflected shock.

Eq. (4) can be plotted as a universal curve if one plots $(\rho_4/\rho_0) \div (\rho_2/\rho_0)$ vs. $[(P_4/P_0)/k_2] - k_3$. The plot is shown as curve I in Fig. 3 and is the mirror image of the curve in Fig. 1. k_1 has been taken equal to 10^3. In general, the template (shaded) should be shifted horizontally so that the arrow is where the abscissa is equal to $10k_1$. To obtain an abscissa equal to $P_4 \div P_0k_2$, the curve should be drawn with the template and then a new curve drawn k_2 units to the right (curve II, Fig. 3). Values of H can then be noted on curve II, using Eq. (5). The entire graph paper can now be positioned appropriately on the graph of gas properties. For example, the point marked with an X in Fig. 3 (at 1,000, 1) can be positioned at

$$P/P_0 = 10^3k_2, \quad \rho/\rho_0 = \rho_2/\rho_0$$

Again, the agreement of enthalpy values on the two graphs gives the solution.

References

[1] Feldman, Saul, *Hypersonic Gas Dynamic Charts for Equilibrium Air*, AVCO Research Laboratory, January, 1957.

[2] Hochstim, A., *Gas Properties Behind Shocks at Hypersonic Velocities I. Normal Shocks in Air*, Convair, San Diego ZPh (GP)-002, AD 134 398, January, 1957.

[3] Huber, P. W., *Tables and Graphs of Normal-Shock Parameters at Hypersonic Mach Numbers and Selected Altitudes*, NACA TN 4352, September, 1958.

[4] Duff, R. E., *Calculation of Reaction Profiles Behind Steady-State Shock Waves*, J. Chem. Phys., Vol. 28, No. 6, p. 1193, 1958.

An Approximation for Subsonic Flow Through an Orifice

P. G. Morgan
Dept. of Engineering, University of Manchester, Manchester, England

October 8, 1959

The mass flow of a compressible fluid through an outlet from a reservoir is given by

$$Q = A\sqrt{2g[\gamma/(\gamma - 1)]P_1p_1[(P_2/P_1)^{2/\gamma} - (P_2/P_1)^{(\gamma+1)/\gamma}]}$$

where

A = area of the outlet
g = acceleration due to gravity
P_1p_1 = pressure and specific weight of the fluid in the reservoir
P_2 = pressure of the fluid outside the reservoir
γ = adiabatic index

Putting

$$\sqrt{2g[\gamma/(\gamma - 1)]} = C, \quad P_2/P_1 = \epsilon$$

and

$$\epsilon^{2/\gamma} - \epsilon^{(\gamma+1)/\gamma} = m$$

we have

$$Q = AC\sqrt{P_1p_1m}$$

and the ratio ϵ determines the character of the flow. If

$$\epsilon \leq \epsilon_* = [2/(\gamma + 1)]^{\gamma/(\gamma-1)}$$

the velocity of the fluid through the orifice is equal to the velocity of sound, and m is constant and equal to

$$m_* = \epsilon_*^{2/\gamma} - \epsilon_*^{(\gamma+1)/\gamma}$$

$$= [2/(\gamma + 1)]^{2/(\gamma-1)} - [2/(\gamma + 1)]^{(\gamma+1)/(\gamma-1)}$$

The mass flow depends only upon the parameters of the fluid and of the reservoir.

When $\epsilon > \epsilon_*$, the value of m depends upon ϵ, and the determination of Q becomes more difficult. For ϵ nearly equal to 1, the compressibility effect may be neglected, and Q may be determined from the equations for incompressible flow. The value of m may be expressed, to a good degree of approximation, over the whole subsonic flow range $\epsilon_* < \epsilon < 1$ by the equation

$$m_{\text{app.}} = k[a - (\epsilon - b)^2]$$

where k, a, and b are constants. These may be obtained from the conditions

$$\epsilon = \epsilon_*, \quad m_{\text{app.}} = m_*$$

$$\epsilon = \epsilon_*, \quad dm_{\text{app.}}/d\epsilon = dm/d\epsilon = 0$$

$$\epsilon = 1, \quad m_{\text{app.}} = m = 0$$

leading to

$$k[a - (\epsilon_* - b)^2] = m_*$$

$$2(\epsilon_* - b) = 0$$

$$k[a - (1 - b)^2] = 0$$

which give

$$k = m_*/(1 - \epsilon_*)^2, \quad a = (1 - \epsilon_*)^2, \quad b = \epsilon_*$$

For $\gamma = 1.4$, we have

$$\epsilon_* = 0.528, \quad m_* = 0.067$$

giving

$$k = 0.300, \quad a = 0.223, \quad b = 0.528$$

Using this approximate method, calculations for the flow rate show a difference between the exact and approximate values of less than 2 per cent over the whole subsonic range.

Error Criterion for Feedback-System Synthesis (*Continued from page 134*)

[29] Laning, J. H., Jr., and Battin, R. H., *Random Processes in Automatic Control*, McGraw-Hill Book Co., Inc., New York, 1956.

[30] Mathews, M. V., and Steeg, C. W., *Final Value Controller Synthesis*, Trans. IRE, PGAC-2, p. 6, February, 1957.

[31] Booton, R. C., Jr., *Optimum Design of Final Value Control Systems*, Proceedings of the Symposium on Nonlinear Circuit Analysis, Brooklyn Polytechnic Institute, New York, 1956.

[32] Peterson, E. T., *Optimization of Multi-Output Linear Time-Varying Systems Subject to Multiple or Redundant Non-Stationary Inputs*, Trans. AIEE, Part II, 1959.

[33] Shinbrot, M., *On the Integral Equation Occurring in Optimization Theory With Nonstationary Inputs*, J. Math. & Phys., Vol. 36, pp. 121–129, 1957.

[34] Guillemin, E. A., *The Mathematics of Circuit Analysis*, John Wiley and Sons, Inc., New York, 1949.

REQUIREMENTS *for* CONTRIBUTIONS

to the publications of the

INSTITUTE *of the* AERONAUTICAL SCIENCES

The Institute of the Aeronautical Sciences invites both members and nonmembers from any country to submit papers for publication in the JOURNAL OF THE AERO/SPACE SCIENCES and AERO/SPACE ENGINEERING. The Institute, following the practice of other societies, does not pay for contributions.

The following directions for the preparation of papers, if followed by authors, will save correspondence, avoid the return of papers for changes, minimize the work of preparation for the printer, and save the expense due to the charges made for "author's corrections."

MANUSCRIPTS: The original typewritten copy of the paper is desired. **To expedite review, an additional copy of both the manuscript and figures should be submitted.** The manuscript must be double or triple spaced on one side of white paper sheets, consecutively numbered. There should be wide margins to allow for the marking of directions to the printer. Correcting, changing, or adding to papers after they are in type is costly. It is, therefore, imperative that papers submitted be in final form. Typographical errors may be corrected on proofs, but if authors wish to add material, they may do so at their own expense. In mailing, drawings may be rolled, but manuscripts should be sent flat. Send by first-class mail (register if you wish for your own protection) to the Editorial Office, Institute of the Aeronautical Sciences, 2 East 64th Street, New York 21, N.Y. All manuscripts will be examined by the Editorial Committee and by the Editor. Authors will be advised as promptly as possible whether the paper is acceptable for publication.

TITLES: The title of the paper should be brief. The name and initials of the author should be written as he prefers. The use of the full name of an author is advocated because of the frequent duplication of initials and surnames which sometimes makes it difficult to establish the identity of the author. This is particularly important for large annual indexing and abstracting services. All titles and degrees or honors are omitted. The name of the organization with which the author is associated should be placed after his name on a separate line. The date on which the paper is received will be inserted by the Editor. The author's title or position should be indicated in a footnote.

SUMMARIES OR ABSTRACTS: An abstract to be printed at the beginning should accompany each article. It should be adequate as an *index* and as a *summary*. It should contain a statement of major conclusions reached, since summaries in many cases constitute the only source of information used in compiling scientific reference indexes. Abstracts printed in other journals, especially foreign, in most cases consist of summaries from printed papers. The summary should explain as adequately as possible the major conclusions to a nonspecialist in the subject and should contain from 100 to 300 words, depending on the length of the paper.

SUBHEADINGS: Subheadings should be inserted by the author at frequent intervals. The work of editorial preparation will be simplified by the author's provision of many subheadings.

MATTER USUALLY DELETED: Photographs or illustrations of little technical interest and not showing advances in general practice. Too detailed tabular matter (general results of such tables may be included in the text). Lengthy descriptions of materials or processes or of preliminary experiments or theories that preceded final results; salient features only are of interest.

REFERENCES: References should be numbered consecutively and grouped together at the end of the manuscript, with only the corresponding number being mentioned in the text. The arrangement should be as follows. For books: [1] Durand, W. F., *Aerodynamic Theory*, 1st Ed., Vol. 1, p. 23; Julius Springer, Berlin, 1934. For magazines: [1]England, C. R., Crawford, A. B., and Mumford, W. W., *Some Results of a Study of Ultra-Short-Wave Transmission Phenomenon*, Proc. IRE, Vol. 20, No. 12, pp. 481–482, March, 1933. Please give author, title, edition, volume, number, page, publisher, and place and date of publication as indicated. Omission of one required fact causes much extra editorial work and possible inaccuracies.

ILLUSTRATIONS: Illustrations should accompany manuscripts and each should always be referred to in the text by number Drawings or graphs should not be larger than 12 × 16 inches, and must be made with jet black India ink on white paper or tracing cloth, the latter being preferred. *Do not use typewriter for lettering.* The smallest lettering on 8 × 10 inch figures should be no less than 1/4 inch high. Cross-section paper (white with black lines) may be used, but it should not have more than 4 lines per inch. If finer ruled paper is used, the major division lines should be drawn in with black ink, omitting the finer divisions. In the case of finely ruled paper, only blue-lined paper can be accepted. *Tracing paper and blueprints* are not acceptable. Lettering and all markings must be large enough to be readable after reduction to single-column width ($3^{3}/_{16}$ in.). Mail rolled or flat; never fold. Drawings that cannot be reproduced (including pencil drawings) will be returned to the author for redrawing, thus delaying publication of the paper. Photographs should be distinct and show clear black and white contrasts. They must be on glossy white paper. Avoid round or oval photographs.

CAPTIONS AND LEGENDS: Legends or captions must accompany each drawing or photograph submitted. If written on the drawing or photograph, they should be placed below and well outside the part to be reproduced. Each table should have a caption such as Table 1, Table 2, Table 3, etc. Captions should be complete in themselves so as to make the data intelligible to the reader without reference to the text. A duplicate list of captions for figures should be included as the last page of the manuscript. Use "Fig. 1" (not Figure 1), "Figs. 3 and 4," etc., in both the text and the numbering of illustrations. In the text, "Eq. (1)" or "Eqs. (1) and (2)" is used, not "Equation (1)." In captions, legends, and in table headings, write all words in full; do not abbreviate, except for "Fig." and "Eq."

MATHEMATICAL WORK: Formulas may be typewritten or carefully written in pen and ink, the writing to be large enough so that it can be marked for the printer. Considerable space for marking should be allowed above and below all equations. All complicated equations should be repeated on separate sheets with plenty of space left for marking. The solidus should be used for simple fractions appearing within the text. Make all expressions clear to the typesetter. Greek letters used in formulas should be clearly designated by name in the margin of the manuscript. The difference between capital and lower-case letters should be clearly distinguished and care taken to avoid confusion between zero (0) and the letter (o), between the numeral (one) and the letter (ell) and the prime (′), between alpha and a, kappa and k, u and mu, v and nu, n and eta. All subscripts and exponents should be clearly distinguished. Avoid complicated exponents and subscripts. Dots and bars over letters or mathematical expressions should also be avoided. When it is necessary to repeat a complicated expression, it should be represented by some convenient symbol.

SYMBOLS AND ABBREVIATIONS: The symbols recommended in the American Standard Association "Letter Symbols for Aeronautical Sciences," ASA Y10.7—1954, should be used wherever practicable. All symbols should be clearly written and carefully checked. Standard abbreviations should be used, and it should be noted that most abbreviations are lower case, such as m.p.h., b.m.e.p., i.h.p. b.hp., hp., etc.

CORPORATE MEMBERS

OF THE

INSTITUTE OF THE AERONAUTICAL SCIENCES

AC SPARK PLUG DIVISION, GENERAL MOTORS CORPORATION

ACADEMY OF AERONAUTICS

AEROJET-GENERAL CORPORATION

AEROLAB DEVELOPMENT COMPANY

AERONCA MANUFACTURING CORPORATION

AERONUTRONIC SYSTEMS, INC.

AEROQUIP CORPORATION

AGAWAM AIRCRAFT PRODUCTS, INC.

ALLIED RESEARCH ASSOCIATES, INC.

ALLISON DIVISION, GENERAL MOTORS CORPORATION

ALUMINUM COMPANY OF AMERICA

AMERICAN AIRLINES, INC.

AMERICAN BOSCH ARMA CORPORATION

AMERICAN STEEL & WIRE DIVISION, UNITED STATES STEEL CORPORATION

AMOCO CHEMICALS CORPORATION

AMPHENOL-BORG ELECTRONICS CORPORATION

ANDERSON, GREENWOOD & CO.

ARDE ASSOCIATES

ASSOCIATED AVIATION UNDERWRITERS

AUTOMATION INDUSTRIES, INCORPORATED

AVCO RESEARCH LABORATORY

AVIEN, INC.

BAKER STEEL & TUBE COMPANY

BEECH AIRCRAFT CORPORATION

BELL AIRCRAFT CORPORATION

BENDIX AVIATION CORPORATION

BOEING AIRPLANE COMPANY

BOOZ, ALLEN & HAMILTON

THE BRISTOL AEROPLANE COMPANY (U.S.A.) INC.

BULOVA RESEARCH AND DEVELOPMENT LABORATORIES, INC.

CANADAIR, LTD.

THE CESSNA AIRCRAFT COMPANY

CHANCE VOUGHT AIRCRAFT, INCORPORATED

THE CHASE MANHATTAN BANK

CHICAGO AERIAL INDUSTRIES, INC.

THE CLEVELAND PNEUMATIC INDUSTRIES, INC.

CONSOLIDATED CONTROLS CORPORATION

CONTINENTAL MOTORS CORPORATION

CORNELL AERONAUTICAL LABORATORY, INC.

CURTISS-WRIGHT CORPORATION

DANIEL, MANN, JOHNSON, & MENDENHALL

DAYSTROM, INC.
DAYSTROM-WESTON SALES DIVISION

THE DECKER CORPORATION

DEL MAR ENGINEERING LABORATORIES

DELCO-REMY DIVISION, GENERAL MOTORS CORPORATION

DOAK AIRCRAFT COMPANY, INC.

DOUGLAS AIRCRAFT COMPANY, INC.

DZUS FASTENER COMPANY, INC.

EASTERN AIR LINES, INC.

EATON MANUFACTURING COMPANY

EDO CORPORATION

ELASTIC STOP NUT CORPORATION OF AMERICA

ENGINEERING SUPERVISION COMPANY

FAIRCHILD CAMERA AND INSTRUMENT CORPORATION

FAIRCHILD ENGINE AND AIRPLANE CORPORATION

THE GARRETT CORPORATION

GENERAL APPLIED SCIENCE LABORATORIES, INC.

GENERAL DYNAMICS CORPORATION

GENERAL ELECTRIC COMPANY

GENERAL PRECISION EQUIPMENT CORPORATION

G. M. GIANNINI & CO., INC.

GIANNINI PLASMADYNE CORPORATION

THE B. F. GOODRICH COMPANY

GOODYEAR AIRCRAFT CORPORATION

GRUMMAN AIRCRAFT ENGINEERING CORPORATION

HYDRO-AIRE CO.

INSURANCE COMPANY OF NORTH AMERICA COMPANIES

INTERNATIONAL BUSINESS MACHINES CORPORATION

THE INTERNATIONAL NICKEL COMPANY, INC.

ITT LABORATORIES, DIVISION OF INTERNATIONAL TELEPHONE AND TELEGRAPH CORPORATION

JANITROL AIRCRAFT, A DIVISION OF MIDLAND-ROSS CORPORATION

JOHNS-MANVILLE SALES CORPORATION

WALTER KIDDE & COMPANY, INC.

KOLLSMAN INSTRUMENT CORPORATION

LAVELLE AIRCRAFT CORPORATION

LEAR, INCORPORATED

C. W. LEMMERMAN, INC.

LIBRASCOPE DIVISION OF GENERAL PRECISION, INC.

THE LIQUIDOMETER CORPORATION

LOCKHEED AIRCRAFT CORPORATION

LOEWY-HYDROPRESS DIVISION OF BALDWIN-LIMA-HAMILTON CORPORATION

THE MARQUARDT CORPORATION

THE MARTIN COMPANY

MARTIN STEEL PRODUCTS CORPORATION

McDONNELL AIRCRAFT CORPORATION

MELETRON CORPORATION

MINNEAPOLIS-HONEYWELL REGULATOR COMPANY

NATIONAL CREDIT OFFICE, INC.

NORTH AMERICAN AVIATION, INC.

NORTHROP CORPORATION

NUCLEAR DEVELOPMENT CORPORATION OF AMERICA

PAN AMERICAN WORLD AIRWAYS, INC.

THE RALPH M. PARSONS COMPANY

PESCO PRODUCTS DIVISION, BORG-WARNER CORPORATION

PHILLIPS PETROLEUM COMPANY

PIASECKI AIRCRAFT CORPORATION

RADIO CORPORATION OF AMERICA
ASTRO-ELECTRONIC PRODUCTS DIVISION
DEFENSE ELECTRONIC PRODUCTS

RAMO-WOOLDRIDGE DIVISION, THOMPSON RAMO WOOLDRIDGE INC.

REPUBLIC AVIATION CORPORATION

ROHR AIRCRAFT CORPORATION

PAUL ROSENBERG ASSOCIATES

RYAN AERONAUTICAL COMPANY

SANDBERG-SERRELL CORPORATION

SHAFER BEARING DIVISION, CHAIN BELT COMPANY

SHELL OIL COMPANY

SIMMONDS AEROCESSORIES, INC.

SOCONY MOBIL OIL COMPANY, INC.

SOLAR AIRCRAFT COMPANY

SOUTHWEST PRODUCTS CO.

SPACE TECHNOLOGY LABORATORIES, INC.

R. DIXON SPEAS ASSOCIATES

SPERRY GYROSCOPE COMPANY DIVISION OF SPERRY RAND CORPORATION

STANDARD OIL COMPANY OF CALIFORNIA

STANDARD OIL COMPANY (INDIANA)

STANDARD-THOMSON CORPORATION
CLIFFORD MANUFACTURING DIVISION

STANLEY AVIATION CORPORATION

THIOKOL CHEMICAL CORPORATION

THOMPSON RAMO WOOLDRIDGE INC.

TRANS WORLD AIRLINES, INC.

TURBO PRODUCTS, INC.

UNION CARBIDE CORPORATION

UNITED AIR LINES, INC.

UNITED AIRCRAFT CORPORATION

UNITED STATES AVIATION UNDERWRITERS, INC.

VARD, INC.

VERTOL AIRCRAFT CORPORATION

VITRO CORPORATION OF AMERICA

WESTERN GEAR CORPORATION

WESTINGHOUSE ELECTRIC CORPORATION

WYMAN-GORDON COMPANY

YOUNG RADIATOR COMPANY